The role of non-myocytes in drug-induced cardiovascular toxicity

A thesis submitted in accordance with the requirements of
the University of Liverpool for the degree of
Doctor in Philosophy

By Stephanie Marianne Ravenscroft

2014

MRC-Centre for Drug Safety Science
Institute of Translational Medicine

List of contents

List of figures

List of tables

Abstract

The role of non-myocytes in drug-induced cardiovascular toxicity.

Stephanie Ravenscroft, The University of Liverpool

Submitted for the degree of Doctor of Philosophy (PhD), 2014

Cardiovascular toxicity is a leading cause of drug attrition at the preclinical and clinical stages of drug development. The specific mechanisms of drug-induced cardiovascular toxicities, however, are not well understood and can occur via direct interactions of the drug with cardiomyocytes or indirectly through interactions with other components of the cardiovascular system. Indirect drug effects can target non-cardiomyocyte cells such as fibroblasts, macrophages, vascular smooth muscle cells and endothelial cells. Evidence suggests interactions between these cell types are essential to the metabolism, growth, contractile performance and rhythmicity of the myocardium (Brutsaert, 2003). Preclinical and clinical drug safety tests primarily focus on cardiomyocytes, ignoring the other cellular components of the myocardium.

High content biology in combination with ATP content as a measure of cytotoxicity was used to assess the sensitivities of endothelial and fibroblast cells from different vascular beds to known structural cardiotoxins. This assay principle has previously been successful in the detection of structural cardiotoxicity in human embryonic stem cell derived cardiomyocytes (hESC-CM's) (Pointon *et al*., 2013). The endothelial cells displayed no significant difference in their compound responses, while the fibroblasts showed variation; imatinib was more potent in the cardiac fibroblasts and lapatinib more potent in the dermal fibroblasts. When the sensitivities of the cells from the myocardium (human cardiac fibroblasts (hCFs), human cardiac microvascular endothelial cells (hCMECs) and hESC-CMs) were globally compared the non-myocytes were sensitive to structural cardiotoxicity at the acute time point of 6 hour (h), whereas the hESC-CMs display toxicity only after 72 h. The conclusions from this work are that non-myocyte cells play a role in drug-induced cardiovascular toxicity since early sensitivity is displayed, however current *in vitro* models lack the complexity required to investigate the translation of this *in vivo*.

Multiple types of cardiac microtissue models were developed and their responses to reference structural cardiotoxins and inotropes evaluated using ATP content and video-based edge monitoring of contractility, respectively. Compound responses highlighted the promotion of maturity in the cardiac tri-cultured microtissue. Further investigations into gene expression and calcium (Ca^{2+}) handling suggested SR function and Ca^{2+} handling maturity had been promoted and that the ca^{2+} handling protein S100A1 plays a critical role in this maturity. These findings show adult cardiac non-myocyte cells can be used to promote contractile maturity of hESC-CM's *in vitro* when co-cultured as a three dimensional (3D) microtissue. The induction of maturity was very much multi-parameter dependent requiring a) both non-myocyte cell types, b) cells of cardiac origin and c) a 3D culture environment. More advanced human relevant *in vitro* models that better reconstitute the *in vivo* cellular physiology of the heart could allow improved *in vitro* to *in vivo* correlation in future drug safety screens.

Declaration

I declare that no portion of the work referred to in this thesis has been submitted in support of an application for another degree or qualification of this or any other university or other institute of learning.

Stephanie Ravenscroft

Institute of translational medicine

Centre for drug safety sciences.

Acknowledgements

Firstly I would like to thank my supervisors Dr Michael Cross and Dr James Sidaway for the support and guidance they have provided throughout my PhD. I'm grateful for the continued encouragement and for giving me the opportunity to attend some brilliant conferences. I have thoroughly enjoyed working for you.

Thank you to the MRC and AstraZeneca for funding this research.

Thank you Dr Amy Pointon for your unbelieveable patience and support for which I will be eternally grateful. Although not officially one of my supervisors, I respect your opinion and ideas therefore I have always considered you as one. Most of all I now consider you a friend.

I would like to thank everyone I have worked with at AstraZeneca, it has been a tough few years of change and yet you made it a pleasure to come to work every day. I wish you all the very best in the future. Thank you Alison Foster, Claire Summers, Julie Eakins, Dr Janet Kelsal, Clare Garner, Dr Helen Garside, Dr Alex Harmer, Dr Chris Pollard, Dr Najah Abi Gerge, Dr Helen Powell and Phil Glaves.

Thank you to my colleagues within the CDSS, Awel Williams, Dr Maxine Seaton and Emma Smith for their assistance and contribution to this project.

And finally thank you to my family and friends for being my life outside science. Scott, I thank you for your constant support, encouragement and for reminding me that I can do this.

Abbreviations

EC_{50}	50% effective concentration
IC_{50}	50% inhibition concentration
acLDL	acetyl low density lipoprotein
AP	Action potential
ATPase	Adenosine triphosphatase
ATP	Adenosine triphosphate
α	Alpha
β	Beta
BSA	Bovine serum albumin
Caff	Caffeine
Caff-ICR	Caffeine-induced calcium release
CICR	Calcium induced calcium release
Ca^{2+}	Calcium ion
CO_2	Carbon dioxide
cTNI	Cardiac troponin I
CM microtissue	Cardiomyocyte microtissue
CME microtissue	Cardiomyocyte/cardiac endothelial microtissue
CMEF microtissue	Cardiomyocyte/cardiac endothelial/cardiac fibroblast microtissue
CMF microtissue	Cardiomyocyte/cardiac fibroblast microtissue
DMEF microtissue	Cardiomyocyte/dermal endothelial/dermal fibroblast microtissue
CV	Cardiovascular
cm	Centimetre
^oC	Degrees celcius
DMSO	Dimethyl sulfoxide
DDR2	Discoidin domain receptor 2
ER	Endoplasmic reticulum
EGF	Epidermal growth factor
ECM	Extracellular matrix
FCS	Foetal calf serum

Xg	Gravitational force
GF	Growth factor
Hz	Hertz
HCB	High content biology
hr	hour
hCFs	Human cardiac fibroblasts
hCMECs	Human cardiac microvascular endothelial cells
hCAECs	Human coronary artery endothelial cells
hDMECs	Human dermal microvascular endothelial cells
hESC-CMs	Human embryonic stem cell derived cardiomyocytes
IGF	Insulin growth factor
LVEF	Left ventricle ejection fraction
L	Litre
Mg^{2+}	Magnesium ion
C_{max}	Maximum exposure concentration
µg	Microgram
µl	Microlitre
µm	Micrometre
µM	Micromolar
mg	Milligram
ml	millilitre
ms or msec	millisecond
Min	Minute
MMP	Mitochondrial membrane potential
M	Molar
ng	Nanogram
nm	Nanometre
-ve	Negative
NOS	Nitric oxide synthase
NE	No effect
NhDFs	Normal human dermal fibroblasts
N	Number

NRG1	Neuregulin-1
PBS	Phosphate buffered saline
PDGF	Platelet derived growth factor
+ve	Positive
K+	Potassium ion
rpm	Revolutions per minute
RT	Room temperature
RyR	Ryanodine receptor
SR	Sarco-endoplasmic reticulum
SERCA	Sarco-endoplasmic reticulum calcium ATPase
Sec or s	Second
ActN2	Smooth muscle alpha actinin type 2
Na+	Sodium ion
NCX	Sodium- calcium exchange
SD	Standard deviation
TI	Therapeutic Index
3D	Three dimensional
t	Time
T-tubule	Transverse tubule
TBS	Tri buffered saline
TMRE	Trimethylrhodamine
2D	Two dimensional
ULA	Ultra low adhesion
VEGF	Vascular endothelial growth factor
vs.	Versus
V	Voltage
v/v	Volume for volume measure
w/v	Weight for volume measure

Chapter One

General Introduction

1.1 Cardiovascular system

In all vertebrates, a complex vascular system is vital for the adequate supply of essential oxygen and nutrients to the organs, and for the concomitant removal of metabolic waste products. The transport of endocrine signals from their sites of secretion to their effector organs and the movement of immune cells to sites of infection and inflammation, are also functions of the vascular system. Hence, the cardiovascular system is the first functional organ to develop during embryogenesis (Rossant & Howard, 2002). The cardiovascular system comprises the heart and the peripheral vascular system, forming part of the closed circulatory system within the body. The peripheral vascular system comprises blood vessels sub-divided into macrovascular and microvascular vessels which extend throughout the body. The heart is central to the cardiovascular system (figure 1.1) and comprises four chambers built from striated cardiac muscle called myocardial tissue. This tissue has a dense coronary microvascular network which allows delivery, via the bloodstream, of the free fatty acids and oxygen required to meet the high metabolic demands of the myocardial tissue (Aird, 2007a) (figure 1.1).

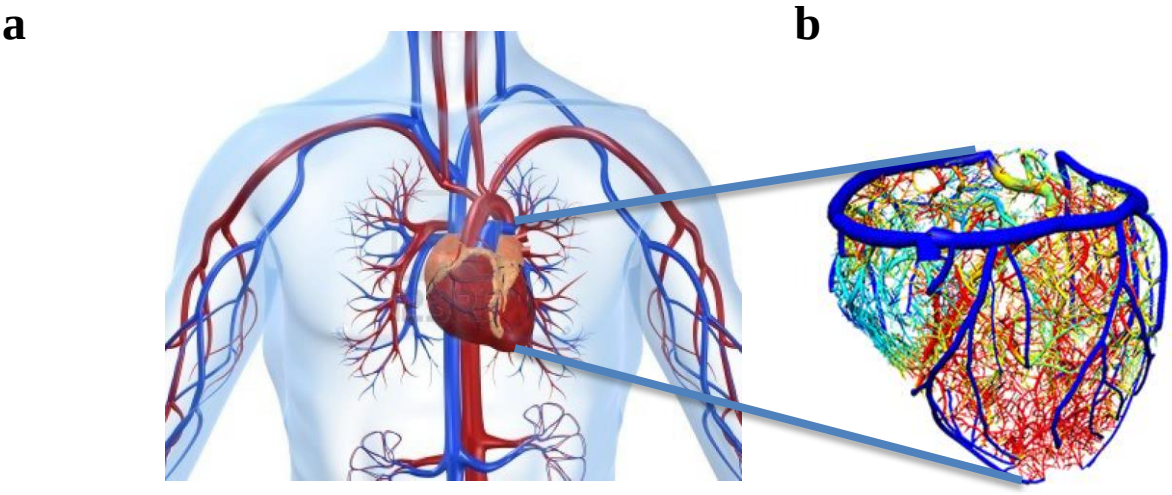

Figure 1.1 Cardiovascular system comprising the peripheral and coronary vasculature.

(a) The macro- and microvasculature of the peripheral vascular system. (b) The macro- and microvasculature of the coronary vascular system*. Image courtesy of Professor Nicholas Smith (Kings College London).*

The structure of the large, macrovascular vessels such as arteries and veins, consists of an inner layer (*tunica intima*) comprising a monolayer of endothelial cells surrounded by a sheet-like basement membrane home to the extracellular matrix proteins (ECM). This basement membrane is surrounded by the *tunica media* layer, which consists of vascular smooth muscle cells, whose function it is to allow vessel contraction. The outmost *tunica adventia* layer provides the supporting connective tissue. By contrast, the structure of the microvascular vessels, such as capillaries and arterioles, comprises a monolayer of endothelial cells surrounded by basement membrane and stabilised by a layer of specialised smooth muscle cells, known as pericytes (figure 1.2) (Aird, 2007b).

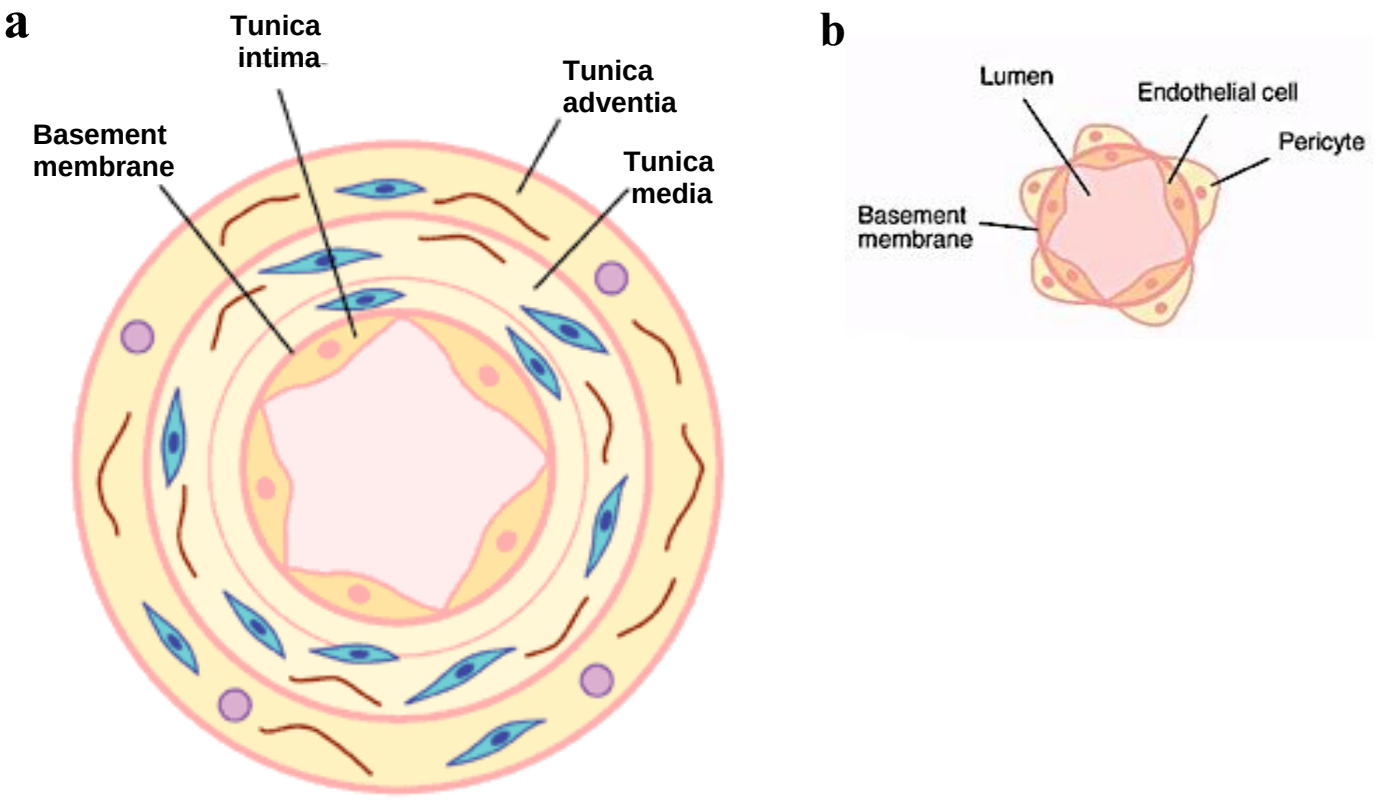

Figure 1.2 Diagram of blood vessel structure.

(a) Macrovascular vessel showing the inner layer (*tunica intima*), the *tunica media* layer and the outmost *tunica adventia*. (b) Microvascular vessel showing the monolayer of endothelial cells surrounded by smooth muscle cells and pericytes.

1.2 Cardiomyocytes- the fundamental work unit of the myocardium

The myocardial tissue (myocardium) is composed of 30% cardiomyocytes (Brutsaert, 2003); the fundamental work unit of the myocardium. The ultimate role of the heart is to maintain a constant circulation of blood around the vascular system which requires a non-stop pumping action by the heart, cycling between relaxing to fill with blood (diastole) and contracting to eject the blood (systole). This rhythmic action is brought about by the tight coordination of cardiomyocyte contractions within the myocardium. Blood circulation is fundamental to life therefore the heart is one of the earliest organs to develop during embryogenesis. Cell tracing studies in mice have suggested that the cardiac lineage arises from a population of cells expressing the vascular endothelial growth factor receptor 2 (VEGFR2, Flk-1) indicating that it may develop from a progenitor with vascular potential (Kattman *et al*., 2006). During embryogenesis, cardiomyocytes differentiate from stem cells. Stem cells are defined as undifferentiated cells capable of self-renewal or propagation as well as the capacity to transform into specialised cells under the appropriate conditions (Kumar, Kamp & LeWinter, 2005). The conditions required for cardiomyocyte differentiation are not fully understood, however the transcription factors Nkx-2.5 and GATA4 are known to play an important role in the specification of myocardial progenitors from the mesoderm since their expression is upregulated during the *in vitro* differentiation of embryonic stem cells into cardiomyocytes (Kumar, Kamp & LeWinter, 2005). Neuregulin-1 (NRG1) has recently been suggested to drive myocardial progenitors towards mature chamber cardiomyocytes (LaFlamme and Murray 2011) with faster conductance and a larger cell size. In the mature form these cells have a highly organised arrangement of functional units termed sarcomeres. Figure 1.3 shows the mature cardiomyocyte ultrastructure. Sarcomeres consist of myofilaments comprising groups of thin actin filaments and thick myosin filaments, which upon activation ‘slide’ past one another to shorten the sarcomere length; coordinated multi-sarcomere shortening thus contracts the cardiomyocyte. With coordinated cardiomyocyte contractions, the ventricular muscle contracts pushing blood out and around the body (Katz, 2006).

As with skeletal muscle, the activation of cardiomyocyte sarcomere filaments is regulated by calcium (Ca^{2+}) binding to elicit contraction, and dissociating to relax the contraction (Fabiato & Fabiato, 1975). Calcium homeostasis is perhaps considered

even more vital in the myocardium since the level of calcium signalling is solely responsible for the contractile force (inotropy) of the cardiomyocyte, whereas in skeletal muscle this depends upon the number of muscle fibers available (Eisner *et al.*, 2012).

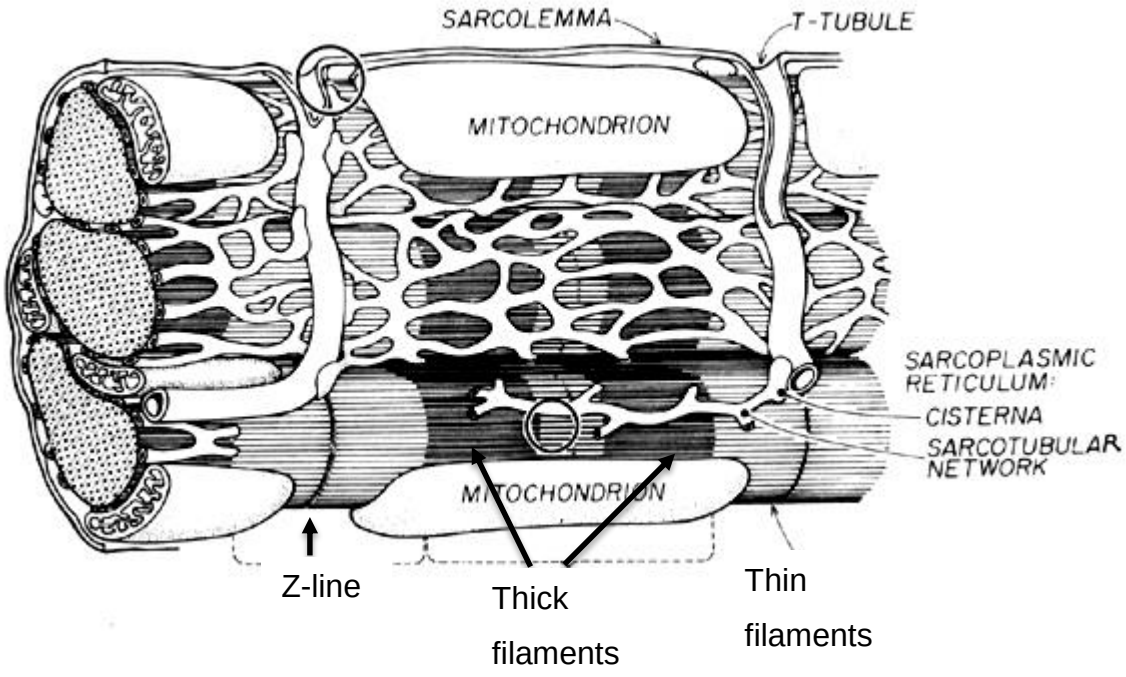

Figure 1.3 Ultrastructure of the cardiomyocyte.
Adapted from *Katz, 2006.*

1.2.1 Excitation-contraction coupling

Excitation-contraction coupling is the translation of an electrical excitation into a mechanical contraction force. A review by Bers in 2002 describes this process. Excitation is in the form of an action potential (AP) initiated by the pacemaker cells of the heart. This action potential travels through the heart causing membrane depolarisation. The action potential travels into the ventricular muscle, along the sarcolemma and deep into the cardiomyocyte by utilising the tranverse tubules (T-tubules). This membrane depolarisation opens the L-type Ca^{2+} channels (LTCC), Ca^{2+} ions now enter the cardiomyocytes. The mature cardiomyocyte has an

abundant T-tubule network, which carries membrane depolarisation deep into the cardiomyocyte and spatially localises Ca^{2+} entering through the L-type Ca^{2+} channels with the ryanodine receptors (RyRs) of the sarcoplasmic reticulum (SR) (McNary *et al.*, 2012). Extracellular Ca^{2+} binds to the RyRs to release a much greater amount of Ca^{2+} from the intracellular calcium stores of the SR (Fabiato & Fabiato, 1977; 1979). This results in a rapid rise in free cytosolic Ca^{2+}. This free Ca^{2+} binds to troponin C of the thin actin filaments causing an allosteric change, freeing the inhibitory troponin I from actin and unblocking the myosin binding site. Cross-bridge cycling can now occur, the myosin 'heads' of the thick filaments bind to the actin of the thin filaments, via the hydrolysis of adenosine triphosphate (ATP) and a resulting conformational change the thick and thin filaments 'slide' past one another shortening the sarcomere (Bers, 2002; Bers, 2001). Muscle contraction is therefore dependent upon Ca^{2+} and ATP. Figure 1.4 illustrates the excitation-contraction coupling network within the cardiomyocyte.

Relaxation of the cardiomyocytes now occurs to allow the heart to re-fill with blood during its diastole phase. Ca^{2+} dissociates from troponin C and is either pumped back into the SR by the sarcoplasmic reticulum Ca^{2+} ATPase (SERCA) or effluxed from the cell using the sodium-calcium exchangers (NCX) which swap the one Ca^{2+} for three Na+ (Bers, 2002; Díaz *et al.*, 2005). This loss of Ca^{2+} inhibits the cross-bridge cycling and relaxation of the ventricular muscle occurs.

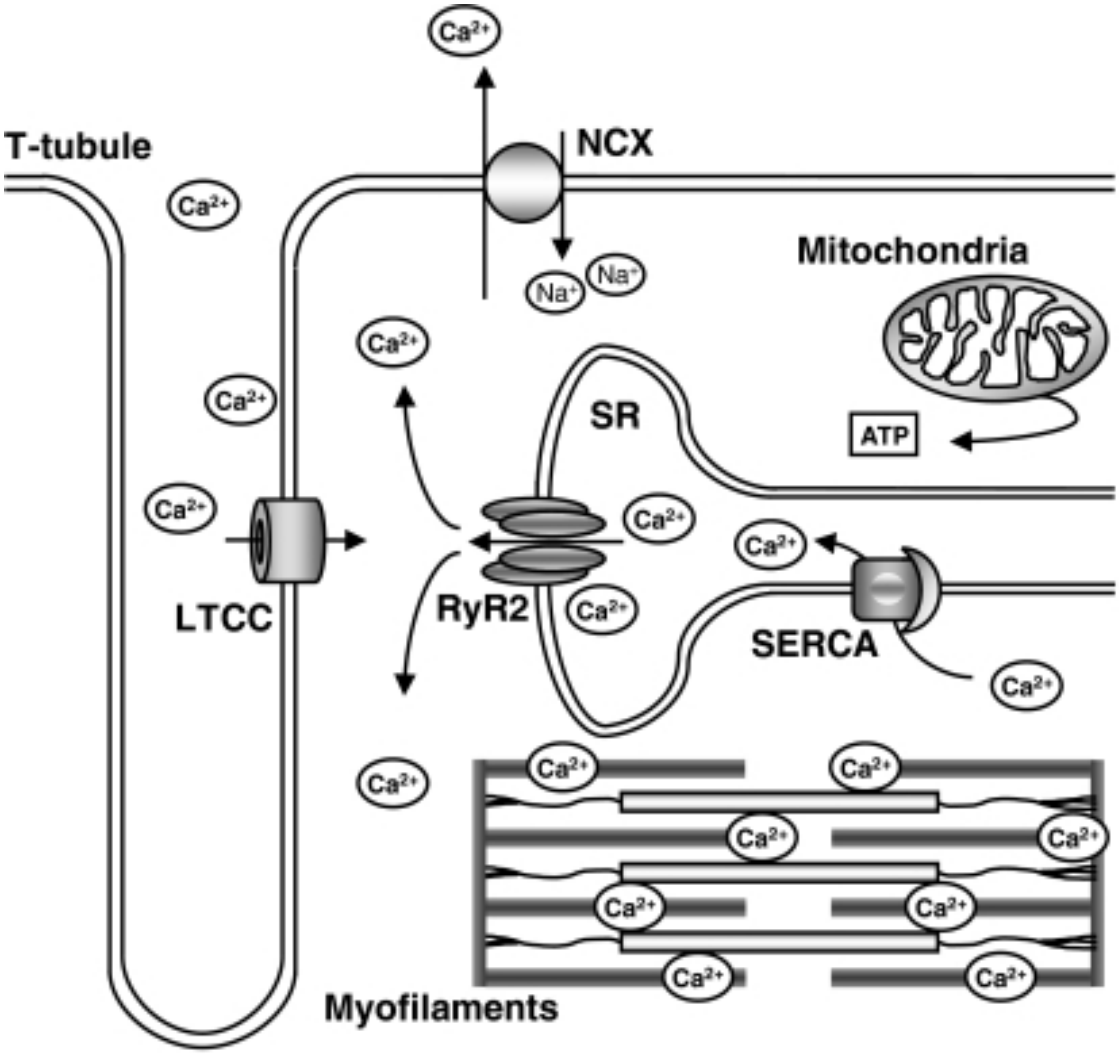

Figure 1.4 Excitation-contraction coupling in the cardiomyocyte.

An action potential enters the tranverse tubules (T-tubules). Membrane depolarisation opens L-type Ca^{2+} channels (LTCC), Ca^{2+} ions enter the cardiomyocytes. Extracellular Ca^{2+} binds to the RyRs to release Ca^{2+} from the sarcoplasmic reticulum (SR). Ca^{2+} binds to troponin C of the myofilaments. Upon repolarisation, sarcoplasmic reticulum Ca^{2+} ATPase (SERCA) loads Ca^{2+} back into the SR, sodium-calcium exchanger (NCX) transports Ca^{2+} out of the cell. Ca^{2+} dissociates from troponin C and the cardiomyocyte relaxes. *Figure adapted from Volkers et al, 2010.*

1.2.2 Role of S100A1 in cardiomyocyte excitation-contraction coupling

S100A1 is a Ca^{2+} binding protein of the EF-hand type and a member of the S100 protein family. The S100 family are a group of low molecular weight proteins found in vertebrates and characterised by their two calcium binding sites that have a helix-loop-helix (EF-hand) conformation. The 19 members of the S100 protein family have varied biological activities including cell differentiation and cell cycle progression but also transduction of intracellular Ca^{2+} signalling. S100A1 is the most abundant S100 protein in striated muscle and shows preferential myocardial tissue expression (Duarte-Costa *et al.*, 2014). Studies have shown co-localisation of S100A1 with the intracellular SR Ca^{2+} stores and the contractile filaments of cardiomyocytes (Völkers *et al.*, 2010). Given its preferential cardiac expression and localisation pattern, S100A1 has become a target of interest with respect to cardiac contractility. S100A1 has been shown to regulate and improve the function of key proteins involved in the control of sarcoplasmic reticulum Ca^{2+} handling as well as myofilament and mitochondrial function, thereby enhancing the heart's inotropic and lusitropic state (Brinks *et al.*, 2011; Duarte-Costa *et al.*, 2014; Ritterhoff & Most *et al.*, 2007; Rohde *et al., 2014*; Völkers *et al.*, 2010). Figure 1.5 illustrates S100A1 interactions duing excitation-contraction coupling within the cardiomyocyte. Additionally, heart failure studies have highlighted a marked reduction in S100A1 protein expression correlating with a reduction in β-adrenergic and inotropy response therefore highlighting S100A1 as a promising target for cardiac gene therapy (Bennett *et al.*, 2014). Other commonly known cardiac calcium binding proteins include the troponins, calmodulin and myosin.

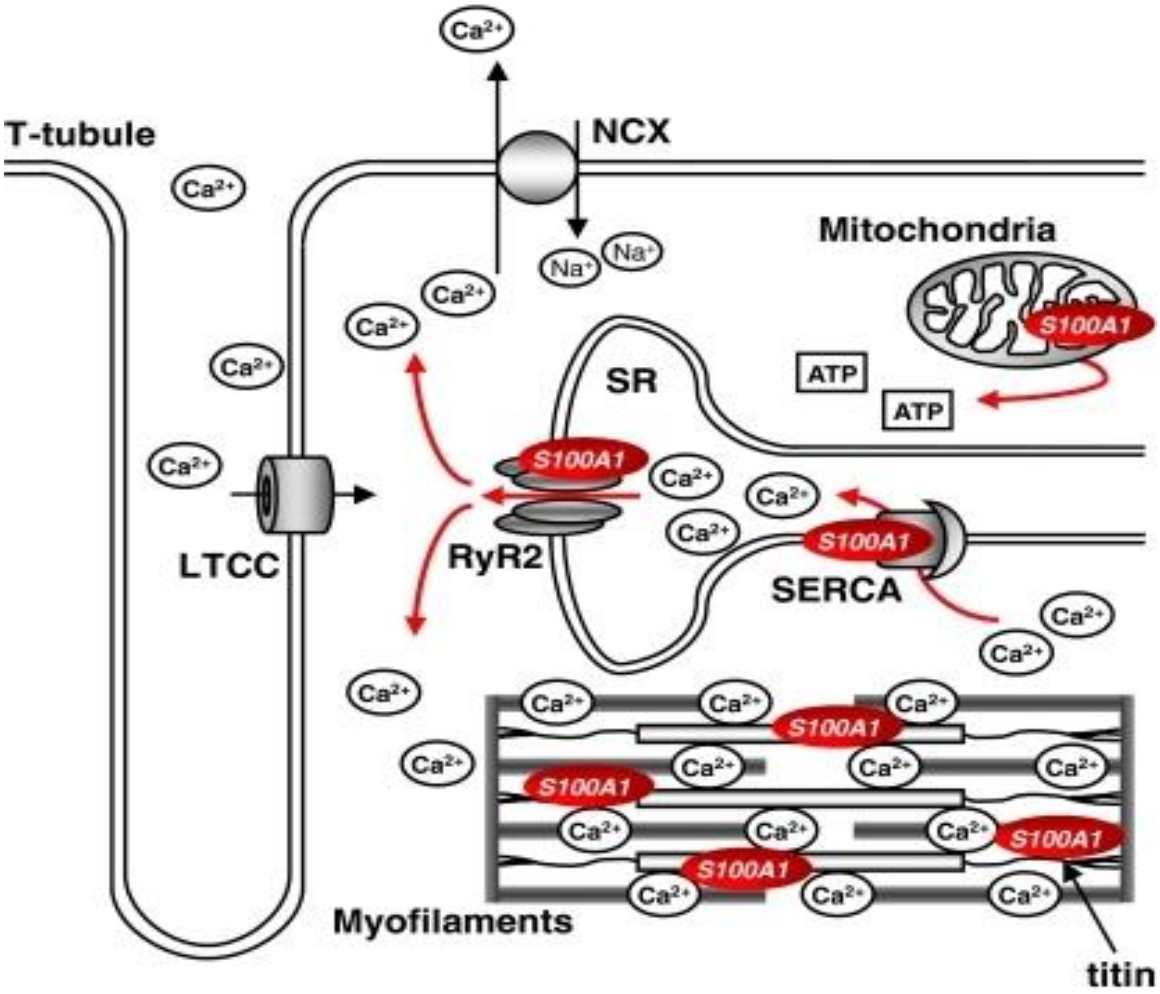

Figure 1.5 S100A1 in cardiomyocyte excitation-contraction coupling.

An action potential enters the tranverse tubules (T-tubules). Membrane depolarisation opens L-type Ca^{2+} channels (LTCC); Ca^{2+} ions enter the cardiomyocytes. Extracellular Ca^{2+} binds to the ryanodine receptors (RyRs) to release Ca^{2+} from the sarcoplasmic reticulum (SR). Ca^{2+} binds to troponin C of the myofilaments. Upon repolarisation, sarcoplasmic reticulum Ca^{2+} ATPase (SERCA) loads Ca^{2+} back into the SR, sodium-calcium exchanger (NCX) transports Ca^{2+} out of the cell. Ca^{2+} dissociates from troponin C and the cardiomyocyte relaxes. S100A1 binds to and improves the functioning of RyR2, SERCA, myofilaments and mitochondria. *Figure adapted from Volkers et al, 2010.*

1.2.3 Caffeine and modulation of Ca^{2+}

In electrophysiology studies using isolated cardiomyocytes a high concentration of caffeine (10 mM) has traditionally been used to measure sarcoplasmic reticulum (SR) function through caffeine-induced calcium release (caff-ICR) (Trafford *et al.*, 1998). Caffeine acts to increase the open probability of the RyRs therefore rendering the SR leaky and allowing the intracellular Ca^{2+} stores to be released into the cytosolic domain (Rousseau & Meissner, 1989; Trafford *et al.*, 1998; Xu & Meissner, 1998). This large and rapid Ca^{2+} signal throughout the cell allows cross-bridge cycling between the thin and thick filaments of the cardiomyocyte sarcomeres. In the myocardium the strength of the contraction (inotropy) is dependent upon the magnitude of Ca^{2+} transient and ATP available, therefore a steep relationship between intracellular Ca^{2+} store concentration and inotropy response exists. This inotropy is short lived however because the bulk of this Ca^{2+} is quickly transported out of the cell on NCX; normal Ca^{2+} reloading into the SR via SERCA is redundant due to the open RyRs on the SR surface therefore intracellular Ca^{2+} stores become depleted. This depletion occurs incredibly rapidly and results in an abrupt halt in cardiomyocyte contractions in unpaced conditions. Upon removal of caffeine, field stimulation of the cells allows an AP to activate the L-type Ca^{2+} channels causing an influx of Ca^{2+}into the cardiomyocyte cytosol and re-loading of the now sealed SR can occur via the SERCA channels. This effect is seen in adult cardiomyocytes because their dominant role for intracellular Ca^{2+} release is gated by RyRs (Liu *et al.*, 2007).

SR are found to be relatively sparse in the immature myocyte with inositol 1,4,5-trisphosphate (IP3)-gated Ca^{2+} release channels (IP3Rs) playing significant roles in Ca^{2+} mobilization from them (Liu *et al.*, 2007). Research has suggested that reliance upon RyRs for intracellular Ca^{2+} release increases with maturity (Liu *et al.*, 2007). Caffeine response can therefore be utilized as a marker of cardiomyocyte maturity; as RyR reliance and SR numbers increase, the magnitude of calcium released increases in correlation with contractile inotropy.

1.3 Non-cardiomyocytes- support cells of the myocardium

1.3.1 Cardiac fibroblasts

The remaining 70% of the cells in the myocardium are non-cardiomyocyte cells, with the majority being cardiac fibroblasts. These fibroblast cells are situated between cardiomyocytes (figure 1.6), their main role being the maintenance of the extracellular matrix (ECM). They are spindle shaped connective tissue cells that do not form a basement membrane but are responsible for the majority of the ECM proteins found in the myocardium. Their close proximity to myocytes and ability to manipulate the ECM provides them with the potential to influence the cardiomyocyte phenotype. Until recent years fibroblasts have been viewed as uniform cells, whereby phenotype is not subject to the local environment but gene expression studies are now suggesting they possess a high degree of phenotypic plasticity. For example, the cell surface receptor discoidin domain receptor 2 (DDR2) is specifically expressed by cardiac derived fibroblasts (Souders *et al.*, 2009). In addition to this, preliminary reporting suggests cardiac fibroblasts possess contractile transducing abilities not seen in other fibroblasts (Kamkin *et al*., 2005), this characteristic may facilitate communications between cardiomyocytes. Fibroblasts also support the microvascular system of the heart by secreting basement membrane proteins; fibronectin, laminin, collagen I and III. In this way they are heavily involved in cardiac remodeling (Calderone *et al.*, 1998; Ottaviano & Yee, 2011; Souders *et al.*, 2009).

The Ca^{2+} binding protein S100A1, (see section 1.2.2), has recently been suggested by Rohde *et al*, (2014) to possess an alarmin role during cardiac damage and a potential interaction with localized cardiac fibroblasts. Alarmin is a relatively new term referring to a protein released from a damaged cell, which acts upon neighbouring cells as a ‘distress’ signal allowing maintenance of tissue homeostasis. Rohde *et al*, have shown that S100A1 protein is released from iscahemic cardiomyocytes following tissue damage. S100A1 is then internalized via endolysosomal trafficking utilizing Toll-like receptor 4 in cardiac fibroblasts. Internalized S100A1 activates MAPK/SAPK and NFkB to initiate an anti-fibrotic immunomodulatory role in cardiac fibroblasts (Rohde *et al.*, 2014). Rohde *et al.* (2014) also highlighted a lack of internalization in endothelial and smooth muscle cells suggesting S100A1 has a specific alarmin role between cardiomyocytes and

cardiac fibroblasts to protect against fibrosis. This is one example of the important interplay that exists between cardiomyocytes and non-myocytes of the myocardium in order to maintain a finely tuned tissue even during times of environmental stress.

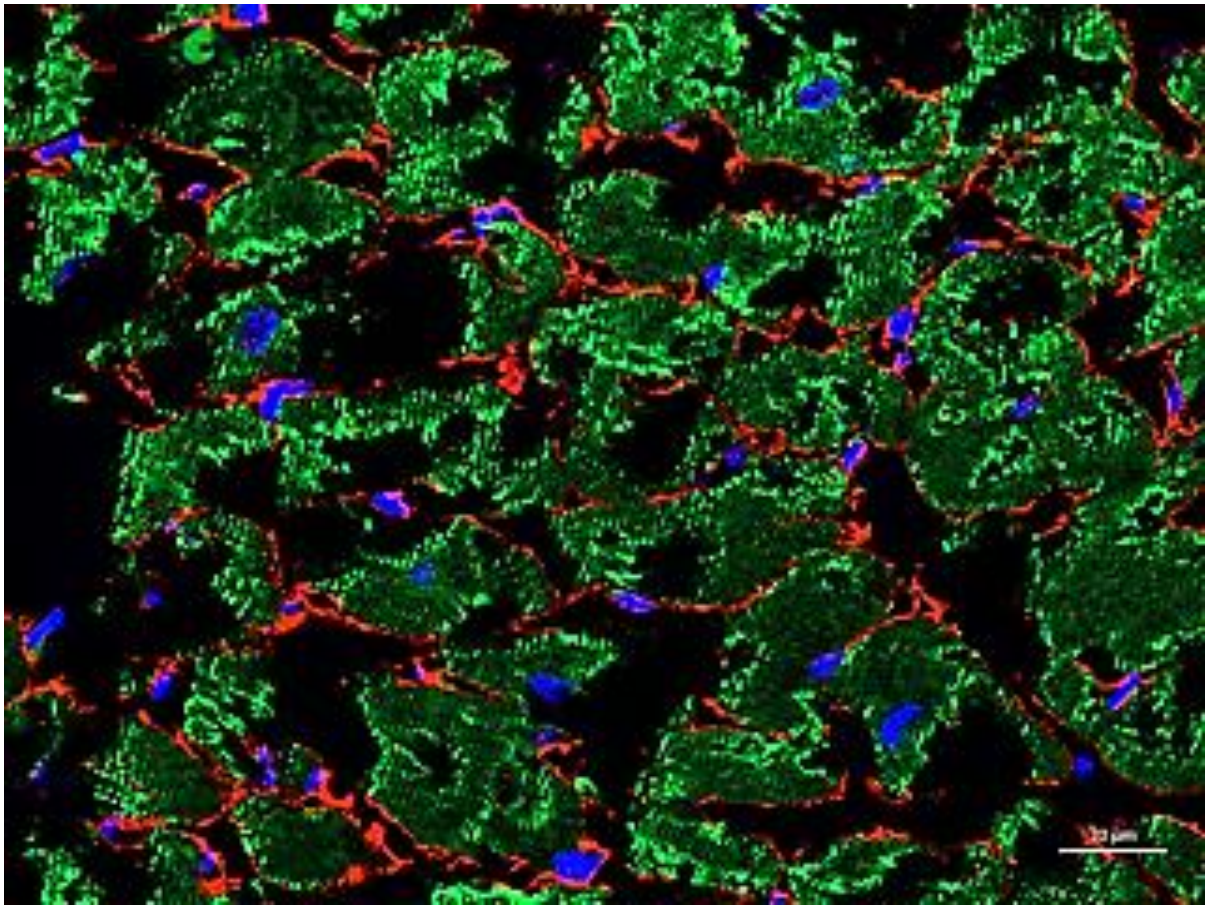

Figure 1.6 Immunofluorescence image of cardiomyocytes and cardiac fibroblasts within a rat heart left ventricle section.

Rat hearts were sectioned at 10 μM and stained with cell specific markers, images use Hoescht as a nuclei stain. Myocytes are stained using cardiac troponin I (cTnI) shown in green and fibroblasts with collagen 1 in red. Scale bar represents 20 μm. *Image courtesy of Emma Smith (The University of Liverpool).*

1.3.2 Cardiac microvascular endothelial cells

The next most abundant cells in the myocardium are the cardiac endothelial cells (figure 1.7). When considering the cardiovascular system, it is important to distinguish between the cardiac endothelium and the vascular endothelium as the latter interacts with smooth muscle cells as opposed to cardiomyocytes. The cardiac

endothelium represents two types of endothelial cells, those present within the endocardium and the microvascular endothelial cells of the intramyocardial capillaries. In the normal myocardium, the ratio of capillaries to myocytes is at least 1:1 with endothelial cells outnumbering myocytes 3:1, this minimal cell-to-cell diffusion distance is crucial to ensure the cardiomyocytes obtain the nutrients and oxygen required to meet their high metabolic demands, while also allowing signalling factors to be communicated between cells (Brutsaert, 2003; Hsieh *et al.*, 2006). Endothelial cells form a barrier to thrombus formation, regulate the adherence of immune cells and maintain vascular homeostasis (Aird, 2007a).

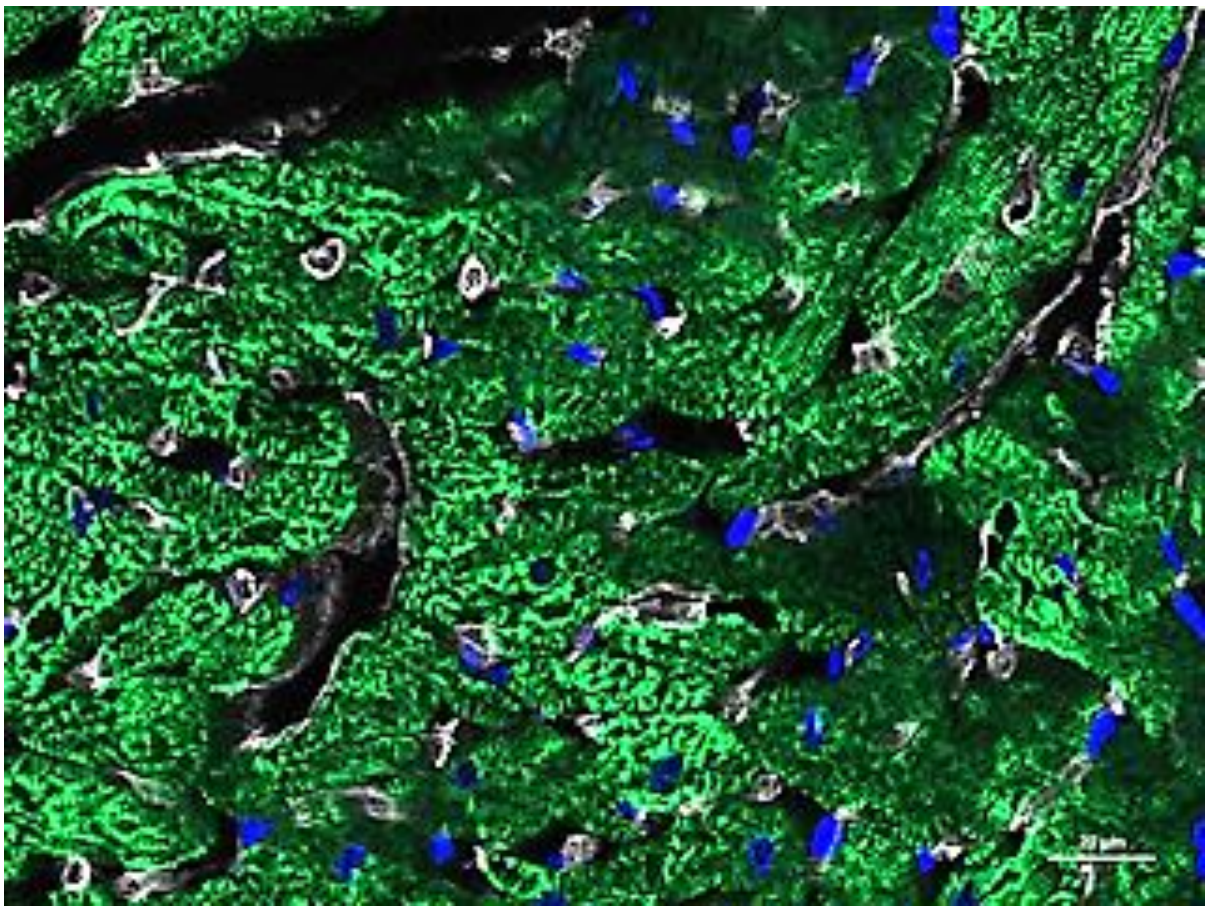

Figure 1.7 Immunofluorescence image of cardiomyocytes and cardiac microvascular endothelial cells within a rat heart left ventricle section.

Rat hearts were sectioned at 10 μM and stained with cell specific markers, images use Hoescht as a nuclei stain. Myocytes are stained using cardiac troponin I (cTnI) shown in green and endothelial cells with rat endothelial cell antibody (RECA1) shown in white. Scale bar represents 20 μm. *Image courtesy of Emma Smith (The University of Liverpool).*

It is generally accepted that the development of blood vessels involves two consecutive processes, vasculogenesis followed by angiogenesis (Starke *et al.*, 2006). Vasculogenesis in the early embryo involves the *in situ* differentiation of pluripotent mesodermal cells from the primitive streak into haemangioblasts which migrate to the extra-embryonic mesodermal layer in the yolk sac (Suburo & D'Amore, 2006). These haemangioblasts form aggregates known as primitive blood islands which comprise an outer layer of primitive endothelial cells, known as angioblasts, and an inner mass of primitive haemapoetic cells, known as haemangioblasts. Cells at the outer aspect of the blood island assume a spindle shape as they undergo differentiation into endothelial cells; whereas the inner cells differentiate into primitive blood cells by progressively losing their intercellular attachments. This results in the formation of mature blood islands. Fusion of these blood islands gives rise to a primary capillary plexus in the yolk sac that surrounds the embryo. A similar, but distinct route of vasculogenesis occurs within the embryo proper whereby the pluripotent mesoderm cells differentiate directly into angioblasts and subsequently into endothelial cells. The establishment of this primary vascular plexus is critical for the survival of murine embryos beyond day 9.5 (E9.5) (Flamme *et al.,* 1997).

Angiogenesis is the subsequent stage of vascular development; it involves the formation of new blood vessels from pre-existing vessels (Clauss & Breier, 2005; Starke *et al.*, 2006). The newly formed primary capillary plexus undergoes vascular remodelling to allow blood vessels to extend into the avascular extremities of the developing embryo (Clauss & Breier, 2005). This stage of vascularisation is critical to embryonic development but is a rare postnatal event in mammals occurring only during specialised physiological processes such as the female reproductive cycle and wound healing (Clauss & Breier, 2005). Angiogenesis plays roles in various pathologies such as rheumatoid arthritis and diabetic retinopathy as well as tumour development and metastasis. A lack of angiogenesis can, in contrast, also be disruptive as in the case of cardiac ischaemia. Many factors are involved in the regulation of sprouting angiogenesis creating a tightly regulated but dynamic multi-step process. Endothelial cells are normally quiescent in mature tissues, however, an upregulation in the concentration of pro-angiogenic factors or a down-regulation in anti-angiogenic factors in the surrounding microenvironment can lead to an

‘angiogenic switch’ and the endothelial cells adopting an angiogenic phenotype. Pro-angiogenic factors include vascular endothelial growth factor (VEGF) and fibroblast growth factor-2 (FGF-2). Anti-angiogenic factors include angiostatin and endostatin.

In recent years it has become increasingly apparent that, like fibroblasts, endothelial cells originating from different vascular beds show considerable heterogeneity (Hendrickx *et al.*, 2004). While endothelial cells are united in certain common features, their heterogeneity has been described at the level of morphology, function, antigen composition and signalling networks, suggesting each endothelial cell type is uniquely adapted to meet the demands of its local environment. Recently, data indicates that the embryological origin of macro- and microvascular endothelium are distinct; evidence suggests that microvasculature arises from vasculogenesis whereby angiogenesis is responsible for the creation of macrovascular segments. Therefore, endothelial cell responses are now thought to be the result of the environment in which an endothelial cell resides and it’s genetically ‘programmed’ function (Aird, 2012), providing endothelial cells residing within different tissues with the potential to respond to a common signal in a unique manner. Research is also suggesting a common ancestry for cardiac microvascular endothelial cells and cardiomyocytes, which could allow a hypothesis for common drug sensitivities (Garry & Olson, 2006; Laflamme & Murry, 2011; Moretti *et al.*, 2006; Wu *et al.*, 2006). Specific progenitor cells, which ultimately make up the myocardium, arise from a common embryonic epiblast. Endothelial cells have two routes to their final endothelial phenotype; the signalling factor wingless-related integration site (wnt) can direct this epiblast into haemangioblast and subsequently endothelium or alternatively, the epiblast is directed towards pre-cardiac mesoderm upon which VEGF directs a subsequent and final endothelial cell fate. Alternatively this pre-cardiac mesoderm can develop into chamber cardiomyocytes directed by neuregulin-1 (NRG-1) (Laflamme & Murry, 2011).

1.3.3 Cardiac pericytes

The microvasculature in human hearts contains abundant pericytes (figure 1.8), and on average each endothelial cell is associated with two to three pericytes (Nees *et*

al., 2013). These pericytes are contractile cells which wrap themselves around the microvasculature and support the normal functioning of the endothelial cells; these cells have only recently been highlighted as a target of interest with respect to cardiotoxicity (Chintalgattu *et al.*, 2013; Nees *et al.*, 2013; Nees *et al.*, 2012). They play many physiological roles from barrier function, regulation of homeostasis, facilitation of angiogenesis to initiation of coagulation.

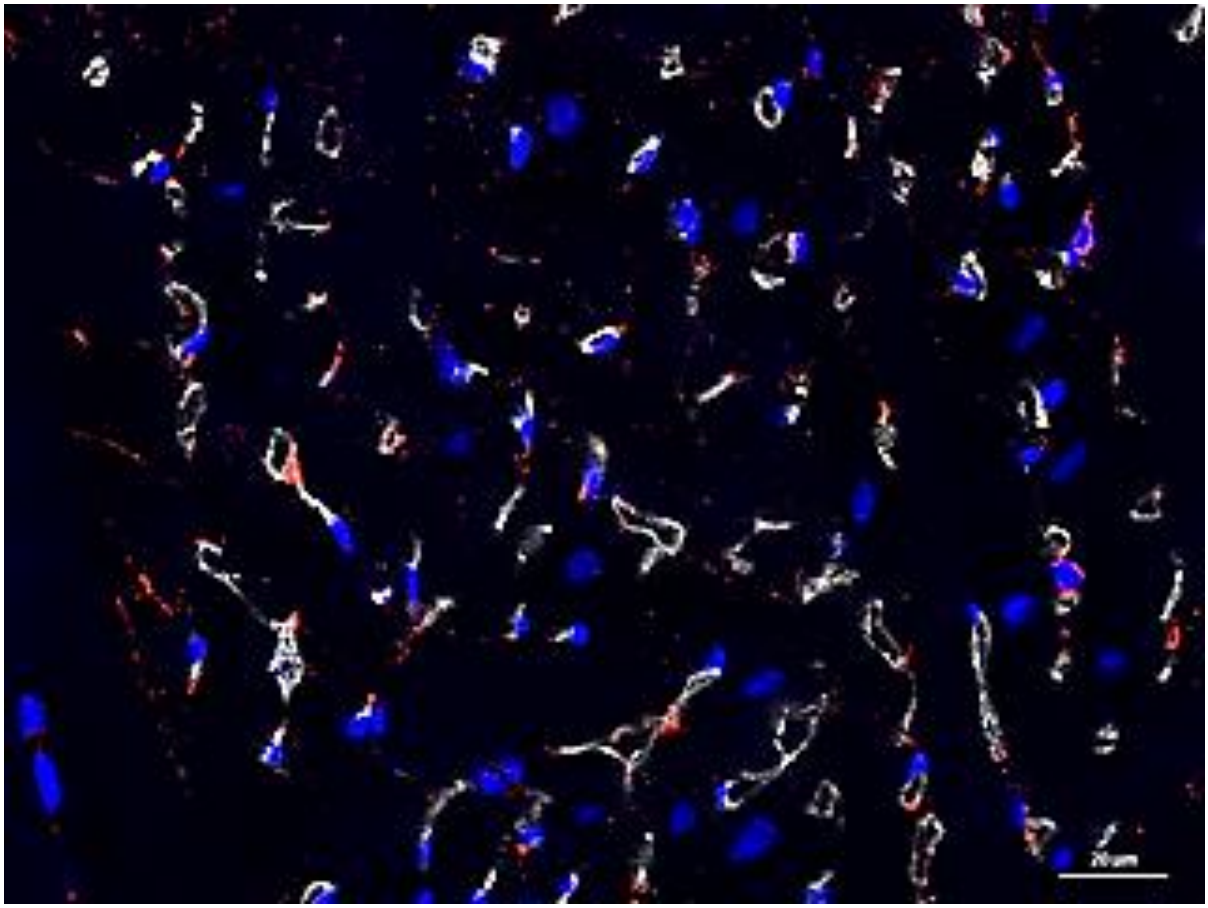

Figure 1.8 Immunofluorescence image of cardiac microvascular endothelial cells and cardiac pericytes within a rat heart left ventricle section.

Rat hearts were sectioned at 10 μm thickness and stained with cell specific markers, images use Hoescht as a nuclei stain. Endothelial cells are stained using rat endothelial cell antibody (RECA1) shown in white and pericytes with chondroitin sulfate proteoglycan (NG2) shown in red. Scale bar represents 20 μm. *Image courtesy of Emma Smith (The University of Liverpool).*

1.4 Cellular communications within the myocardium

1.4.1 Physical communications

As with many organs, cell communications within the myocardium are highly abundant in order to coordinate the fast and continual rhythmic contractions. Both cardiomyocytes and non-cardiomyocyte cells are rich in gap junctions, and as with other cell types this allows the direct passage of ions and small solutes between cells. These types of gap junctions are important in the myocardium for the transfer of oxygen and nutrients between the cardiomyocytes and the endothelial cells of the microvasculature. Gap junctions play an additional role between cardiac cells; a family of gap junction proteins, known as connexins, are critical in the fast conduction of electrical impulses. Global deletion of Connexin 43 (Cx43) in mice causes neonatal death (Tirziu *et al.*, 2010). The role of gap junctions has been best described between cells of the same type i.e. cardiomyocyte to cardiomyocyte (homotypic), but heterotypic connections also exist, for example cardiomyocytes form gap junctions with other cell types such as adjacent cardiac fibroblasts (Tirziu *et al.*, 2010) or endothelial cells of neighbouring microvasculature (Brutsaert, 2003; Hsieh *et al*., 2006). These connections allow an uninterrupted conduction of electrical impulses throughout the myocardium. Cells of the myocardium also form connections with the extracellular matrix. The synthesis and degradation of the ECM is primarily the role of the cardiac fibroblasts; it provides a 3D scaffold for the cardiomyocytes and microvasculature. Cardiac fibroblasts are able to respond to extracellular stimuli (chemical, mechanical or electrical) in order to maintain a healthy 3D scaffold (Souders *et al.*, 2009).

1.4.2 Chemical communications

In addition to physical communications between cells; autocrine and paracrine signalling is present within the myocardium as a dense and complex cross-talk between cardiomyocytes and non-cardiomyocytes in order to regulate cardiac structure and function. Combinations of secretion factors act to regulate cardiomyocyte health and therefore cardiac performance. It is widely accepted that cardiomyocytes, as with most muscle cell types including vascular smooth muscle cells, respond to increased cellular demands by increasing in cell size rather than

number (Brutsaert, 2003). Numerous signalling pathways are involved in the hypertrophy and survival of cardiomyocytes. Nitric oxide (NO) is a low molecular weight signalling molecule which acts by passively diffusing through target cell membranes to regulate intracellular signalling. NO is synthesised by the enzyme nitric oxide synthase (NOS) expressed under normal physiological conditions in cardiac endothelial cells (Brutsaert, 2003). The major eicosanoids synthesised by endothelial cells are prostacyclin (PGI_2) and prostaglandin E2 (PGE_2) which are synthesised by the enzyme cyclooxygenase (COX) (Campbell and Falck, 2007). It has been suggested that NO and PGI_2 have an anti-growth effect on the heart (Calderone *et al*., 1998; Harding *et al*., 1995; Hayakawa and Railj, 1997). Bradykinin has been shown to induce a direct growth response on cardiomyocytes in monoculture, however when co-cultured with cardiac endothelial cells, this growth response is inhibited (Ritchie *et al.*, 1998a; 1998b). It was therefore suggested that bradykinin stimulates endothelial release of NO and PGI_2 by acting upon the B_2 receptors on the endothelial cell surface which would therefore explain the beneficial effects of the angiotensin converting enzyme (ACE) inhibitors (ACEI) on ventricular remodelling; ACE breaks down bradykinin thereby inhibition results in an accumulation of bradykinin. The mechanism through which NO and PGI_2 block hypertrophy is unclear, however evidence suggests an increase in cGMP levels in the cardiomyocytes (Calderone *et al*., 1998).

An additional role for NO released by endothelial cells is to regulate the onset of ventricular relaxation, however it can also be synthesised by eNOS and nNOS present within cardiomyocytes (Grocott-Mason, 1994; Paulus, 1999). This autocrine signalling from cardiomyocytes can regulate β-adrenergic and muscarinic control of contractile state. NO diffuses into cardiomyocytes and can activate soluble guanylate cyclase leading to an increase in cGMP levels within the cell (Castro, 2010). This increased concentration of cGMP activates cGMP-dependent protein kinase which acts via numerous pathways e.g inhibition of ATP synthesis and closure of voltage-gated calcium channels (Brutsaert, 2003). Endothelin-1 (ET-1) is also thought to be involved in cardiac contractility (Iwanaga, 1998; Cingolani *et al.*, 2006). It is released by endothelial cells and activates two endothelin-1 receptors, ET-A and ET-B, found on cardiomyocytes; ET-B is also found on endothelial cells. These receptors are coupled to a G_q-protein and activation leads to an increase in IP_3. IP_3 stimulates

enhanced calcium release from the sarcoplasmic reticulum; this causes muscle contraction therefore increasing contractility and heart rate. As a second route of action to allow tight control of contractility, ET-1 acts to activate ET-B receptors on the endothelial cell surface (Hsieh *et al*., 2006). This receptor activation induces NO synthesis (Hsieh *et al*., 2006), which can diffuse into the cardiomyocyte and counteract the contraction signal produced by the ET-A and ET-B receptors.

Cardiac rhythmicity is thought to be a principle role of the endocardial endothelial cells rather than the microvascular capillary endothelium. However, NO released by human cardiac microvascular endothelial cells (hCMECs) is also suggested to play a role in the regulation of myocardial rhythmicity; although this is not fully understood it is thought that NO together with PGI_2 is involved in the tight balancing of cGMP:cAMP levels in cardiomyocytes (Brutsaert, 2003).

A final role for NO within the myocardium is regulation of cardiac metabolism; it has been shown to decrease myocardial tissue oxygen consumption in the normal as well as failing human heart (Brutsaert, 2003). This reduction in myocardial oxygen consumption was further reduced by ACE inhibitors (Loke, 1999); ACE inhibitors prevent the breakdown of bradykinin which leads to an increase in NO levels and therefore reduced oxygen consumption.

Growth factors also play complex roles within the myocardium. VEGF is a potent mitogen whose activity is specific to endothelial cells. Substantial amounts of VEGF mRNA expression have been determined in cardiac microvascular endothelial cells (CMEC's) as well as cardiomyocytes (Maruyama, 1999). mRNA of the VEGF receptor KDR/Flk-1 was found in the CMECs but not the cardiomyocytes (Maruyama, 1999) therefore explaining the lack of mitogenic activity on cardiomyocytes. Platelet derived growth factor (PDGF-AB/PDGF-α) signalling pathway between cardiomyocytes, cardiac fibroblasts and CMEC's was found to increase expression of VEGF and its receptor FLK-1 in the CMEC's (Edelberg, 1998). VEGF produced either by the cardiomyocytes or the CMECs can in turn influence the expression of NO and PGI_2 by the endothelial cells, thereby effecting cardiomyocyte remodelling and performance (Murphy, 2001; Ziche, 1997).

Cardiomyocyte survival is regulated by several signalling molecules. Growth factors such as insulin, IGF-1, erythropoietin and cytokines can antagonise apoptosis by activating PI3K which acts through Akt/PKB (Chen *et al*., 2010). Activated Akt acts to inhibit the pro-apoptotic Bcl-2 family member Bad, Bax, caspase-9, GSK-3 and FOX01 by phosphorylation (Chen *et al.*, 2010; Oudit, 2009). PTEN negatively regulates the PI3K/Akt pathway (Oudit, 2009). An alternative activation route involves the activation of G-protein coupled receptors by peptide agonists or B_2-adrenergic stimulation. Endothelial cell survival is also regulated in this way. These examples highlight the vast complexity of the signalling interplay that exists between cells of the myocardium. This expanse communication network is susceptible to interruptions by cardiotoxic drugs.

While fibroblasts and endothelial cells share many of the same activating stimuli such as hypoxia (Brutsaert, 2003; Souders, 2009; Pohlman & Harlan, 2000), more recently data suggests cardiac non-myocytes can also respond to mechanical strain (Tirziu et al., 2010). Activation of angiogenesis or fibroblast proliferation can lead to changes in the vasculature or cardiac remodeling, this can be beneficial to the cardiomyocytes or as is the case in drug-induced cardiotoxicity, it can be detrimental and lead to reduced cardiac output.

1.5 Introduction to cardiovascular toxicity

Cardiovascular toxicity can be defined as ‘chemically induced heart disease’, which can occur with many different drug classes treating a range of diseases (Brana & Tabernero, 2010). Drug development has improved drastically over recent years, particularly with respect to cancer therapeutics. The cardiac safety of drugs, however, is slow to catch up meaning we are now facing an era of replacing one disease with another. Anthracyclines, such as doxorubicin, are a common form of chemotherapy used in anti-cancer treatment. It has been estimated that two million women in the USA are at risk of delayed anthracycline toxicity as a result of breast cancer treatment (Gianni *et al.,* 2008). Not only are these drug-induced cardiovascular toxicity events a cause of serious health problems in patients, they are also the primary cause of drug withdrawal from the market and attrition during drug development; 28% over the past ten years (Laverty *et al.*, 2011). For example, the non-steroidal anti-inflammatory drug (NSAID) rofecoxib (Vioxx®) was withdrawn

in 2004 due to fatal cardiotoxicity in man and the anti-diabetic drug rosiglitazone (Avandia®) is now withdrawn or greatly restricted due to an increased risk of cardiovascular events (Laverty *et al*., 2011).

Ultimately the problematic endpoint of drug-induced cardiotoxicity is the inability of the heart to efficiently pump blood around the body. The specific mechanisms of drug-induced cardiovascular toxicities, however, are not well understood and can occur via direct interactions of the drug with cardiomyocytes or indirectly through interactions with other components of the cardiovascular system. Drug induced cardiovascular toxicity results from both functional effects (acute alteration of the mechanical function of the myocardium) and structural changes (morphological damage to cardiomyocytes or loss of viability) to the heart (figure 1.9). These adverse effects result in conditions such as arrhythmia or a more serious reduction in left ventricular ejection fraction (LVEF), which can lead to heart failure and death (Senkus, 2011; Minami, 2010). Indirect drug effects can target non-cardiomyocyte cells such as fibroblasts, macrophages, vascular smooth muscle cells and endothelial cells. Evidence suggests interactions between these cell types are essential to the metabolism, growth, contractile performance and rhythmicity of the myocardium (Brutsaert, 2003). Preclinical and clinical drug safety tests primarily focus on cardiomyocytes, ignoring the other cellular components of the myocardium (*see section 1.7*).

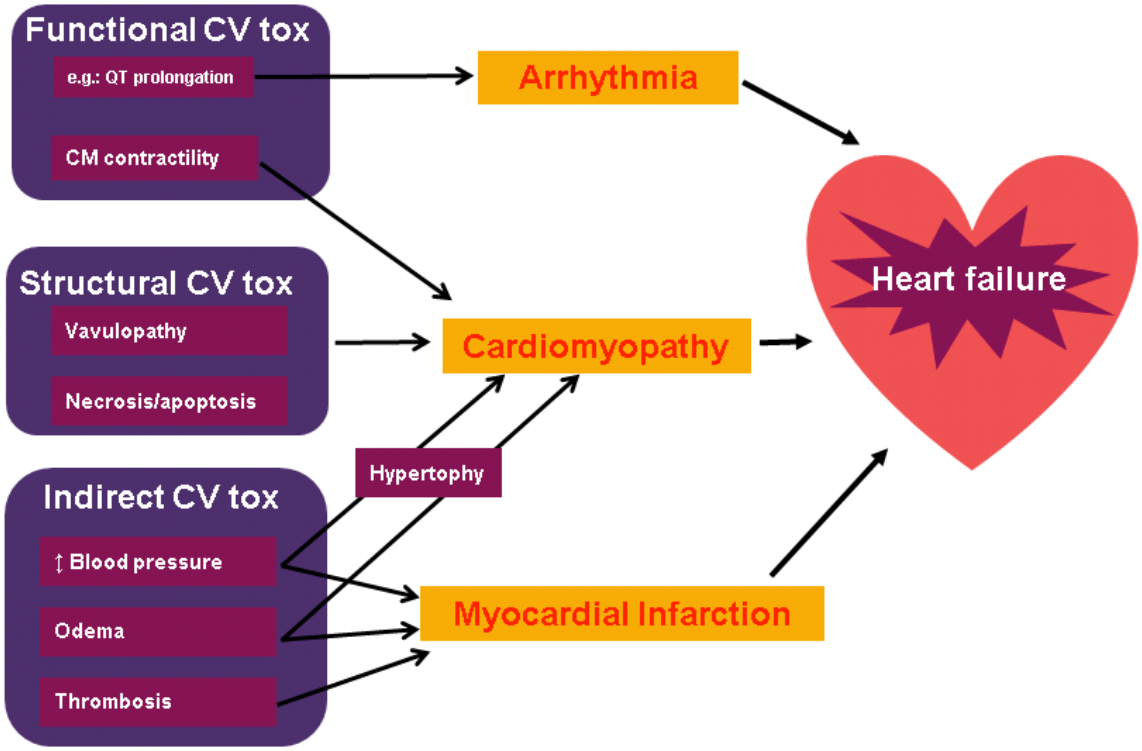

Figure 1.9 Functional, structural or indirect drug-induced cardiovascular toxicities.

1.5.1 Drug-induced structural cardiotoxicity

Damage to the myocardial cells can occur due to reduced blood supply in ischaemia or via direct drug-induced toxicity, leading to changes in myocardial morphology, physiology and biochemistry. This compromises cardiac function and can lead to cardiac failure (Brana & Tabernero, 2010) (figure 1.9). Figure 1.10 provides an overview of the changes that can occur as a result of drug-induced cardiovascular injury. The initiating event in cardiac dysfunction was originally believed to be at the myocyte level. However, it is now becoming apparent that endothelial dysfunction can influence surrounding cells (Ajithkumar *et al.*, 2011; Mikaelian *et al.*, 2010; Ritchie *et al.*, 1998a; Higashi *et al.*, 2009). Furthermore, cardiac fibroblasts are known to affect both cardiac myocyte and endothelial cell function (Calderone *et al.*, 1998; Ottaviano & Yee, 2011; Rohde *et al.*, 2014). Recent data have shown that drugs associated with clinical cardiotoxicity such as doxorubicin and tubulin-binding drugs (Mikaelian *et al.*, 2010) can adversely affect cardiac endothelial cells. Doxorubicin (Adriamycin) is a member of the anthracycline family and many studies have highlighted doxorubicin-induced hydrogen peroxide production in endothelial cells and cardiomyocytes as a cause of cellular dysfunction (Ajithkumar *et al*., 2011). This oxidative stress is thought to have the ability to modulate the production levels

of NO and ET-1 leading to decreased NO and increased ET-1 (Ajithkumar *et al*., 2011). This could potentially perturb cardiomyocyte-endothelial interactions. In addition to this doxorubicin is thought to lead to reactive oxygen species (ROS) and iron accumulation within the mitochondria of cardiomyocytes (Ichikawa *et al.*, 2014). Oxidative stress can result in the activation of mitogen or stress activated kinases involved in an apoptotic response, this would explain the high level of cardiomyocyte cell death seen with doxorubicin (Ajithkumar *et al*., 2011). The redox cycling and generation of reactive oxygen species by doxorubicin has long been acknowledged and recently a mechanism for the initiation of this toxicity has been suggested. Zhang *et al* have shown that cardiomyocyte specific deletion of Top2b (encoding topoisomerase-IIβ) protects cardiomyocytes from doxorubicin-induced DNA double-strand breaks that are responsible for defective mitochondrial biogenesis and ROS formation (Zhang *et al., 2012*). Doxorubicin has also been shown to increase endothelial apoptosis in the coronary microvasculature of the myocardium. Wu *et al*, measured an increase in Caspase 3 activity and resulting apoptosis in adriamycin-induced cardiomyopathy both *in vitro* and *in vivo* (Wu *et al.,* 2002; Ueno *et al*., 2006).

The advent of molecularly targeted cancer therapy and concomitant development of protein kinase inhibitors represents an emerging cardiovascular toxicity problem (Mellor *et al.*, 2011). These drugs have the potential to interfere with the autocrine and paracrine growth factor/cytokine-stimulated signalling pathways utilized by the cardiomyocytes, endothelial cells and fibroblasts to maintain cellular homeostasis and respond to environmental factors (Brutsaert, 2003; Chintalgattu *et al.*, 2010; Chintalgattu & Khakoo, 2010; Chintalgattu *et al.*, 2013; Ottaviano & Yee, 2011; Chiusa *et al.*, 2012). Examples include bevacizumab, sunitinib and sorafenib, all of which are protein kinase inhibitors (PKI). Inhibition of VEGF activity inhibits NO release (Mellor *et al.,* 2011), since NO is thought to have cardioprotective roles in the myocardium it seems likely that this inhibition of endothelial cell activity would have an effect on cardiomyocytes. Sorafenib is a multi-kinase inhibitor which acts upon several protein kinases including the Raf family of kinases; Raf-1, β-Raf, VEGFR1, 2, 3 and PDGFR members (Mellor *et al*., 2011). Alternative multi-kinase inhibitors exist with different PKI specificities, for example dasatinib targets Bcr-Abl, c-kit, PDGF-β and members of the Src family (Mellor *et al.,* 2011). Recent data has shown

that the PKI sunitinib (Sutent), which also targets a range of kinases (VEGF receptors, c-Kit, PDGF receptors and Flt-3) in order to inhibit tumour angiogenesis, can adversely affect cardiac pericytes resulting in cardiac toxicity (Chintalgattu *et al.*, 2013; Nees *et al.*, 2013; Nees *et al.*, 2012).

A potent method of chemotherapy treatment is often a combination of an anthracycline and an ErbB2 inibitor, for example breast cancer patients are often treated with lapatinib and doxorubicin. Seemann *et al* investigated whether this presents further complications with regard to cardiotoxicity. Cardiac irradiation of mice decreased microvascular density and increased endothelial damage in surviving capillaries but these changes were not exacerbated when followed with lapatinib treatment. Lapatinib pre-treatment did not enhance the risk of radiation or anthracycline-induced cardiac toxicity in mice up to 40 weeks after treatment, but endothelial and myocyte mitochondrial damage was more severe with doxorubicin-lapatinib combination therapy (Seemann *et al.*, 2014). One mechanism being explored is the hypothesis that ErbB2 receptors, expressed abundantly in mature cardiomyocytes, offer anti-apoptotic protection against anthracycline toxicity when activated by endothelial released NRG-1, thus inhibition of this interaction facilitates anthracycline toxicity. An alternative hypothesis by Hasinoff *et al*, is the blockade of doxorubicin efflux transporters by lapatinib thus increasing intracellular doxorubicin concentrations and cardiotoxic effects (Hasinoff *et al.*, 2013).

Cancer chemotherapies are not alone in their cardiotoxicity, Refocoxib is a NSAID which was withdrawn in 2004 due to adverse cardiovascular events; it inhibits COX-2 which is responsible for the conversion of arachidonic into prostaglandin E2, a hormone involved in inflammation (Nalbant *et al.*, 2006). Since prostaglandins are thought to have an anti-growth effect on cardiomyocytes, it could be hypothesised that this reduction in the optimisation of cardiomyocyte hypertrophy and rthythmicity is responsible for the adverse cardiovascular events witnessed.

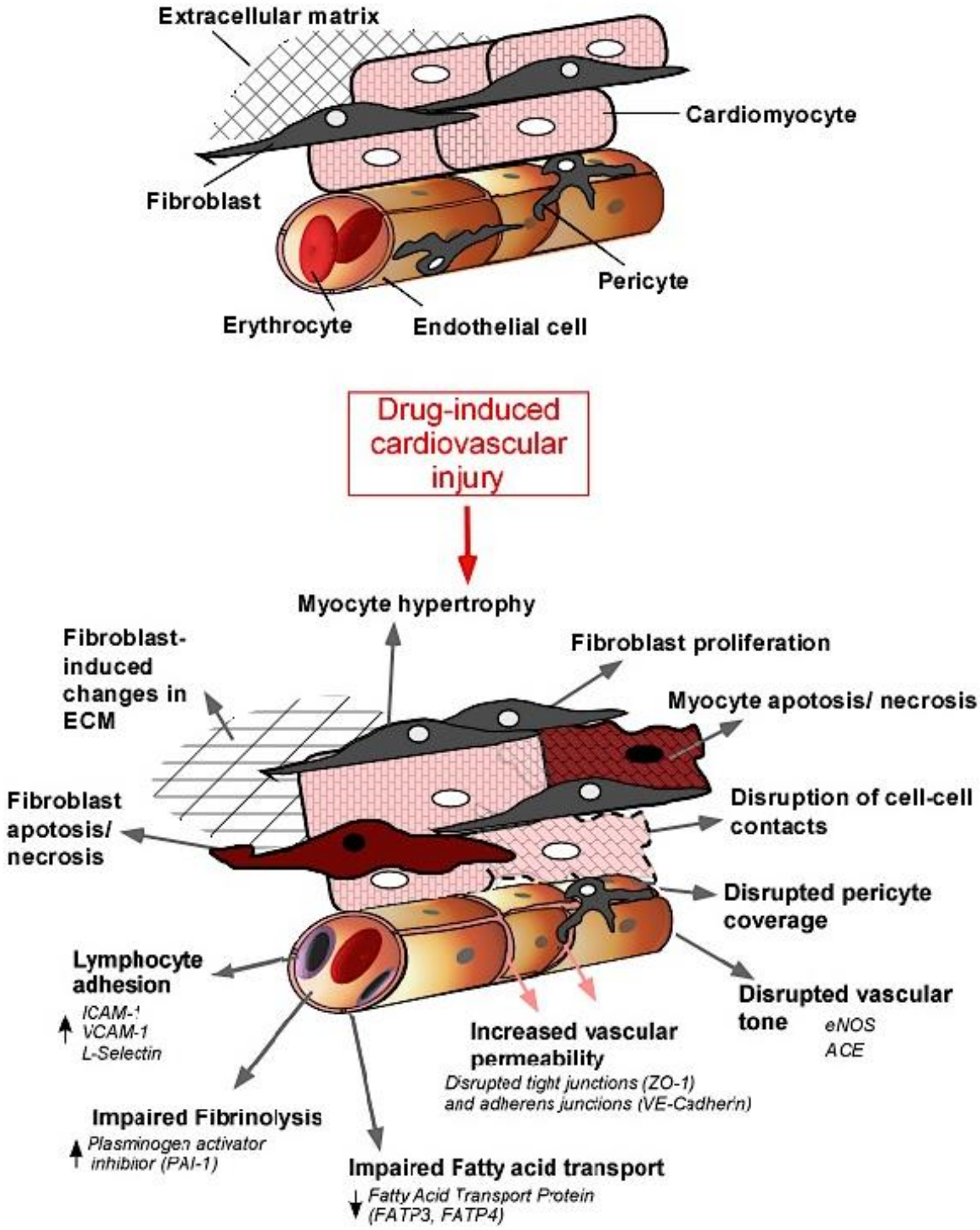

Figure 1.10 Mechanisms of drug-induced structural cardiovascular toxicity.

1.5.2 Drug-induced functional cardiotoxicity

Functional cardiotoxicity is essentially disruption of the contraction strength (left ventricular ejection fraction; LVEF) or rhythm of the heart (arrthymia, QT prolongation), ultimately resulting in heart failure. Functional cardiotoxicity can be secondary to structural cardiotoxicity i.e. damage to the muscle tissue results in weaker myocardial contraction and a reduction in LVEF. Alternatively, functional cardiotoxicity can arise from the direct effects of a drug, for example the antagonistic effect of atenolol at the beta-1 (β1)-adrenergic receptor allows atenolol to reduce hypertension but this can also lead to bradycardia (slow beat rate) and a reduction in LVEF. In this study, drug-induced changes to myocardial contraction force (negative and positive inotropy) will be focused on. An inotrope is defined as an agent that alters the force or energy of muscular contractions. Negatively inotropic agents weaken the force of muscular contractions. Positively inotropic agents increase the strength of muscular contraction. Very little is known regarding the role of non-myocytes in drug-induced functional cardiotoxicity. Recent data has begun to suggest that cardiac fibroblasts have electro-competence; this could potentially be perturbed by functional cardiotoxins (Souders *et al.*, 2009).

1.6 Current *in vitro* models and assays of cardiotoxicity

Cardiovascular toxicity can be structural, involving morphological change or necrosis of cardiomyocytes, reduced myocardial microvascular density and fibrosis, or functional cardiotoxicity whereby the mechanical contractions of the heart are altered in frequency or strength. These toxicities can ultimately lead to a reduction in LVEF, meaning blood is not pumped around the body efficiently and can lead to heart failure. Cardiovascular toxicities are one of the leading causes of drug attrition at the clinical level of drug development suggesting our current pre-clinical models lack human *in vivo* relevance. This section will cover current *in vitro* models and assays utilised to study drug-induced structural and functional cardiovascular toxicity.

1.6.1 Human stem cell-derived cardiomyocytes and their immature phenotypes

Recent *in vitro* assays for structural and functional cardiovascular toxicity are utilising human embryonic and pluripotent stem cell derived cardiomyocytes monolayer models (Goldring *et al.*, 2011; Srivastava & Ivey, 2006; Gepstein, 2002). These cell models lack the mature phenotype of an adult cardiomyocyte (Liu *et al.*, 2007), they are however, considered more *in vivo* relevant than traditional cell line models such as the immortalised rat cardiomyoblast H9c2 cell line. The stem cell models, whether embryonic or induced pluripotent derived, exhibit a spontaneous beat, immunofluorescent staining for cardiac striations and expression of important ion channels/ receptors validated through gene expression and electrophysiology analysis. Classically these cells are seeded as confluent spontaneously beating monolayer models. Human embryonic stem cell derived cardiomyocytes will be utilised during this study.

It has been widely reported that hESC-CMs structurally resemble embryonic or fetal cardiomyocytes (Kehat *et al.*, 2003; Robertson *et al.*, 2013). In a review by Robertson *et al* the various differences between embryonic cardiomyocytes and mature cardiomyocytes are discussed. Adult cardiomyocytes (CM) are large and cylindrical, approximately 150 μm (micrometer) in length, while embryonic and fetal cardiomyocytes are smaller (~30 μm). In addition, most adult CM are bi- or multinucleated, whereas hESC-CMs are mononucleated. The extensive t-tubule network present in adult ventricular CM is absent in hESC-CMs (Kehat *et al.*, 2003; Lieu *et al.*, 2009; Robertson *et al.*, 2013), resulting in slower excitation-contraction coupling and calcium entry primarily through the sarcolemma instead of releasing from the sarcoplasmic reticulum (SR). Experiments with long-term monolayer culture of hESC-CMs has shown a degree of maturity towards adult CM morphology but never development of a T-tubule network or multinucleation (Lieu *et al.*, 2009). Contractile machinery and mitochondria fill two-thirds of the cytoplasmic volume in adult CM, where as in hESC-CMs we see smaller sarcomeric regions and have more moderate numbers of mitochondria. Similarly,

expression of contractile and cytoskeletal genes is much lower compared to fetal (20 weeks) or adult cardiomyocytes (Robertson *et al.*, 2013).

In the adult CM, isoproterenol, a β_1-adrenergic receptor agonist displays positive inotropy (increase in contraction force) and positive chronotropy (increase in contraction rate). With hESC-CMs we see positive chronotropy but no positive inotropy suggesting hESC-CMs have some degree of β_1-adrenergic receptor expression but again highlighting the immaturity of this cell model (Robertson *et al.*, 2013).

In adult CM, calcium induced calcium release (CICR) from the SR contributes almost 70% of the total calcium release. In contrast, immature cardiomyocytes demonstrate calcium transients that are smaller and slower (Robertson *et al.*, 2013), with most cation influx of Ca^{2+} through the cell membrane (Liu *et al.*, 2007). This results in abnormal diffusion of calcium into the cell and reduces the synchrony in contraction necessary for large force generation. There is also consensus that intracellular calcium stores are smaller than in adult CM. Calcium handling and response to compounds that modify calcium handling varies greatly between immature and mature CMs. However, over time in culture increased sarcoplasmic reticulum function is seen, as assessed by caffeine-induced calcium release (caff-ICR) (see section 1.3.3 for details on caffeine effects on cardiomyocyte Ca^{2+} homeostasis).

For a cardiomyocyte to respond with positive inotropy i.e. increase its contraction force, an extensive t-tubule network is thought to be required to ensure that the entire cell depolarizes rapidly and homogeneously. Immature cardiomyocytes rely primarily on calcium entry through the cell across the cell membrane which diffuses though the cytoplasm, a slower process. Some evidence suggests that non-SR calcium stores play a key role in excitation-contraction coupling in immature cardiomyocytes. IP3 receptor (IP3R) is expressed and colocalizes with

sarcomeres, suggesting it may play a role in release of non-SR calcium stores. In adult CM, IP3R appears to regulate non-contractile calcium signalling only, with greater reliance upon ryanodine receptors for calcium induced calcium release (CICR).

Despite these immaturities, the lack of a readily available source of human adult CM for routine drugs testing means these cells along with human induced pluripotent stem cell derived cardiomyocytes (IPS-CMs) have become fundamental to many *in vitro* cardiotoxicity assays.

1.6.2 3D in vitro cell culture models

Various types of 3D cell culture techniques have been developed, some utilising scaffolds, others utilising the innate interactions of cells (Breslin & O'Driscoll, 2013; Hirt *et al.*, 2014), all developed with the aim of reconstituting the *in vivo* cellular morphology and physiology (Maltman & Przyborski, 2010). The most traditional scaffold-free 3D cell culture technique is the hanging drop method, whereby cells are suspended in a droplet of cell culture media where they aggregate to form a 'ball' of cells. More recently this technique has been replaced with the use of ultra low adhesion round bottomed plates whereby the cells sink to the well bottom and aggregate into a spheroid. The use of scaffolds to 'manually' manipulate a cell into a more *in vivo* like shape are popular since this maintains a 2D platform that allows visualisation of the cells for image-based cytotoxicity assays (see section 1.7.3), which becomes technically challenging with spheroid models. One example are NanoFiber™ plates; a nanofiber matrix of approximately 700 nm (nanometer) diameter electrospun polycaprolactone (PCL) which creates an artificial tissue matrix for cells to adhere to. Although 3D cell culture techniques have existed for some time, it is only since the recent development of stem cell derived cardiomyocytes that efforts have been directed towards utilizing these techniques to potentially increase model maturity for cytotoxicity screening.

1.6.3 In vitro structural cardiotoxicity assays

Until recently structural cardiotoxicity detection *in vitro* went largely untested in preclinical studies. In 2013 Pointon *et al* developed an approach whereby structural cardiotoxicity could be predicted in multiple cardiomyocyte cell models by staining cells with fluorescent dyes towards mitochondria, Ca^{2+} mobilisation, endoplasmic reticulum integrity and membrane permeability (Pointon *et al.*, 2013). This is a method whereby fluorescently labelled cells are utilised as the basic unit of molecular discovery is known as high-content biology (HCB).

Healthy active mitochondria have a relative negative charge. Upon damage or inactivity, depolarisation occurs and this negative charge is reduced. Tetramethylrhodamine ethyl ester (TMRE) is a cell permeant, positively charged, red-orange fluorescent dye which is readily sequestered by active, negatively charged mitochondria (Life Technologies™ (Paisley, U.K.)). A change in mitochondrial membrane potential can therefore be detected by staining cells with TMRE and fluorescently imaging with an orange-red excitation filter.

Structural changes to the endoplasmic reticulum, in particular a loss of ER density, can be detected using cell permeant, live cell dyes highly selective for the ER. ER dyes are available at the DAPI, FITC and TRITC wavelengths to allow multiplexing of dyes. Various dyes exist to allow the detection of Ca^{2+} mobilisation; the most commonly used for cell-based high-throughput drug discovery are the Fluo-calcium indicators. Fluo-3 was developed by Tsien (Tsien *et al*., 1988) and colleagues and has been utilised in drug discovery since about 1996. It is essentially non-fluorescent unless bound to Ca^{2+} and exhibits at least a 100-fold Ca^{2+}-dependent fluorescence enhancement (Life Technologies™ (Paisley, U.K.)). Fluo-3 & 4, a new derivative of 3, are essentially identical except Fluo-4 exhibits stronger fluorescence at the FITC (488 nm) wavelength. For this reason Fluo-4 AM was selected to monitor Ca^{2+} changes.

The endpoint of toxicity is generally cell death (necrosis); this is detected by staining cells with a cell membrane impermeable, dimeric cyanine nucleic acid dye which exhibits 100-1000 fold DNA-dependent fluorescence enhancement (Life Technologies™ (Paisley, U.K.)). The fluorescence spectra of the 10 available dimeric cyanine dyes covers the entire visible wavelength range. Given TMRE and Fluo-4 AM are only available as dyes detectable at the red-orange (~555 nm; TRITC) and green (488 nm; FITC) wavelengths, respectively, the blue-white ER Tracker dye will be used (~350 nm; DAPI) and a far red (633 nm;Cy5) nuclei acid dye, TOTO-3, will be multiplexed. With each dye emitting fluorescence at a different wavelength, MMP, ER integrity, Ca^{2+} mobilization and cell death can be simultaneously monitored as shown in figure 4.2. This HCB approach was combined with a cytotoxicity assay to measure intracellular adenosine triphosphate (ATP) content (Promega., Southhampton, U.K.). Figure 1.11 summarises the parameters measured by HCB and ATP assessment. By combining the two assay types Pointon *et al* were able to increase the predictive strength of the overall assay (Pointon *et al*., 2013).

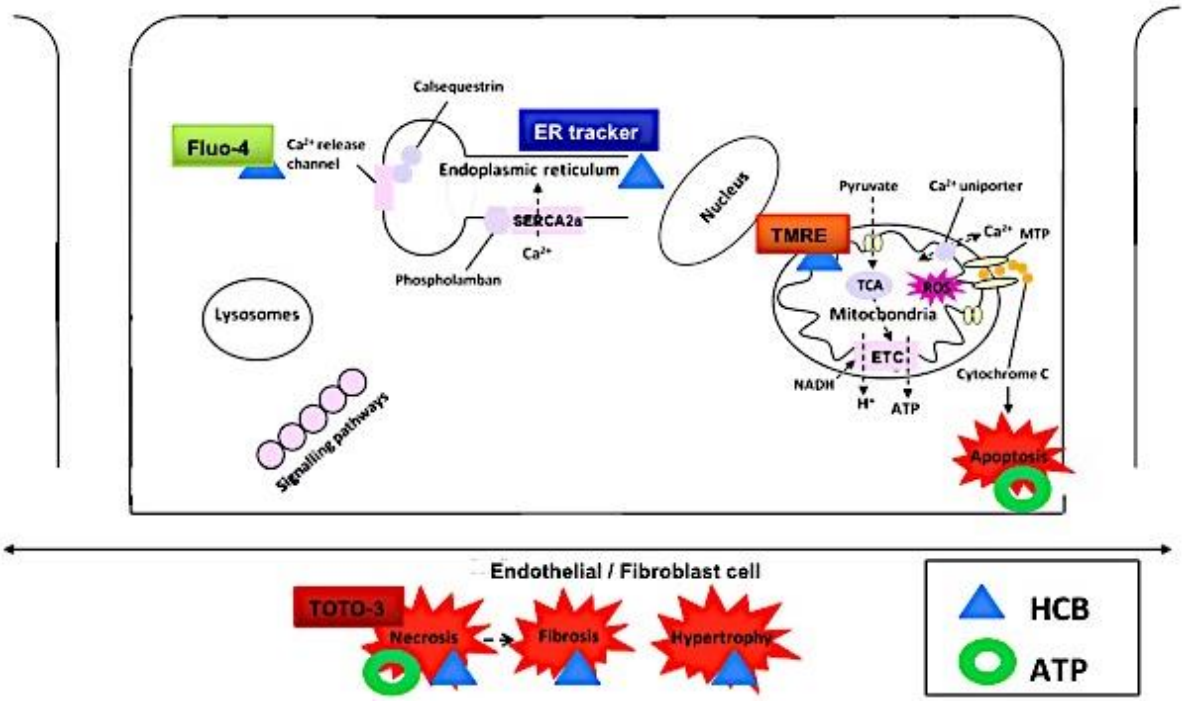

Figure 1.11 High content biology approaches to simultaneously monitor MMP, ER integrity, Ca^{2+} mobilisation and cell death in endothelial & fibroblast cells.

Tetramethylrhodamine ethyl ester (TMRE) (30 pM) to measure mitochondrial membrane potential (MMP), ER-Tracker™ blue-white (1 nM) to measure ER integrity, Fluo-4 AM (1 nM) to measure calcium mobilization and TOTO®-3 (1 nM) to indicate necrosis of cells. CellTiter-Glo reagent to measure intracellular ATP content to indicate apoptosis/ necrosis. Stained cells were subjected to automated live-cell fluorescent image acquisition using an ImageXpress high content analysis system (Molecular Devices, 20x objective). Fluorescent images were captured according to the optimal excitation and emission wavelengths of each probe. ATP luminescence was recorded using a Wallac 1450 Microbeta Trilux Scintillation Counter (PerkinElmer Life Sciences, Fremont, CA, U.S.A.).

1.6.4 In vitro functional cardiotoxicity assays

Current functional cardiotoxicity assays involve classical electrophysiology techniques such as patch clamping whereby an individual cardiomyocyte is either impaled or suctioned onto a microelectrode and ion currents throughout the membrane of a cell are measured. Ion channels perform many essential roles and specifically regulate electrical activity in excitable cells such as muscles and neurons (Harmer *et al.*, 2008). Alternatively, changes in the contractility parameters of isolated cardiomyocytes can be monitored by utilizing the IonOptix cell geometry system which utilises video-based detection of sarcomere shortening (Harmer *et al.*, 2012). In this technique optical intensity data is collected representing dark and light bands present within the sarcomere, the movement of these bands translates into transients of peaks and troughs. These contractility transients are analysed using IonWizard software to provide quantification of contractility (contraction displacement measurements). These animal models however, are relatively poor predictors of human responses.

With the development of human stem cell derived cardiomyocyte monolayer models (described in *section 1.6.1*) a new era of multi-electrode array (MEA) technology has arrived. MEAs are plate based assays whereby a monolayer of cells are seeded on to an electrode array printed to the well bottom. MEA recordings allow the simultaneous electrophysiological measuring of beat rate, field potential duration, amplitude and conduction velocity. Unlike the traditional patch-clamp assays which look at one ion channel at a time, MEA assesses changes in all major ion channels implicated in an action potential. Human stem cell derived cardiomyocyte monolayer models are also being utilized in calcium fluorescence based electrophysiology assays. The FLIPR system developed by Molecular Devices is one such system. Monolayer cells are pre-incubated with an intracellular calcium indicator dye, as the cells spontaneously beat and their intracellular Ca^{2+} levels flux, these peaks and troughs in fluorescence intensity are recorded. This system allows changes in contraction force i.e. peak

amplitude and frequency to be quantified. Despite these assays advancing to multi-parameter, higher throughput levels, their predictive strengths are often limited by the models applied to them. The non-human models are poor at predicting human-specific toxicities and the human stem cell derived cardiomyocyte monolayer models lack the mature complexity of myocardial tissue.

1.7 Aims

The high prevalence of drug-induced cardiovascular events at the pre-clinical and clinical stages of drug development suggests our current models of cardiovascular toxicity are lacking human *in vivo* relevance. Current *in vitro* models focus mainly on the cardiomyocytes of the myocardium, however data is mounting suggesting important roles for the non-cardiomyocytes in maintaining normal heart function.

The aim of this study is to firstly determine the cardiotoxin sensitivities of cardiac microvascular endothelial and cardiac fibroblast cells relative to cardiomyocytes in order to highlight potential roles for non-myocytes in drug-induced cardiovascular toxicity. Dermal endothelial and fibroblast cells will be used alongside coronary artery endothelial cells in order to elucidate any myocardial specific cardiotoxic sensitivities. A high content biology assay, which uses fluorescently labelled cells as the basic unit of molecular discovery, will be combined with a measure of cytotoxicity. This assay principle has previously been successful in the detection of structural cardiotoxicity in human ESC cardiomyocytes (Pointon *et al.*, 2013)

The ultimate aim of this work is to develop a human relevant *in vitro* model, which better reconstitutes the *in vivo* cellular physiology of the heart. Multiple types of cardiac microtissue models will be developed and their responses to reference inotropes evaluated using video-based edge monitoring of contractility. The microtissues will be further assessed for calcium handling and gene expression maturity. More advanced human relevant *in vitro* models will mean improved *in vitro* to *in vivo* correlation in future drug safety screens.

Chapter three will discuss the development of *in vitro* cell based models to study cardiovascular toxicity, *chapter four* will evaluate the sensitivities of non-myocytes to structural cardiotoxins using high content biology and cytotoxicity while *chapter five* will discuss contractile maturity in multicellular cardiac microtissues.

Chapter Two

Materials & Methods

2.1 Materials

2.1.1 Reagents

5-Tetramethylrhodamine (TMRE); endoplasmic reticulum (ER)-Tracker™ Blue-White DPX; Fluo-4 AM; TOTO®-3 Iodide; MitoTracker® Deep Red FM; Hoescht 33342; DiI-AcLDL (Human Plasma Acetylated LDL, DiI complex (1,1′-dioctadecyl-3,3,3′,3′-tetramethyl-indocarbocyanine perchlorate)) and Alexa Fluor® 568 phalloidin were purchased from Molecular Probes (Life Technologies™ (Paisley, U.K.). CellTiter-Glo® Luminescent Cell Viability Assay Kit was purchased from Promega (Madison, WI). Lactate dehydrogenase (LDH) cytotoxicity detection kit was purchased from Roche Applied Science (Welwyn Garden City, U.K.). Triton X-100; dimethyl sulfoxide (DMSO), 37% Formaldehyde and Tris buffered saline (10x, pH 8.0) were purchased from Sigma-Aldrich (Poole, U.K.). RNeasy mini RNA (RiboNucleic Acid) extraction kit was bought from Qiagen (Crawley, U.K.). Lipofectamine™ RNAiMAX transfection reagent was purchased from Life Technologies™ (Paisley, U.K.).

Water

Distilled, deionised water (ddH2O) was passed through a 0.22 µm filter and treated with ultra violet (UV) light in a Millipore Synergy 185 unit (Millipore Ltd., Watford, U.K.) prior to use in the preparation of buffers and solutions.

2.1.2 Cell types

Table 2.1 Cell types

Name	Cell Type	Source
hCMECs	Human cardiac microvascular endothelial cells (Lot-No. 9090701.2 and 1122702)	PromoCell (Heidelberg, Germany)
hCAECs	Human coronary artery endothelial cells (Lot-No. 1111804.1 and 113008.7)	PromoCell (Heidelberg, Germany)
hDMECs	Human dermal microvascular endothelial cells (Lot-No. 0092101.2)	PromoCell (Heidelberg, Germany)
hCFs	Human cardiac fibroblasts (Lot-No. 1062201.5)	PromoCell (Heidelberg, Germany)
NhDFs	Normal human dermal fibroblasts (Lot-No. 2061206.2)	PromoCell (Heidelberg, Germany)
hESC-CMs	Cytiva human embryonic stem cell cardiomyocytes (Lot-No. 7396634)	GE Healthcare Life Sciences (Buckinghamshire, U.K.)

2.1.3 Cell culture media & solutions

Table 2.2 Cell culture media

Name	Composition	Source
Endo FGM	Endothelial MV2 basal medium supplemented with 5% (v/v) foetal calf serum (FCS), EGF (5.0 ng/ ml), hydrocortisone (0.2 µg/ ml), VEGF (0.5 ng/ ml), FGF-2 (10.0 ng/ ml), insulin-like growth factor-1 (20.0 ng/ ml) and ascorbic acid (1.0 µg/ ml), (Cat. No.: C-22121).	PromoCell (Heidelberg, Germany).
Endo SFM	Endothelial MV2 basal medium supplemented with EGF (5.0 ng/ ml), hydrocortisone (0.2 µg/ ml), VEGF (0.5 ng/ ml), FGF-2 (10.0 ng/ ml), insulin-like growth factor-1 (20.0 ng/ ml) and ascorbic acid (1.0 µg/ ml) (Cat. No.: C-22121).	PromoCell (Heidelberg, Germany).
Endo LSM	Endothelial MV2 basal medium supplemented with 1% (v/v) foetal calf serum (FCS).	PromoCell (Heidelberg, Germany).
Endo -GF	Endothelial MV2 basal medium supplemented with 5% (v/v) foetal calf serum (FCS).	PromoCell (Heidelberg, Germany).
F2 media	Fibroblast growth medium 2 supplemented with 2% (v/v) foetal calf serum (FCS), basic FGF (1.0 ng/ ml) and human recombinant insulin (5 µg/ ml), (Cat. No.: C-23120).	PromoCell (Heidelberg, Germany).
F3 media	Fibroblast growth medium 3 supplemented with 10% (v/v) foetal calf serum (FCS), basic FGF (1.0 ng/ ml) and human recombinant insulin (5 µg/ ml), (Cat. No.: C-23130).	PromoCell (Heidelberg, Germany).
CM media	RPMI 1640 + glutamax (Cat. No.: 61870044) supplemented with B27 supplement (Cat. No.: 17504-044).	Life Technologies™ (Paisley, U.K.)
5050 Microtissue media	50% CM media mixed with 50% Endo FGM	In-house

Table 2.3 Cell culture solutions

Solution	Composition	Source
1x ACCUTASE enzymes in Dulbecco's PBS	KCl (0.2 g/L), KH2PO4 (0.2 g/L), NaCL (8 g/L) and Na_2HPO_4 (1.15 g/L) containing 0.5 mM EDTA·4Na and Phenol Red (3 mg/L).	Sigma-Aldrich (Poole, U.K.).
0.1% (w/v) gelatin solution	0.1% (w/v) gelatin from porcine skin, (type A, cell culture tested) in ddH_2O, autoclaved and filter sterilised.	Sigma-Aldrich (Poole, U.K.).
Dulbecco's phosphate-buffered saline (without Ca^{2+}/Mg^{2+})	KCl (200 mg/l), KH_2PO_4 (200 mg/l), NaCl (8,000 mg/l), $Na_2HPO_4•7H_2O$ (2,160 mg/l).	Lonza (Basel, Switzerland).

2.1.4 Cell culture materials

Polystyrene, filter cap cell culture flasks with growth areas of 25 cm², 75 cm² and 175 cm², 6-, 12-, 24- and 96-well cell-culture plates, black-walled clear bottomed 96-well cell culture plates, centrifuge tubes, cryovials, filter pipette tips and serological pipettes were bought from Greiner Bio-One (Stonehouse, U.K.). Corning® Costar® round bottomed ultra-low adhesion plates (CLS7007) from Sigma-Aldrich (Poole, U.K.). Nunc™ Thermanox Coverslips, 13 mm diameter from Thermo Fisher Scientific (Loughborough, U.K.).

2.1.5 Compounds

Table 2.4 Compounds

Compound	Known targets	Total C_{max} / μM	Source	Catalogue no.
Imatinib Mesylate	Inhibitor of the Bcr-Abl, PDGF & c-kit receptors.	3.54	AZ in house supply	AZ10049442
Sunitinib malate	Inhibitor of PDGFRa, PDGFRb, VEGFR1, VEGFR2, VEGFR3, KIT, FLT3, CSF-1R, and RET.	0.25	AZ in house supply	AZ11755299
Sorafenib tosylate	Inhibitor of KIT, FLT-3, VEGFR-2, VEGFR-3, and PDGFR-ß.	16.57	AZ in house supply	AZ10406510
Dasatinib	Inhibitor of BCR-ABL, SRC family (SRC, LCK, YES, FYN), c-KIT, EPHA2, and PDGFRβ.	0.0072	AZ in house supply	AZ12384652
Lapatinib	Inhibitor of HER1/EGFR/ERBB1 and HER2/ERBB2	4.18	AZ in house supply	AZ10402704
Doxorubicin HCl	Intercalation of DNA, inhibits topoisomerase II activity	15.34	Sigma-Aldrich (Poole, U.K.).	D1515
Idarubicin HCl	Intercalation of DNA, inhibits topoisomerase II activity	0.12	Sigma-Aldrich (Poole, U.K.).	I1656
Fluorouracil HCl	Pyrimidine analogue. Irreversible inhibition of thymidylate synthase.	4.61	AZ in house supply	AZ10090045
Amoxacillin	β-lactam antibiotic	0.87	AZ in house supply	AZ12192757
Sildenafil	PDE-5 inhibitor	0.24	AZ in house supply	AZ11779205

Enalapril	Angiotensin-converting enzyme inhibitor	0.83	AZ in house supply	AZ10215522
Tolbutamide	ATP-sensitive potassium channel inhibitor	203	AZ in house supply	AZ10013036
Paracetamol	Cyclooxygenase inhibitor	33.08	AZ in house supply	AZ10009025
Verapamil	L-type Ca^{2+} channel blocker	0.6	AZ in house supply	AZ10049213
Flecainide	Cardiac Na+ channel block	0.36	AZ in house supply	AZ10591336
Haloperidol	Dopamine D_2-receptor antagonist	0.024	AZ in house supply	AZ10047978
Ivabradine	Inhibits pacemaker I_f current	0.04	AZ in house supply	AZ13525484
Phentolamine	Non-selective α adrenergic receptor antagonist	0.0097	AZ in house supply	AZ10039017
Nifedipine	L-type Ca^{2+} channel blocker	0.39	AZ in house supply	AZ10027237
Bepridil	L-type Ca^{2+} channel blocker	1.9	AZ in house supply	AZ10134609
Atenolol	β_1 receptor antagonist	0.0023	AZ in house supply	AZ10000568
Diltiazem	L-type Ca^{2+} channel blocker	0.38	AZ in house supply	AZ10180667

Milrinone	PDE-3 inhibitor	1.43	AZ in house supply	AZ10064577
Glibenclamide	ATP-sensitive potassium channel inhibitor	0.73	AZ in house supply	AZ10102123
Dobutamine	β_1-adrenergic agonist	0.44	AZ in house supply	AZ10471493
Digoxin	Inhibits Na+ / K+ ATPase membrane pump	0.0032	AZ in house supply	AZ12127481
Levosimenden	Calcium sensitiser (binds to cardiac troponin C)	0.22	AZ in house supply	AZ13401595
Isoproterenol	β -adrenergic receptor agonist	0.0071	AZ in house supply	AZ10064045
Epinephrine	Non-selective adrenergic receptor agonist	0.17	AZ in house supply	AZ12136154

Total plasma C_{max} (bound and unbound drug) values taken from FDA approval packages accessed through *Pharmapendium*.

2.1.6 Antibodies and fluorescent dyes

Table 2.5 Fluorescent dyes

Stain	Target	Wavelength	D.F	Source	Catalogue no.
TMRE	Mitochondrial Membrane Potential	TRITC	1:2000	Life Technologies™ (Paisley, U.K.)	T-668
ER-Tracker™ Blue-White DPX	Endoplasmic Reticulum integrity	DAPi	1:1000	Life Technologies™ (Paisley, U.K.)	E12353
Fluo-4 AM	Ca^{2+} mobilization	FITC	1:650	Life Technologies™ (Paisley, U.K.)	F36205
TOTO®-3 Iodide	Dead cell indicator	Cy5	1:1000	Life Technologies™ (Paisley, U.K.)	T3604
DiI-AcLDL	ac-Low Density Lipoprotein uptake	TRITC	1:1000	Life Technologies™ (Paisley, U.K.)	L3484
Alexa Fluor® 568 phalloidin	F-actin	Texas Red	1:500	Life Technologies™ (Paisley, U.K.)	A12380
Hoescht 33342	Nuclei	DAPi	1:5000	Life Technologies™ (Paisley, U.K.)	H3470

Table 2.6 Primary Antibodies

Host	Target	Dilution factor	Supplier	Catalogue no.
Mouse	Alpha sarcomeric actinin (ActN2)	1:500	Thermo Scientific™ Pierce™	MA1 22863
Sheep	CD31	1:500	R&D systems	AF806
Rabbit	Collagen I	1:500	Abcam	Ab34710
Rabbit	Cardiac troponin I (cTNI)	1:200	Abcam	Ab47003
Goat	Discoidin domain receptor 2 (DDR2)	1:200	Santa Cruz Biotechnology	SC-7555

Table 2.7 Secondary Antibodies

Host	Target	Dilution factor	Wavelength	Supplier	Catalogue no.
Donkey	Sheep	1:1000	Alexa Fluor 488	Life Technologies™ (Paisley, U.K.)	A11015
Donkey	Rabbit	1:1000	Alexa Fluor 568	Life Technologies™ (Paisley, U.K.)	A10042
Donkey	Mouse	1:1000	Alexa Fluor 680	Life Technologies™ (Paisley, U.K.)	A10038
Donkey	Goat	1:1000	Alexa Fluor 488	Life Technologies™ (Paisley, U.K.)	A11055

2.1.7 RT-PCR probes

Table 2.8 TaqMan® Probes

Gene	TaqMan® gene expression assay probe	Catalogue no.	Source
ADRB1	Hs02330048_s1	Cat. # 4331182	Life Technologies™ (Paisley, U.K.)
ATP2A1	Hs01092295_m1	Cat. # 4331182	Life Technologies™ (Paisley, U.K.)
ATP2A2	Hs00544877_m1	Cat. # 4331182	Life Technologies™ (Paisley, U.K.)
ATP5B	Hs00969569_m1	Cat. # 4331182	Life Technologies™ (Paisley, U.K.)
CACNA1C	Hs00167681_m1	Cat. # 4331182	Life Technologies™ (Paisley, U.K.)
CACNA1H	Hs00234934_m1	Cat. # 4331182	Life Technologies™ (Paisley, U.K.)
GAPDH	Hs02758991_g1	Cat. # 4331182	Life Technologies™ (Paisley, U.K.)
GJA1	Hs00748445_s1	Cat. # 4331182	Life Technologies™ (Paisley, U.K.)
IRX4	Hs00212560_m1	Cat. # 4331182	Life Technologies™ (Paisley, U.K.)
KCND3	Hs00542597_m1	Cat. # 4331182	Life Technologies™ (Paisley, U.K.)
KCNH2	Hs04234270_g1	Cat. # 4331182	Life Technologies™ (Paisley, U.K.)
KCNJ2	Hs01876357_s1	Cat. # 4331182	Life Technologies™ (Paisley, U.K.)
KCNQ1	Hs00923522_m1	Cat. # 4331182	Life Technologies™ (Paisley, U.K.)
MYH6	Hs01101425_m1	Cat. # 4331182	Life Technologies™ (Paisley, U.K.)

MYH7	Hs01110632_m1	Cat. # 4331182	Life Technologies™ (Paisley, U.K.)
NKX2.5	Hs00231763_m1	Cat. # 4331182	Life Technologies™ (Paisley, U.K.)
NOS3	Hs01574659_m1	Cat. # 4331182	Life Technologies™ (Paisley, U.K.)
PDE3A	Hs01012698_m1	Cat. # 4331182	Life Technologies™ (Paisley, U.K.)
PECAM1	Hs00169777_m1	Cat. # 4331182	Life Technologies™ (Paisley, U.K.)
RYR2	Hs00892883_m1	Cat. # 4331182	Life Technologies™ (Paisley, U.K.)
S100A1	Hs00984741_m1	Cat. # 4331182	Life Technologies™ (Paisley, U.K.)
SCN5A	Hs00165693_m1	Cat. # 4331182	Life Technologies™ (Paisley, U.K.)
TCAP	Hs00985784_g1	Cat. # 4331182	Life Technologies™ (Paisley, U.K.)
THY1	Hs00264235_s1	Cat. # 4331182	Life Technologies™ (Paisley, U.K.)
TNNC1	Hs00896999_g1	Cat. # 4331182	Life Technologies™ (Paisley, U.K.)
TNNI3	Hs00165957_m1	Cat. # 4331182	Life Technologies™ (Paisley, U.K.)

2.2 Methods

2.2.1 Manipulation of mammalian cells

2.2.1.1 Cell culture techniques

Sterile conditions were maintained at all times during culturing and manipulation of mammalian cells by wearing nitrile examination gloves, using sterile cell culture equipment and working in a BioMAT^2 Class II Microbiological Safety Cabinet (Medical Air Technology, Oldham, U.K.). Culture medium was warmed to 37 degrees celcius (°C) in a water bath prior to use. All work surfaces were disinfected by wiping with 70% (v/v) ethanol before and after cell culture work.

2.2.1.2 Gelatin-coating of cell culture plates and dishes

Primary cells were routinely cultured in sterile polystyrene, filter cap cell culture flasks. Flasks were coated with 10 ml of autoclaved and sterile-filtered gelatin solution (0.1% (w/v) in ddH2O) per 75 cm^2 growth area, and incubated at 37 °C in a humidified, 5% (v/v) carbon dioxide (CO_2), atmosphere in a Heraeus® HERAcell® CO_2 Incubators (Thermo Scientific, Hampshire, U.K.) for 15 minutes (min) prior to use. Gelatin was aspirated from the flasks prior to the seeding of cells.

2.2.1.3 Thawing of cryopreserved cell stocks

Cryopreserved cells stored at -135 °C were thawed in a 37 °C water bath for 2-3 min with gentle agitation. The exterior of each cryovial was carefully disinfected with 70% (v/v) ethanol prior to pipetting the contents of the vial into a falcon tube containing 8 ml of pre-warmed growth medium. One millilitre (ml) of growth media was used to wash the cryovial before also being added to the falcon tube. The cell suspension was centrifuged at 1200 revolutions per minute (rpm) for 2 mins and the cells re-suspended in 16 ml of growth media which was

subsequently transferred into two T25 cell culture flasks. The flasks were then incubated at 37 °C, 5% CO_2.

2.2.1.4 Passaging of primary cells and routine cell culture

Following incubation at 37 °C, 5% CO_2, for 3-5 days in the appropriate cell growth culture medium, to expand cell numbers, cells were briefly washed with 10 ml of Dulbecco's-Phosphate Buffered Saline (D-PBS) (without Ca^{2+}/Mg^{2+}) per 75 cm^2 growth area. D-PBS was then aspirated, and 10 ml of 1x accutase enzymes in Dulbecco's PBS per 75 cm^2 was added. Flasks were returned to the incubator for 5 min and tapped gently to aid cell detachment. When 95-100% of the cells had detached, as judged by viewing under an inverted light microscope, the cell suspension was transferred to a falcon tube and centrifuged at 1200 rpm for 3 min. The supernatant was aspirated and the cells re-suspended in the appropriate cell culture medium and split as described in Table 2.9.

Table 2.9 Summary of cell usage

Cell Type	Cell culture medium used for routine culture	Cell splits	*Passages* used	Seeding density in 96 well plate (cells $well^{-1}$)
hCMECs	Endo FGM	1:4, every 4-5 days	*p2-p9*	6,000
hCAECs	Endo FGM	1:5, every 4-5 days	*p2-p9*	6,000
hDMECs	Endo FGM	1:4, every 4-5 days	*p2-p9*	8,000
hCFs	F3 media	1:4, every 4-5 days	*p2-p15*	6,000
NhDFs	F2 media	1:6, every 4-5 days	*p2-p15*	3,000

2.2.1.5 Thawing of hESC-CMs

Cytiva 1E5 hESC-CMs were purchased cryopreserved and stored at -135°C until use. Each vial was thawed in a 37 °C water bath for 2-3 min with gentle agitation. The exterior of each cryovial was carefully disinfected with 70% (v/v) ethanol prior to pipetting the contents of the vial into a falcon tube. One millilitre of CM media was used to wash the cryovial before also being added to the falcon tube. Eight millilitres of CM media was slowly added to the cells over 2-3 mins. The cell suspension was centrifuged at 400 rpm for 4 mins and the cells re-suspended in CM media. Fifty microlitres of the cell suspension was then pipetted onto a Fast-Read 102® (0.0025 mm^2 and 0.100 mm depth) haemocytometer (Immune Systems Ltd, Paignton U.K.) for counting. The cell suspension was diluted to the appropriate cell density ml^{-1} and used in the downstream experiment.

2.2.1.6 Cell plating for experiments

Prior to use in experiments, cells growing in a cell culture flask were detached by briefly washing with 10 ml of D-PBS (without Ca^{2+}/Mg^{2+}) per 75 cm^2 growth area. D-PBS was then aspirated, and 10 ml of 1x accutase enzymes in D-PBS per 75 cm^2 was added. Flasks were returned to the incubator for 5 min and tapped gently to aid cell detachment. When 95-100% of the cells had detached, as judged by viewing under an inverted light microscope, the cell suspension was transferred to a falcon tube and centrifuged at 1200 rpm for 3 min. The supernatant was aspirated and the cells re-suspended in the appropriate volume of cell culture medium. Fifty microlitres of the cell suspension was then pipetted onto a Fast-Read 102® (0.0025 mm^2 and 0.100 mm depth) haemocytometer (Immune Systems Ltd, Paignton U.K.) for counting. The cell suspension was diluted to the appropriate cell density ml^{-1} for the required seeding density (Table 2.9) using cell culture medium and 95 µL pipetted into each well of a black-walled, 96 well plate. Plates were incubated for 4 days with media replaced every 48 h.

2.2.1.7 Freezing of cell stocks

Cells were purchased cryopreserved at passage 2 (*p*2). Following their initial thawing, cells were passaged twice and prepared for freezing at *p*4, by detachment and re-suspension of confluent T25 cell culture flasks. Re-suspension followed a ratio of one T25: 1 ml of cell freezing medium (90% (v/v) cell culture medium and 10% (v/v) DMSO). Resultant cell suspensions were aliquotted into sterile cryovials and stored overnight at -80 ^{o}C before being transferred to the -135 °C freezer for long-term storage.

2.2.1.8 Preparation of cardiac microtissues

All primary cells were sub-cultured prior to microtissue formation, see section 2.2.1.4. All primary cells were detached and counted according to section 2.2.1.6. Cell suspensions were diluted and stored at 37^{o}C, 5% CO_2 for up to one hour while hESC-CM cell suspensions were prepared. A vial of Cytiva cardiomyocytes was thawed and suspended in CM media according to section 2.2.1.5. Cell suspensions were mixed together at desired ratio, see table 2.10 for details on ratios, total cell numbers and cell media used. 100 µl of cell suspension was subsequently seeded into round bottom ultra- low adhesion 96-well plates (Corning® Costar®, CLS7007). Plates were incubated at 37^{o}C, 5% CO_2. At day 4 100 µl of appropriate cell culture media (see table 2.10) was added to each well. Microtissues were incubated for a further 10 days with 100 µl media refreshed every 3-4 days.

Table 2.10 Summary of microtissue combinations, ratios and media types

Microtissue type	Cell types used	Total cells well^{-1}	Cell ratio (CM:Fibro:Endo)	Cell culture media
CM	hESC-CMs	1000	-	CM
CMEF	hESC-CMs hCFs hCMECs	500	4:2:1	5050 microtissue
DMEF	hESC-CMs NhDFs hDMECs	500	4:2:1	5050 microtissue
CME	hESC-CMs hCMECs	500	2:1	5050 microtissue
CMF	hESC-CMs hCFs	500	2:1	5050 microtissue

2.2.2 Fluorescent imaging techniques

2.2.2.1 DiI-ac-LDL uptake

Cells in a black-walled, 96 well plate were stained with DiI-acLDL and Hoescht 33342 in Endothelial basal media (EBM) MV2 growth medium for 4 h at dilutions shown in Table 2.5. Following staining, media was replaced with 100 µL D-PBS (without Ca^{2+}/Mg^{2+}) and the cells subjected to automated live-cell fluorescent image acquisition using an ImageXpress high content analysis system (Molecular Devices, 20x objective). Fluorescent images were captured according to the optimal excitation and emission wavelengths of each probe (Table 2.5).

2.2.2.2 Fixation and labeling of F-actin

Immediately after the DiI-AcLDL imaging assay was performed, the imaging medium was replaced with fixing solution; 3.7 % (v/v) paraformaldehyde (PFA) and 0.1% (v/v) Triton X-100 (polyethyrene glycol mono-*p*-iso-octylphenyl ether) in D-PBS (without Ca^{2+}/Mg^{2+}) (pH 7.4), the cells were then incubated at 37 ^{o}C, 5% CO_2 for 20 mins. Paraformaldehyde fixes the cells by forming crosslinks between proteins. These crosslinks are methylene bridges formed between nitrogen

containing side chains of basic amino acids. Following fixation, the cells were washed twice in D-PBS (without Ca^{2+}/Mg^{2+}) and blocking solution was added (0.2 % (v/v) Triton X-100 and 1.1 % (w/v) bovine serum albumin (BSA) in Tris buffered saline (TRIS) (10x)) for 30 mins at room temperature. Following this incubation period, the blocking solution was removed and 50 µL/ well of Alexa Fluor® 568 phalloidin in D-PBS (without Ca^{2+}/Mg^{2+}) at a 1:500 dilution was added and the cells incubated in the dark for 1h at room temperature. The cells were washed once with D-PBS (without Ca^{2+}/Mg^{2+}) and 50 µL/ well of Hoescht 33342 in D-PBS (without Ca^{2+}/Mg^{2+}) at a dilution of 1:12500 was added and the cells incubated in the dark for 20 mins at room temperature. Following incubation, the cells were washed twice with D-PBS (without Ca^{2+}/Mg^{2+}) and a final volume of 100 µL added. The cells were subjected to automated live-cell fluorescent image acquisition using an ImageXpress high content analysis system (Molecular Devices, Sunnyvale, CA, U.S.A., 20x objective) or stored in the dark at 4 ^{o}C until needed. Fluorescent images were captured according to the optimal excitation and emission wavelengths of each probe (Table 2.5).

2.2.2.3. Monolayer Immunofluorescence

Monolayer cell media was replaced with 4% (v/v) formaldehyde in D-PBS and cells incubated at 37^{o}C, 5% CO_2 for 20 mins. Cells were washed in D-PBS three times. They can now be stored at 4^{o}C. Cells were permeabilised with 0.2% (v/v) triton X-100/ PBS at room temperature for 10 mins and then blocked in 1.1% (w/v) BSA /TBST block (with 0.2% (v/v) Triton X-100) for 30 mins at room temperature. Primary antibody was diluted as required in 1.1% (w/v) BSA /TBST (with 0.2% (v/v) Triton X-100), block reagent was removed and primary antibody added for 2 h at room temperature. Cells were washed in D-PBS and secondary antibody applied at desired concentration in 1.1% (w/v) BSA/TBST (with 0.1% (v/v) Triton X-100) for 1 hour at room temperature. Finally cells were stained with Hoescht 33342 in D-PBS (with 0.1% (v/v) Triton X-100) (1:5000 dilution) for 10 mins at room temperature. Cells were washed and imaged in D-PBS.

2.2.2.4 Microtissue immunofluorescence

Microtissues are washed in D-PBS until no remaining media can be seen. Microtissues are fixed in 4% (v/v) formaldehyde for 1 hour at 4^{o}C, following which they are washed 6 times in PBS. They can now be stored at 4^{o}C. Microtissues were permeabilised with 0.5% (v/v) triton X-100/ PBS overnight at 4^{o}C then blocked in 3% (w/v) BSA /TBST block (with 0.1% (v/v) Triton X-100) for 2 h at room temperature. Primary antibody was diluted as required in 1% (w/v) BSA /TBST (with 0.1% (v/v) Triton X-100), block reagent was removed and primary antibody added overnight at 4°C. Microtissues were washed three times with TBST (with 0.1% (v/v) Triton X-100) at room temperature, each time incubated for 1 hour. Secondary antibody was diluted 1:1000 in 1% (w/v) BSA/TBST (with 0.1% (v/v) Triton X-100) and added to the microtissues overnight at 4°C. Microtissues were washed for 1 hour with TBST (with 0.1% (v/v) Triton X-100) at room temperature and stained with Hoescht 33342 in TBST (with 0.1% (v/v) Triton X-100) (1:5000 dilution) for 1 hour at room temperature. Microtissues were washed briefly in TBST (with 0.1% (v/v) Triton X-100) before mounting onto a microscope slide with ProLong Gold. Microtissues were imaged using a Zeiss fluorescence microscope.

2.2.4 Gene expression analysis & manipulation techniques

2.2.4.1 RNA samples

All stages of the RNA extraction procedures were carried out using sterile, RNase-free plastic ware, filter-tip pipette tips, and RNase-free water. RNA samples were kept on ice at all times, to minimise the possibility of RNA degradation by RNases. Adult left ventricle, foetal heart and smooth muscle total RNA were purchased from US Biological life sciences. hESC-CM total RNA was purchased from GE Healthcare. All primary cells were washed twice in DPBS (without Ca^{2+}/Mg^{2+}), detached with pre-warmed Accutase (Sigma, A6964) for 5 mins at 37ºC, 5% CO_2, centrifuged for 3 mins at 1200 xg before lysis in 500 µl Buffer RLT containing 1% (v/v) 2-mercaptoethanol and stored at −80 °C until processing. Microtissues were pooled and transferred into a falcon tube, centrifuged at 1200 xg for 2 mins and re-suspended in pre-warmed DPBS. Microtissues were re-centrifuged at 1200 xg for 2 mins and lysed in 500 µl Buffer RLT containing 1% (v/v) 2-mercaptoethanol. Total RNA was extracted from cells using the RNeasy mini kit (Qiagen, Crawley, U.K.). A NanoDrop spectrophotometer (NanoDrop Technologies) was used to quantify RNA samples.

2.2.4.2 Preparation of cDNA

Total RNA was used for cDNA synthesis. Reverse transcription reactions were carried out in sterile, RNase- and DNase-free 0.2 ml PCR tubes. Total RNA was diluted to 20 ng and reverse transcribed using a SuperScript® III first-strand synthesis supermix kit (Life Technologies™ (Paisley, U.K.)) following manufacturers instructions. cDNA was stored at -80 °C, or immediately preamplified. cDNA samples were preamplified using the TaqMan® PreAmp Master mix kit with TaqMan® Probes (see table 2.8), manufacturers instructions were followed using 10 cycles and final stock diluted 1:250.

2.2.4.3 Quantitative real-time polymerase chain reaction (qRT-PCR)

QRT-PCR reactions were performed in a 7900 HT Fast Real-Time PCR System (Applied Biosystems, Foster City, CA, U.S.A.), 2.5 µl of preamplified cDNA was used with TaqMan® Gene Expression probes (Table 2.8) and master mix to monitor amplification under standard cycling conditions. All reagents were thoroughly mixed by vortexing prior to use. Following the loading of each 384-well PCR plate, plates were sealed with optically clear sealing film, and the plate was vortexed gently. Sealed plates were centrifuged for 1 min at 3,000 r.p.m. at 4 °C in a Beckman Coulter Allegra™ 25R centrifuge (Beckman Coulter (U.K.) Ltd, High Wycombe, U.K.) prior to loading the plate into the RT-PCR machine.

Absolute quantification and relative quantification are the most commonly used methods to analyze data from qRT-PCR experiments (Livak & Schmittgen, 2001). Both methods of qRT-PCR data analysis involve the use of cycle threshold (*C*T) values. *C*T values can be defined as the number of cycles at which the amplification curve of a gene crosses a certain threshold of fluorescence. *C*T values were recorded by SDS2.3 software linked to the 7900 HT Fast Real-Time PCR machine. The expression of an invariant endogenous control (housekeeping gene) can be used as an active reference to correct minor intra- and inter-assay variations (sample-to-sample and run-to-run variations respectively) (Pfaffl & Hageleit, 2001). In each case, the level of expression of the mRNA of interest was normalized to the expression level of *GAPDH* mRNA. Three identical replicates of each sample were included on each plate. *C*T values for the mRNA of the gene of interest and for the *GAPDH* control were recorded, and changes in gene expression were determined by the comparative *C*T ($2^{-\Delta\Delta C}$T) method.

Firstly, the mean, and standard deviation (SD), of three replicate samples was calculated. Secondly, the Δ*C*T value of each sample was calculated by subtracting the *C*T value for *GAPDH* from the *C*T value of the target gene (gene of interest). Thirdly, the ΔΔ*C*T value was then calculated by subtracting the Δ*C*T

of the reference sample from the Δ*C*T of the test sample. Finally, the fold-change in gene expression was calculated using the following formula:

Fold change= 2^-ΔΔCT

As the SD of the ΔCT values is the same as the SD ΔΔCT value in each case, this value was used to calculate the range of the fold-change in expression of the target relative to that of the *GAPDH,* which was calculated as follows:

From: 2−(ΔΔ*C*T) + (SD(ΔΔ*C*T)) To: 2−(ΔΔ*C*T) - (SD(ΔΔ*C*T))

2.2.4.4 Microtissue transfection with small interfering RNA (siRNA)

Microtissues were formed and incubated for 14 days prior to use (see section 2.2.1.8). Microtissues were transfected with siRNA and Lipofectamine™ RNAiMAX transfection reagent. S100A1 siRNA was purchased from Life Technologies™ (Paisley, U.K.). Negative control siRNA was purchased from Life Technologies™ (Paisley, U.K.). SiRNA stock solution was diluted in 250 µl of OptiMEM®, and in a separate tube, Lipofectamine™ RNAiMAX transfection reagent was diluted to give a 0.1% (v/v) final concentration in 250 µl of OptiMEM® per sample. The diluted Lipofectamine™ RNAiMAX and siRNA components were combined, mixed well by gentle pipetting and incubated for 5 min at room temperature. One hundred microliters of cell culture media was removed from the microtissues and replaced with 100 µl of transfection solution, this was repeated twice to dilute the remaining cell culture media. The plates were swirled gently to ensure even distribution of the siRNA. Microtissues were incubated with the transfection solution at 37 °C, 5% CO_2 for 24 h prior to use.

2.2.5 Compound preparation and treatment

2.2.5.1 HCB and cytotoxicity assay compounds

All compounds were dissolved in 100% dimethyl sulfoxide (DMSO) as 20 mM (milimolar) stock solutions. At 20 mM no insolubility and precipitation were observed with any compound (assessed by visual inspection). Test compounds were prepared using 6 concentrations in a 3-fold dilution scheme. An initial compound plate was produced in a polypropylene 96-well plate by serially diluting the 20 mM stock 1 in 5 to generate 6 concentration points. Intermediate plates were generated by transferring 10 µL from each well of the compound plate to the corresponding wells of a polypropylene plate containing 90 µL of cell culture media and mixed thoroughly. From one compound plate, two intermediate plates were produced. 5 µL from each well of an intermediate plate was added to the corresponding wells of a black-walled, 96-well plate containing cells previously seeded at the appropriate density in a volume of 95 µl (Table 2.9) and incubated at 37 ^{o}C for 4 days. One intermediate plate was used to treat one black-walled, 96-well plate which was then incubated at 37 ^{o}C, 5 % CO_2. Final DMSO concentration was 0.5% (v/v). Compounds were screened in duplicates on separate plates, on three separate occasions. The final compound concentrations were 0.01 µM-100 µM.

2.2.5.2 IonOptix contractility assay compounds

Compounds were obtained from Sigma-Aldrich (Dorset, UK) or the AstraZeneca compound collection. Compounds were initially formulated in DMSO as a 1000x stock solution. This stock solution was subsequently serially diluted down to lower concentrations using DMSO. The DMSO stock solutions were diluted 1000x into the 5050 microtissue media to give the final test concentrations. The final DMSO concentration was 0.1% (v/v). Where compounds were insoluble in DMSO, Dulbecco's PBS (Lonza (Basel, Switzerland)) was used. Caffeine was formulated directly in 5050 microtissue media at 10 mM.

2.2.6 Cytotoxicity assays

2.2.6.1 LDH cytotoxicity detection

After compound treatment, 50 µL of conditioned growth medium from each well of the treated black-walled, 96-well plate was transferred into a clear 96-well cell-culture plate and 50 µL of LDH cytotoxicity reaction reagent added (prepared as per the manufacturer's instructions). The reaction was incubated in the dark for 30 mins at room temperature and fluorescence recorded using an EnVision® multilabel reader (PerkinElmer Life Sciences, Fremont, CA, U.S.A.).

2.2.6.2 Measuring cellular ATP content

Immediately after the imaging assay was performed, a commercially available CellTiter-Glo® luminescent cell viability kit (Promega, Southampton, U.K.), was used to determine the number of viable cells in culture. This assay utilises the luciferin-luciferase reaction to detect the amount of ATP present in cultured cells, which is directly correlated with the number of viable cells, and has been shown to be an accurate measure of cytokine-dependent proliferation in cultured cells (Crouch *et al.*, 1993). CellTiter-Glo® reagent lyses cell membranes to release ATP and inhibits endogenous ATPases, whilst also providing beetle luciferin and recombinant firefly luciferase to the reaction mixture. The manufacturer's instructions were followed, however, media was removed and replaced with 100 µl of fresh cell culture media prior to the addition of the CellTiter-Glo® reagent. Luminescence was recorded using a Wallac 1450 Microbeta Trilux Scintillation Counter (PerkinElmer Life Sciences, Fremont, CA, U.S.A.).

2.2.7 High content biology

2.2.7.1 Mitochondrial and nuclei staining

Cells were stained with fluorescent probes in D-PBS (without Ca^{2+}/Mg^{2+}) at 37°C for 20 mins. The fluorescent probes used were MitoTracker® Deep Red FM and Hoescht

33342 at dilutions shown in Table 2.5. Following staining, staining media was replaced with 100 µL D-PBS (without Ca^{2+}/Mg^{2+}) and the cells subjected to automated live-cell fluorescent image acquisition using an ImageXpress high content analysis system (Molecular Devices, 20x objective). Fluorescent images were captured according to the optimal excitation and emission wavelengths of each probe (Table 2.5).

2.2.7.2 Multiplex imaging assay

After 6, 24 or 72 h of compound treatment at 37ºC, 5% CO_2, the media was removed and the cells were stained with fluorescent probes in serum-free medium at 37ºC for 1 h. The fluorescent probes used were 5-Tetramethylrhodamine (TMRE); ER-Tracker™ Blue-White DPX; Fluo-4 AM and TOTO®-3 Iodide at dilutions shown in Table 2.5. Following staining, staining media was replaced with 100 ul D-PBS (without Ca^{2+}/Mg^{2+}) and the cells subjected to automated live-cell fluorescent image acquisition using an ImageXpress high content analysis system (Molecular Devices, Sunnyvale, CA, U.S.A., 20x objective). Fluorescent images were captured according to the optimal excitation and emission wavelengths of each probe (Table 2.5). Immediately after imaging, cellular ATP content was measured as described in *section 2.2.6.2.*

Image analysis was performed using metaXpress software (Molecular Devices, Sunnyvale, CA, U.S.A.). A series of measurements of each fluorescent probe were obtained for each drug. They were mean nuclei integrated intensity for TOTO®-3 (wavelength Cy5), and mean cell integrated intensity for the three remaining wavelengths. The sum of these numerical measurements from the four image fields within the same well were divided by the sum of the nuclei count from the same four image fields to obtain values that were standardised by cell number. Values were normalized by the average values from the 6 vehicle treated wells and then wells of the same treatment on duplicate plates were averaged.

Cellular ATP data was normalized by the average values from the 6 vehicle treated wells and then wells of the same treatment on duplicate plates were averaged.

Concentration-effect curves were plotted for each compound and expressed relative to vehicle (0.5% (v/v) DMSO). The molar concentration of test compound producing 50% inhibition (IC_{50}) or 50% response (EC_{50}) for each cellular parameter; mitochondrial membrane potential, ER integrity, Ca^{2+} mobilization and cellular ATP content, were calculated using Graphpad Prism™ (La Jolla, CA). IC_{50} values for each parameter were divided by the total C_{max} of the test compound to give the therapeutic index; a comparison of the amount of a therapeutic agent that causes the therapeutic effect to the amount that causes toxicity. The cellular parameter with the lowest therapeutic index was selected for each compound and correlations between cell types were generated using Graphpad Prism™ (La Jolla, CA).

2.2.8 IonOptix contractility and calcium flux analysis

2.2.8.1 Video-based edge detection of contractions

Microtissues were transferred onto 0.1% (w/v) gelatin-coated 13 mm plastic coverslips (Thermanox) within a 12 well plate and incubated at 37°C, 5% CO_2 for at least one hour before mounting onto the IonOptix contractility system. Contractile properties of spheroids were assessed using a video-based edge detection method (IonOptix™, Dublin, Ireland). A gelatin-attached microtissue was placed in a perfusion chamber (FHC Inc., Bowdoinham, ME, USA) mounted on the stage of an inverted Nikon TE200 microscope (Nikon UK, Surrey, UK). The microscope stage (Prior Scientific Instruments, Cambridge, U.K.) was motorized and controlled remotely. Microtissues were continuously perfused from a gravity fed system at 2 mL/ min with microtissue media heated to 35.5 ± 1 °C using a line heater (Cell MicroControls, Norfolk, VA, USA). The microtissues were field stimulated with suprathreshold voltage at a pacing frequency of 1 or 1.5 Hertz (Hz), with a bipolar pulse of 6 miliseconds (ms) duration, using a pair of platinum wires placed on opposite sides of the chamber connected to a MyoPacer EP stimulator (IonOptix™). Microtissues were imaged at 240 Hz using an IonOptix™ Myocam-S CCD camera. Digitised images were displayed within the IonWizard™ acquisition software (IonOptix™). The edge of the microtissue of interest was aligned parallel to the video raster line, by means of a semi-automated dovecote prism optical

system that could be controlled remotely (Cairn Research, Faversham, UK). Optical intensity data was collected representing dark and light bands at the edge of the spheroid of interest. The IonWizard™ software analyzes the periodicity in the optical density by means of a fast Fourier transform algorithm. The output of this analysis is a direct real-time measurement of microtissue contraction displacement.

Compound response was measured from one microtissue on triplicate occasions. After microtissues were added to the microscope stage, perfusion with microtissue media (with 0.1% DMSO as the vehicle control) was immediately started. At this time field stimulation was also started, and microtissues were left to acclimatise for approximately 2 mins at ~ 37 °C, after which at least 30 seconds (s) of basal contractions were recorded for each spheroid. Test compounds were applied in a cumulative manner with each concentration applied for 250 s or until steady-state was achieved. Every 3-4 days, 10 μM verapamil was applied as a positive control.

Initial analysis was performed using the IonWizard™ software. For each test condition, data for 10 to 15 contractions were averaged, using the stimulation time as common reference point, to give a single representative monotonic contractility transient. This transient was analysed using the “monotonic transient analysis” function of the IonWizard™ software. From this analysis, 3 key parameters were used to quantify microtissue dynamics: 1) peak height, which indicates the percentage of peak contraction displacement relative to the resting length. 2) Maximum contraction velocity, calculated as the maximum rate of change in peak height during the contraction phase. 3) Maximum relaxation velocity, calculated as the maximum rate of change in peak height during the relaxation phase. Concentration-effect curves were plotted for each compound and expressed relative to vehicle (0.1% (v/v) DMSO). The molar concentration of test compound producing 50% inhibition (IC_{50}) or 50% response (EC_{50}), were calculated using Graphpad Prism™ (La Jolla, CA).

2.2.8.2 Ca^{2+} transient measurements

Microtissues were loaded with 0.2 µmol/L Fura-2-acetoxymethyl ester (Invitrogen), a calcium-sensitive, ratiometric fluorescence dye, for 30 min at room temperature (RT) and kept in the dark. The same experimental design used for performing contractility recordings was applied to carry out intracellular calcium measurements. An IonOptix system was used to conduct the experiments, including the Xenon arc lamp, hyperswitch and myopacer for microtissue stimulation and fluorescence excitation, myocam-S for the measurement of edge contraction, and a fluorescence system interface to integrate the different components (IonOptix Ltd). The Xenon arc lamp and fluorescence hyperswitch containing a galvanised mirror were used to alternate between wavelengths of 340 and 380 nm (nanometer) at a high frequency. Calcium fluorescence was recorded at 510 nm. Calcium traces represent the ratio of calcium bound: calcium free Fura-2- acetoxymethyl ester dye, and hence changes in free intracellular calcium. Simultaneous contraction and calcium recordings for microtissues were taken while perfusing with their standard cell culture media (see table 2.10) containing DMSO 0.1% (v/v) as the vehicle control when appropriate. A transition period of 250 s was conducted between test concentrations, allowing any compound induced effects to reach a steady state. Analysis was performed using the IonWizard™ software as for contractility measurements.

2.2.9 Statistical analysis

In order to define statistical significance the unpaired students t-test function in Graphpad Prism™ (La Jolla, CA) was used to calculate P values of significance. The t test investigates the likelihood that the difference between the means of the two groups could have been caused by chance. P values of less than 0.05 are deamed significant.

Chapter Three

Development of *in vitro* cell models for the study of drug-induced cardiotoxicity

3.1 Introduction

Routine cardiac safety screens primarily focus on cardiomyocytes in isolation, ignoring other cellular components of the myocardium such as the endothelial and fibroblast cells. However, it is now becoming apparent that endothelial dysfunction can influence neighbouring cells (Ajithkumar *et al.*, 2011; Brutsaert, 2003; Chen *et al*., 2010; Chiusa *et al.*, 2012; Jiang, 2007; Mikaelian *et al.*, 2010; Ritchie *et al.*, 1998a) and cardiac fibroblasts are known to affect both cardiac myocyte and endothelial cell function (Calderone *et al*., 1998; Ottaviano & Yee, 2011). Aberration of these interactions could lead to changes in myocardial morphology, physiology and biochemistry and ultimately cardiac failure.

This chapter describes, firstly, the optimisation of human primary endothelial and fibroblast monolayer models originating from cardiac and dermal origins. These models are optimised as a confluent cell monolayer for use in plate based cytotoxicity assays. In recent years it has become clear that the same cell type originating from different organs show considerable heterogeneity. While endothelial and fibroblast cells are united in certain common features, their heterogeneity is becoming increasingly apparent. Endothelial heterogeneity has been described at the level of morphology, function, antigen composition and signalling networks suggesting each endothelial cell type is uniquely adapted to meet the demands of its local environment (Aird, 2012; Hendrickx *et al.*, 2004; Ishii *et al.*, 2009). Recent data also indicates that the embryological origin of macro- and microvascular endothelium are distinct (Rossant & Howard, 2002). Therefore, cell responses are now thought to be the result of the environment in which a cell resides combined with it's genetically 'programmed' function, providing cells residing within different tissues with the potential to respond to a common signal in a unique manner. Monolayer models will be developed for human coronary artery endothelial cells (hCAECs), human dermal microvascular endothelial cells (hDMECs) and normal human dermal fibroblast (NhDFs) alongside human cardiac microvascular endothelial cells (hCMECs) and human cardiac fibroblasts (hCFs) to eventually allow any cardiac myocardial specific toxicities to be highlighted.

Secondly, this chapter describes the development of *in vitro* 3D cardiac microtissue models for use in both structural and functional cardiotoxicity assays. The aim of 3D cell culture is to increase the physiological relevance of the cells microenvironment and therefore create an *in vitro* model which better recapitulates the *in vivo* tissue. Here a technique based on the more traditional scaffold-free hanging drop technique will be used to generate microtissue spheroids.

3.2 Optimisation of primary human endothelial monolayer models

3.2.1 High seeding density for short term culture

Initial experiments using primary human cardiac microvascular endothelial cells (hCMECs) investigated seeding cells at a high density using cell attachment overnight to create a usable model the following day, however preliminary experiments to establish the optimal number of hCMECs per well repeatedly displayed a significant loss in cell number. hCMECs were seeded into gelatin-coated 96 well plates at 10,000; 15,000; 20,000 and 25,000 cells per well (well^{-1}) in endothelial full growth media (FGM). Following 24h incubation, nuclei were stained with Hoescht 33342, fluorescent images taken and automated algorithms used to approximate cell numbers per well. When seeded at 20,000 cells well^{-1}, the resulting cell number was approximately 60% lower than the initial seeding density (figure 3.1). There are numerous reasons why this “cliff-edge effect” should be avoided. Firstly, the ethical issues, the high costs and limited supply of human primary cells mean efficient use of available stock is highly important. Secondly, prior to cell treatment it is important that the cells are in a stable, healthy environment; a drastic increase in cell death is likely to influence the interactions and survival of the remaining cells. Therefore, an alternative approach was considered whereby cells were seeded at a lower density and incubated for a longer time period to allow a confluent monolayer to develop (section 3.2.3), thus reducing the “cliff- edge effect” seen with the overnight method, maintaining cell health and improving stock utility. First optimal cell culture media was established.

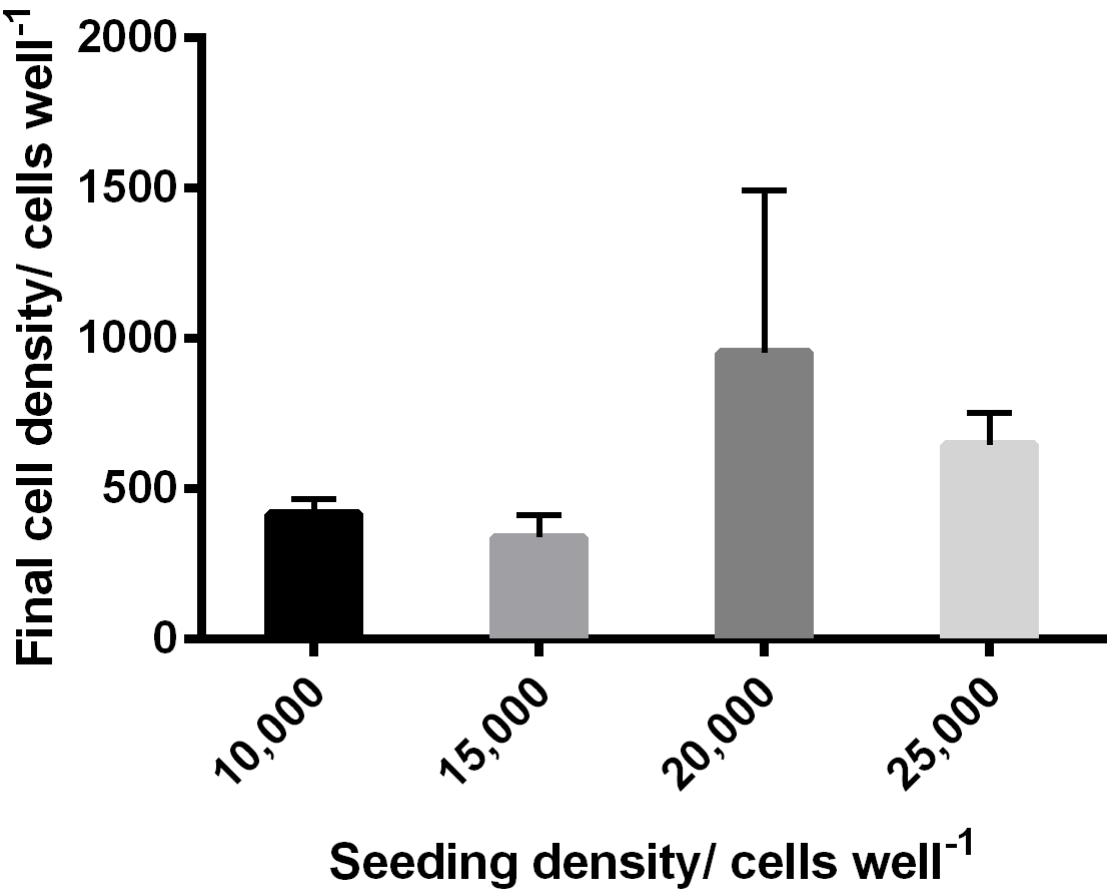

Figure 3.1 Number of cells well^{-1} 24 h post seeding at varying densities.

hCMECs were seeded at 10,000, 15,000, 20,000 and 25,000 cells well^{-1} on gelatin-coated 96 well plates in endothelial full growth media (Endo-FGM) for 24 h. The cells were stained with Hoescht 33342 and fluorescent images taken at the DAPI wavelength using an ImageXpress machine (MolecularDevices, Sunnyvale, CA, U.S.A., 20x objective). From these images nuclei were counted to give the number of cells well^{-1}. Data shown is from a single experiment mean of n=6 with *SD error bars*. *hCMEC, human cardiac microvascular endothelial cells.*

3.2.2 Selection of assay media

The survival of the hCMECs under differing media conditions was studied. Endothelial MV2 basal medium supplemented with 5% (v/v) foetal calf serum (FCS), EGF (5.0 ng/

ml), hydrocortisone (0.2 µg/ ml), VEGF (0.5 ng/ ml), FGF-2 (10.0 ng/ ml), insulin-like growth factor-1 (20.0 ng/ ml) and ascorbic acid (1.0 µg/ ml), (Cat. No.: C-22121) was the full growth media (Endo FGM) recommended by the manufacturers, PromoCell (Heidelberg, Germany). However when studying the toxicity of kinase inhibitors upon endothelial cells the capability to treat the cells in the absence of growth factors was desirable. hCMECs were therefore cultured at 20,000 cells well^{-1} in gelatin-coated 96 well plates in three subtypes of endothelial media; Endothelial full growth media (Endo-FGM), Endothelial low serum media (Endo-LSM) (1% (v/v) foetal calf serum (FCS)) and Endothelial media without growth factors (Endo–GF) (5% (v/v) FCS for 5 days to cover the maximum treatment period of 72 h.

Figure 3.2 shows that when hCMECs are cultured in 5% FCS in the absence of any supplemented growth factors (Endo -GF), an initial increase in cell number is followed by a steep decline until a recovery period appears to begin. When hCMECs are cultured in low serum and no supplemented growth factors (Endo LSM), a gradual decline in cell number can be seen over the experiment time course. These preliminary experiments suggested that endo FGM would be the only media capable of maintaining a stable cell monolayer over the treatment period.

Data shown in figure 3.2 for hCMECs grown in endo FGM shows a slight decline in cell number from the initial seeding density of 20,000 cells well^{-1} to a baseline density of approximately 15,000 cells well^{-1} between days 3 and 4. This suggested that a seeding density of 20,000 was still too high to allow avoidance of an initial death phase, therefore further seeding density optimisation was required using densities below that of 20,000 cells well^{-1}.

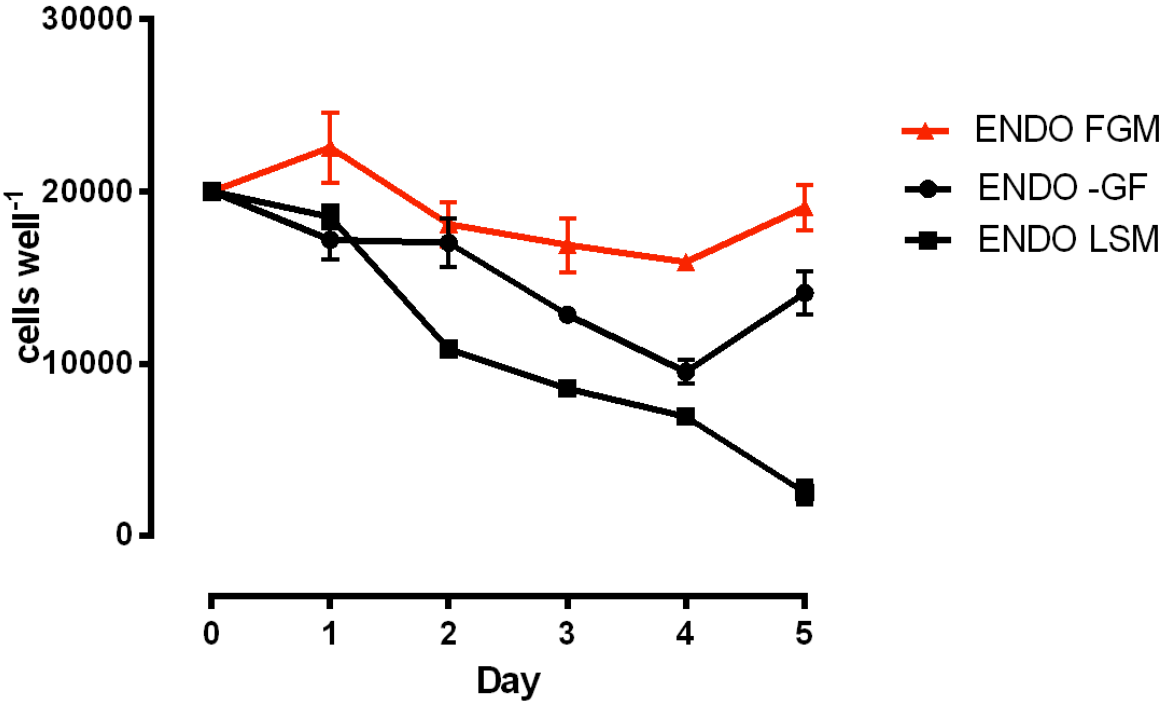

Figure 3.2 Effect of various endothelial media subtypes upon hCMEC survival. hCMECs were seeded at 20,000 cells well^{-1} on gelatin-coated 96 well plates in Endo FGM, Endo LSM (1% (v/v) foetal calf serum (FCS)) and Endo –GF (5% (v/v) foetal calf serum (FCS)). At 24 h intervals for 5 consecutive days, cells were stained with Hoescht 33342 and fluorescent images taken at the DAPI wavelength using an ImageXpress high content analysis system (MolecularDevices, Sunnyvale, CA, U.S.A., 20x objective). From these images nuclei were counted to give the number of cells well^{-1}. Data shown is from a single experiment mean of n=3 with *SD error bars*. *hCMEC, human cardiac microvascular endothelial cells; FGM, full growth media; GF, growth factor; FCS, Foetal calf serum.*

3.2.3 Optimisation of seeding density in endothelial full growth media

hCMECs were seeded into gelatin-coated 96 well plates at densities of 6,000; 8,000 and 10,000 cells well^{-1} in endothelial full growth media (FGM). Previous data (figure 3.1 and figure 3.2) suggested 10,000 cells well^{-1} as a maximum seeding density therefore

this was selected as a maximum cell density with 6,000 and 8,000 as lower densities. The aim of this experiment was to determine a seeding density which avoids an initial death phase and after a period of incubation allows the formation of a stable confluent endothelial cell monolayer capable of surviving the maximum treatment period with minimal fluctuations in cell number. Using Hoescht nuclei staining as a measure of cell number, figure 3.3 shows that when hCMECs were seeded at 10,000, 8,000 and 6,000 cells well^{-1}, an increase in cell number to approximately 15,000 to 20,000 cells well^{-1} occurs until day 3. The 10,000 cells well^{-1} sample displays a subtle decline in cell number from 20,000 to 15,000 cells well^{-1} followed by a cell number recovery between days 6 and 7 (figure 3.3). When seeded at 8,000 cells well^{-1}, cell number fluctuates throughout the treatment period (figure 3.3). A seeding density of 6,000 cells well^{-1} proved optimal for the following reasons; hCMECs gradually increase in cell number until approximately 20,000 cells well^{-1} is reached, this occurs by day 4 (figure 3.3). From day 4 until day 7, no large fluctuations in cell number were seen suggesting a healthy equilibrium has been reached whilst avoiding a so called “cliff-edge effect”. Furthermore, as discussed previously, the cost and availability of human primary cells greatly limits their use as a cell model; shown here a low seeding density of 6,000 cells well^{-1} is enough to provide a stable cell monolayer over the maximum treatment period of 72 h (days 4-7), while also increasing throughput capabilities. This data has also identified day 4 as the optimal time to dose the cells; this is the beginning of the stable growth period.

Similar experiments were performed to optimise the seeding densities of hDMECs and hCAECs, again, with the aim of achieving a confluent stable monolayer for plate based toxicity assays. hDMECs were seeded into gelatin-coated 96 well plates at densities of 6,000, 8,000 and 10,000 cells well^{-1} in endothelial FGM. Previous work with hCMECs (figure 3.1, 3.2 & 3.3) directed these selections. Figure 3.3 shows adult hDMEC cell number is most stable between days 4 and 7 when seeded at a density of 8,000 cells well^{-1}, this time frame corresponds with that of the hCMEC model. hCAECs were seeded into gelatin-coated 96 well plates at densities of 6,000 and 8,000 cells well^{-1} in

endothelial FGM. Previous work with hCMECs and adult hDMECs (figures 3.1, 3.2, 3.3) was used to guide the selection of these two densities. Figure 3.3 shows hCAEC number is most stable between days 4 and 7 when seeded at a density of 6,000 cells well^{-1}. From day 4 until day 7, no significant fluctuations in cell number were seen suggesting a healthy equilibrium has been reached, a time frame we also see with hCMEC and hDMECs. These results already show endothelial heterogeneity; the cardiac cells (hCMEC & hCAEC) require a lower cell seeding number compared with the dermal endothelial cells (hDMEC).

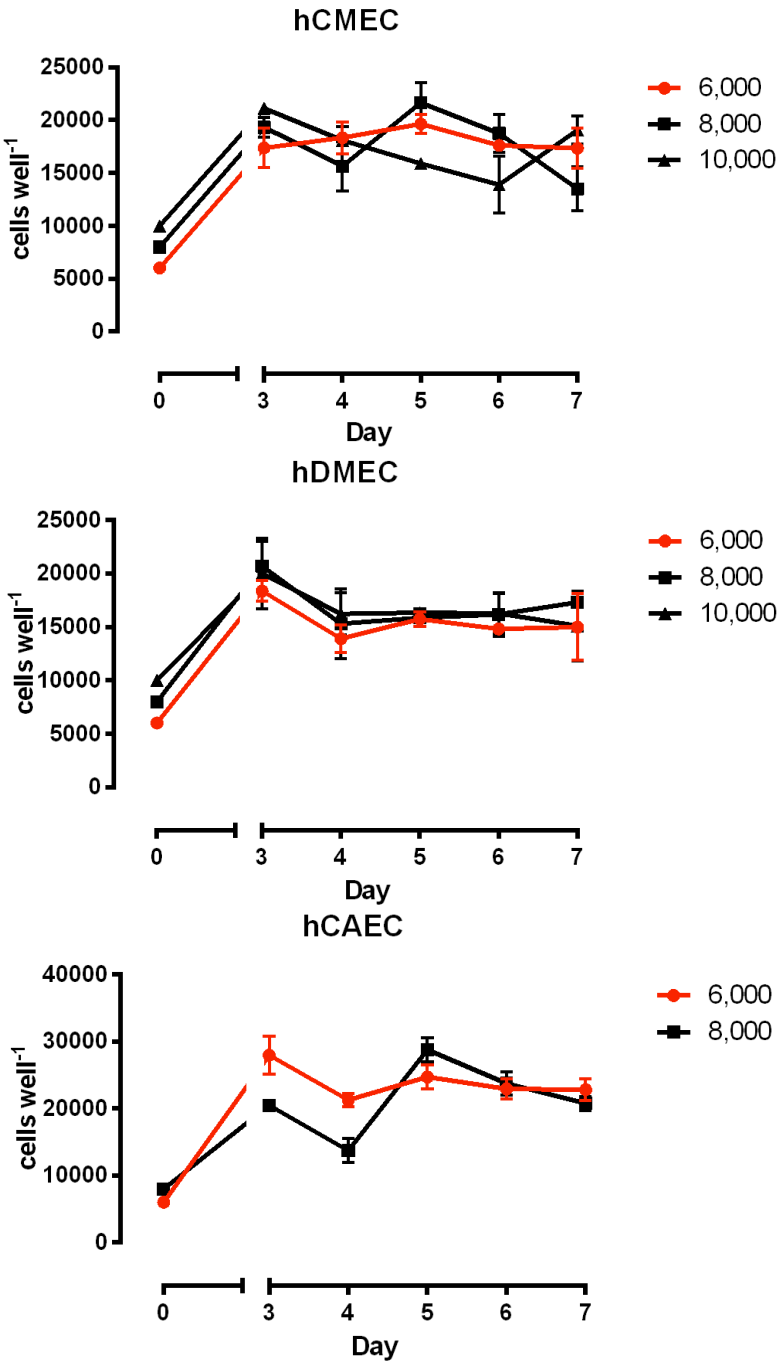

Figure 3.3 Optimisation of endothelial seeding density.

Endothelial cells were seeded on gelatin-coated 96 well plates at differing densities on day 0 and incubated for 3 days in endothelial FGM. From day 3, cells were stained with Hoescht 33342 at 24 h intervals for 5 consecutive days and fluorescent images taken at the DAPI wavelength using an ImageXpress high content analysis system (MolecularDevices, Sunnyvale, CA, U.S.A., 20x objective). From these images nuclei were counted to give the number of cells well^{-1} at each time point. Data shown is from a single experiment mean of n=6 with *SD error bars*. *hCMEC, human cardiac microvascular endothelial cells; hDMEC, human dermal microvascular endothelial cells; hCAEC, human coronary artery endothelial cells; FGM, full growth media.*

3.2.4 Endothelial cellular stability over time course

Having established optimal seeding densities of 6,000 cells well^{-1} (hCMEC and hCAEC) and 8,000 cells well^{-1} (hDMEC) with an incubation period of 4 days prior to cell treatment; mitochondrial staining and intracellular ATP content were used as a measure of intracellular health and monitored over this chosen time period. Endothelial cells were seeded on gelatin-coated 96 wells plates and incubated for 4 days. Every 24 h for 5 consecutive days cells were stained with MitoTracker and Hoescht 33342 and imaged at the TRITC and DAPI wavelengths using an ImageXpress machine (Molecular Devices, Sunnyvale, CA, U.S.A., 20x objective). Automated algorithms were used to give the percentage mitochondrial staining per cell, which provides a measure of mitochondrial health over the time course. Following imaging, cells were lysed for intracellular ATP content using CellTiter- Glo reagent. Figure 3.4 shows mitochondrial health is unchanged over the course of the experiment for all endothelial models. ATP content relative to maximal ATP content varies over the time course in all endothelial models. hCMEC intracellular ATP content increases by 75% from day 4 to day 5 and decreases by 75% from day 5 to day 6. PromoCell have recorded the population doubling time of this cell type to be approximately 30-40 h, therefore this peak in ATP may be a result of a population doubling which should be considered in future cytotoxicity measures. Additionally cell culture media is refreshed between days 4 and 5, this replenishment of metabolic nutrients could explain the shorterm increase in cellular ATP synthesis. hDMEC and hCAEC ATP content relative to maximal ATP content also peaks on day 5, as was seen with the hCMEC model (figure 3.4); this again could be a result of a population doubling as suggested by the manufacturer (PromoCell) or cell culture replenishment. At 24h intervals endothelial cells were stained for acetyl low density lipoprotein (Dil-acLDL) uptake and nuclei (Hoescht 33342), the cells were imaged at the TRITC and DAPI wavelengths using a ImageXpress high content analysis system and automated algorithms used to determine the percentage acLDL uptake per cell. AcLDL uptake is a characteristic specific to endothelial cells therefore it can be used to monitor the endothelial phenotype of the cell model. Figure 3.4 shows acLDL uptake was stable for each endothelial model over the time course.

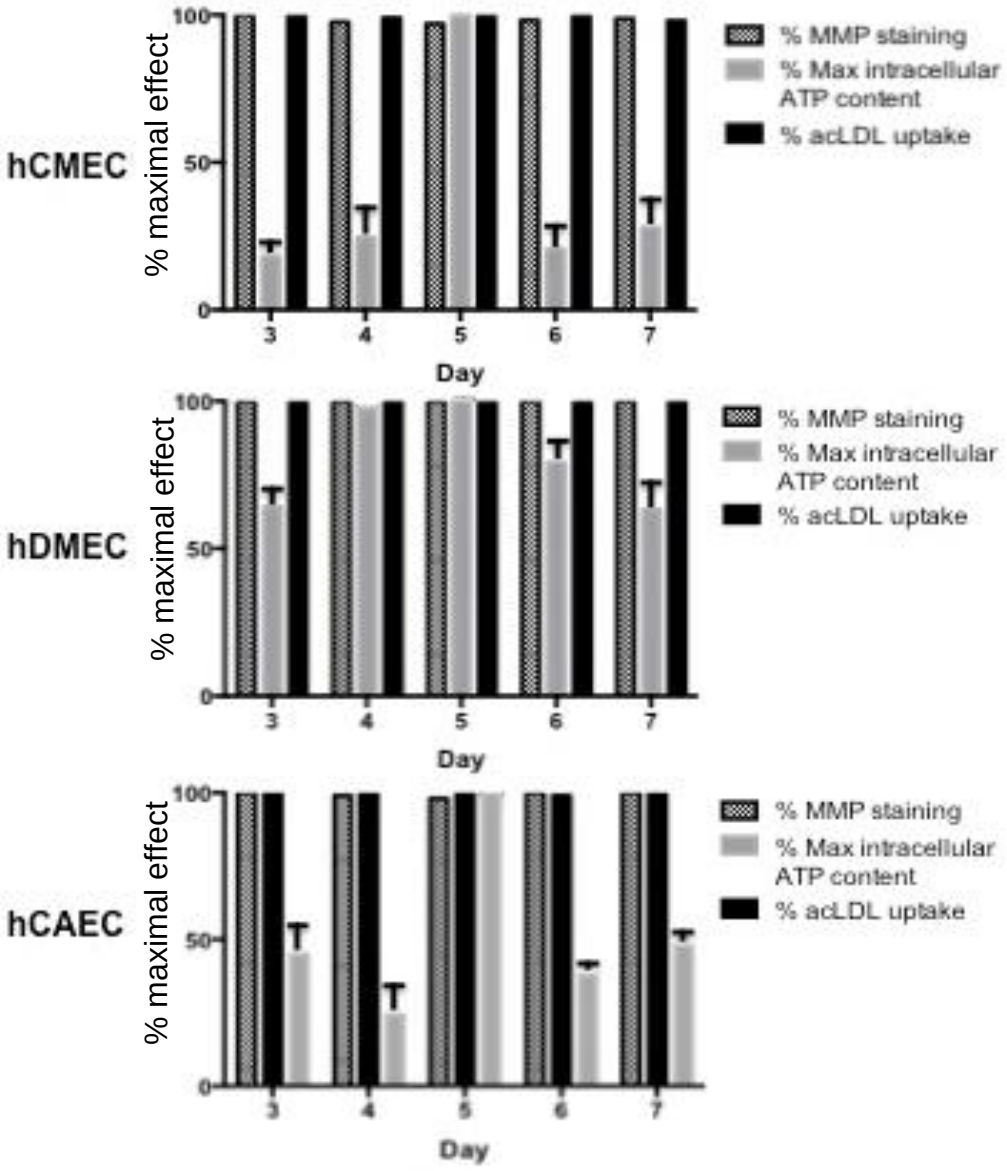

Figure 3.4 Endothelial cell health over treatment period.

Endothelial cells were seeded on gelatin-coated 96 well plates at their optimal seeding densities (see *section 3.2.3*) and incubated for 3 days in endothelial FGM. Cells were then monitored at 24 h intervals over 5 consecutive days for various parameters of intracellular health. Cells were stained with MitoTracker and Hoescht 33342 and imaged at the TRITC and DAPI wavelengths using an ImageXpress high content analysis system (Molecular Devices, Sunnyvale, CA, U.S.A., 20x objective). Cells were stained for acLDL uptake and nuclei (Hoescht 33342), the cells were imaged at the TRITC and DAPI wavelengths. In both assays, automated algorithms were used to determine the percentage staining per cell. Cells were lysed for intracellular ATP content using CellTiter-Glo reagent (Promega, Southampton, U.K.). Data shown is from a single experiment mean of n=6 with *SD error bars*. *hCMEC, human cardiac microvascular endothelial cells; hDMEC, human dermal microvascular endothelial cells; hCAEC, human coronary artery endothelial cells; FGM, full growth media.*

3.2.5 Visualisation of endothelial health, confluency and phenotype

Mitochondrial health was maintained throughout the treatment period for each endothelial monolayer model as discussed in *section 3.2.4*. Figure 3.5 displays this mitochondrial staining (MitoTracker dye) alongside stained nuclei (Hoescht 33342), these figures (only treatment period shown) show the maintenance of a healthy monolayer of cells for each endothelial model throughout the maximum treatment period of 72 h.

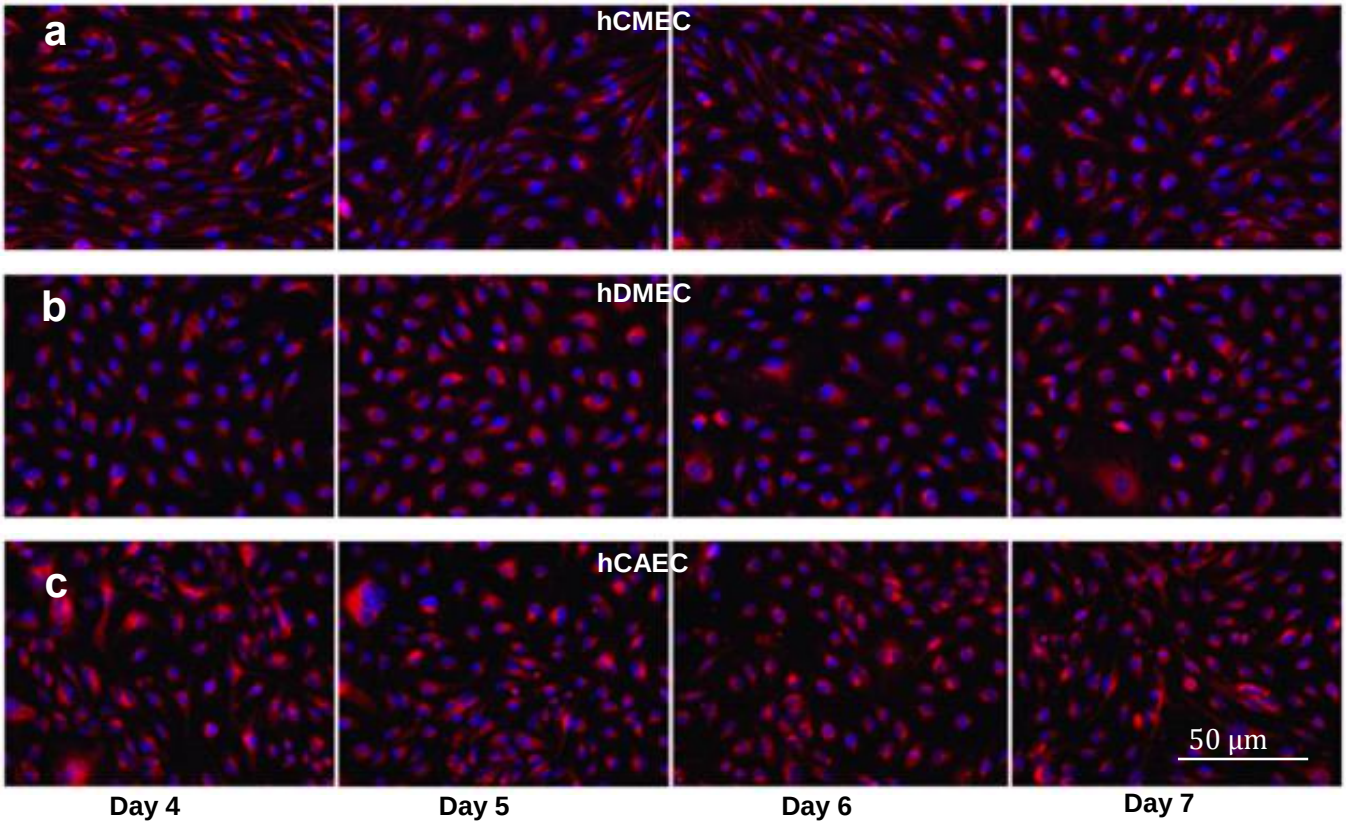

Figure 3.5 Visualisation of endothelial mitochondrial health.

Endothelial cells were seeded on gelatin-coated 96 well plates at their optimal seeding densities (see *section 3.2.3*) and incubated for 3 days in endothelial FGM. Cells were then monitored at 24 h intervals over 5 consecutive days (only 4 day treatment period shown here) for mitochondrial health. (a) hCMEC, (b) hDMEC and (c) hCAEC were stained with MitoTracker (shown in red) and Hoescht 33342 (shown in blue) and imaged at the TRITC and DAPI wavelengths using an ImageXpress high content analysis system (Molecular Devices, Sunnyvale, CA, U.S.A., 20x objective). Representative images of triplicate samples. Scale bar represents 50 μm.

In vivo endothelial cells are in close contact and exhibit acetyl low-density lipoprotein uptake, therefore the monolayer models were assessed for confluency using a phalloidin dye towards F-actin, a structure of the cytoskeleton and acLDL uptake using a fluorescently labelled acLDL dye. Figure 3.6 (a,b,c) shows F-actin staining of each endothelial monolayer model at the end of the compound treatment time course; we can see that the endothelial cells are in contact with one another and this was maintained until the end of the treatment period. Figure 3.6 (d,e,f) shows acLDL uptake for each endothelial monolayer model at the end of the treatment period. Each endothelial model maintains the ability to take up acLDL and therefore it's endothelial phenotype.

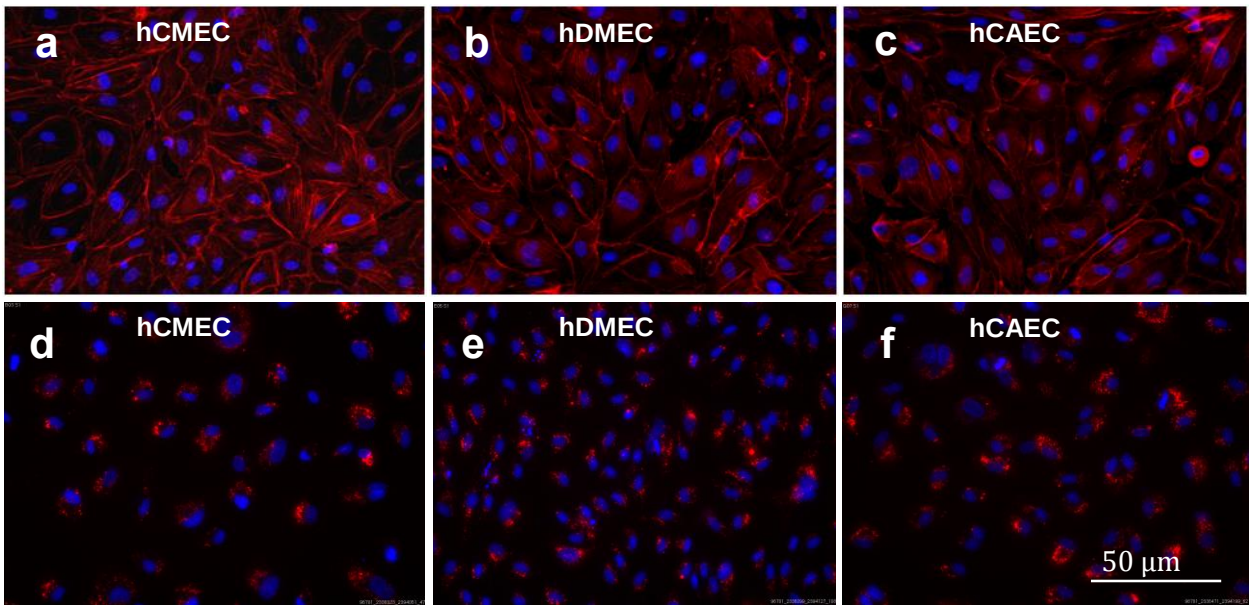

Figure 3.6 Visualisation of endothelial confluency and acLDL uptake.

Endothelial cells were seeded on gelatin-coated 96 well plates at their optimal seeding densities (see *section 3.2.3*) and incubated for 3 days in endothelial FGM. Cells were then monitored at 24 h intervals over 5 consecutive days (only final day of treatment period shown here) for F-actin and acLDL uptake. (a) hCMEC, (b) hDMEC and (c) hCAEC were fixed with 3.7% (v/v) formaldehyde and stained with phalloidin 647 and Hoescht 33342 for F-actin and nuclei, respectively. (d) hCMEC, (e) hDMEC and (f) hCAEC were stained for acLDL uptake and nuclei (Hoescht 33342), the cells were imaged at the TRITC and DAPI wavelengths. *hCMEC, human cardiac microvascular endothelial cells; hDMEC, human dermal microvascular endothelial cells; hCAEC, human coronary artery endothelial cells; FGM, full growth media; acLDL, acetyl low-density lipoprotein.* Representative images of triplicate samples. Scale bar represents 50 μm.

3.3 Development of primary human fibroblast monolayer models

3.3.1 Optimisation of seeding density in fibroblast FGM

Again the aim of these model optimisation experiments was to achieve a confluent fibroblast monolayer with reasonable cellular stability over the treatment period. Optimal cell number utility is beneficial both ethically and financially since these cells are primary sourced. Previous work with the endothelial monolayer models has allowed tight direction of these experiments. Both fibroblast models were developed in the manufacturers recommended full growth medias (FGM) to maintain consistency with the previously developed endothelial models; hCFs were cultured in F3 media (fibroblast growth medium 3 supplemented with 10% (v/v) foetal calf serum (FCS), basic FGF (1.0 ng/ ml) and human recombinant insulin (5 µg/ ml) and NhDFs were cultured in F2 media (fibroblast growth medium 2 supplemented with 2% (v/v) foetal calf serum (FCS), basic FGF (1.0 ng/ ml) and human recombinant insulin (5 µg/ ml), both purchased from PromoCell (Heidelberg, Germany).

hCFs were seeded into uncoated 96 well plates at densities of 6,000 and 8,000 cells well^{-1} in F3 media and incubated for 3 days as with the endothelial monolayer models. From day 3 for 5 consecutive days at 24h intervals, hCFs were stained with Hoescht 33342 and fluorescent images taken at the DAPI wavelength using an ImageXpress high content analysis system (MolecularDevices, Sunnyvale, CA, U.S.A., 20x objective). A seeding density which forms a confluent fibroblast monolayer with minimal cell number fluctuations was desired. Figure 3.7 shows hCF number was most stable between days 4 and 7 when seeded at a density of 6,000 cells well^{-1}; where as a steep rise and fall was displayed with a density of 8,000 cells well^{-1}. This corresponds with the seeding/ stability pattern displayed by the cardiac endothelial cells (hCMEC & hCAEC) suggesting the cardiac derived cell types share similar growth rates.

The growth rate of NhDFs was known to be significantly quicker than the endothelial and cardiac fibroblasts therefore a wider range of seeding densities was selected for optimisation, 1,500; 3,000; 5,500 and 8,000 cells well^{-1}. Again NhDFs were seeded into uncoated 96 well plates, this time in F2 media and incubated for 3 days as with the previous models. From day 3 for 5 consecutive days at 24h intervals, NhDFs were stained with Hoescht 33342 and fluorescent images taken at the DAPI wavelength using an ImageXpress high content analysis system (MolecularDevices, Sunnyvale, CA, U.S.A., 20x objective). Figure 3.7 shows NhDF number was most stable between days 4 and 7 when seeded at a density of 3,000 cells well^{-1}; this reduced cell number compared with the previous monolayer models reflects the increased growth rate of this cell type.

3.3.2 Fibroblast cellular stability over maximum treatment period

Having established the fibroblast optimal seeding densities of 6,000 and 3,000 cells well^{-1} for hCFs and NhDFs respectively, with a pre-incubation period of 4 days, mitochondrial staining and intracellular ATP content were monitored over the proposed treatment period to ensure reasonable cellular stability. Fibroblasts were seeded onto uncoated 96 well plates and incubated for 3 days. Every 24 h for 5 consecutive days mitochondrial health and intracellular ATP content were monitored. Figure 3.8 shows mitochondrial health was unchanged over the treatment period (days 4-7). ATP content relative to maximal ATP content shows an increase from days 4 and 5 to days 6 and 7, suggesting a population doubling has occurred during this time frame.

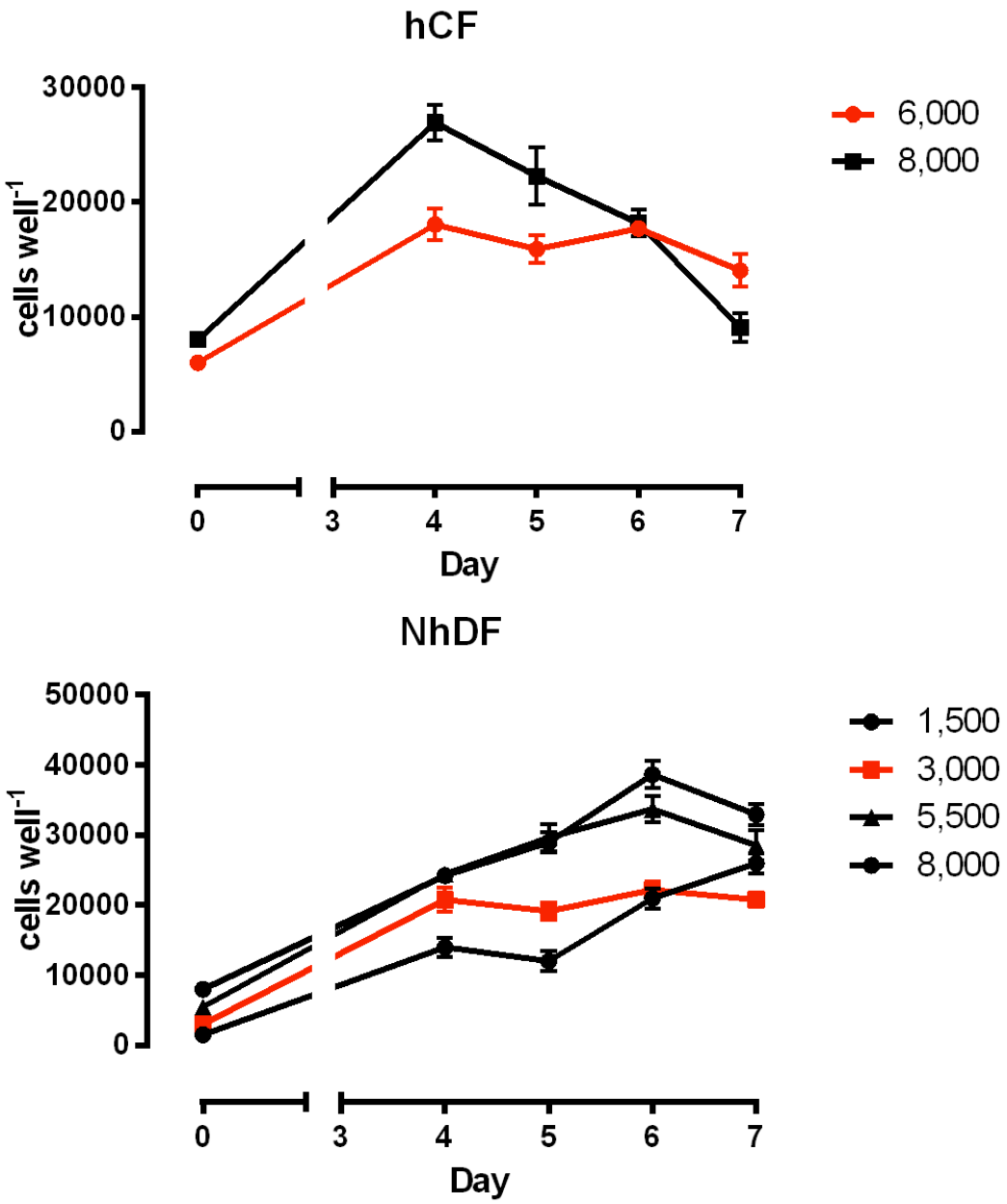

Figure 3.7 Optimisation of fibroblast seeding density.

Fibroblasts were seeded in 96 well plates at differing densities on day 0 and incubated for 3 days in their cell culture media. From day 3, cells were stained with Hoescht 33342 at 24 h intervals for 5 consecutive days and fluorescent images taken at the DAPI wavelength using an ImageXpress high content analysis system (MolecularDevices, Sunnyvale, CA, U.S.A., 20x objective). From these images nuclei were counted to give the number of cells per well at each time point. Data shown is from a single experiment mean of n=6 with *SD error bars*. *hCF, human cardiac fibroblasts; NhDF, normal human dermal fibroblasts*

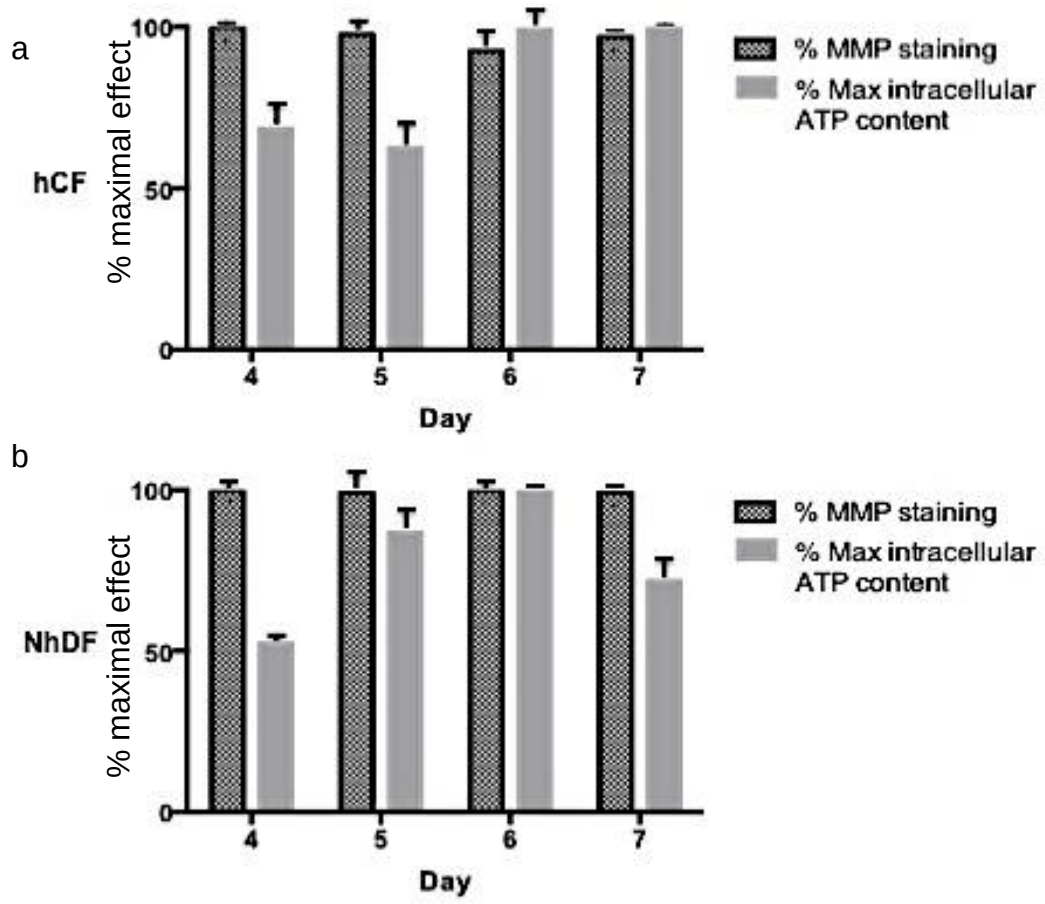

Figure 3.8 Fibroblast cell health over treatment period.

(a) hCF and (b) NhDF. Fibroblasts were seeded on uncoated 96 well plates at their optimal seeding densities (see *section 3.3.1*) and incubated for 3 days. Cells were then monitored at 24 h intervals over 5 consecutive days for various parameters of intracellular health. Red; cells were stained with MitoTracker and Hoescht 33 342 and imaged at the TRITC and DAPI wavelengths using an ImageXpress high content analysis system (Molecular Devices, Sunnyvale, CA, U.S.A., 20x objective). Automated algorithms were used to determine the percentage staining per cell. Blue; cells were lysed for intracellular ATP content using CellTiter-Glo reagent (Promega, Southampton, U.K.). Data shown is from a single experiment mean of n=6 with *SD error bars*. *hCF, human cardiac fibroblasts; NhDF, normal human dermal fibroblasts.*

3.3.3 Visualisation of fibroblast health, confluency and phenotype

Mitochondrial health was maintained throughout the treatment period for each fibroblast monolayer model as discussed in *section 3.3.2*. Figure 3.9 displays this mitochondrial staining (MitoTracker dye) alongside stained nuclei (Hoescht 33342), these figures (only treatment period shown) show the maintenance of a healthy monolayer of cells for each fibroblast model (hCF and NhDF) throughout the maximum treatment period of 72 h. This figure allows the confluency of the fibroblasts to be highlighted; both hCFs and NhDFs show a confluent monolayer with MitoTracker stain that was maintained over the treatment period. This figure also displays the significant heterogeneity between the two fibroblast cell types; NhDFs have a more spindle like cell morphology (figure 3.9b) compared to the larger more rounded hCFs (figure 3.9a).

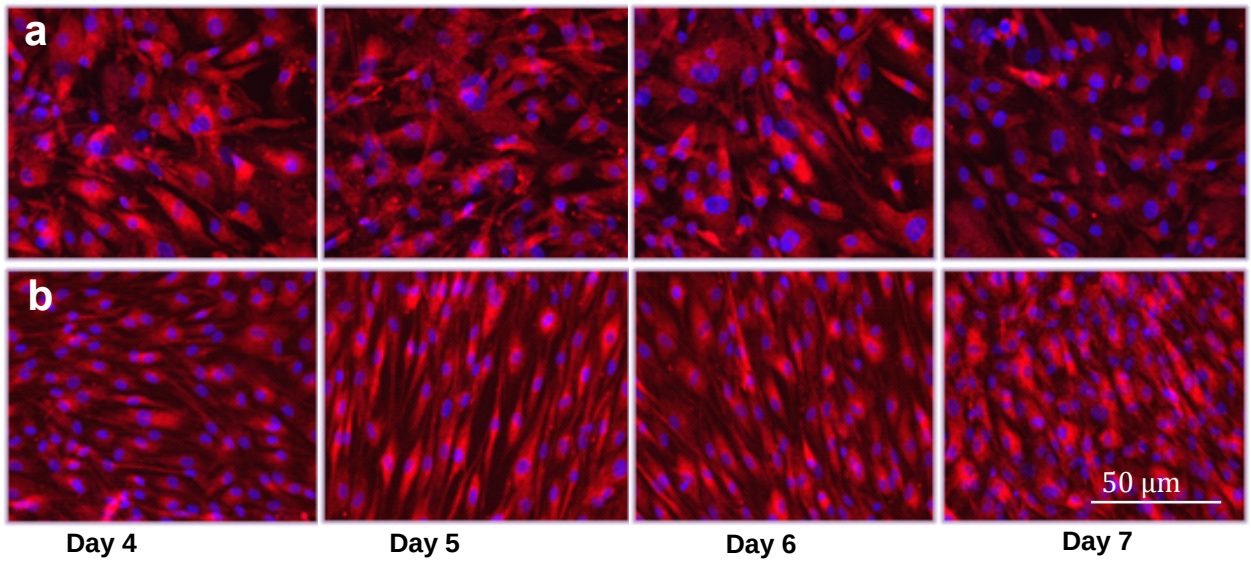

Figure 3.9 Visualisation of fibroblast mitochondrial health and confluency.

Fibroblast cells were seeded on uncoated 96 well plates at their optimal seeding densities (see *section 3.3.1*) and incubated for 3 days in F2/3 media. Cells were then monitored at 24 h intervals over 5 consecutive days (only 4 day treatment period shown here) for mitochondrial health. (a) hCF and (b) NhDF were stained with MitoTracker (shown in red) and Hoescht 33342 (shown in blue) and images captured at the TRITC and DAPI wavelengths using an ImageXpress high content analysis system (Molecular Devices, Sunnyvale, CA, U.S.A., 20x objective). Representative images of triplicate samples. Scale bar represents 50 μm.

Unlike the endothelial cells that display an endothelial specifc trait in the form of acLDL uptake that can be monitored with flourescently labelled acLDL, no active marker of fibroblast health is available and antibody/ gene markers of fibroblast specific phenotype are difficult to come by. In recent years, however, research has suggested that discoidin domain receptor 2 (DDR2) can be used as a specific marker to cardiac derived fibroblasts. Figure 3.10 shows immunofluorescent staining for DDR2 in hCFs.

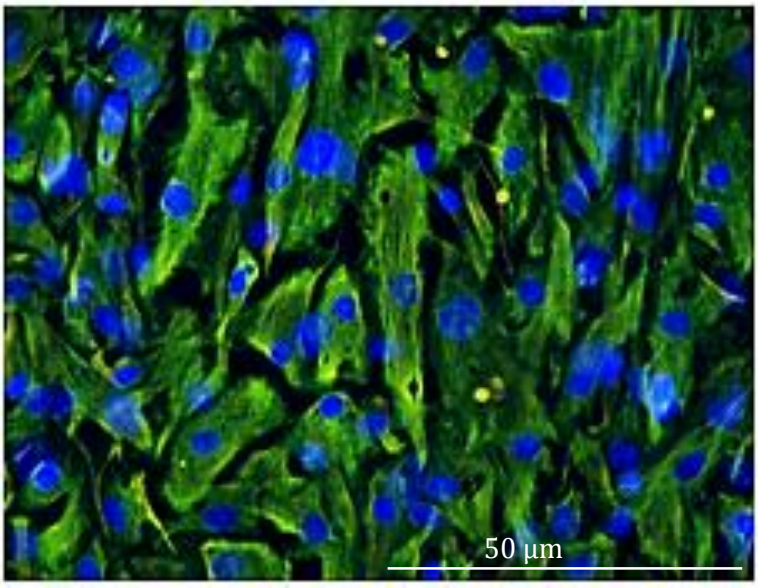

Figure 3.10 Immunofluorescent staining of DDR2 in hCFs.

hCFs were seeded on uncoated 96 well plates at 6,000 cells well^{-1} and incubated for 4 days in F3 media. Cells were then fixed for 20 mins in 3.7% (v/v) formaldehyde before undergoing immunofluorescent staining for discoidin domain receptor 2 (DDR2) (goat anti-human DDR2 antibody, donkey anti-goat Alexa fluor 488 antibody) and nuclei (Hoescht 33342). Images captured at the FITC and DAPI wavelengths using an ImageXpress high content analysis system (Molecular Devices, Sunnyvale, CA, U.S.A., 20x objective). *hCF, human cardiac fibroblasts.* Representative images of triplicate samples. At the same instrument settings no visible fluorescence from primary only or secondary only controls was visible. Scale bar represents 50 μm.

3.4 Development of microtissue models to study drug-induced cardiotoxicity

3.4.1 Cardiomyocyte- cardiac endothelial- cardiac fibroblast (CMEF) microtissue

The aim of 3D cell culture is to increase the physiological relevance of the cells microenvironment and therefore create an *in vitro* model which better recapitulates the *in vivo* tissue. The utilisation of a round bottom ultra low adhesion (ULA) cell culture plate means that cells have a higher affinity for cell-cell adhesion than culture plate adhesion and a microtissue forms at the bottom of the well. The fundamentals of this technique are similar to the more traditional hanging drop technique but with advantages in robustness and user handling. Figure 3.11 is a diagram summarising the protocol for multicell microtissue formation. The initial step in microtissue development is selection of cell seeding number; literature has suggested that approximately 1000 cells should form a microtissue of approximately 200 µm in diameter (Mehta *et al.*, 2012). This diameter is desirable to avoid a hypoxic centre when developing microtissues for drug safety assays. Figure 3.12 shows microtissue formation when seeded at 1000 and 500 cells well^{-1} using a 'general' starting ratio of 3 hESC-CMs: 1 hCFs: 1 hCMECs. This ratio using a higher proportion of cardiomyocytes was selected to account for the proliferation of the primary fibroblast and endothelial cells- work was later done to optimise this ratio. The primary cells were subcultured prior to detachment for cell counting and subsequent suspension with thawed and counted cardiomyocytes (see *materials and methods*). 100 ul of mixed cell suspension was added to each well of a 96 well round bottom ULA plate and incubated at 37^{o}C, 5% CO_2. After 2-3 days the cells have aggregated to form one microtissue in each well. Figure 3.12 shows that with 1000 cells in total the microtissues are surrounded by excess cells and cell debris, whereas with a total of 500 cells a microtissue of 200 µm forms with very few loose cells suggesting optimal use of cell numbers.

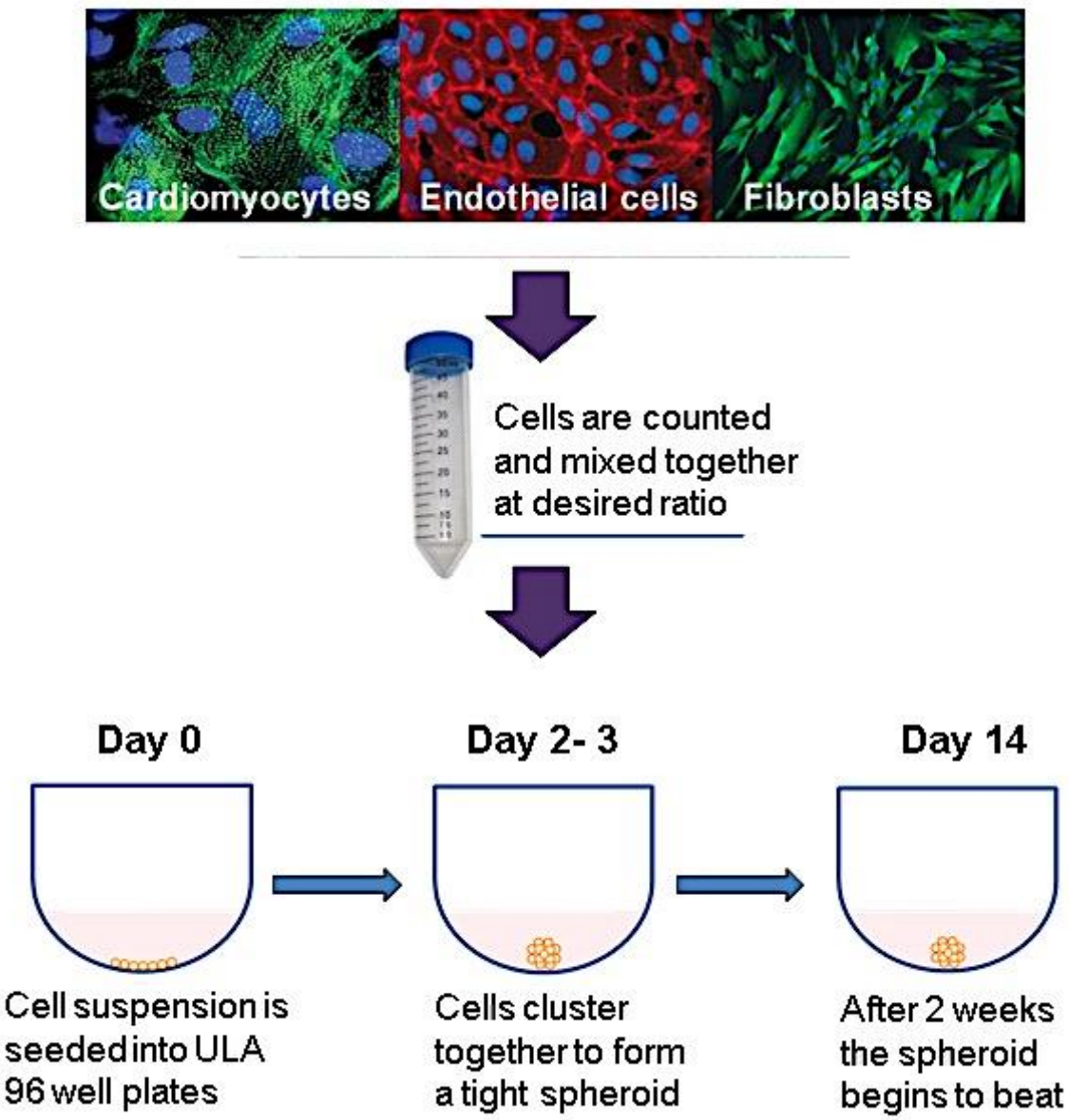

Figure 3.11 Diagram outlining the protocol for microtissue formation.

Endothelial and fibroblast cells are subcultured prior to microtissue formation. Primary cells are detached using Accutase solution at 37ºC for 5 mins, subsequently counted and mixed with a suspension of thawed and counted cardiomyocytes (see *materials and methods*). 100 µl of mixed cell suspension was added to each well of a 96 well round bottom ULA plate and incubated at 37ºC, 5% CO_2. After 2-3 days the cells have aggregated to form one tight microtissue in each well. After 2 weeks the microtissues spontaneously beat.

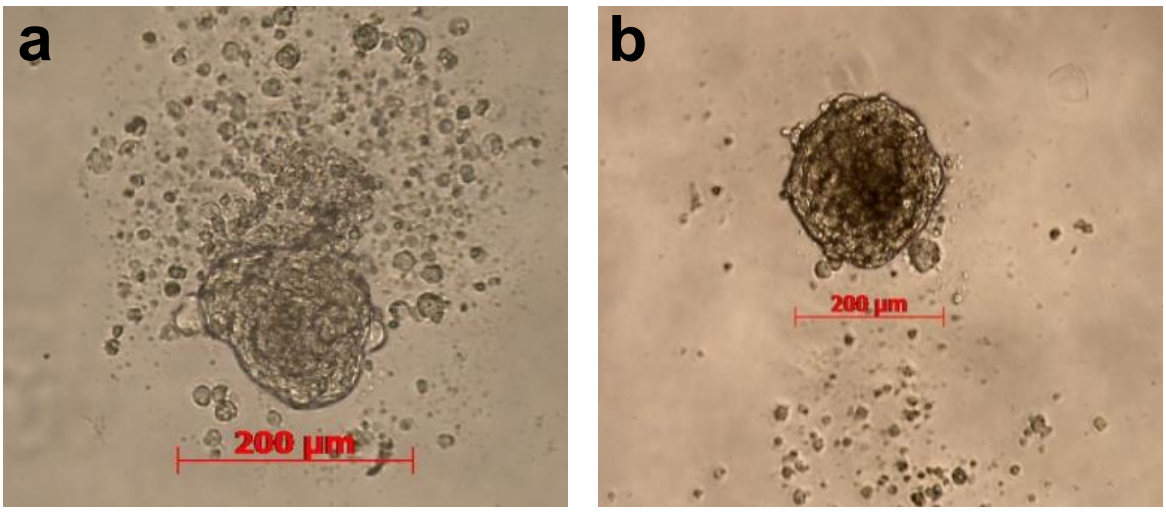

Figure 3.12 CMEF microtissues seeded at (a) 1000 cells well^{-1} and (b) 500 cells well^{-1}.

Endothelial and fibroblast cells are subcultured prior to microtissue formation. Primary cells are detached using Accutase solution at 37^{o}C for 5 mins, subsequently counted and mixed with a suspension of thawed and counted cardiomyocytes using a 'general' starting ratio of 3 hESC-CMs: 1 hCFs: 1 hCMECs (see *materials and methods*). 100 µl of mixed cell suspension was added to each well of a 96 well round bottom ULA plate and incubated at 37^{o}C, 5% CO_2 for two weeks. A full 96 well plate of each spheroid type was seeded to visualise variability across the plate. Images shown are representatives of the seeded plates. Microtissues imaged using a Leica DMLB microscope.

Using this total cell number (500 cells well^{-1}) the microtissue cell ratios could now be optimised with the aim of achieving a spontaneously beating vascularised microtissue displaying markers of each cell type and longevity. Literature suggests the myocardium comprises 70% non-myocytes with the majority of these being cardiac fibroblasts followed by cardiac microvascular endothelial cells (Brutsaert, 2003), this in combination with the proliferative nature of the primary cells was considered when selecting the cell ratios. Figure 3.13 summarises the trialled cell ratios (hESC-CMs: hCFs: hCMECs) and corresponding phase contrast image of the resulting CMEF microtissue. Various criteria

was used to select the optimal ratio; microtissue diameter of 200 μm, regular round shape, regular spontaneous contractions of ~1.5Hz, low cell debris/ excess cells and no visible necrosis/ hypoxia. Each ratio forms a microtissue of approximately 200 μm with mostly uniform shaping. A ratio of 4 hESC-CMs: 2 hCFs: 1 hCMEC was selected as it forms microtissues with the least debris, no visible necrosis, a consistent regular spontaneous contraction of approximately 1-1.5Hz (*see chapter five*) after incubation for 14 days and good uniformity across the 96 well plate. The alternative microtissue ratios displayed some of these criteria but with less consistency.

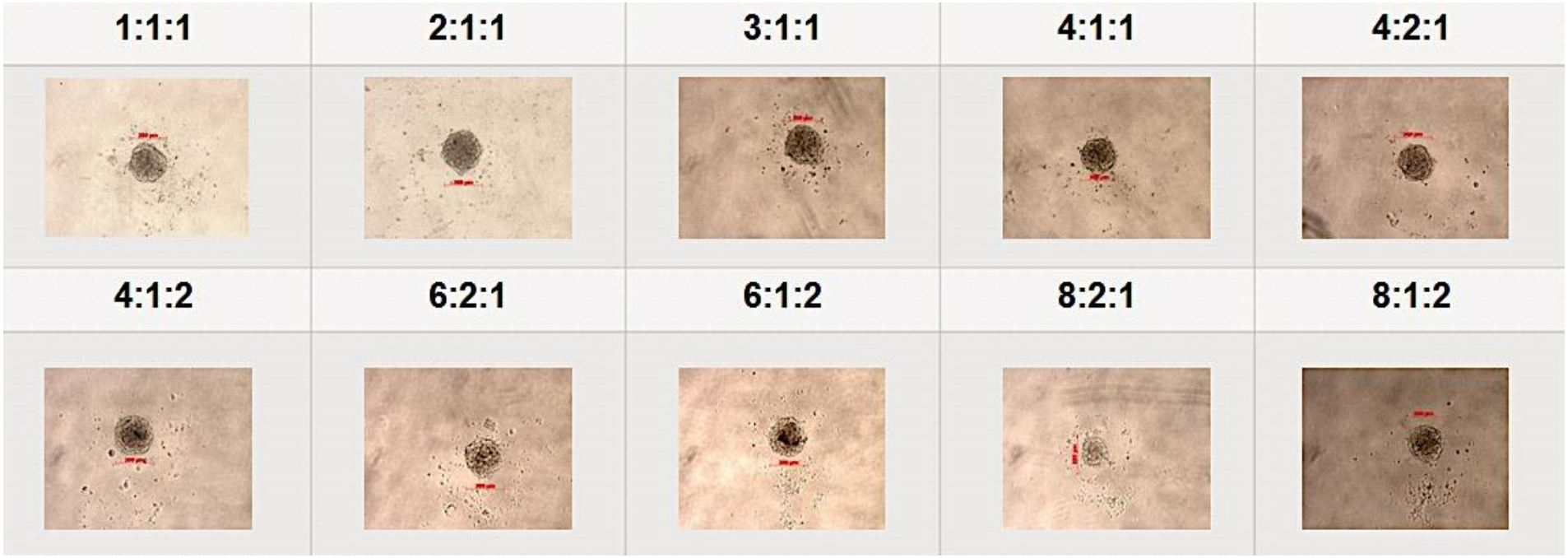

Figure 3.13 CMEF microtissues seeded at differing ratios of hESC-CMs: hCFs: hCMECs.

Endothelial and fibroblast cells are subcultured prior to microtissue formation. Primary cells are detached using Accutase solution at 37ºC for 5 mins, subsequently counted and mixed with a suspension of thawed and counted cardiomyocytes at the following ratios of hESC-CMs: hCFs: hCMECs; 1:1:1, 2:1:1, 3:1:1, 4:1:1, 4:2:1, 4:1:2, 6:2:1, 6:1:2, 8:2:1 and 8:1:2 (see *materials and methods* for more details on culturing techniques). 100 µl of mixed cell suspensions was added to each well of a 96 well round bottom ULA plate and incubated at 37ºC, 5% CO_2 for two weeks. Images were taken on day 14, when the uniform spontaneous beat was present, using a Leica DMLB microscope. Representative images of 16 microtissues per ratio type.

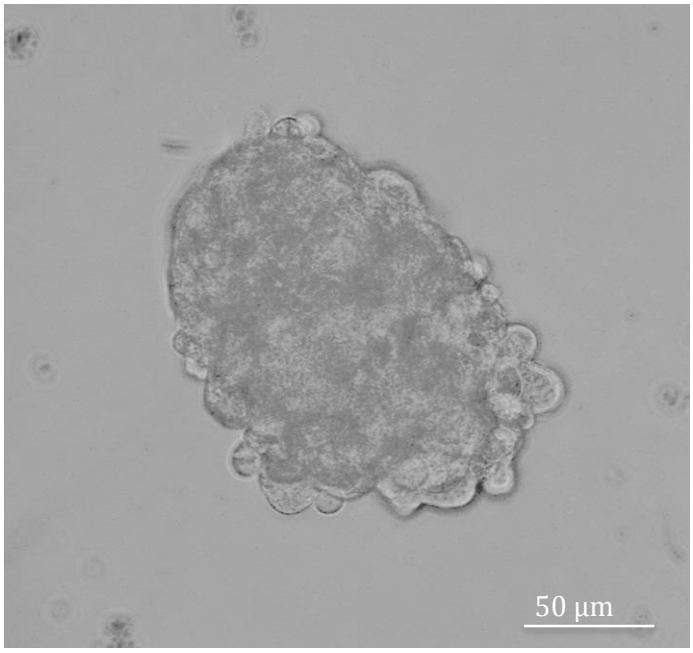

Figure 3.14 Phase contrast image of CMEF microtissue.

hCMECs and hCFs are subcultured prior to microtissue formation. Primary cells are mixed with a suspension of thawed and counted cardiomyocytes at a density of 500 cells well^{-1} and a ratio of 4 hESC-CMs: 2 hCFs: 1 hCMECs. 100 µl of mixed cell suspension was added to each well of a 96 well round bottom ULA plate and incubated at 37^{o}C, 5% CO_2 for two weeks. Microtissues imaged using a Leica DMLB microscope. Scale bar represents 50 μm.

Structural characterisation of CMEF microtissues (shown in figures 3.15 and 3.16) using cardiac troponin I (cTNI) as a cardiomyocyte specific marker, alpha actinin N2 to highlight myocyte striations, CD31 as a endothelial specific marker and collagen I as a relatively specific cardiac fibroblast marker was performed via wholemount immunofluorescence on 4% (v/v) formaldehyde fixed microtissues. This allowed visualisation of the cellular arrangement within the microtissue; good spatial distribution of the cell markers can be seen (Figure 3.15) suggesting adequate interactions of the different cell types in forming the microtissue. Figures 3.15 and 3.16 also display a higher abundance of myocyte striations than seen in the CM microtissues (Figure 3.21). Figure 3.16 shows a fixed CMEF microtissue immunofluorescently stained for cTNI, CD31 and the cardiac specific fibroblast marker discoidin domain receptor 2 (DDR2) at 20x and 40x objectives. At the 40x objective we can clearly visualise the arrangement of the cardiac troponin striations within the CMEF microtissue.

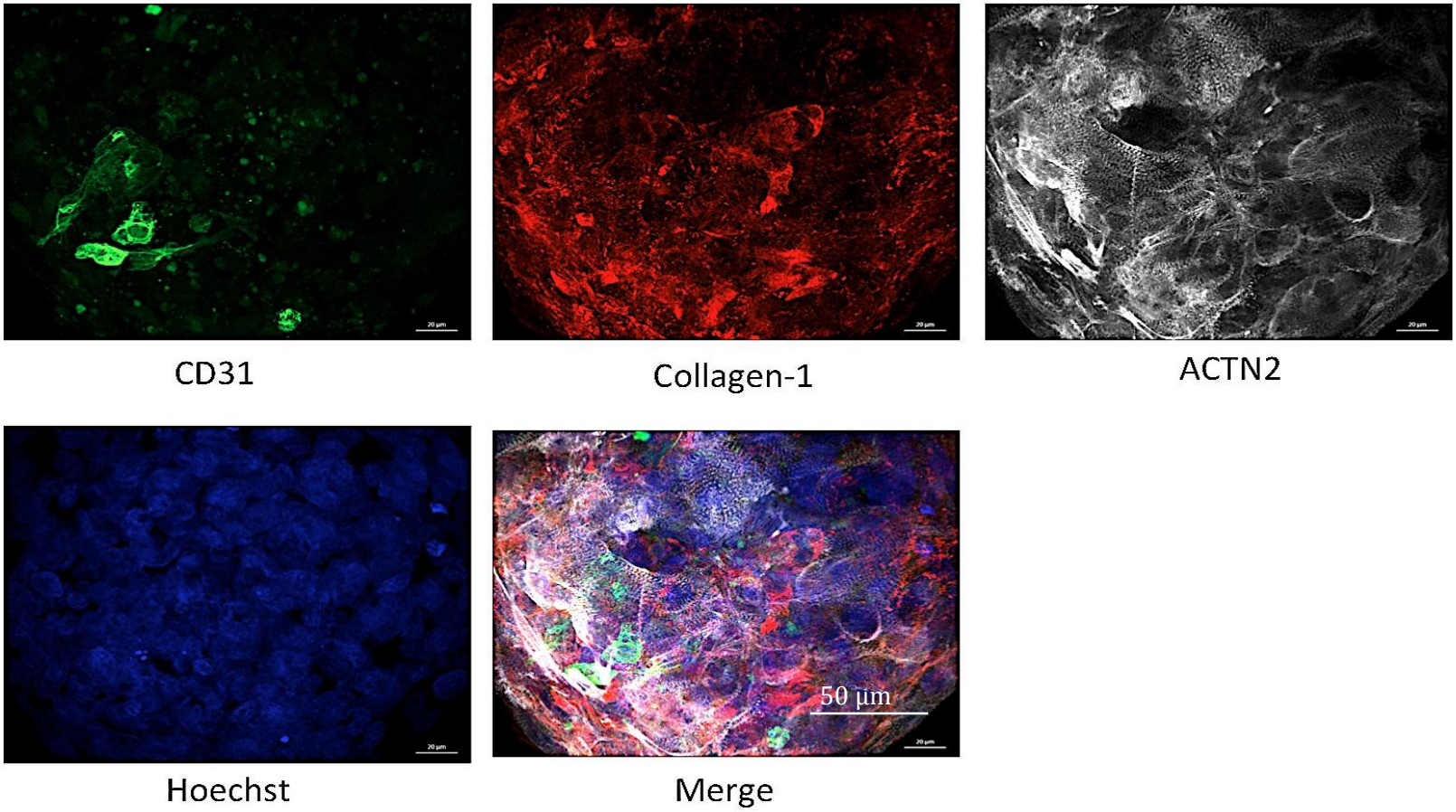

Figure 3.15 Structural characterisation of CMEF microtissues by immunofluorescent imaging.
hCMECs and hCFs are subcultured prior to microtissue formation. Primary cells are mixed with a suspension of thawed and counted cardiomyocytes at a density of 500 cells well^{-1} and a ratio of 4 hESC-CMs: 2 hCFs: 1 hCMECs. 100 µl of mixed cell suspension was added to each well of a 96 well round bottom ULA plate and incubated at 37^{o}C, 5% CO_2 for two weeks before formaldehyde fixation and staining with cell specific markers. CD31, endothelial marker; Collagen-1, fibroblast marker; sarcomeric alpha actinin 2 (ACTN2), cardiomyocyte marker; Hoescht 33342, nuclei stain. At the same instrument settings no visible fluorescence from primary only or secondary only controls was visible. *Immunofluorescence performed by Awel Williams (The University of Liverpool).* Scale bar represents 50 µm.

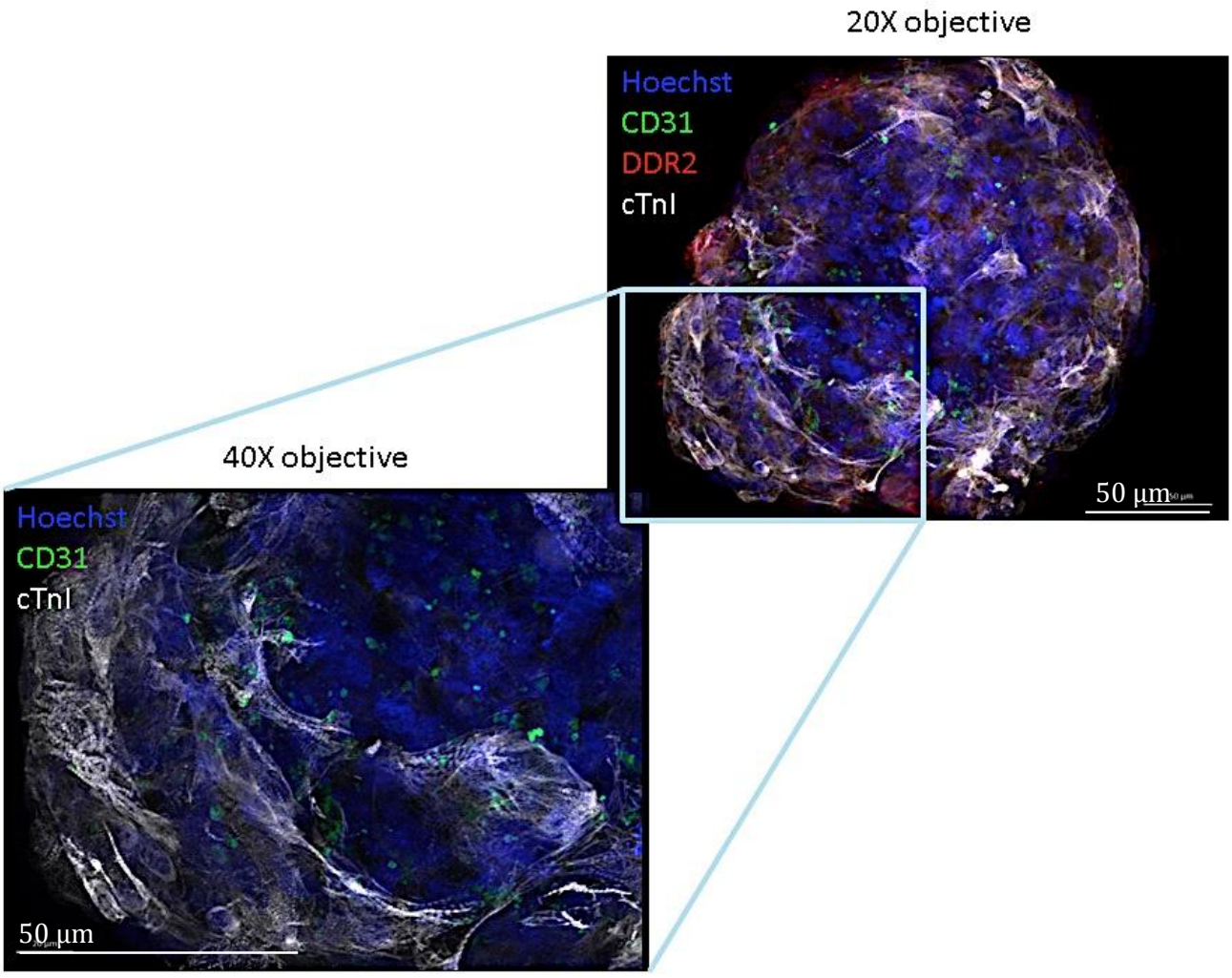

Figure 3.16 Visualisation of troponin striations within CMEF microtissues by immunofluorescent imaging.

hCMECs and hCFs are subcultured prior to microtissue formation. Primary cells are mixed with a suspension of thawed and counted cardiomyocytes at a density of 500 cells well^{-1} and a ratio of 4 hESC-CMs: 2 hCFs: 1 hCMECs. 100 µl of mixed cell suspension was added to each well of a 96 well round bottom ULA plate and incubated at 37ºC, 5% CO_2 for two weeks before formaldehyde fixation and staining with cell specific markers. CD31, endothelial marker; DDR2, cardiac fibroblast marker; cTNI, cardiomyocyte marker; Hoescht 33342, nuclei stain. At the same instrument settings no visible fluorescence from primary only or secondary only controls was visible. *Immunofluorescence performed by Awel Williams (The University of Liverpool).* Scale bar represents 50 µm.

3.4.2 Cardiomyocyte- dermal endothelial- dermal fibroblast (DMEF) microtissue

When investigating the role of cardiac endothelial and cardiac fibroblast cells in drug-induced cardiovascular toxicity, various control spheroids will be needed in order to establish any non-myocyte cell type and/ or tissue origin specific toxicity. An alternative tri-culture microtissue was developed containing hESC-CMs with dermal microvascular endothelial cells (hDMECs, previously used as a monolayer model, see section 3.2) and normal dermal fibroblasts (NhDFs, previously used as a monolayer model, see section 3.3) called a DMEF microtissue. These microtissues were formed using the same method as the CMEF microtissues; cell number total of 500 cells well^{-1} and a ratio of 4 hESC-CMs: 2 NhDFs: 1 hDMEC. Microtissues of 200 µm diameter, uniform round shape and spontaneous contractions formed after 14 days incubation. Figure 3.17 shows a phase contrast image of a representative DMEF microtissue taken using a Leica DMLB microscope at day 14. Morphologically no significant differences between these microtissues and the CMEF microtissues can be seen. Figure 3.18 shows the presence of dermal non-myocytes within the DMEF microtissues; hDMECs marked by CD31 expression and NhDFs marked by collagen-1 expression. Alpha actinin (ActN2) expression was used to highlight striations within the cardiomyocytes. DMEF microtissues display striations, however the level of organisation appears slightly reduced compared with CMEF microtissues (figure 3.16).

Figure 3.17 Phase contrast image of DMEF microtissue.

hDMECs and NhDFs are subcultured prior to microtissue formation. Primary cells are mixed with a suspension of thawed and counted cardiomyocytes at a density of 500 cells well^{-1} and a ratio of 4 hESC-CMs: 2 NhDFs: 1 hDMECs. 100 µl of mixed cell suspension was added to each well of a 96 well round bottom ULA plate and incubated at 37ºC, 5% CO_2 for two weeks. Microtissues imaged using a Leica DMLB microscope. Scale bar represents 50 μm.

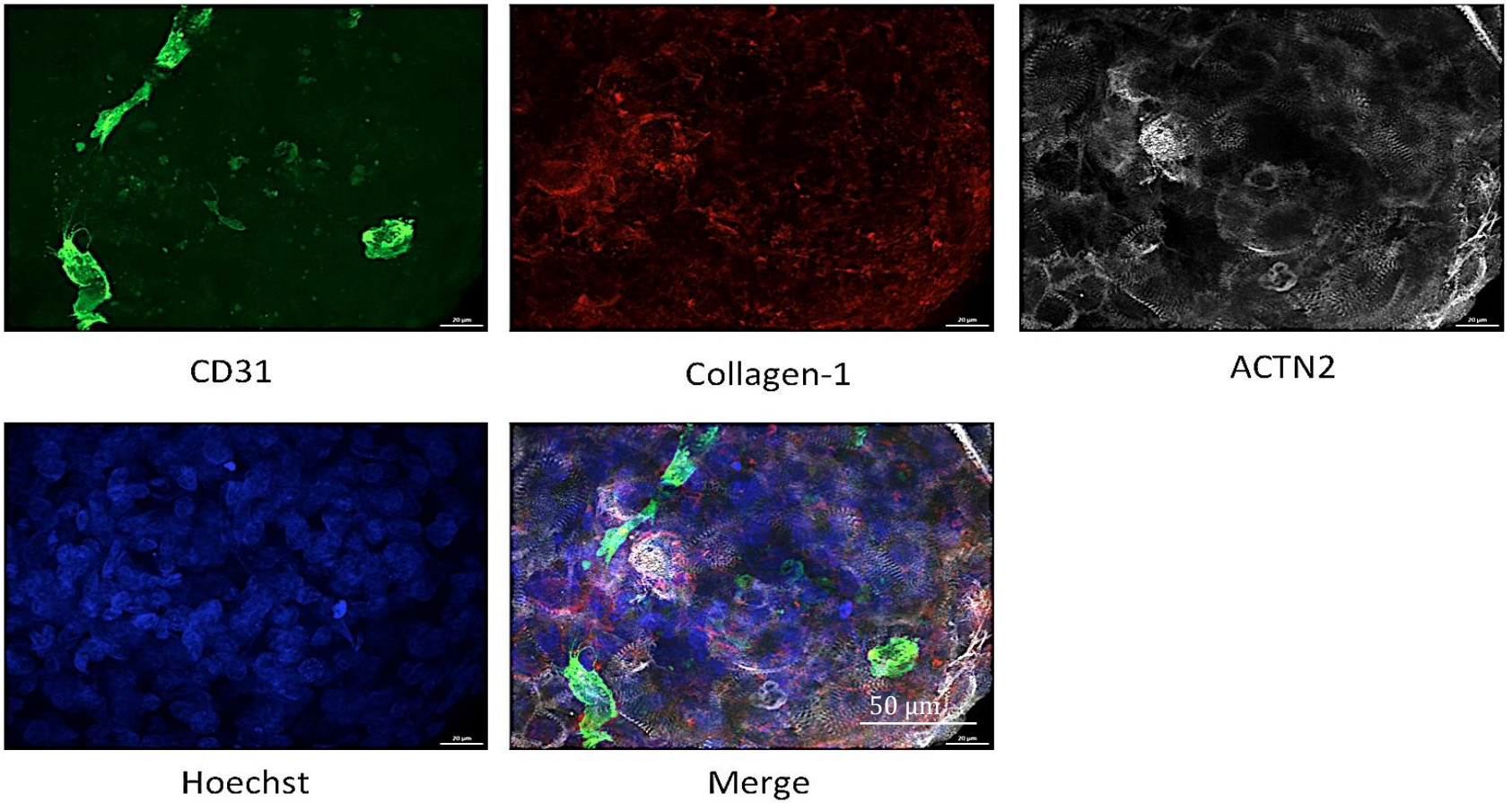

Figure 3.18 Structural characterisation of DMEF microtissues by immunofluorescent imaging.
hDMECs and NhDFs were subcultured prior to microtissue formation. Primary cells were mixed with a suspension of thawed and counted cardiomyocytes at a density of 500 cells well^{-1} and a ratio of 4 hESC-CMs: 2 NhDFs: 1 hDMECs. 100 µl of mixed cell suspension was added to each well of a 96 well round bottom ULA plate and incubated at 37^{o}C, 5% CO_2 for two weeks before formaldehyde fixation and staining with cell specific markers. CD31, endothelial marker; Collagen-1, fibroblast marker; sarcomeric alpha actinin 2 (ACTN2), cardiomyocyte marker; Hoescht 33342, nuclei stain. At the same instrument settings no visible fluorescence from primary only or secondary only controls was visible. *Immunofluorescence performed by Awel Williams (The University of Liverpool).* Scale bar represents 50 µm.

3.4.3 human ESC cardiomyocyte (CM) microtissue

The DMEF microtissue described above can be used to distinguish any differences between cardiac and dermal non-myocytes, a model comprising solely cardiomyocytes was required in order to highlight compound sensitivities brought about by the non-myocyte cells. A starting cell density of 1000 cells well^{-1} was used alongside 500 cells well^{-1} as this forms microtissues of 200 µm diameter in the tri-cultured instance and an additional density of 2000 cells well^{-1} was tested to account for the non-proliferative nature of the hESC-CMs. Figure 3.19 shows that 1000 cells well^{-1} forms a tight spheroid of 200 µm diameter with minimal cell debris, whereas the alternative densities do not efficiently aggregate to form good size microtissues.

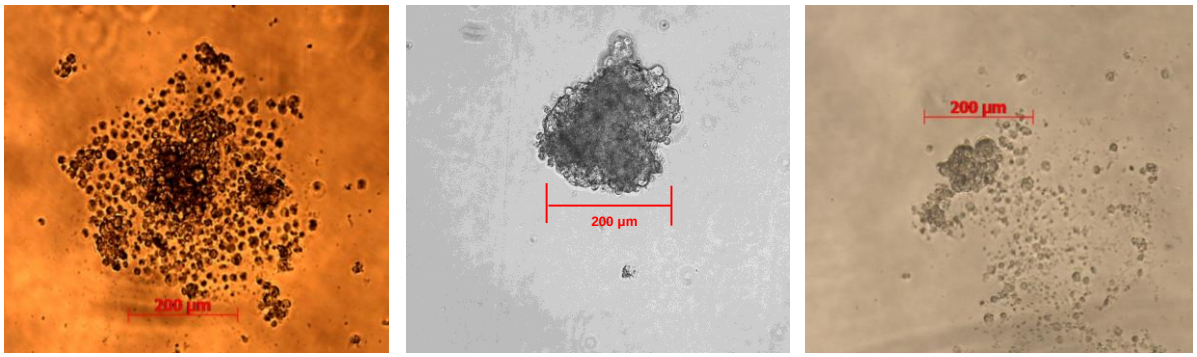

Figure 3.19 CM microtissues seeded at (a) 2000, (b) 1000 and (c) 500 cells per well.

A vial of hESC-CMs are thawed, counted and 100 µL of cell suspension seeded into 96 well round bottom ULA plate at densities of 2000, 1000 and 500 cells well^{-1} and incubated at 37^{o}C, 5% CO_2 for two weeks. Microtissues imaged using a Leica DMLB microscope.

hESC-CM microtissues have spontaneous contractions of ~1Hz after 14 days; slightly slower frequency that tri-cultured microtissues (see chapter 5 for functional analysis). CM microtissues also lack the smooth appearance displayed by the tri-culture spheroids suggesting the cells are not aggregating as strongly with solely cardiomyocytes, possibly due to a lack of extracellular matrix proteins normally secreted by fibroblasts. The CM microtissues display key cell markers;

immunofluorescence for the cardiac gap junction, connexin43 (GJA1) and cardiac troponin I (cTNI) shows gap junction formation and low levels of cardiac striations (figure 3.20). When immunostained for alpha actinin (ActN2) we also see low levels of striations (figure 3.21) compared with DMEF and CMEF microtissues (figure 3.16 & 3.18).

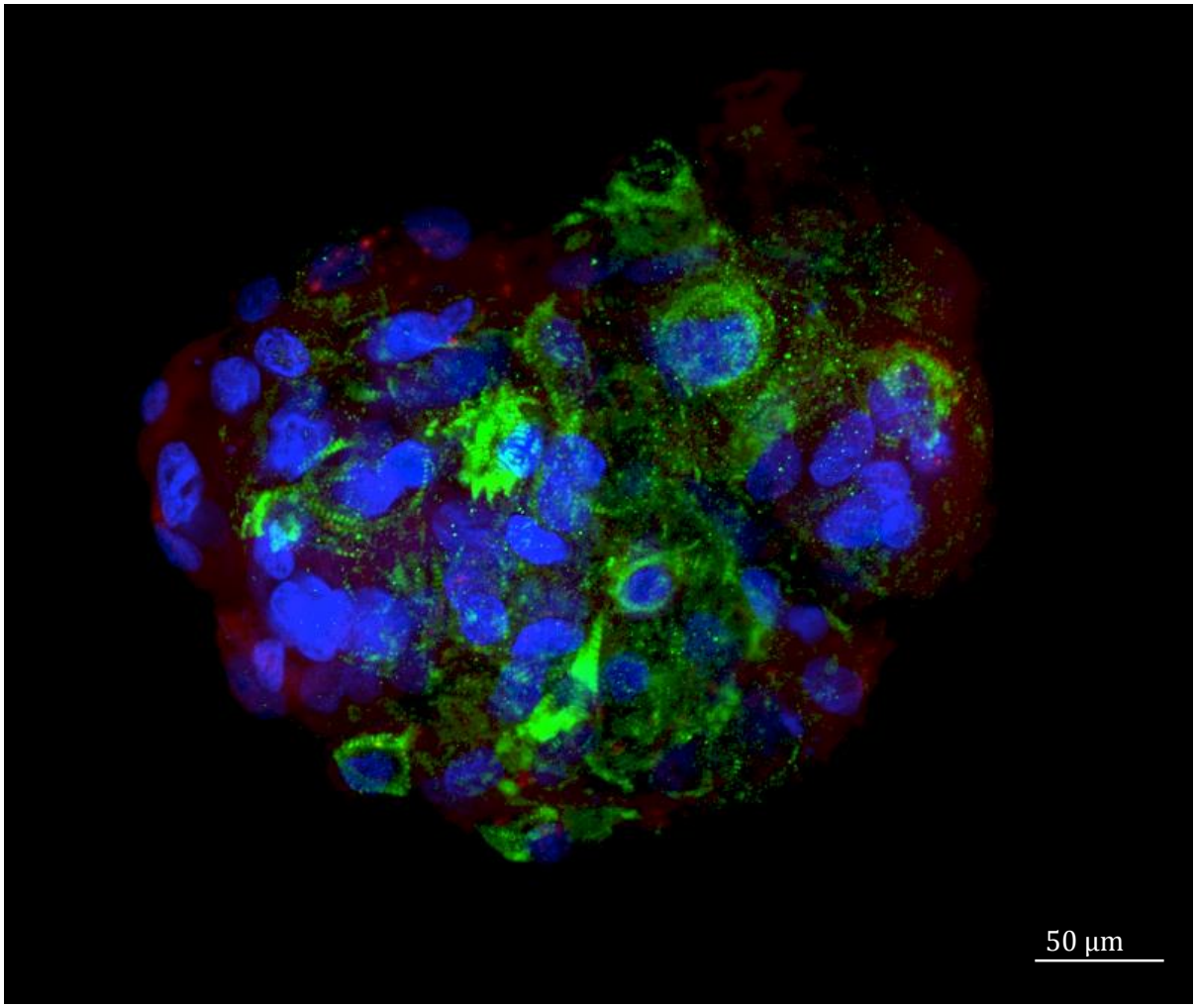

Figure 3.20 Structural characterisation of CM microtissues using immunofluorescent imaging.

A vial of hESC-CMs were thawed, counted and 100 µL of cell suspension seeded into 96 well round bottom ULA plate at a density of 1000 cells well^{-1} and incubated at 37ºC, 5% CO_2 for two weeks before formaldehyde fixation and staining for connexin43 showin in red, cTNI shown in green and nuclei shown in blue. At the same instrument settings no visible fluorescence from primary only or secondary only controls was visible. Scale bar represents 50 μm.

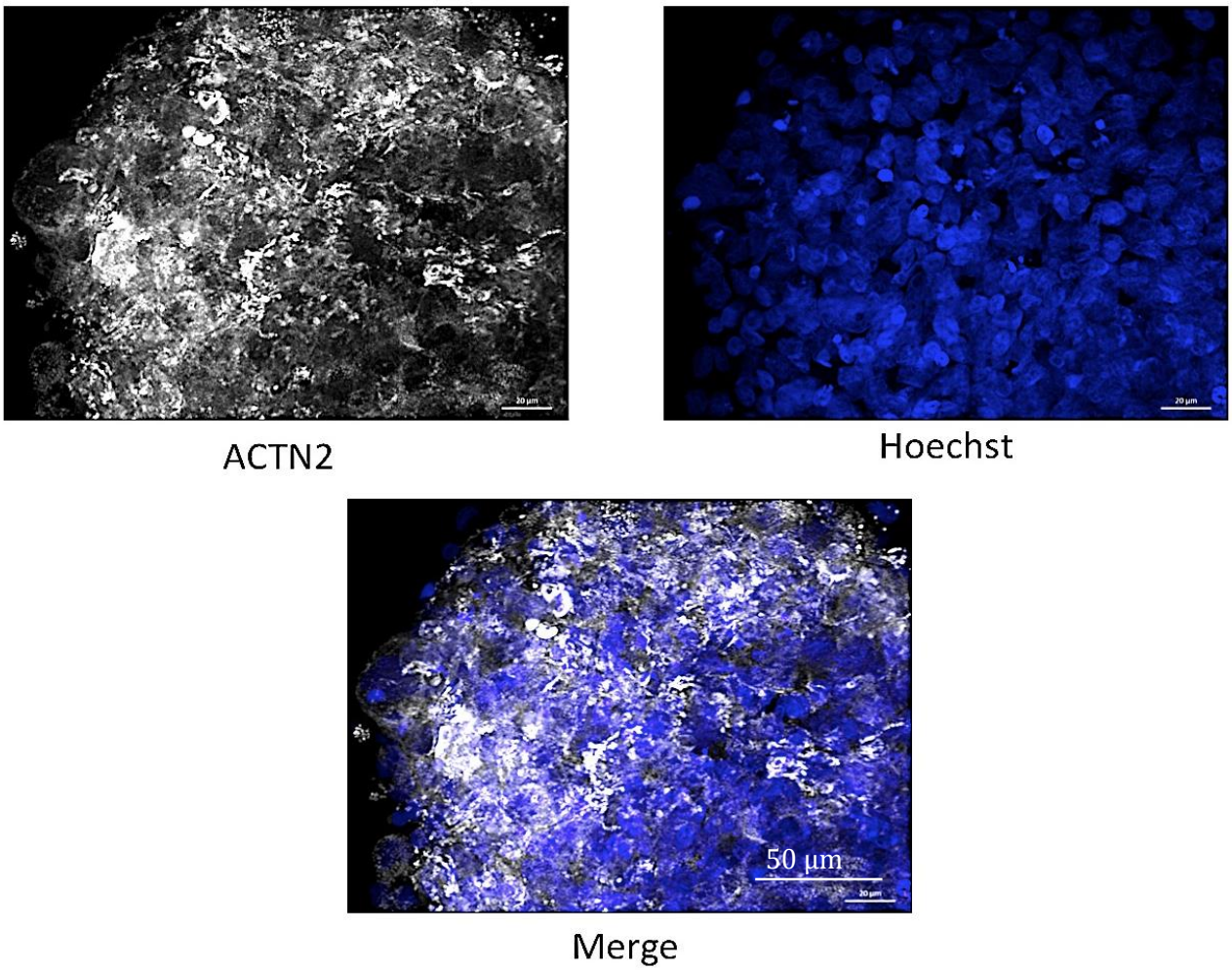

Figure 3.21 Structural characterisation of CM microtissues using immunofluorescent imaging.

A vial of hESC-CMs were thawed, counted and 100 µL of cell suspension seeded into 96 well round bottom ULA plate at a density of 1000 cells well^{-1} and incubated at 37ºC, 5% CO_2 for two weeks before formaldehyde fixation and staining for sarcomeric alpha actinin 2 (ACTN2) shown in white and nuclei shown in blue. At the same instrument settings no visible fluorescence from primary only or secondary only controls was visible. *Immunofluorescence performed by Awel Williams (The University of Liverpool).* Scale bar represents 50 µm.

3.4.4 Cardiomyocyte- cardiac fibroblast (CMF) and cardiomyocyte- cardiac endothelial (CME) microtissues

DMEF and CM microtissues can be used to study cardiac and non-myocyte affects respectively, di-culture models of hESC-CMs and either endothelial (hCMECs; CME microtissues) or fibroblast cells (hCFs; CMF microtissues) have subsequently been developed to distinguish between endothelial or fibroblast effects. A seeding density of 500 cells well^{-1} was selected based on previous development of the tri-culture models. Various different ratios of hESC-CMs to non-myocyte cell were tested (data not shown), microtissues form well with a ratio of 2 hESC-CMs: 1 non-myocyte. This 2:1 ratio differs slightly from the overall 4:3 ratio used for the tri-culture microtissues but has similarities in that extra cardiomyocytes were required to overcome the proliferative nature of the primary non-myocytes. Immunofluorescence of CD31 was used to highlight hCMECs within the CME microtissues (figure 3.22b,d) and DDR2 was used to highlight hCFs within the CMF microtissues (figure 3.22a,c). A spontaneous contraction was used to highlight cardiomyocyte cell health within the microtissues. Again, under phase contrast, very little morphological difference can be seen between the di-culture and tri-culture microtissues (figures 3.14, 3.17 & 3.22).

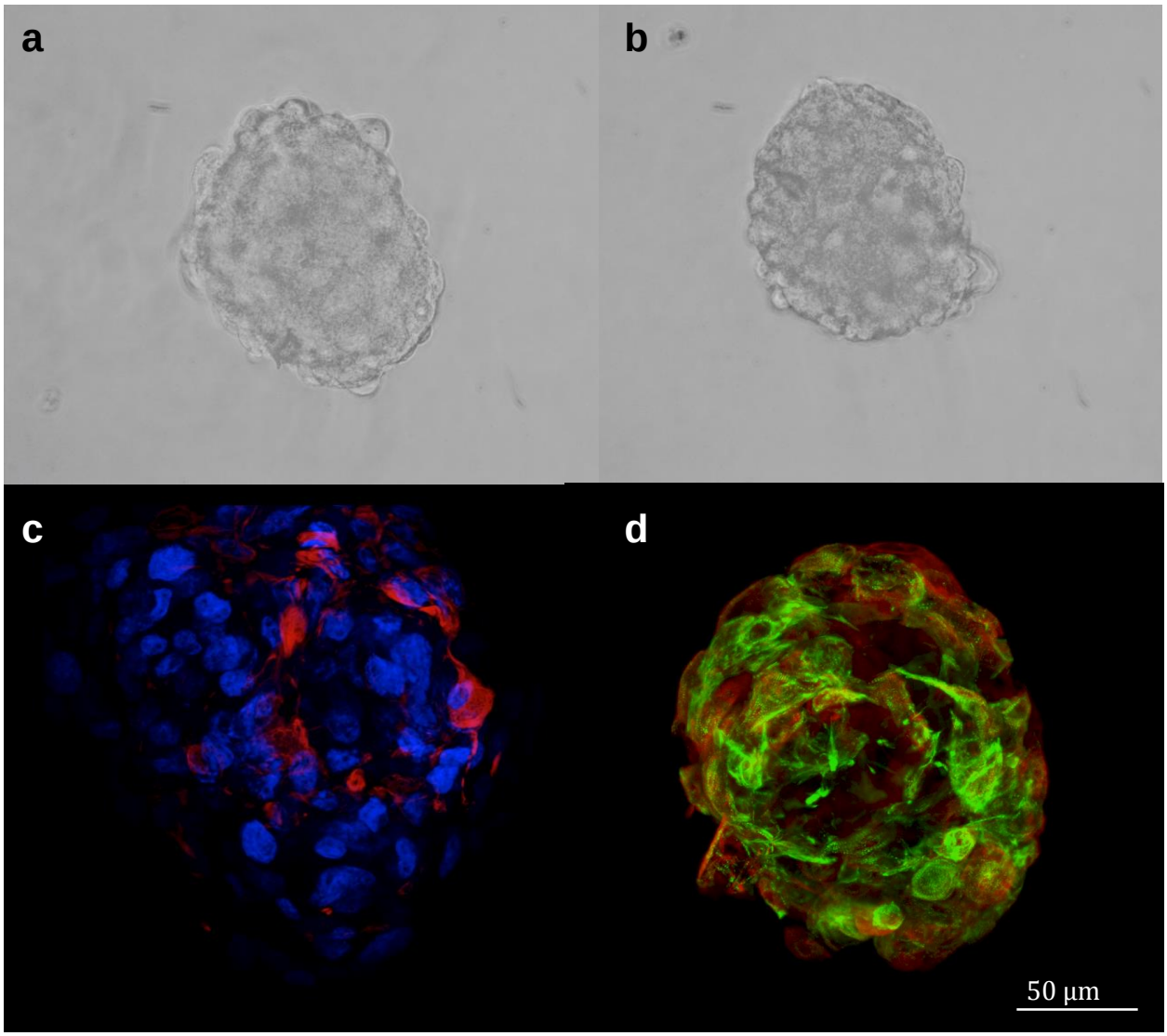

Figure 3.22 Structural characterisation of CMF & CME microtissues by phase contrast & immunofluorescent imaging.

hCMECs and hCFs were subcultured prior to microtissue formation. Primary cells were mixed with a suspension of thawed and counted cardiomyocytes at a density of 500 cells well^{-1} and a ratio of 2 hESC-CMs: 1 hCFs (CMF microtissue) or 2 hESC-CMs: 1 hCMECs (CME microtissue). 100 µl of mixed cell suspension was added to each well of a 96 well round bottom ULA plate and incubated at 37^{o}C, 5% CO_2 for two weeks before formaldehyde fixation and staining for cell specific markers. (a) Phase contrast image of CMF microtissue, (b) phase contrast image of CME microtissue, (c) Immunofluorecently labelled CMF microtissue displaying; DDR2, cardiac fibroblast marker shown in red and Hoescht, nuclei stain, shown in blue, (d) Immunofluorescently labelled CME microtissue displaying; CD31, endothelial marker shown in green and cTNI, cardiomyocyte marker shown in red. At the same instrument settings no visible fluorescence from primary only or secondary only controls was visible. Scale bar represents 50 µm.

3.4.5 Expression of cell marker genes in microtissue models

Cardiac troponin I gene TNNI3 was used as a cardiomyocyte cell marker alongside the connexin43 gene GJA1. The CD31 gene PECAM1 was used as an endothelial marker and the CD90 gene THY1 as a fibroblast marker. Total RNA was extracted and reverse transcribed into cDNA following which preamplification and qRT-PCR was performed. Figure 3.23 shows cell marker gene expression in individual cells, microtissue models and foetal heart tissue relative to adult ventricle tissue. This analysis shows each microtissue expresses similar levels of TNNI3 but less than adult ventricle. GJA1 expression was similar in all models. PECAM1 expression was approximately 10-fold higher in the CMEF model compared with all other microtissue models but still reduced compared with adult ventricle. THY1 expression was higher than adult ventricle in all microtissue models with CM microtissues sitting alongside foetal heart as the most upregulated models.

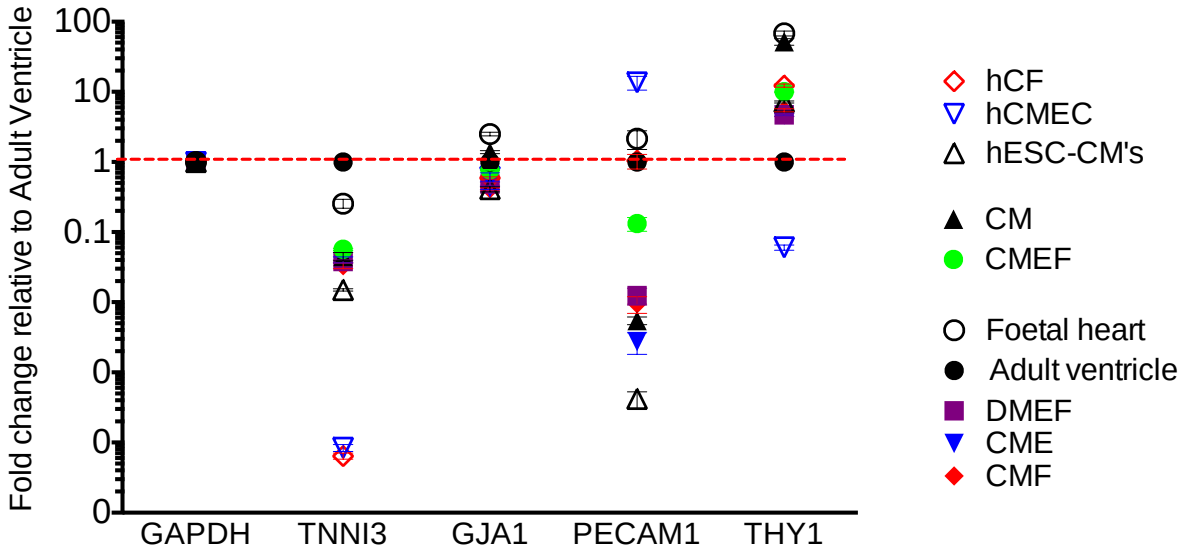

Figure 3.23 Expression of cell marker genes in microtissue models. Total RNA extracted using RNeasy mini kit (Qiagen, Crawley, U.K.). Total RNA was diluted to 20 ng and reverse transcribed using a SuperScript® III first-strand synthesis supermix kit (Life technologies). cDNA samples were preamplified using the TaqMan® PreAmp Master mix kit. QRT-PCR reactions were performed using TaqMan® Gene Expression probes and master mix to monitor amplification under standard cycling conditions. Gene expression is expressed as fold change relative to GAPDH and adult ventricle using the ΔΔ*C*T method. Fold change relative to adult ventricle is plotted for tissues, adult ventricle and foetal heart; microtissues, CMEF, DMEF, CM, CME and CMF; and cells, hESC-CMs, hCFs, hCMECs. Triplicate experiments of duplicate samples*, SD error bars.*

3.5 Discussion

The overall aim of this chapter was to develop *in vitro* cell based cardiac models for the study of drug-induced cardiovascular toxicity. As mentioned earlier routine cardiac safety screens primarily focus on cardiomyocytes in isolation, ignoring other cellular components of the myocardium such as the endothelial and fibroblast cells.

3.5.1 Microvascular cardiac, dermal and macrovascular endothelial monolayer models

Endothelial cells originating from the microvasculature of the human myocardium (hCMEC) have been used to generate a confluent and stable *in vitro* monolayer model which, as will be shown in the following chapter, enables the study of structural cardiotoxicity. The majority of current microvascular studies utilise endothelial cells originating from either dermal or umbilical sources since these tissues are often 'waste' products of plastic surgery or child birth. In recent years, however it has become increasingly apparent that the same cell type originating from different organs show considerable heterogeneity. While endothelial cells are united in certain common features, their heterogeneity is becoming increasingly apparent (Aird, 2007). For this reason monolayer models were developed using human dermal microvascular endothelial cells (hDMECs) and human macrovascular endothelial cells from the coronary artery (hCAECs).

Recently, data indicates that the embryological origin of macro- and microvascular endothelium are distinct; evidence suggests that microvasculature arises from vasculogenesis whereby angiogenesis is responsible for the creation of macrovascular segments (Suburo & D'Amore, 2006), suggesting we should perhaps expect to see closer similarities between the microvascular cells; hCMECs and hDMECs than the coronary artery cells; hCAECs. However optimisation of the endothelial seeding density shows more hDMECs are needed to achieve a stable confluent monolayer (8,000 cells^{-1} well compared to 6,000 cells well^{-1} for cardiac originating endothelial cells). In addition to this, the intracellular ATP content over the treatment period displays a very similar pattern in the cardiac endothelials (hCMEC & hCAEC) but differs to the dermal endothelials (hDMECs). The seeding density and

peak in ATP content at day five suggests the cardiac cells share the same proliferation rate. This data suggests that *in vitro* the cardiac originating endothelial cells, despite macro- and microvascular origins, may share more homogeneity than the microvascular endothelial cells (hDMECs & hCMECs). The significance of these differences with regard to compound toxicities are not yet known, but suggest that a dermal source of endothelial cells for drug screening is not suitable for a cardiac study.

A limitation to these monolayer models is the lack of any vascular structure. These models have been optimised to study structural cardiotoxicity using fluorescent-based imaging (high content biology- see *chapter four*) for which a monolayer of cells works optimally. It may only be upon the formation of a vasculature that the heterogeneity of the macro- and microvascular endothelial cells becomes apparent.

3.5.2 Cardiac and dermal fibroblast monolayer models

As with endothelial cells, fibroblast heterogeneity is also becoming increasingly apparent (Souders, 2009) and yet many studies utilise fibroblasts from dermal origins for a vast array of organ toxicity studies. Monolayer models of cardiac and dermal fibroblasts have been developed for structural cardiovascular toxicity assays in order to assess whether their suggested heterogeneity affects their prediction of structural cardiotoxicity. This will be assessed in chapter four.

Interestingly, the first clear difference between the fibroblasts is their morphology; the dermal fibroblasts have a spindle-like structure whereas the cardiac fibroblasts appear larger and rounder. This was surprising given that the endothelial cells showed no clear morphological differences. Secondly, the dermal fibroblasts (NhDFs) required a lower seeding density (3,000 cells well^{-1} as opposed to 6,000 cells well^{-1} for hCFs) suggesting a quicker proliferation rate. This data shows once again the heterogeneity between cells of cardiac and dermal origin.

3.5.3 Development of microtissues for drug-induced cardiotoxicity testing

Current preclinical *in vitro* models focus primarily on a single cell type cultured in a restrictive two-dimensional (2D) format only suitable for short-term toxicity studies due to rapid de-differentiation (Harmer et al., 2012; Pollard et al., 2010). In the past few years there have been significant advances in the field of *in vitro* three-dimensional (3D) cellular models. The environment created by a 3D culture model allows reconstitution of the natural cellular physiology by promoting the complex cell-cell and cell-matrix network communications found *in vivo* (Breslin & O'Driscoll, 2013). The utilisation of a round bottom ultra low adhesion (ULA) cell culture plate overcomes the handling difficulty of the traditional hanging drop technique while maintaining the same principles. Microtissues have advantages over other 3D cell culture techniques in that they allow the cells to position themselves into a 3D format of their chosing and can generally be formed using a lower cell number than monolayer and scaffold models allow.

The microtissues developed within this chapter show sutble differences in morphology. Firstly, the incorporation of fibroblasts into the spheroid models, whether cardiac or dermal derived fibroblasts, improves cell aggregation and therefore spheroid formation but also appears to visibly enable better synchronisation of the spontaneous contractions (discussed further in *chapter 5*). Since the main function of fibroblasts is to maintain the extracellular matrix (ECM) (Souders, 2009), which provides a scaffold for tissue formation *in vivo*, it is likely that they are using this ability to improve cell contacts during spheroid formation this could potentially help enable efficient conductance of the cardiomyocyte contractions. In addition to this role, cardiac fibroblasts are also becoming known for their electrocompetence. Recent findings suggest cardiac specific fibroblasts are capable of conducting electrical currents between cardiomyocytes (Kamkin *et al.*, 2005). Chapter five will cover functional analysis of the microtissues.

Immunofluorescent analysis of the microtissue models showed differences in striations. The cardiac tri-cultured CMEF microtissues show more elongated

striations than the dermal tri-cultured DMEF microtissues whose striations were less frequent and appeared shorter. During cardiomyocyte maturation the cells become larger and contractile machinery develops into a highly organised structure creating more defined striations throughout the cardiomyocyte (Robertson *et al*., 2013). Interestingly the CM microtissues show no clear striations, this was the first sign that co-culturing can promote cardiomyocyte maturation (discussed further in *chapter five*).

Disappointingly the microtissues displayed no obvious vascularisation when analysed by immunofluorescence. This could be due to the size of the microtissues; a microtissue of 200 μm was desired since sizes greater than this can develop hypoxic/necrotic centres. The small microtissue diameter means there is no requirement for a vascular system to transport oxygen or nutrients; therefore perhaps a larger microtissue is needed to induce vascularisation.

Curiously, all microtissue models only begin to spontaneously contract around 14 days post-seeding, whereas the hESC-CMs monolayer model begins to contract around 3-4 days post-seeding. During the 3-4 days post-seeding of the monolayer model, the cardiomyocytes are attaching to the tissue culture plates and setting up cellular interactions to form a synchronised monolayer. The increased time period of the microtissues could suggest the formation of more complex cell interactions.

3.5.4 Conclusion

This chapter has seen the development of dermal and cardiac non-myocyte monolayer models that can be utilized to study individual cell sensitivities to drug-induced cardiotoxcity but also the development of three dimensional (3D) microtissue models. Structural and gene expression analysis have shown these 3D models represent human *in vitro* models that better reconstitute the *in vivo* cellular physiology and can be used to provide improved *in vivo* relevance to our current *in vitro* toxicity assays. The use of these models will be discussed in chapters four and five.

Chapter Four

Sensitivity of non-myocytes to known structural cardiotoxins

4.1 Introduction

Numerous drugs are now being highlighted for their toxic effects upon non-myocyte cells (Ajithkumar *et al*., 2011; Gianni *et al.*, 2008; Mellor *et al.*, 2011; Minami *et al*., 2010; Palella, 2011; Senkus, 2011), although very little is known with regard to the cardiac microvasculature and its potential role in cardiotoxicity. Given the known heterogeneity of endothelial cells originating from different vascular beds and the increasing emergence of fibroblast heterogeneity research, the use of large-vessel or non-cardiac derived cells may provide relatively little useful information regarding cardiac toxicity. For example, angiogenesis is a process largely confined to the microvasculature therefore the *in vitro* study of human endothelial cells of microvascular origin, as opposed to large vessel endothelial cells, may enhance target relevance when considering the toxicity of kinase inhibitors designed to block tumour angiogenesis *per se*.

The first aim of this chapter will be to assess the sensitivities of human endothelial and fibroblast cells from cardiac (human cardiac microvascular endothelial cells, hCMECs and human cardiac fibroblasts, hCFs) and dermal origins (human dermal microvascular endothelial cells, hDMECs and human dermal fibroblasts, NhDFs) as well as endothelial cells from macrovasculature (human coronary artery endothelial cells, hCAECs) to highlight their capabilities in predicting drug-induced cardiovascular toxicities. The ultimate aim of this chapter will be to compare the structural cardiotoxin sensitivities of the myocardial non-myocytes (microvascular endothelial and fibroblasts) with those of the cardiomyocytes to gain a possible insight into the role of non-myocytes in drug-induced cardiovascular toxicity. In order to assess the sensitivities of the non-myocyte cells a high content biology approach combining a cytotoxicity assay previously developed by Pointon *et al* (Pointon *et al*., 2013) to successfully predict structural cardiotoxicity in hESC-CMs will be utilised.

High content biology (HCB) is essentially the visual monitoring of phenotypic changes within a whole cell, utilising fluorescent images as the basic unit of molecular discovery (Pointon *et al*., 2013). Various cellular and subcellular structures can be monitored simultaneously by utilising cellular dyes exhibiting fluorescence at different wavelengths. HCB is a popular choice for high-throughput drug screening due to the level of information that can be obtained from a single experiment. The

cellular and subcellular targets of toxicity and molecular mechanisms of toxicity are thought to vary from agent to agent. Currently the molecular mechanisms of structural cardiotoxins remain poorly understood. Mitochondrial damage either directly or indirectly (e.g. sorafenib) (Will *et al.*, 2008) is thought to be one major route of cellular toxicity. Endoplasmic reticulum (ER) stress (Kerkelä *et al.*, 2006; Minamino & Kitakaze, 2010) and disruption in calcium (Ca^{2+}) homeostasis are also thought to be important mechanisms of structural cardiotoxicity within the myocardium.

The final part of this chapter will utilise various microtissue models for assessment of intracellular ATP content following exposure to a set of known structural cardiotoxins. The aim of these experiments being to investigate compound sensitivities in an environment which permits interactions between the non-myocyte and myocyte cells.

4.2 Assay development

4.2.1 Compound classification

Compound classification of structural cardiotoxins was gathered using two commercially available clinical databases: Pharmapendium and Biowisdom. Classical terminologies for cardiac injury (i.e. cardiomyopathy, myocarditis, heart failure) were used to identify compounds in Pharmapendium with clinical adverse event reports for cardiotoxicity, whereas Biowisdom enables automated full-text searches of literature, again using the same classical terminologies. A compound was classified as a structural cardiotoxin if it was associated with structural cardiotoxicity in the two databases (Pointon *et al*., 2013). Additionally, all classifications were manually checked for the occurrence of structural cardiotoxicity in the FDA approval package. Therapeutic plasma exposure levels (C_{max}) were obtained from Pharmapendium for all compounds with the exception of fluorouracil (Bocci *et al*, 2000). For AstraZeneca's proprietary compounds, the classification was based on the occurrence of histopathological abnormalities in one month pre-clinical toxicology studies.

Compounds were selected that are chemically diverse representatives of the different classes of structural cardiotoxins. For example sunitinib malate and sorafenib tosylate are both tyrosine kinase inhibitors, however their specific targets differ. Doxorubicin and idarubicin were selected as representatives of the anthracycline family, while fluorouracil is the sole representative of the anti-metabolite family.

4.2.2 Controls: the effect of foetal calf serum and DMSO

Protein binding can have a marked effect upon compound distribution therefore the initial step in developing the toxicity assay was to establish whether the foetal calf serum (FCS) present within the cell culture media has a significant effect upon compound dose response; if protein binding is occurring then we would expect to see less sensitivity of the cell model when FCS is present. Sunitinib malate was selected as a representative of the kinase inhibitor family and doxorubicin as a representative of the anthracycline family of compounds. Both compounds are known to cause structural cardiotoxicity. hCMECs were seeded on gelatin-coated 96 well plates at 6,000 cells well^{-1} and incubated for 3 days before treatment with a 6-point concentration set of sunitinib or doxorubicin (100 – 0.032 μM) in endothelial full growth media (Endo FGM) which contains 5% FCS and endothelial serum free media (Endo SFM). An early time point of 6 h (figure 4.1a & b) and a late time point of 72 h (figure 4.1c & d) of compound treatment was performed, following which cells were lysed for intracellular ATP content using CellTiter-Glo reagent (Promega, Southampton, U.K.) as a measure of cytotoxicity. At the early and late time points, no difference in dose response can be seen for sunitinib or doxorubicin when 5% FCS is present; the data points correlate closely as do the IC_{50} values. Sunitinib has an IC_{50} of 10 μM and 2 μM at 6 h and 72 h, respectively, in both media conditions. Doxorubicin has an IC_{50} of 1 μM and 0.02 μM at 6 h and 72 h respectively, in both media conditions.

All structural cardiotoxins that were studied were reconstituted to a stock concentration of 20 mM in dimethyl sulfoxide (DMSO) and subsequently diluted in cell culture media to a final concentration of 0.5% (v/v) DMSO and top compound concentration of 100 μM. A 0.5% concentration of DMSO within the assay maintained compound solubility. A control experiment was performed to assess the toxicity of DMSO. hCMECs and hCFs were seeded in 96 well plates at their optimal seeding densities and incubated for 3 days in their full growth cell culture media (see *chapter 3* for model optimisation details). Cells were subjected to a range of DMSO concentrations (0.1, 0.25, 0.5, 0.75 & 1%) for 72 h, then lysed for intracellular ATP content using CellTiter-Glo reagent (Promega, Southampton, U.K.) as an indicator of cytotoxicity. Figure 4.1e shows intracellular ATP content relative to 0% DMSO for both hCMECs and hCFs after 72 h. 0.1, 0.25 and 0.5% DMSO show no significant decrease in ATP content in either cell type. Final DMSO concentrations higher than 0.5% (v/v) begin to decrease the relative cellular ATP content.

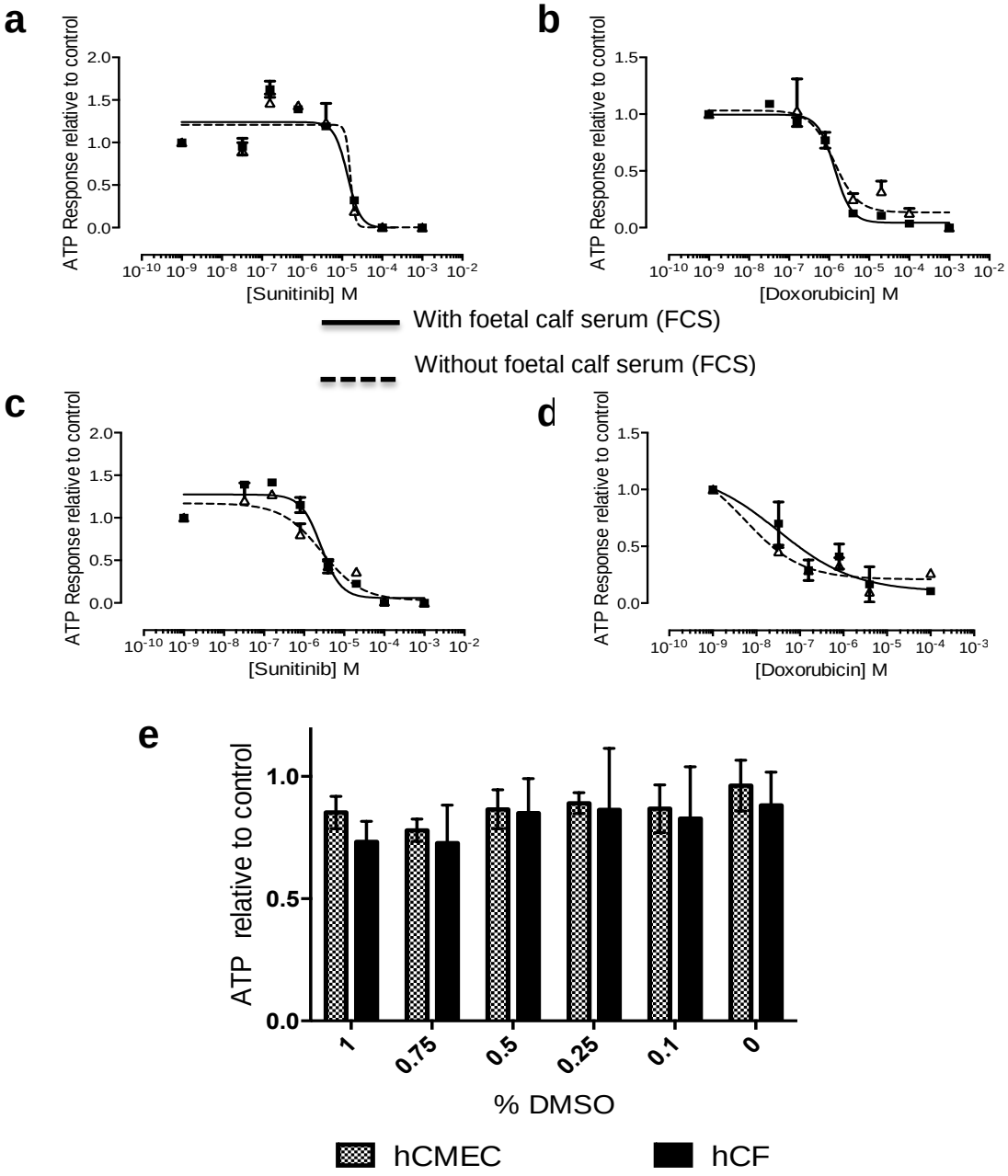

Figure 4.1 Assay controls: the effect of 5% FCS and DMSO.

hCMECs were seeded at 6,000 cells well^{-1} on gelatin-coated 96 well plates for 3 days. Cells were then treated with sunitinib (100 – 0.032 μM) for 6 h (a) and 72 h (b) or doxorubicin (100 – 0.032 μM) for 6 h (b) and 72 h (d) in endo FGM or endo SFM or (e) DMSO (0.1-1%) in endo FGM. Intracellular ATP content was assessed using CellTiter-Glo® luminescent cell viability kit (Promega, Southampton, U.K.) and luminescence was recorded using a Wallac 1450 Microbeta Trilux Scintillation Counter (PerkinElmer Life Sciences, Fremont, CA, U.S.A.). ATP values shown are relative to 0.5% DMSO control (a,b,c,d) or media without vehicle (e), single experiment mean of n=3 with SD error bars. *hCMEC, human cardiac microvascular endothelial cells. hCMEC, human cardiac microvascular endothelial cells; FCS, foetal calf serum; FGM, full growth media; SFM, serum free media.*

4.2.3 Assay work flow

All human primary cells studied (hCMECs, hCFs, hDMECs, hCAECs & NhDFs) were thawed from the manufacturers (PromoCell, Germany) cryovial and pre-cultured before seeding into black-walled 96 well plates (endothelial cells on gelatin-coated plates). Cells were incubated for 3 days at 37^{o}C, 5% CO_2 before compound treatment (see *materials and methods*). Following 6, 24 or 72 hour treatment, cells were stained with fluorescent dyes towards MMP, ER integrity, Ca^{2+} mobilisation and membrane permeability for 1 hour at 37^{o}C, 5% CO_2. Dye was then washed off and each well of cells fluorescently imaged using TRITC, FITC, DAPI and Cy5 filter settings on an ImageXpress high content analysis system (Molecular Devices, Sunnyvale, CA, U.S.A., 20x objective). Immediately after imaging cells were lysed for intracellular ATP content using CellTiter-Glo reagent (Promega, Southampton, U.K.). This cytotoxicity assay represents an additional measure of cell necrosis and apoptosis. Fluorescent images were analysed using metaXpress software (Molecular Devices, Sunnyvale, CA, U.S.A) to provide a series of measurements for each fluorescent probe; mean cell integrated intensity for each wavelength measured. The sum of these numerical measurements from 4 image fields within a single well was combined to give an overall quantification of each fluorescent signal from each well therefore each compound concentration. Dose response curves for ATP content and the HCB parameters were generated and used to calculate IC_{50} / EC_{50}'s. hESC-CMs data was obtained from Pointon *et al*., 2013. Figure 4.2 summarises this assay work flow.

4.2.4 Endothelial and fibroblast characterization

Acetyl low-density lipoprotein (AcLDL) uptake is a phenotype characteristic of endothelial cells, therefore all cell models were assessed for acLDL uptake at each assay time point to ensure endothelial phenotype (Data not shown; see *chapter 3* for more detail). Similarly, discoidin domain receptor 2 (DDR2) was used as a cardiac specific fibroblast marker to ensure cardiac phenotype of the hCFs (Data not shown; see *chapter 3* for more detail).

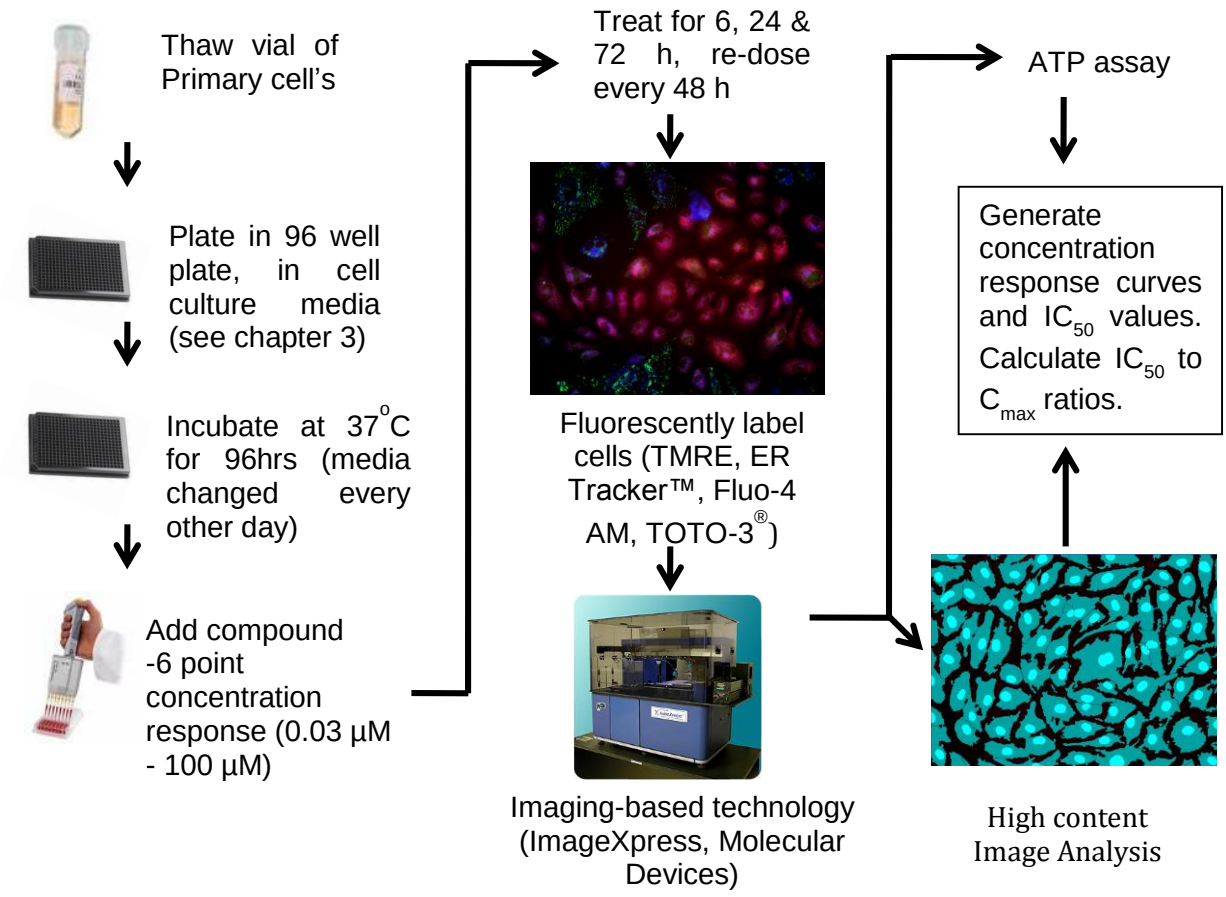

Figure 4.2 Assay work flow.

hCMECs, hCFs, hDMECs, hCAECs & NhDFs were thawed from the manufacturers (PromoCell, Germany) cryovial and pre-cultured before seeding into black-walled 96 well plates (endothelial cells on gelatin-coated plates). Cells were incubated with a 6-point concentration (0.03-100 µM) compound treatment for 6, 24 or 72 h then stained with fluorescent dyes towards Mitochondrial membrane potential (MMP), Endoplasmic Reticulum (ER) integrity, Ca^{2+} mobilisation (Ca^{2+}) and membrane permeability for 1 hour at 37ºC, 5% CO_2. Cells were fluorescently imaged using TRITC, FITC, DAPI and Cy5 filter settings on an ImageXpress high content analysis system (Molecular Devices, Sunnyvale, CA, U.S.A., 20x objective). Immediately after imaging cells were lysed for intracellular ATP content using CellTiter-Glo reagent (Promega, Southampton, U.K.).

4.3 Detecting structural cardiotoxicity in non-myocyte cells

4.3.1 Generating therapeutically relevant data from dose response curves

Each cell model (hCMEC, hDMEC, hCAEC, hCF and NhDF) was treated with a 6-point concentration set (100 – 0.032 μM) of each compound for 6, 24 or 72 h before being stained for MMP, ER integrity, Ca^{2+} mobilization and dead cells. Immediately after imaging the cells were lysed for intracellular ATP content using CellTiter-Glo reagent. Concentration-effect curves were plotted for each parameter of each compound treatment using GraphPad Prism (LA Jolla, CA) and expressed relative to vehicle (0.5% DMSO). Figure 4.3 shows representative fluorescent images of hCMECs displaying the effect of doxorubicin on fluorescent staining. With doxorubicin treatment a decrease in ER integrity (ER tracker) and mitochondrial membrane potential (MMP) (TMRE) fluorescence was seen while an initial increase in Ca^{2+} mobilization (Fluo-4 AM) was seen. Figure 4.4 shows cellular ATP content relative to control for each compound at each time point in hCMECs. As the dose response curves show in the case of some compounds i.e. sorafenib tosylate (IC_{50}), full toxicity can be predicted as early as 6 h since beyond this time point there was no significant shift in the dose response curve. For other compounds such as Doxorubicin, 72 h was needed in order to predict toxicity (IC_{50}). Figure 4.5 shows a similar trend for the high content biology (HCB) parameters. Here the most sensitive parameter either MMP, Ca^{2+} or ER integrity at each time point 6, 24 and 72 h is plotted for each compound. Figure 4.5 shows 72 h compound exposure is required to predict fluorouracil toxicity whereas 6 h exposure is adequate for Idarubicin toxicity. From the concentration- effect curves generated for each parameter, the molar concentration of test compound producing 50% inhibition (IC_{50}) or 50% response (EC_{50}) was generated (summary of IC_{50}'s for each cell type can be found in the appendix; *tables 1, 2 and 3*). In order to relate this therapeutically, all IC_{50} values were divided by the total C_{max} (see table 2.4, *materials & methods*) of the test compound to give the therapeutic index (TI); a ratio of the amount of therapeutic agent that causes the therapeutic effect to the amount that causes toxicity.

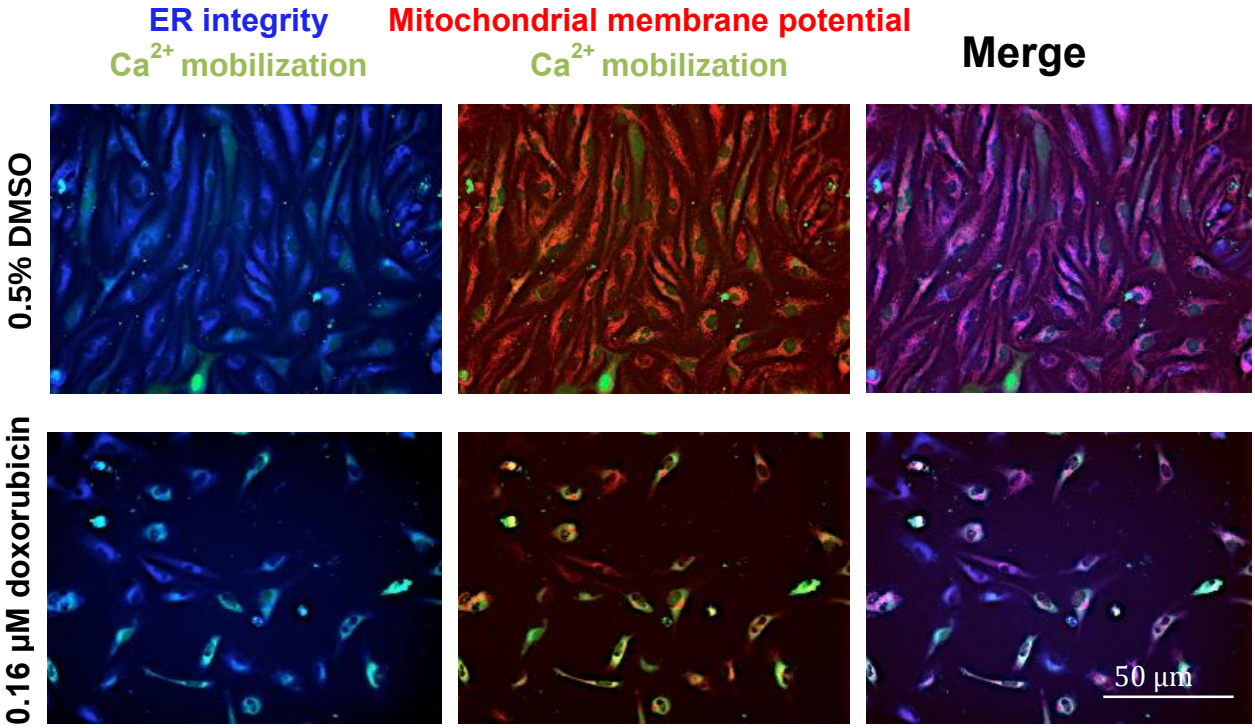

Figure 4.3 Representative images of hCMECs stained for MMP, ER integrity and Ca^{2+} mobilization following treatment with 0.16 µM doxorubicin.

hCMECs were seeded at 6,000 cells well-1 on gelatin-coated 96 well plates and incubated for 3 days in endo FGM before compound treatment. After 72 h, cells were incubated for 1 h in serum- free media with TMRE (30 pM) to measure MMP, ER-Tracker™ blue-white (1 nM) to measure ER integrity, Fluo-4 AM (1 nM) to measure Ca^{2+} mobilization and TOTO®-3 (1 nM) to indicate dead cells. Following staining, cells were subjected to automated live-cell fluorescent image acquisition using an ImageXpress high content analysis system (Molecular Devices, 20x objective). Fluorescent images were captured according to the optimal excitation and emission wavelengths of each probe. Red, Mitochondrial membrane potential (MMP); Blue, ER integrity; Green, Ca^{2+} mobilization. *TOTO-3 staining not shown due to high background levels in the absence of high cell death.* Representative images of duplicate samples over triplicate experiments. Scale bar represents 50 µm.

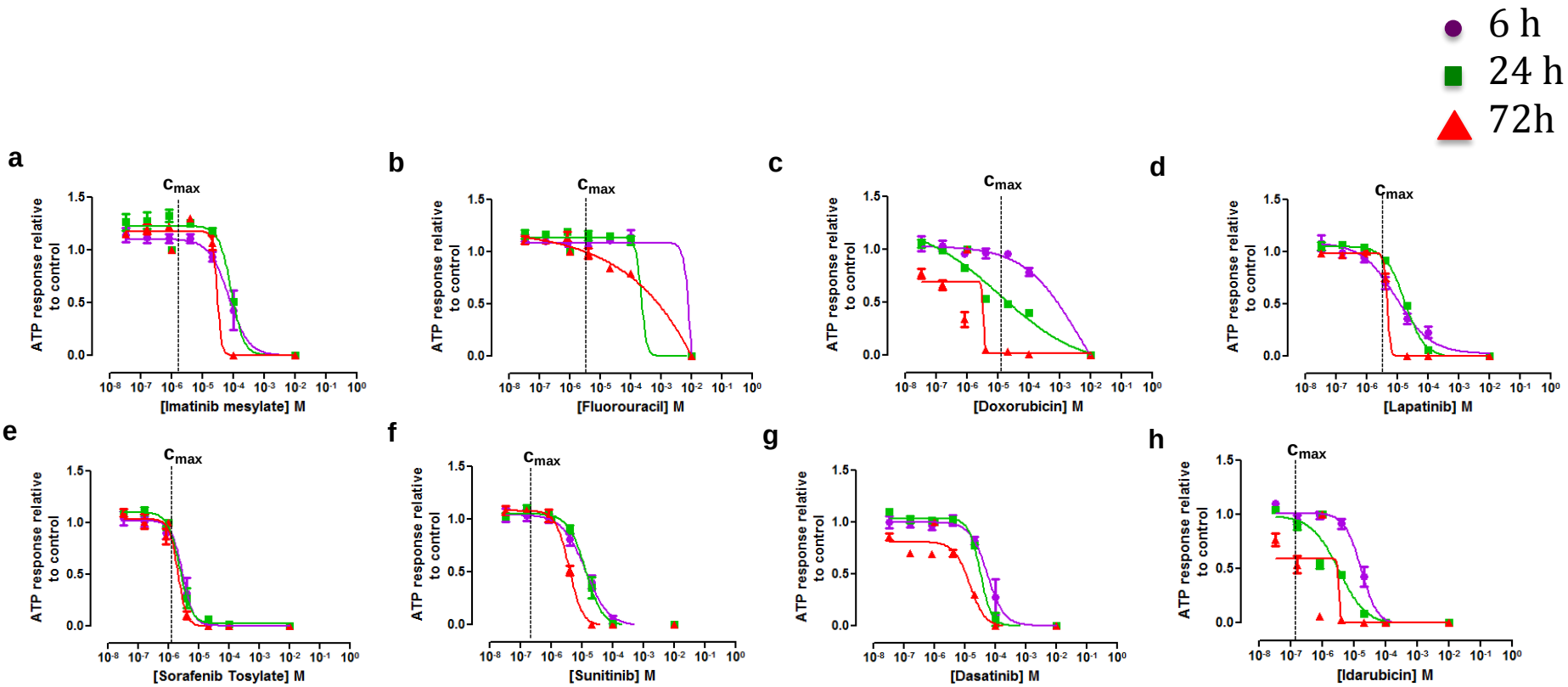

Figure 4.4 Intracellular ATP content concentration-effect curves for 8 structural cardiotoxins in hCMECs following 6, 24 and 72 h exposure.

hCMECs were seeded at 6,000 cells well^{-1} on gelatin-coated 96 well plates and incubated for 3 days in endo FGM before compound treatment. Cells were treated with a 6-point concentration set (100 – 0.032 μM) of either (a) imatinib mesylate, (b) fluorouracil, (c) doxorubicin HCl, (d) lapatinib, (e) sorafenib tosylate, (f) sunitinib malate, (g) dasatinib or (h) idarubicin for 6 (shown in purple), 24 (shown in green) and 72 h (shown in red) before being stained for MMP, ER integrity, Ca^{2+} mobilization and dead cells. The cells were lysed for intracellular ATP content using CellTiter-Glo reagent. Concentration-effect curves were plotted for all 8 compounds using GraphPad Prism (LA Jolla, CA) and expressed relative to vehicle (0.5% DMSO). Data represents the mean ATP measurements of duplicate wells on separate plates from three separate experiments for each timepoint. *hCMEC, human cardiac microvascular endothelial cells; FGM, full growth media. SD error bars.*

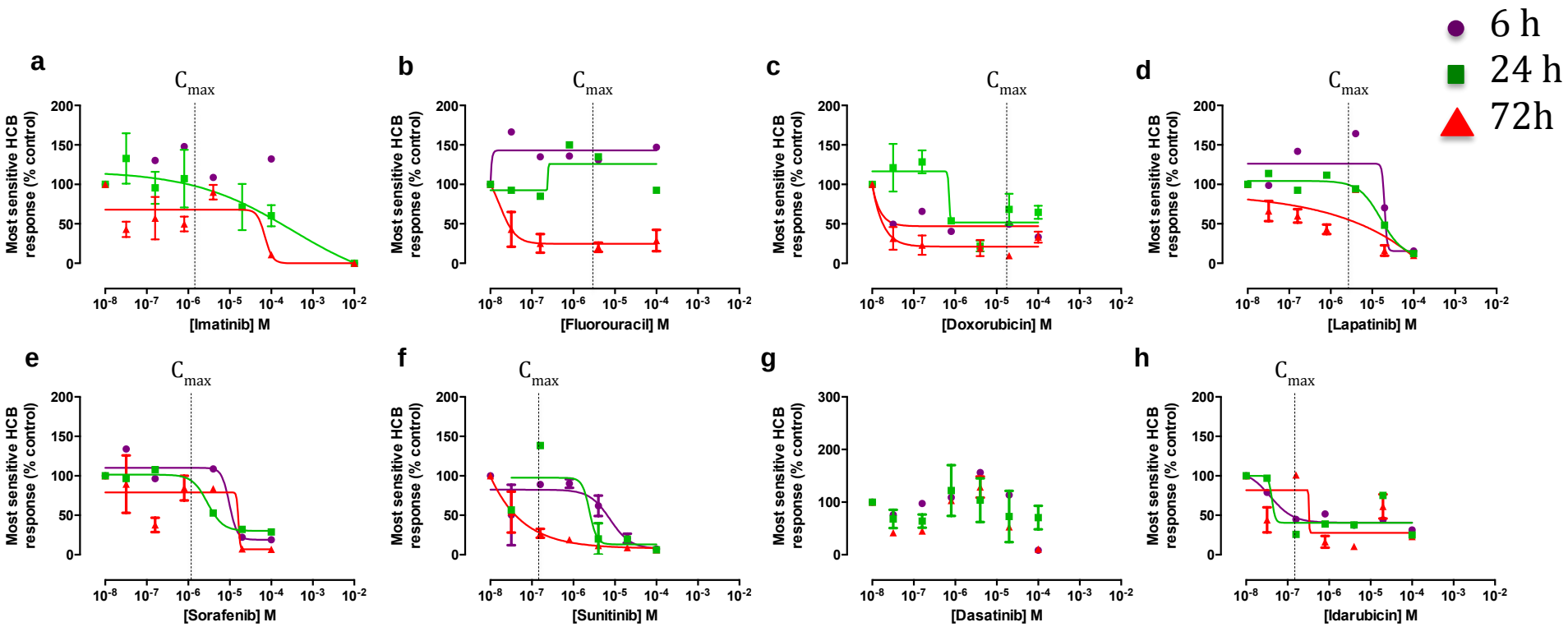

Figure 4.5 Most sensitive HCB parameter concentration-effect curves for 8 structural cardiotoxins in hCMECs following 6, 24 and 72 h exposure.

hCMECs were seeded at 6,000 cells well^{-1} on gelatin-coated 96 well plates and incubated for 3 days in endo FGM before compound treatment. Cells were treated with a 6-point concentration set (100 – 0.032 µM) of either (a) imatinib mesylate, (b) fluorouracil, (c) doxorubicin HCl, (d) lapatinib, (e) sorafenib tosylate, (f) sunitinib malate, (g) dasatinib or (h) idarubicin for 6 (shown in purple), 24 (shown in green) and 72 h (shown in red) after which cells were incubated for 1 hour in serum- free media with TMRE (30 pM) to measure MMP, ER-Tracker™ blue-white (1 nM) to measure ER integrity, Fluo-4 AM (1 nM) to measure Ca^{2+} mobilization and TOTO®-3 (1 nM) to indicate dead cells. Automated live-cell fluorescent image acquisition using an ImageXpress high content analysis system (Molecular Devices, 20x objective). Fluorescent images were analysed using metaXpress software (Molecular Devices, Sunnyvale, CA, U.S.A) to quantify mean cell integrated intensity for each wavelength measured. Concentration-effect curves were plotted using GraphPad Prism (LA Jolla, CA) and expressed relative to vehicle (0.5% DMSO) (n=3). The imaging parameter with the lowest IC_{50} is shown. Data represents the mean of duplicate wells on separate plates from three separate experiments for each timepoint. *hCMEC, human cardiac microvascular endothelial cells; FGM, full growth media. SD error bars.*

4.3.2 HCB combined with a cytotoxicity assay allows earlier prediction of toxicity

From the concentration- effect curves, all IC_{50} values were divided by the total C_{max} of the test compound to give the therapeutic index (TI); a ratio of the amount of therapeutic agent that causes the therapeutic effect to the amount that causes toxicity. A value of 1 arises when the IC_{50} concentration is equal to the C_{max} concentration for that compound. Only the compounds that have a therapeutic index (TI) below 1 have shown therapeutically relevant toxicity. For each test compound the TI of each parameter (MMP, ER, Ca^{2+} and ATP) was plotted as a dot plot showing each cell type (hCFs, NhDFs, hCMECs, hDMECs, hCAECs and hESC-CMs) at each time point (6, 24 & 72 h) using GraphPad Prism (La Jolla, CA) (figure 4.6-4.12) with a red line drawn to indicate a therapeutic index value of 1.

If we first consider the tyrosine kinase inhibitor imatinib mesylate (figure 4.6) whose pharmacological targets are Bcl-Abr, platelet-derived growth factor (PDGF) and c-kit, the most striking characteristic of this plot is the specific potency of imatinib in cardiac fibroblasts; after a 72hexposure imatinib has a TI value of 0.0001 in hCFs detected by MMP, ER and Ca^{2+}. This TI value is lower than all other cell types tested and the ATP parameter for hCFs (10,000 fold lower) and significantly lower than the TI displayed by hESC-CMs (TI; 10, p=0.0445). This differentiation between the HCB parameters and ATP shows early prediction of imatinib structural toxicity indicated by changes in MMP, ER integrity and Ca^{2+} mobilisation within the hCFs prior to gross cell death indicated by a loss of intracellular ATP.

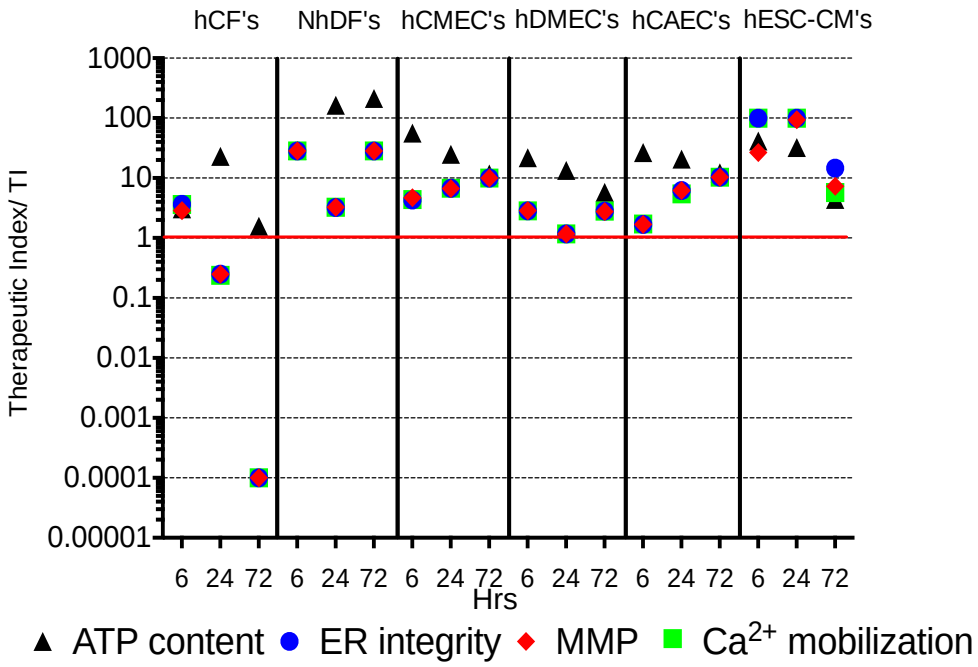

Figure 4.6 Therapeutically relevant toxicity of imatinib mesylate in endothelial, fibroblast and cardiomyocytes.

Cells were treated with a 6-point concentration set (100 – 0.032 μM) of imatinib mesylate for 6 h, 24 hand 72 h before being stained and imaged for MMP, ER integrity, Ca^{2+} mobilization then lysed for cellular ATP content using CellTiter-Glo reagent. Concentration-effect curves were plotted to calculate IC_{50} values, which were then divided by the total C_{max} to give the therapeutic index (TI). *hCF, human cardiac fibroblasts; NhDFs, normal human dermal fibroblasts; hCMEC, human cardiac microvascular endothelial cells; hDMECs, human dermal microvascular endothelial cells; hCAECs, human coronary artery endothelial cells; hESC-CMs, human embryonic stem cell derived cardiomyocytes*

Interestingly with lapatinib (figure 4.7), an epidermal growth factor receptor (EGFR) inhibitor, we see significantly enhanced sensitivity of all non-myocytes when compared with hESC-CMs at the 6 and 24 h timepoints ($p< 0.0001$). After at least 24 h exposure dermal fibroblasts (NhDFs) have shown structural changes with an overall TI value of ~ 0.02; approximately 10-fold less than cardiac fibroblasts (hCFs). A similar pattern exists between the endothelial cells; despite them showing less sensitivity overall, after 24 h lapatinib has induced changes in the ER integrity of the hDMECs with a TI value of 0.3, approximately 10-fold less than any parameter in the other endothelial cell

types (hCMECs & hCAECs). After 72 h this toxicity is reduced in relevance (TI; ~2), possibly due to a cell doubling, a caveat of the endothelial cell model. After a 72 h exposure to lapatinib the cardiomyocytes have also undergone changes in ER integrity in combination with Ca^{2+} mobilisation, once again prior to gross cell death.

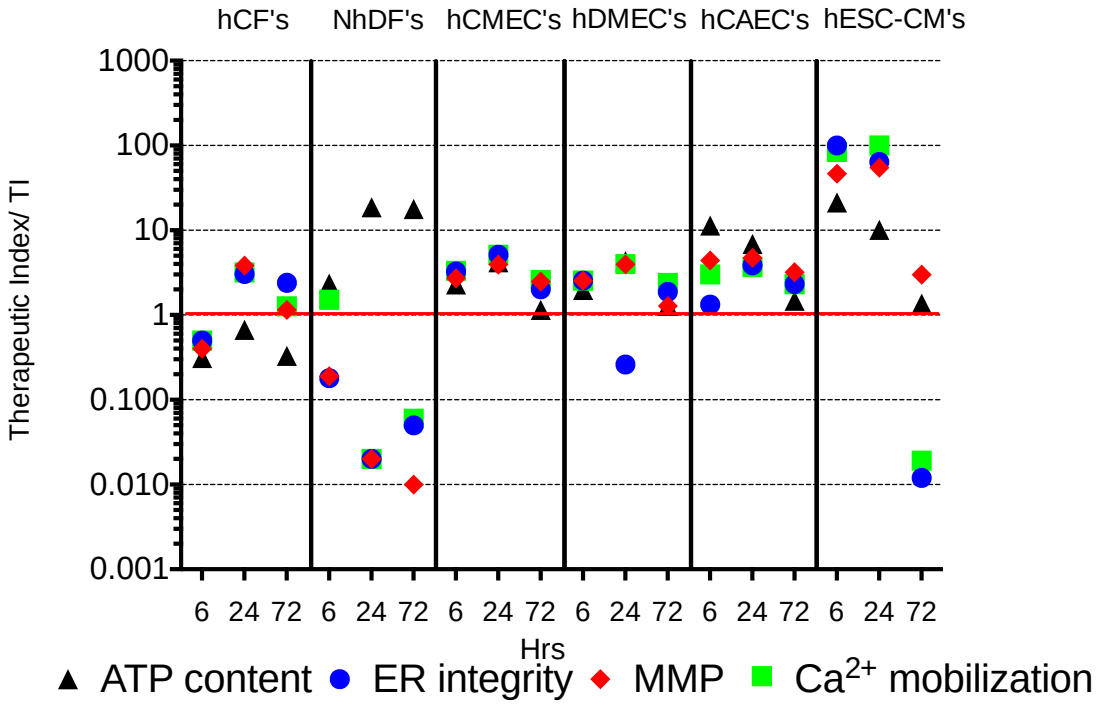

Figure 4.7 Therapeutically relevant toxicity of lapatinib in endothelial, fibroblast and cardiomyocytes.

Cells were treated with a 6-point concentration set (100 – 0.032 μM) of lapatinib for 6 h, 24 h and 72 h before being stained and imaged for MMP, ER integrity, Ca^{2+} mobilization then lysed for cellular ATP content using CellTiter-Glo reagent. Concentration-effect curves were plotted to calculate IC_{50} values, which were then divided by the total C_{max} to give the therapeutic index (TI). *hCF, human cardiac fibroblasts; NhDFs, normal human dermal fibroblasts; hCMEC, human cardiac microvascular endothelial cells; hDMECs, human dermal microvascular endothelial cells; hCAECs, human coronary artery endothelial cells; hESC-CMs, human embryonic stem cell derived cardiomyocytes.*

Sorafenib, sunitinib and dasatinib are multi-tyrosine kinase inhibitors. The therapeutic index values of sorafenib are shown in figure 4.8, all cell models show therapeutically relevant toxicity to sorafenib. The endothelial cells show no significant difference in sensitivities ($p>0.99$) and their MMP, ER, Ca^{2+} and ATP TI values all tightly correlate suggesting gross cell death has occurred as early as 6 h. In contrast the fibroblasts, particurlarly NhDFs, have displayed therapeutically relevant structural toxicity (MMP, ER and Ca^{2+}) and not intracellular ATP depletion. This fibroblast therapeutic toxicity was significantly enhanced compared to hESC-CMs at the 6 and 24 hr timepoints ($p<0.0001$).

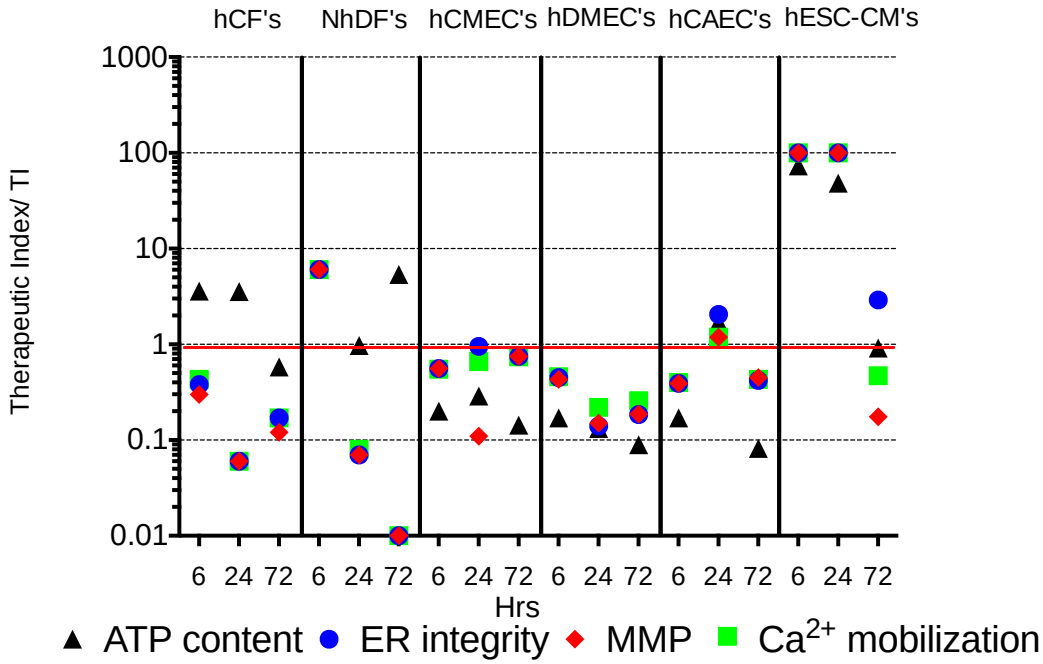

Figure 4.8 Therapeutically relevant toxicity of sorafenib in endothelial, fibroblast and cardiomyocytes.

Cells were treated with a 6-point concentration set (100 – 0.032 µM) of sorafenib for 6 h, 24 h and 72 h before being stained and imaged for MMP, ER integrity, Ca^{2+} mobilization then lysed for cellular ATP content using CellTiter-Glo reagent. Concentration-effect curves were plotted to calculate IC_{50} values, which were then divided by the total C_{max} to give the therapeutic index (TI). *hCF, human cardiac fibroblasts; NhDFs, normal human dermal fibroblasts; hCMEC, human cardiac microvascular endothelial cells; hDMECs, human dermal microvascular endothelial cells; hCAECs, human coronary artery endothelial cells; hESC-CMs, human embryonic stem cell derived cardiomyocytes.*

Sunitinib (figure 4.9) has shown therapeutically relevant toxicity in the NhDFs as early as 6 h exposure, detected by a change in MMP (TI; 1), after 24 h this toxicity was lead by changes to the ER integrity (TI; 0.1). However, after 72 h of compound exposure the NhDFs appear to have recovered from these structural changes and the TI values of all parameters sit at 100. The only cell type which displays maintained structural toxicity was the cardiomyocytes (hESC-CMs), Ca^{2+} mobilisation has a TI value of 0.005 after 72 h exposure; another example of mechanistic prediction using high content biology.

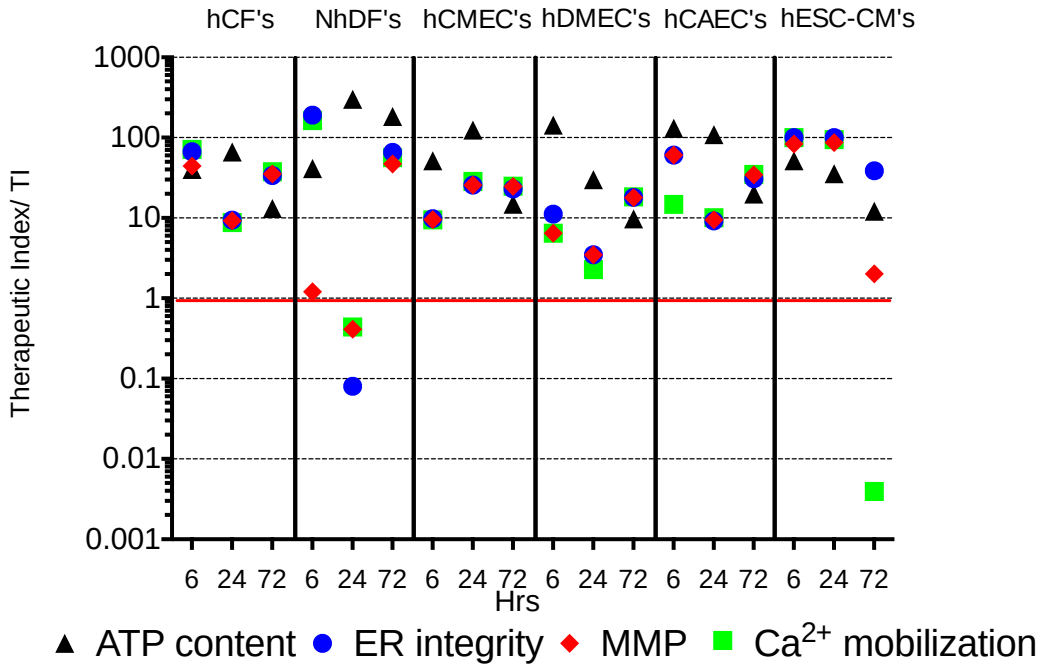

Figure 4.9 Therapeutically relevant toxicity of sunitinib in endothelial, fibroblast and cardiomyocytes.

Cells were treated with a 6-point concentration set (100 – 0.032 µM) of sunitinib for 6 h, 24 h and 72 h before being stained and imaged for MMP, ER integrity, Ca^{2+} mobilization then lysed for cellular ATP content using CellTiter-Glo reagent. Concentration-effect curves were plotted to calculate IC_{50} values, which were then divided by the total C_{max} to give the therapeutic index (TI). *hCF, human cardiac fibroblasts; NhDFs, normal human dermal fibroblasts; hCMEC, human cardiac microvascular endothelial cells; hDMECs, human dermal microvascular endothelial cells; hCAECs, human coronary artery endothelial cells; hESC-CMs, human embryonic stem cell derived cardiomyocytes.*

Dasatinib (figure 4.10), the final tyrosine kinase tested, shows no therapeutically relevant toxicity in any of the cell models except hESC-CMs; after a 24 h exposure a therapeutically relevant change in MMP was seen (TI; 0.7). Following a 72 h exposure this toxicity was no longer relevant, something which displays the importance of multiple time points.

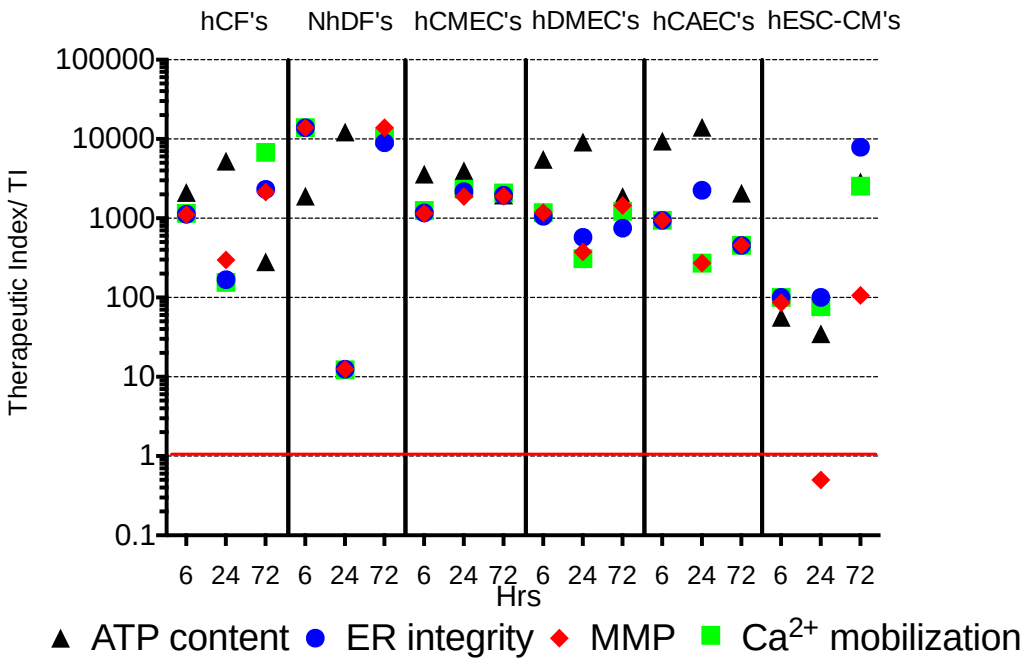

Figure 4.10 Therapeutically relevant toxicity of dasatinib in endothelial, fibroblast and cardiomyocytes.

Cells were treated with a 6-point concentration set (100 – 0.032 μM) of dasatinib for 6 h, 24 h and 72 h before being stained and imaged for MMP, ER integrity, Ca^{2+} mobilization then lysed for cellular ATP content using CellTiter-Glo reagent. Concentration-effect curves were plotted to calculate IC_{50} values, which were then divided by the total C_{max} to give the therapeutic index (TI). *hCF, human cardiac fibroblasts; NhDFs, normal human dermal fibroblasts; hCMEC, human cardiac microvascular endothelial cells; hDMECs, human dermal microvascular endothelial cells; hCAECs, human coronary artery endothelial cells; hESC-CMs, human embryonic stem cell derived cardiomyocytes.*

Fluorouracil is a member of the anti-metabolite drug class and irreversibly inhibits the thymidylate synthase enzyme. The most striking characteristic of figure 4.11 is the complete correlation of all of the HCB parameters and while the endothelial cell toxicity was predicted by the HCB parameters, fibroblast toxicity was either not relevant (hCFs) or intracellular ATP predicted (NhDFs). The hESC-CMs, however show the most sensitivity to fluorouracil with MMP, Ca^{2+} and ER predicting toxicity at TI values of ~0.01 after a 72 h exposure.

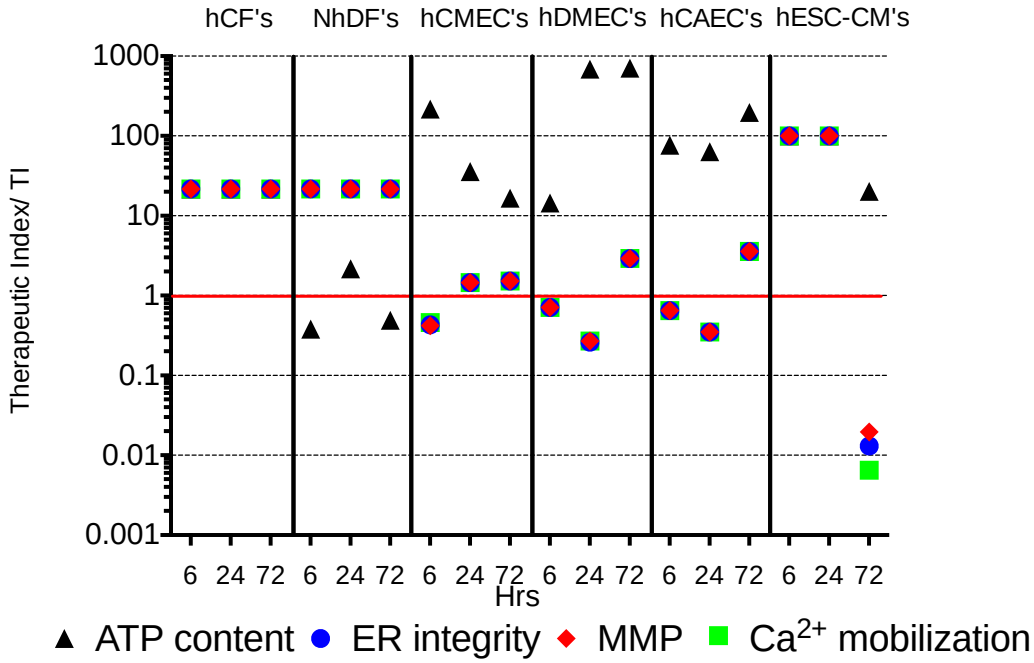

Figure 4.11 Therapeutically relevant toxicity of fluorouracil in endothelial, fibroblast and cardiomyocytes.

Cells were treated with a 6-point concentration set (100 – 0.032 µM) of fluorouracil for 6 h, 24 h and 72 h before being stained and imaged for MMP, ER integrity, Ca^{2+} mobilization then lysed for cellular ATP content using CellTiter-Glo reagent. Concentration-effect curves were plotted to calculate IC_{50} values, which were then divided by the total C_{max} to give the therapeutic index (TI). *hCF, human cardiac fibroblasts; NhDFs, normal human dermal fibroblasts; hCMEC, human cardiac microvascular endothelial cells; hDMECs, human dermal microvascular endothelial cells; hCAECs, human coronary artery endothelial cells; hESC-CMs, human embryonic stem cell derived cardiomyocytes.*

The final group of compounds tested for structural cardiotoxicity were the anthracyclines, doxorubicin and idarubicin. Figure 4.12a and figure 4.12b show therapeutically relevant toxicity in all cell models with doxorubicin exposure, the most sensitive being the hESC-CMs after 72 h (ATP TI; 0.0001), however, idarubicin shows hCF and hESC-CM specific potency. hCFs show a TI of 0.0001 (ER & Ca^{2+}) after 72 h exposure to idarubicin, 100-fold lower than the next most sensitive cell model, hESC-CM with a lowest TI value of 0.01 (ER).

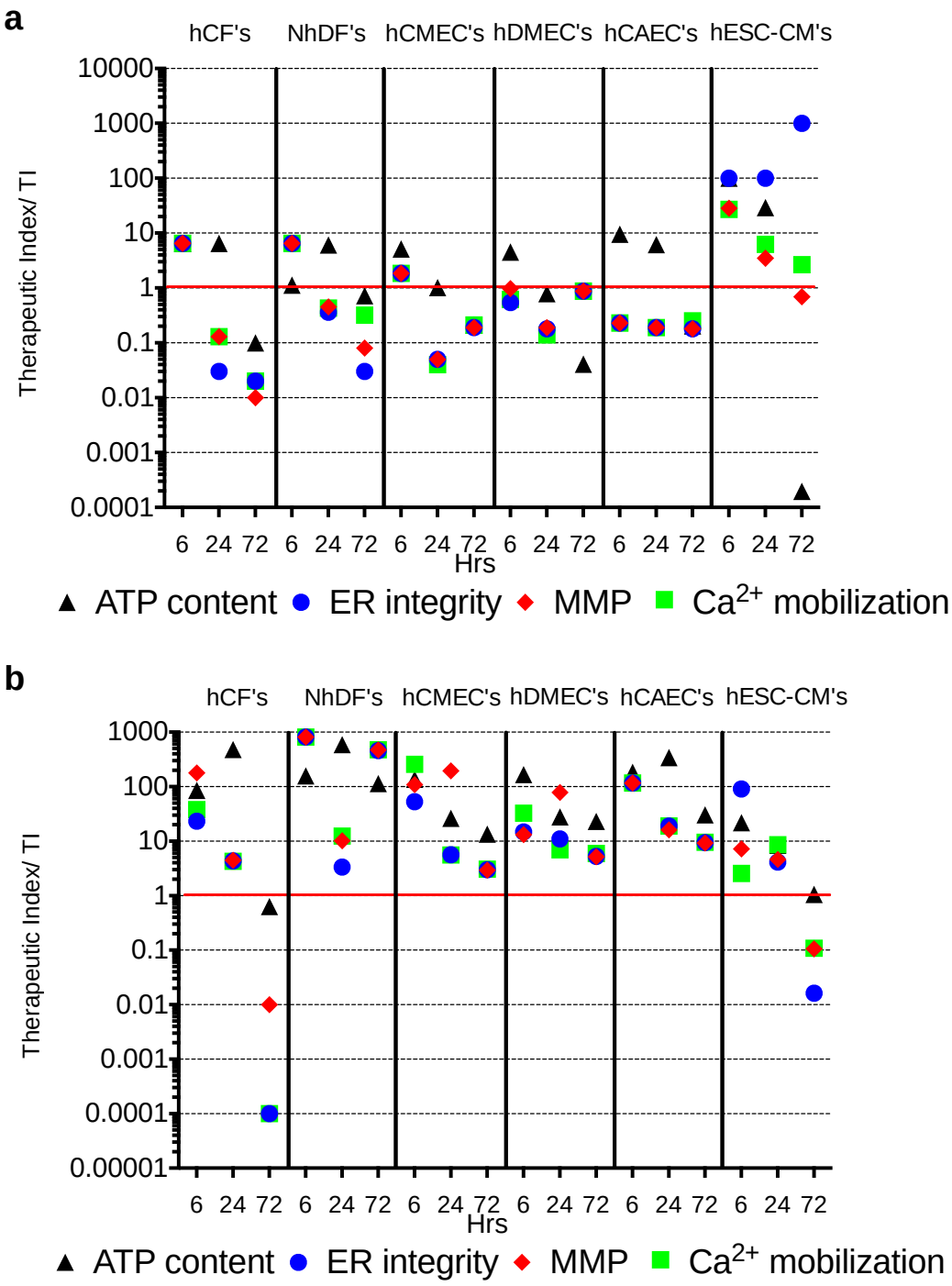

Figure 4.12 Therapeutically relevant toxicity of (a) doxorubicin and (b) idarubicin in endothelial, fibroblast and cardiomyocyte cells.

Cells were treated with a 6-point concentration set (100 – 0.032 µM) for 6, 24 and 72 h before staining and imaging for MMP, ER integrity, Ca^{2+} mobilization then lysed for cellular ATP content using CellTiter-Glo reagent. Concentration-effect curves were plotted to calculate IC_{50} values, which were then divided by the total C_{max} to give the therapeutic index (TI). *hCF, human cardiac fibroblasts; NhDFs, normal human dermal fibroblasts; hCMEC, human cardiac microvascular endothelial cells; hDMECs, human dermal microvascular endothelial cells; hCAECs, human coronary artery endothelial cells; hESC-CMs, human embryonic stem cell derived cardiomyocytes.*

4.4 Relative sensitivities of endothelial cells from different vascular beds to structural cardiotoxins

From the concentration- effect curves of the 8 structural cardiotoxins (imatinib, fluorouracil, doxorubicin, lapatinib, sorafenib, sunitinib, dasatinib and idarubicin), all IC_{50} values were divided by the total C_{max} of the test compound to give the therapeutic index (TI); a ratio of the amount of therapeutic agent that causes the therapeutic effect to the amount that causes toxicity. The parameter with the lowest TI was selected for each compound in each cell type and correlation graphs of hCMEC against hCAECs and hDMECs were generated using GraphPad Prism. Figure 4.13 shows a global comparison whereby the endothelial cell sensitivities to all 8 structural cardiotoxins are compared at (a) 6 h, (b) 24 h and (c) 72 h. This type of analysis was used to highlight any correlations in sensitivity.

After 6 h exposure (figure 4.13a), each data point correlates tightly with the line of unity suggesting there is very little difference in the compound sensitivity of these three cell types. Each endothelial cell was sensitive below therapeutically relevant levels to sorafenib and fluorouracil (TI; <0.2 & <0.7 respectively). Slight differences in sensitivity to doxorubicin can be seen at this point also; the hCAEC and hDMEC were relevantly sensitive to doxorubicin (TI; <0.6) where as the hCMECs were not (TI; 1.85) (Figure 4.13a) (IC50, TI).

Following 24 h of exposure (figure 4.13b), slightly less correlation around the line of unity can be seen. Each endothelial cell type now shows therapeutically relevant sensitivity to doxorubicin (TI; <0.2), however lapatinib shows therapeutically relevant toxicity specifically in the hDMECs (TI; 0.26) but not in the hCMECs (TI; 3.95) or hCAECs (TI; 3.7). Fluorouracil remains therapeutically relevant in the hDMECs and hCAECs (TI; <0.35) but the IC_{50} of hCMECs has risen slightly to above C_{max} (greater than 1) (TI; 1.45). Sorafenib remains equally potent in the hCMECs and hDMECs (TI; 0.1), where as the hCAECs appear less sensitive at 24 h (TI; 1.19).

Figure 4.13c shows afters 72 h exposure the endothelial cells correlate even tighter around the line of unity suggesting no significant difference in sensitivities between the cell models at this time point. All three endothelial cell models were sensitive to doxorubicin (TI; <0.2) and sorafenib (TI; 0.15) at therapeutically relevant levels following 72 h exposure.

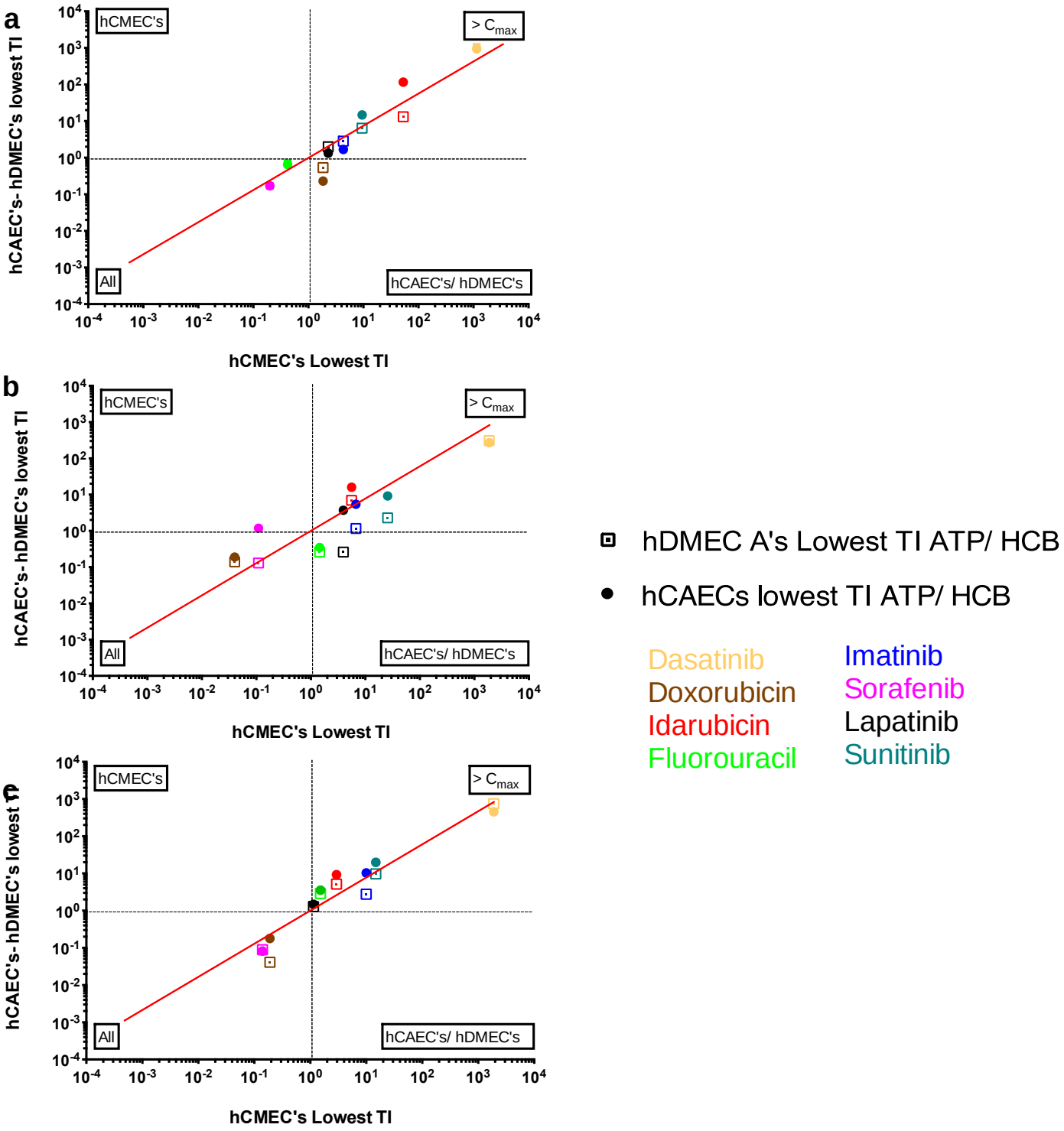

Figure 4.13 Global comparison of endothelial structural cardiotoxin sensitivities following 6, 24 & 72 h exposure to 8 structural cardiotoxins.

Cells were seeded at their optimal seeding densities and incubated for 3 days prior to treatment with 8 structural cardiotoxins for (a) 6 h, (b) 24 h and (c) 72 h. Cells were labelled with fluorescent probes for MMP, ER integrity, Ca^{2+} mobilization and lysed for cellular ATP content. Concentration-effect curves were plotted for all compounds and expressed relative to vehicle (0.5% DMSO). IC_{50} values were obtained and divided by the total Cmax for each test compound to give the therapeutic index (TI). The parameter with the lowest TI was selected and correlation graphs were generated using GraphPad Prism. *hCMEC, human cardiac microvascular endothelial cells; hDMECs, human dermal microvascular endothelial cells; hCAECs, human coronary artery endothelial cells.*

4.5 Relative sensitivities of cardiac and dermal fibroblast cells to structural cardiotoxins

From the concentration- effect curves of the 8 structural cardiotoxins (imatinib, fluorouracil, doxorubicin, lapatinib, sorafenib, sunitinib, dasatinib and idarubicin), all IC_{50} values were divided by the total C_{max} of the test compound to give the therapeutic index (TI); a ratio of the amount of therapeutic agent that causes the therapeutic effect to the amount that causes toxicity. The parameter with the lowest TI was selected for each compound in each cell type and correlation graphs of hCFs against NhDFs were generated using GraphPad Prism. Figure 4.14 shows a global comparison of the fibroblast cell sensitivities to the 8 structural cardiotoxins after 6, 24 and 72 h exposure.

After 6 h exposure (figure 4.14a) both fibroblast cell models show equal sensitivity to lapatinib (TI; 0.3), gradually this sensitivity increases in the NhDFs i.e. IC_{50} values become lower in NhDF's (TI 24 & 72; 0.02 & 0.0001, respectively). Imatinib, sorafenib and sunitinib show differential sensitivities between the cardiac and dermal fibroblasts at the 6 h time point; imatinib and sorafenib have displayed therapeutically relevant toxicity in the hCF model (TI; 0.6 & 0.3, respectively) but not the NhDFs that have a TI value at least 10-fold higher (TI; 23 & 4, respectively). Sunitinib, although not therapeutically relevant, has a TI value approximately 10-fold lower in the NhDFs than the hCFs (TI; 10 & 1.2, respectively).

Figure 4.14b shows the 24 h global fibroblast comparison, here we see imatinib has maintained its hCF specific sensitivity when compared with NhDFs (TI; 0.22 & 3.24, respectively), sorafenib is now equally as toxic to both fibroblast models (TI; 0.06), therapeutically relevant doxorubicin toxicity has developed in both models (TI; <0.2) and NhDF have displayed increased sensitivity to lapatinib while the hCFs have reduced in sensitivity (TI; 0.02 & 0.67, respectively).

After 72h exposure the fibroblast models have shown even more variation in their sensitivity; while only the hCFs show therapeutically relevant sensitivity to imatinib, sunitinib and idarubicin (hCFs TI; 0.0001, 0.66, 0.001, respectively & NhDFs TI; 28, 47, 67, respectively), the NhDFs are 1,000-fold more sensitive to sorafenib and lapatinib (NhDFs TI; 0.0001). Dasatinib has no therapeutically relevant toxicity in either model (TI; >250) and both NhDF's and hCF's have equal sensitivity to doxorubicin (TI; 0.02 & 0.01, respectively).

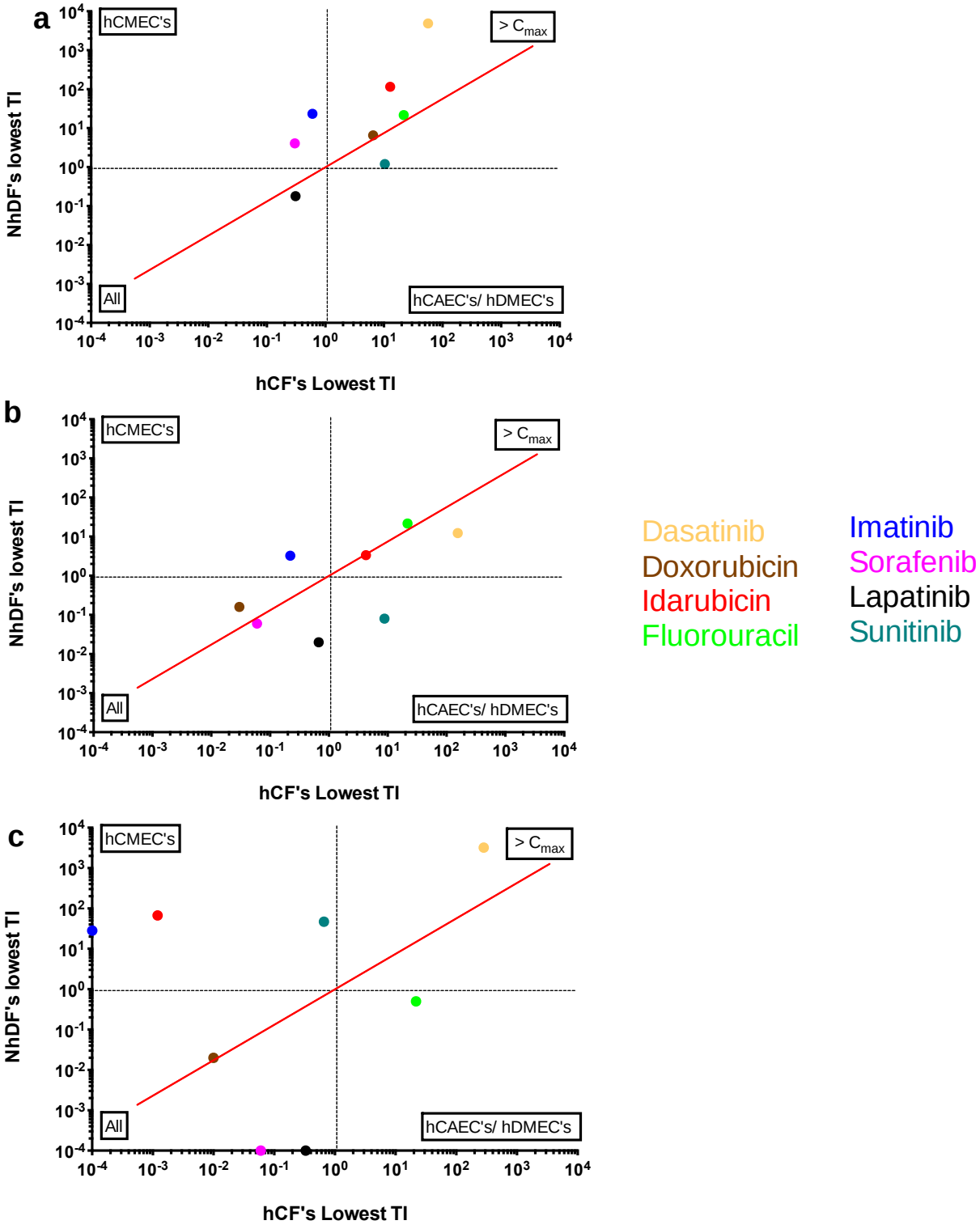

Figure 4.14 Global comparison of fibroblast structural cardiotoxin sensitivities following 6, 24 & 72 h exposure to 8 structural cardiotoxins.

Fibroblasts were seeded in 96 well plates and incubated for 3 days prior to treatment with 8 structural cardiotoxins for (a) 6 h, (b) 24 h and (c) 72 h. Cells were labelled with fluorescent probes for MMP, ER integrity, Ca^{2+} mobilization and lysed for cellular ATP content. Concentration-effect curves were plotted for all compounds and expressed relative to vehicle (0.5% DMSO). IC_{50} values were obtained and divided by the total C_{max} for each test compound to give the therapeutic index (TI). The parameter with the lowest TI was selected and correlation graphs were generated using GraphPad Prism. *hCF, human cardiac fibroblasts; NhDF, normal human dermal fibroblasts.*

4.6 Relative sensitivities of non-myocytes and myocytes to structural cardiotoxins

From the concentration- effect curves of the 8 structural cardiotoxins (imatinib, fluorouracil, doxorubicin, lapatinib, sorafenib, sunitinib, dasatinib and idarubicin), all IC_{50} values were divided by the total C_{max} of the test compound to give the therapeutic index (TI); a ratio of the amount of therapeutic agent that causes the therapeutic effect to the amount that causes toxicity. The parameter with the lowest TI was selected for each compound in each cell type and correlation graphs of cardiac non-myocytes (hCFs & hCMECs) against cardiomyocytes (hESC-CMs) were generated using GraphPad Prism. Figure 4.15 shows a global comparison of the cardiac myocyte and non-myocyte cell sensitivities to the 8 structural cardiotoxins after 6 and 72 h exposure.

If we compare figure 4.15 (a) and (b) we can clearly see an overall shift in data points from the right hand side of the correlation graph at the 6 h timepoint (a) to the left hand side at the 72 h timepoint (b). This means the compounds either have an IC_{50} greater than C_{max} (top right box, figure 4.15a) and are therefore not therapeutically relevant, or have therapeutic relevance solely in one or both of the non-myocytes (hCF or hCMEC) (bottom right box, figure 4.15a). After 72 h exposure all the compounds (except imatinib) show therapeutically relevant toxicity either in the myocyte and non-myocyte models (bottom left box, figure 4.15b) or solely the myocytes (top left box, figure 4.15b). Overall this suggests the non-myocytes are sensitive to structural cardiotoxicity earlier than the cardiomyocytes.

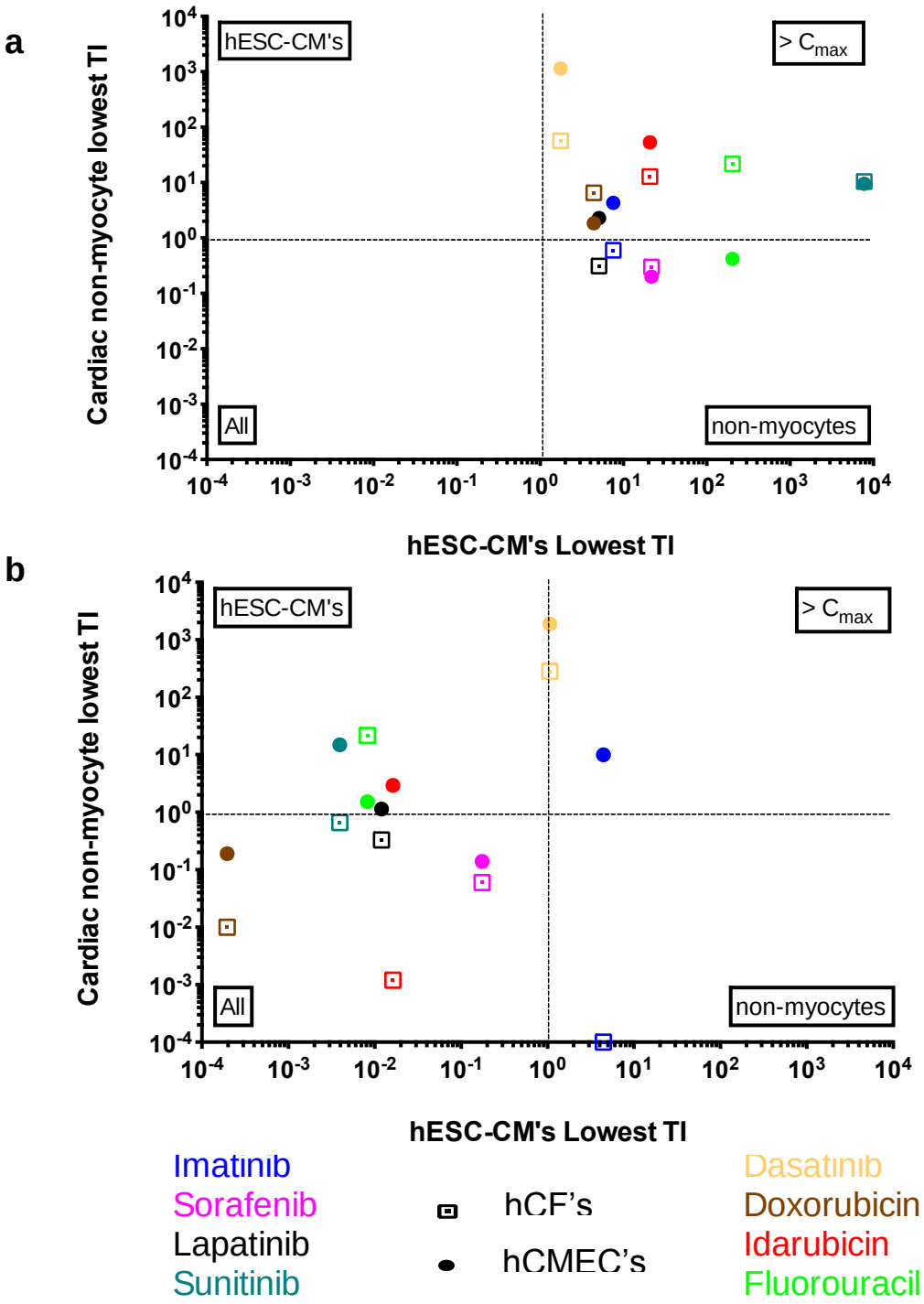

Figure 4.15 Comparison of myocyte (hESC-CMs) and non-myocyte (hCFs & hCMECs) structural cardiotoxin sensitivities at 6 and 72 h.

Cells were treated with a 6-point concentration (0.03-100 µM) response of 8 structural cardiotoxins for (a) 6 h and (b) 72 h. Cells were then labelled with fluorescent probes for MMP, ER integrity, Ca^{2+} mobilization and lysed for cellular ATP content. Concentration-effect curves were plotted and expressed relative to vehicle (0.5% DMSO). From here IC_{50} values were obtained and divided by the total C_{max} for each test compound to give the therapeutic index (TI). The parameter with the lowest TI was selected for each compound in each cell type and correlation graphs were generated using GraphPad Prism (LA Jolla, CA). *hCF, human cardiac fibroblasts; hCMEC, human cardiac microvascular endothelial cells; hESC-CM, human embryonic stem cell cardiomyocytes.*

The only test compound to show a therapeutically relevant toxicity specific to one of the cell models across both acute and chronic exposure is imatinib in the hCF model (figure 4.15a & b) (6 hr TI; 0.6 & 72 hr TI; 0.0001). At 6 h the hCF model also shows sensitivity to lapatinib but following 72 h the cardiomyocytes have also developed this relevant toxicity. At the 6 h timepoint we see fluorouracil sensitivity solely in the hCMECs (TI; 0.4), but after 72 h the cardiomyocytes have also developed sensitivity. Both non-myocytes are sensitive to sorafenib after 6 h but again the cardiomyocytes develop this toxicity at 72 h. At 72 h exposure (figure 4.15b) we see doxorubicin, lapatinib and sorafenib therapeutically relevant sensitivity across all cardiac cell models, sunitinb and idarubicin toxicity was relevant specifically in the cardiac fibroblasts and cardiomyocytes.

4.7 Detection of structural cardiotoxins in microtissue models

The previous sections have discussed the structural cardiotoxin sensitivities of 2D cell models (hCMECs, hDMECs, hCAECs, hCFs, NhDFs and hESC-CMs) comprised of an individual cell type and has suggested the non-myocytes are sensitive to structural cardiotoxins earlier than the cardiomyocytes but with the majority toxicity eventually present within the cardiomyocytes. Given the dependency of cardiomyocytes on the microvascular system for the supply of oxygen and nutrients, the next question was to investigate whether this early non-myocyte toxicity could translate into enhanced cardiomyocyte toxicity. In order to assess this an *in vitro* model with increased physiological relevance was required whereby the cardiomyocytes can directly interact with the non-myocytes (hCFs & hCMECs). 3D cell culture allows better recapitulation of a cells '3D' *in vivo* morphology. Round bottom ultra low adhesion (ULA) cell culture plates were used to form microtissues. Chapter 3 discusses microtissue development in detail. Briefly however, 500 cells at a ratio of 4 hESC-CMs: 2 fibroblasts: 1 endothelial cell (tri-culture; cardiac MEF (CMEF) & dermal MEF (DMEF)) or 2 hESC-CMs: 1 endothelial or fibroblast cell (di-cultures; endothelial CME or fibroblast CMF) or solely hESC-CMs were seeded into each well of an ULA plate in 100 µl of cell culture media. Following 2 weeks of incubation at 37^{o}C, 5% CO_2, the cells have aggregated

to form a tight 200 μm spontaneously beating microtissue. The microtissues have uniform size and shape with possible longevity beyond 2 months (data not shown) however the toxicity assays discussed here were performed with microtissues up to 4 weeks post seeding.

All microtissue models were exposed for 6 and 72 h to 5 structural cardiotoxins selected for their different cell model sensitivities. Fluorouracil displayed therapeutically relevant toxicity specifically in the endothelial cells after a 6 h exposure (figure 4.15a). Imatinib displayed therapeutically relevant toxicity specifically in the cardiac fibroblasts at both 6 and 72 h exposure (figure 4.15a & b). Sunitinib was highlighted for its therapeutically relevant toxicity specifically in the cardiac fibroblasts and cardiomyocytes (figure 4.15b). Lapatinib and doxorubicin were selected as compounds with different mechanistic targets that cause relevant toxicity in all cardiac cell models (figure 4.15a & b). All models were treated with a 6-point concentration set (100 – 0.032 μM) of compound for 6 or 72 h then intracellular ATP content was used as a measure of cytotoxicity; microtissues were lysed on a plate shaker for 20 mins in CellTiter-Glo reagent (Promega, Southampton, U.K.).

From the concentration-effect curves in figure 4.16 and the plotted IC_{50} values in figure 4.21, we can see that exposure to fluorouracil has no effect on intracellular ATP content at either timepoint (6 (figure 4.16a) or 72 h (figure 4.16b)) in any of the cell models tested (IC_{50} > 100 µM).

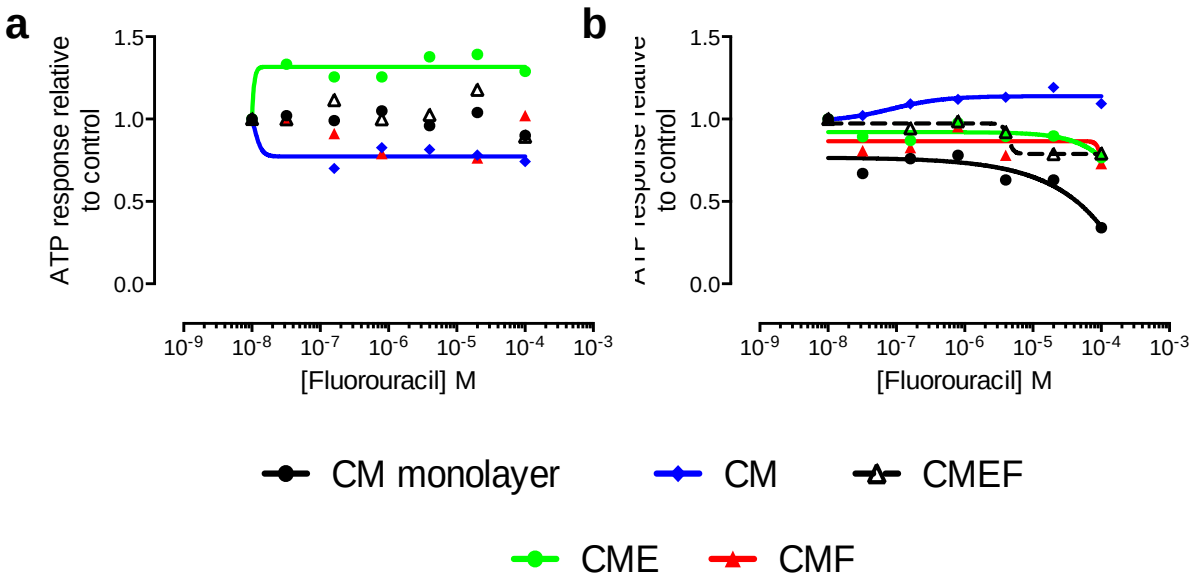

Figure 4.16 Intracellular ATP concentration-effect curves of CM monolayer and CM, CMEF, CME, CMF microtissues following (a) 6 h and (b) 72 h exposure to fluorouracil.

Cells were seeded into each well of an ULA plate at optimal ratio and density in 100 µl of cell culture media and incubated for 2 weeks. All models were treated with a 6-point concentration set (100 – 0.032 µM) of compound for 6 or 72 h then intracellular ATP content was used as a measure of cytotoxicity (CellTiter Glo, Promega, Southampton, U.K.). *CM monolayer, human embryonic stem cell cardiomyocytes; CM, hESC-CM microtissue; CMEF, hESC-CM/ hCF/ hCMEC; CME, hESC-CM/ hCMEC; CMF, hESC-CM/ hCF.*

Doxorubicin has no effect on intracellular ATP content in the cell models after a 6 h exposure (figure 4.17a). However after 72 h exposure all models were sensitive to doxorubicin (IC_{50} < 0.4 µM). The CM monolayer model (hESC-CMs) leads with the lowest IC_{50} at 72 h (0.02 µM; figure 4.21), a 10-fold increase in sensitivity compared with the microtissue models (IC_{50}'s > 0.2 µM; figure 4.21).

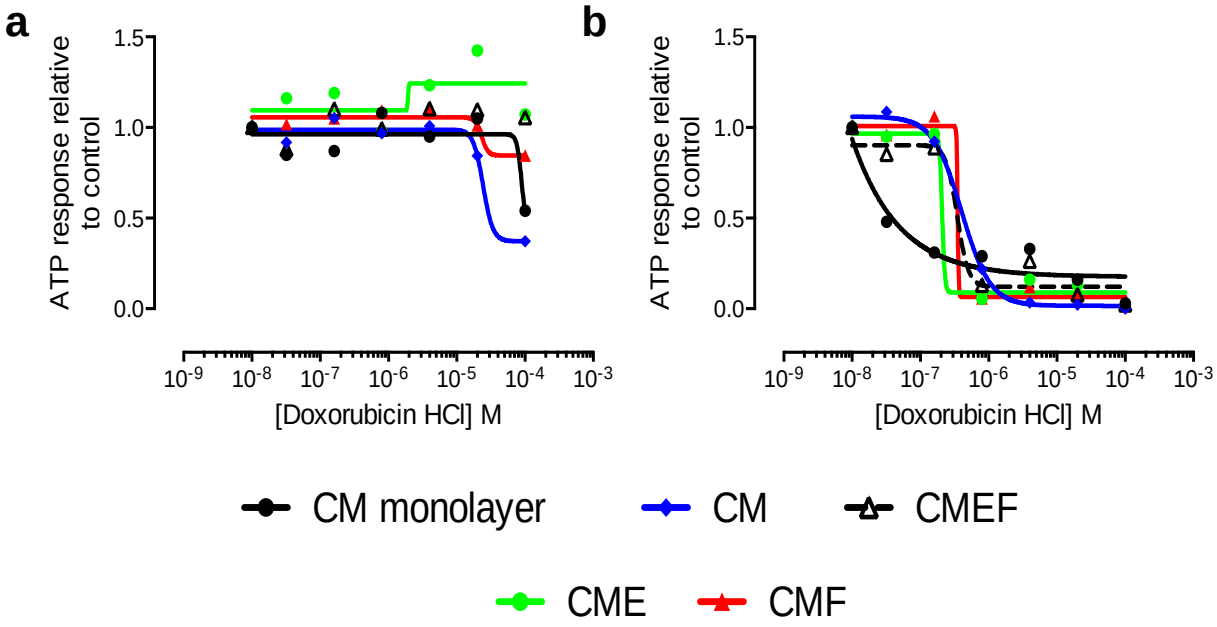

Figure 4.17 Intracellular ATP concentration-effect curves of CM monolayer and CM, CMEF, CME, CMF microtissues following (a) 6 h and (b) 72 h exposure to doxorubicin.

Cells were seeded into each well of an ULA plate at optimal ratio and density in 100 µl of cell culture media and incubated for 2 weeks. All models were treated with a 6-point concentration set (100 – 0.032 µM) of compound for 6 or 72 h then intracellular ATP content was used as a measure of cytotoxicity (CellTiter Glo, Promega, Southampton, U.K.). *CM monolayer, human embryonic stem cell cardiomyocytes; CM, hESC-CM microtissue; CMEF, hESC-CM/ hCF/ hCMEC; CME, hESC-CM/ hCMEC; CMF, hESC-CM/ hCF.*

Figures 4.18a and 4.21 show lapatinib sensitivity in the CM monolayer model after 6 h exposure (IC_{50}, 21.25 µM), however the ATP content of the microtissue models was not affected (IC_{50} > 100 µM). Following 72 h exposure (figure 4.18b) we see a slightly lower IC_{50} (figure 4.21) in the microtissue models compared with the CM monolayer model (microtissues IC_{50}< 5 µM; CM monolayer IC_{50}, 13.8 µM).

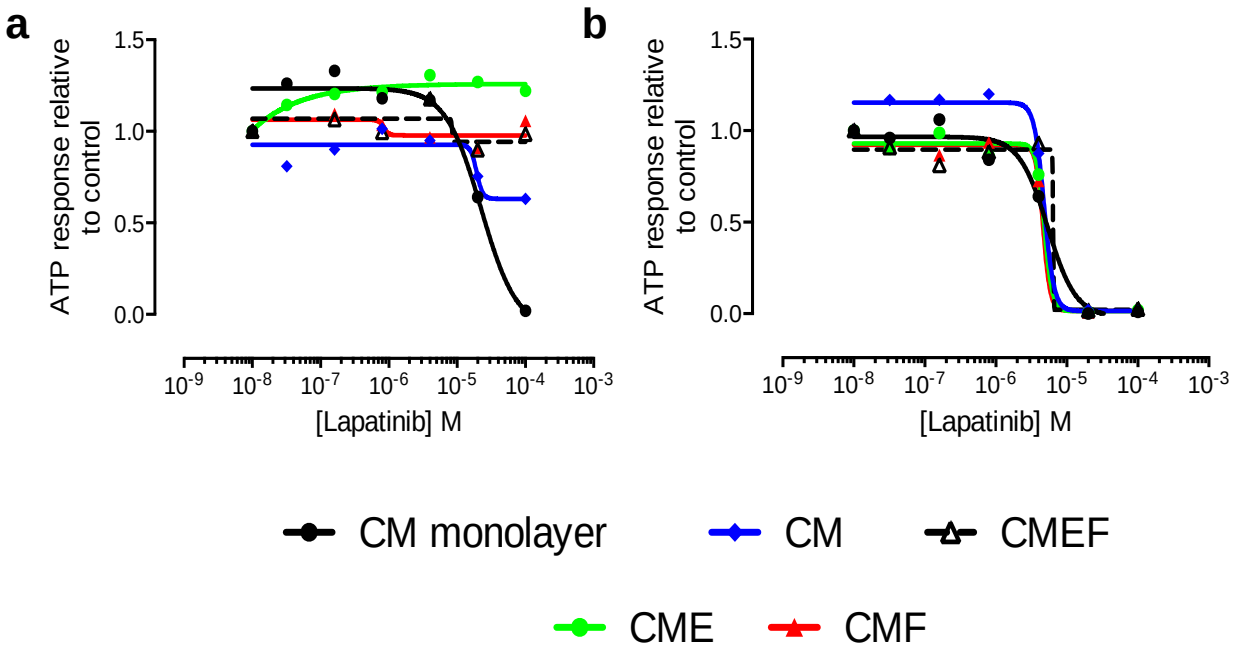

Figure 4.18 Intracellular ATP concentration-effect curves of CM monolayer and CM, CMEF, CME, CMF microtissues following (a) 6 h and (b) 72 h exposure to lapatinib.

Cells were seeded into each well of an ULA plate at optimal ratio and density in 100 µl of cell culture media and incubated for 2 weeks. All models were treated with a 6-point concentration set (100 – 0.032 µM) of compound for 6 or 72 h then intracellular ATP content was used as a measure of cytotoxicity (CellTiter Glo, Promega, Southampton, U.K.). *CM monolayer, human embryonic stem cell cardiomyocytes; CM, hESC-CM microtissue; CMEF, hESC-CM/ hCF/ hCMEC; CME, hESC-CM/ hCMEC; CMF, hESC-CM/ hCF.*

Sunitinib decreased intracellular ATP content in all cell models at both 6 h (figure 4.19a) and 72 h (figure 4.19b) exposure with very little variation in the IC_{50} values (figure 4.21)

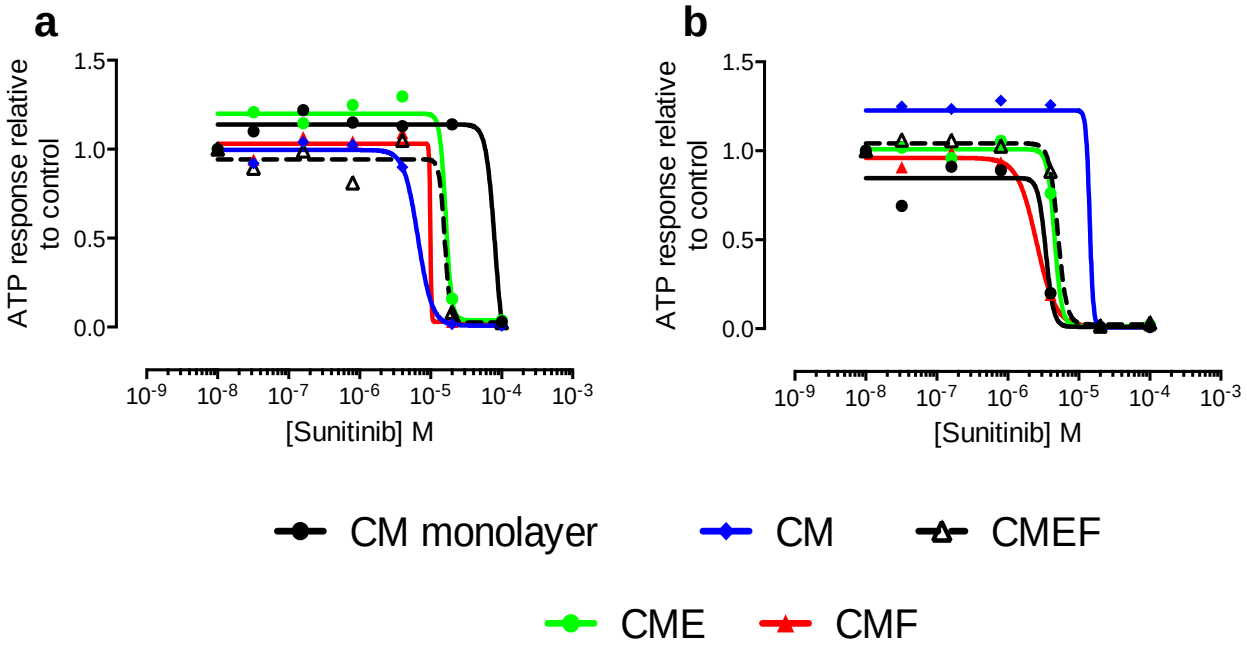

Figure 4.19 Intracellular ATP concentration-effect curves of CM monolayer and CM, CMEF, CME, CMF microtissues following (a) 6 h and (b) 72 h exposure to sunitinib.

Cells were seeded into each well of an ULA plate at optimal ratio and density in 100 µl of cell culture media and incubated for 2 weeks. All models were treated with a 6-point concentration set (100 – 0.032 µM) of compound for 6 or 72 h then intracellular ATP content was used as a measure of cytotoxicity (CellTiter Glo, Promega, Southampton, U.K.). *CM monolayer, human embryonic stem cell cardiomyocytes; CM, hESC-CM microtissue; CMEF, hESC-CM/ hCF/ hCMEC; CME, hESC-CM/ hCMEC; CMF, hESC-CM/ hCF.*

All cell models show a decrease in intracellular ATP content following imatinib exposure for 6 and 72 h. The concentration-effect curves (figure 4.20) and the plot of IC_{50} values (figure 4.21) show a pattern whereby the CMF model was slightly more sensitive at both time points (6 h IC_{50}, 6 μM; 72 h IC_{50}, 2 μM) than all other models (6 h IC_{50}, >10 μM; 72 h IC_{50}, >15 μM), with the CME model following closely after 72 h exposure (IC_{50}, 4 μM).

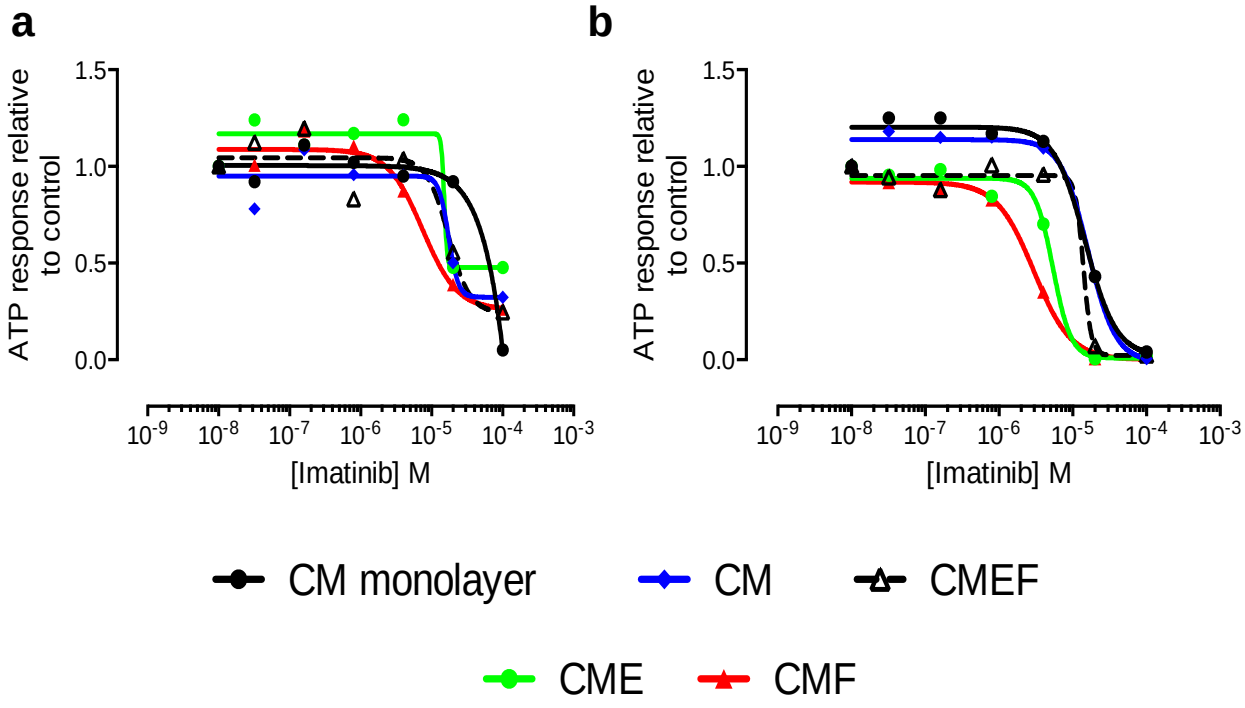

Figure 4.20 Intracellular ATP concentration-effect curves of CM monolayer and CM, CMEF, CME, CMF microtissues following (a) 6 h and (b) 72 h exposure to imatinib.

Cells were seeded into each well of an ULA plate at optimal ratio and density in 100 μl of cell culture media and incubated for 2 weeks. All models were treated with a 6-point concentration set (100 – 0.032 μM) of compound for 6 or 72 h then intracellular ATP content was used as a measure of cytotoxicity (CellTiter Glo, Promega, Southampton, U.K.). *CM monolayer, human embryonic stem cell cardiomyocytes; CM, hESC-CM microtissue; CMEF, hESC-CM/ hCF/ hCMEC; CME, hESC-CM/ hCMEC; CMF, hESC-CM/ hCF.*

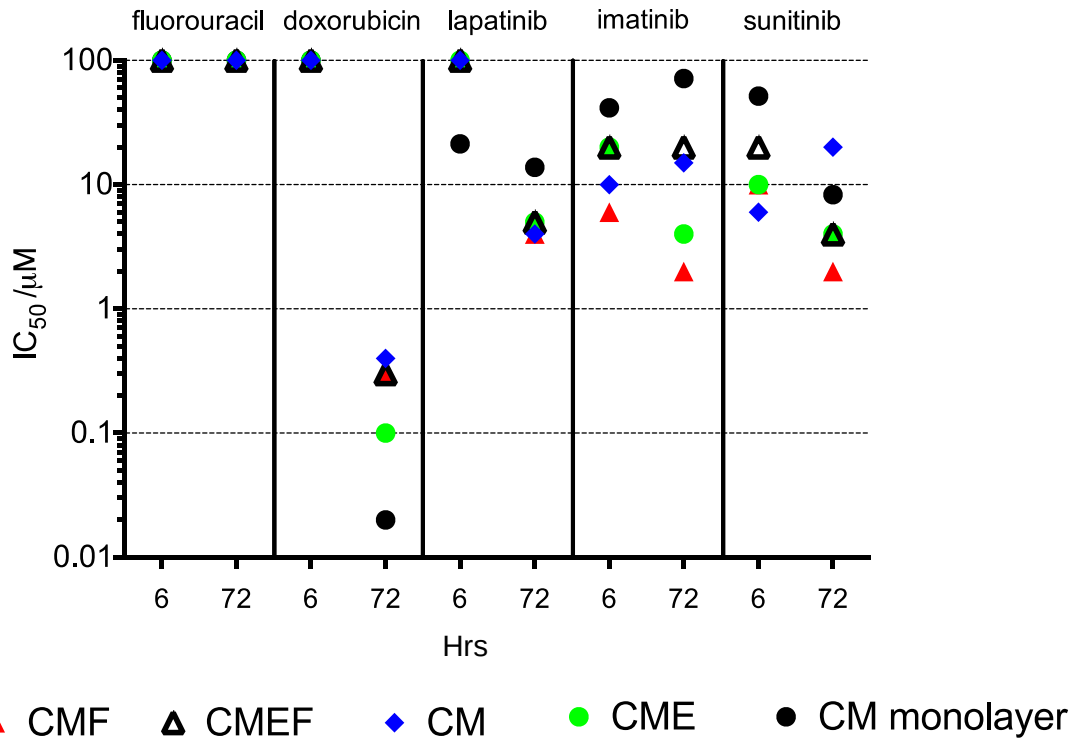

Figure 4.21 Intracellular ATP IC_{50} values for CM monolayer and CM, CMEF, CME, CMF microtissues following 6 and 72 h exposure to 5 structural cardiotoxins.

Cells were seeded into each well of an ULA plate at optimal ratio and density in 100 µl of cell culture media and incubated for 2 weeks. All models were treated with a 6-point concentration set (100 – 0.032 µM) of compound for 6 or 72 h then intracellular ATP content was used as a measure of cytotoxicity (CellTiter Glo, Promega, Southampton, U.K.). Concentration-effect curves were plotted using GraphPad Prism and IC_{50} values calculated. *CM monolayer, human embryonic stem cell cardiomyocytes; CM, hESC-CM microtissue; CMEF, hESC-CM/ hCF/ hCMEC; CME, hESC-CM/ hCMEC; CMF, hESC-CM/ hCF.*

4.8 Discussion

This chapter describes the utilization of a high content biology and cytotoxicity assay approach to measure structural cardiotoxin sensitivities in non-myocyte cells from various different tissue beds. The first aim was to determine the need for non-myocytes from a cardiac origin in structural cardiotoxicity prediction and secondly to compare the sensitivities of cardiac non-myocytes with cardiomyocytes in order to establish a role for non-myocytes in drug-induced structural cardiotoxicity.

4.8.1 Combining HCB with a cytotoxicity assay to increase predictive strength

The data from this chapter firstly shows that the combination of high content biology (HCB) with a cytotoxicity endpoint improves the overall predictive strength of the assay. This was also shown by Pointon *et al* (2013) using multiple cardiomyocyte cell models. For example imatinib mesylate toxicity in hCFs was predicted by the high content biology parameters while doxorubicin toxicity in hESC-CMs was predicted by ATP content. Secondly, we have seen that HCB can predict these toxicities prior to gross cell death and therefore has the potential to provide insight into the mechanism of toxicity (Pointon *et al*., 2013). As will be discussed further on in this section, the non-myocytes showed cytotoxic sensitivity to the structural cardiotoxins at the acute time point of 6 h therefore most mechanistic insight was lost. In hindsight an earlier time point may have allowed better elucidation of the mechanisms of structural toxicity taking place in the non-myocytes but this was not necessary for a global study comparing many different cell types and their sensitivities.

The utilisation of an early and late timepoint also improves the predictive strength of the assay. For example the therapeutic index of fluorouracil increases with increased exposure in endothelial cells. Fluorouracil irreversibly inhibits the enzyme thymidylate synthase therefore enzyme turnover between the early and late timepoint could explain the reduction in potency. An assay solely utilising a late time point would have missed the endothelial fluorouracil therapeutically relevant sensitivity all together.

4.8.2 Structural cardiotoxin sensitivities in non-myocytes from cardiac, dermal and macrovascular origin.

No major difference in structural compound sensitivities were observed between the endothelial cells from different vascular beds. This is perhaps not surprising given the limitations of the cell model. Endothelial cells are highly adaptive cells designed to rapidly respond to changes in their microenvironment in order to maintain the flow of oxygen and nutrients to their tissue (and removal of waste products). A major but unavoidable draw back of this study is that the primary endothelial cells have been removed from their specific microenvironments *in vivo* and cultured alone *in vitro* under general endothelial cell culture conditions. The endothelial cell models were cultured in almost identical conditions therefore it is not surprising that they should respond to compounds in an almost identical manner. This highlights the need for more complex *in vitro* cell models that better reconstitute the *in vivo* cellular physiology when studying drug toxicity.

Interestingly, much more variation in structural cardiotoxin sensitivity was observed between the cardiac and dermal fibroblasts, this suggests that the fibroblasts perhaps are not as dependent upon their microenvironment for their phenotype as the endothelial cells are. For example the compound imatinib mesylate, an inhibitor of the Bcr-Abl, PDGF & c-kit receptors, shows at the therapeutically relevant level cardiac fibroblast specific structural toxicity detected by the high content biology parameters. PDGF receptors are known to play an important role in cardiac fibrosis and angiogenesis (Takeda & Manabe, 2011) therefore inhibition of this signalling could present one mechanism of imatinib cardiotoxicity. Bcr-Abl silencing in myocytes and fibroblasts showed no significant difference in imatinib sensitivity suggesting this is not the mechanism of cardiotoxicity (Wolf *et al*., 2010). This cardiac fibroblast specific toxicity highlights a) the need for cell models derived from the tissue of interest and b) a potential role for non-myocytes in drug-induced cardiovascular toxicity.

Lapatinib, sorafenib, sunitinib and although not therapeutically relevant, dasatinib show enhanced structural toxicity in the dermal fibroblasts compared to the other non-myocytes. Many tyrosine kinase inhibitors are now being highlighted for their incidence of skin rashes (Huang *et al*., 2008), the data in this chapter suggests that dermal fibroblasts could be the target of this skin toxicity.

4.8.3 Role of non-myocytes in drug-induced structural cardiovascular toxicity

As described above the endothelial cells displayed no significant difference in their compound responses, while the fibroblasts showed variation; imatinib was more potent in the cardiac fibroblasts and lapatinib more potent in the dermal fibroblasts. These findings were potentially disappointing although unsurprising. However, when the sensitivities of the cells from the myocardium (hCFs, hCMECs and hESC-CMs) were globally compared we see that the non-myocytes are sensitive to structural cardiotoxicity at the acute time point of 6 h, whereas the hESC-CMs display toxicity only after 72 h. *In vivo* the early compound toxicity of the non-myocytes could potentially translate into enhanced cardiomyocyte sensitivity. Fibroblasts are in close proximity to myocytes and their ability to manipulate the ECM provides them with the potential to influence cardiomyocyte phenotype. Cardiomyocytes are highly energetic cells that require an abundance of oxygen and nutrients from the dense microvasculature. Loss or damage to the microvasculature would ultimately affect cardiomyocyte health and mechanical output.

4.8.4 Structural cardiotoxicity in cardiac microtissues

In order to overcome some of the limitations of the cell models used within this chapter, co-cultured microtissue models were utilised to study structural cardiotoxicity. Chapter three saw the development of multiple microtissue models comprising different co-culture compositions. hESC-CMs were cultured alone and co-cultured with either or both cardiac fibroblasts and cardiac microvascular endothelial cells as three dimensional (3D) microtissues. These models have improved *in vivo* relevance compared with the monolayer assays previously used, since they conform the cells into their natural 3D structure and allow multicellular

interactions. Microtissues were exposed to a subset of the initial structural cardiotoxin compound set and cytotoxicity measured using an intracellular ATP measurement. Compound selection was based upon potency in the non-myocyte monolayer models. Ideally this assay would have been combined with the high content biology approach however, high throughout imaging of 3D samples is technically challenging for automated imaging platforms with regard to locating and focusing on 3D samples. This limited the study quite dramatically since the only available endpoint was ATP content and this parameter was not particularly predictive of toxicity in the monolayer models. For example, no sensitivity to fluorouracil by the microtissue models was detected by measuring ATP content. This is not surprising given that previous monolayer sensitivities were detected by the high content biology parameters and not ATP content.

Despite this ATP measurement allowed some differences in microtissue sensitivities to be detected. The cardiomyocyte-cardiac fibroblast microtissues showed enhanced sensitivity to the tyrosine kinase inhibitors imatinib and sunitinib. This imatinib response supports the earlier findings with the hCF monolayer model in suggesting cardiac fibroblasts are the target of imatinib cardiotoxicity. Interestingly, however, the cardiac tri-culture model CMEF shows a reduction in imatinib sensitivity compared with the di-culture models suggesting a tri-cultured environment provides some protection against this toxicity. Doxorubicin shows a similar pattern except the most sensitive microtissue was the cardiomyocyte-cardiac endothelial microtissue suggesting the endothelial cells play a role in doxorubicin cardiotoxicity potentially through redox disruption since we know endothelial cells utilise nitric oxide as a signalling factor with cardiomyocytes or disruption of the endothelial mitochondrial membrane potential (Chiusa *et al*., 2012). However, once again when tri-cultured we see less sensitivity suggesting some protection is at play.

4.8.5 Conclusion

The ultimate conclusion from this chapter is non-myocyte cells are involved in drug-induced cardiotoxicity and can be used to enhance our current preclinical safety

assessments. These sensitivities are not limited to any one class of compounds. Tyrosine kinase inhibitors, anthracyclines and enzyme inhibitors have been studied and each class has shown toxicity. However, co-cultured microtissue models, despite assay limitations, have suggested that more *in vivo* relevant models are not as sensitive to these toxicities and therefore they may not translate *in vivo.*

Chapter Five

Contractile maturity in cardiac microtissue models

5.1 Introduction

As well as structural cardiotoxicity, drug induced cardiovascular toxicity results from functional effects (acute alteration of the mechanical function of the myocardium) on the heart. These adverse effects can also result in conditions such as arrhythmia or a more serious reduction in left ventricular ejection fraction (LVEF), which can lead to heart failure and death (Brana & Tabernero, 2010; Gianni *et al.*, 2008; Mellor *et al*., 2011). This chapter will firstly describe the detection of positive and negative inotropic agents in cardiac microtissues. A positive inotrope acts to increase the force of cardiomyocyte contraction while a negative inotrope reduces cardiomyocyte contraction. Data suggests that only a matured adult CM can respond to a positive inotrope with positive inotropy and positive chronotropy (increase in contraction rate); hESC-CMs are suggested to respond with only positive chronotropy (Lieu *et al.*, 2009; Robertson *et al.*, 2013). For a cardiomyocyte to respond with positive inotropy they are thought to require an extensive t-tubule network to ensure that the entire cell depolarizes rapidly and homogeneously, a larger intracellular Ca^{2+} store and more dependence upon ryanodine receptors for calcium-induced calcium release (CICR). Immature CM's rely on extracellular Ca^{2+} therefore their Ca^{2+} transients are smaller and slower, lacking the synchrony needed to increase contraction force (Robertson *et al.*, 2013). Microtissues will also be assessed for an increase in sarcoplasmic reticulum function by caffeine-induced calcium release, see section 1.3.3 for details on caffeine effects on cardiomyocyte Ca^{2+} homeostasis.

The current widely used contractility assay uses canine cardiomyocytes and applies them to the IonOptix cell geometry system that utilizes video-based detection of sarcomere shortening (Harmer *et al*, 2012). This technique relies upon optical intensity data that translates into transients of peaks and troughs. These contractility transients are analysed using IonWizard software to provide quantification of contractility (contraction displacement measurements). This animal model, however is a relatively poor predictor of human specific responses. The microtissues will be applied to a similar contractility assay to study their responses to known inotropes and caffeine.

These compound responses will be used alongside a gene expression study of all microtissues in order to highlight any cardiac maturity brought about by a) 3D culturing and b) multicellular culturing.

The ultimate aim of this chapter is to show that the cardiac microtissues can provide a human relevant contractile mature alternative for studying drug-induced functional cardiotoxicity *in vitro*.

5.2 Microtissue functional characterisation

5.2.1 Spontaneous contractions

Human ESC-cardiomyocytes (hESC-CMs) were cultured either alone (CM microtissues) or with human cardiac microvascular endothelial cells (hCMECs) and human cardiac fibroblasts (hCFs) (CMEF microtissues) in 96 well round-bottomed ultra-low adhesion plates. This method can allow the production of microtissues with uniform size and shape. After two weeks all cultures formed a single spontaneously beating microtissue with a 200 μm diameter in each well. Microtissues were transferred onto 0.1% (w/v) gelatin-coated 13 mm plastic coverslips (Thermanox,) within a 12 well plate and incubated at 37ºC, 5% CO_2 for at least one hour before mounting onto the IonOptix contractility system. Contractile properties of spheroids were assessed using a video-based edge detection method (IonOptix™, Dublin, Ireland). A gelatin-attached microtissue was placed in a perfusion chamber (FHC Inc., Bowdoinham, ME, USA) mounted on the stage of an inverted Nikon TE200 microscope (Nikon UK, Surrey, UK). Microtissues were continuously perfused from a gravity fed system with warmed microtissue media. Figure 5.1 shows a 10 secrecording of spontaneous contractions in CM and CMEF microtissues using video-based edge detection. The rate of contraction varies between the microtissue types; CM microtissues contract 0.4 beats per sec (b/s) (figure 5.1a) whereas the CMEF microtissues have a rate of 0.9 b/s (figure 5.1b).

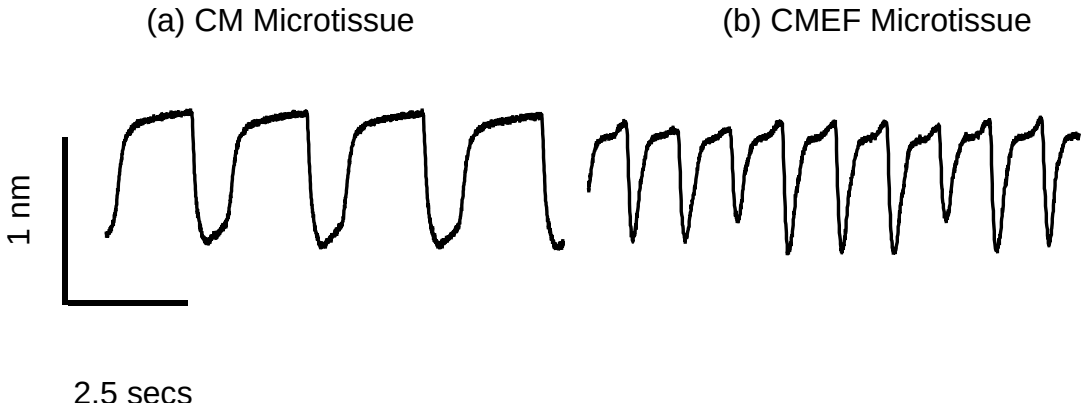

Figure 5.1 Spontaneous contractions in (a) CM and (b) CMEF microtissues.

hESC-CMs were cultured either alone (CM microtissues) or with hCMECs and hCFs (CMEF microtissues) in 96 well round-bottomed ULA plates. After 2-3 days the cells have aggregated to form one tight microtissue in each well. After 2 weeks the microtissues spontaneously beat. Microtissues were transferred onto 0.1% gelatin-coated coverslips for at least one hour before mounting onto the IonOptix contractility system. Contractile properties were assessed using a video-based edge detection method (IonOptix™, Dublin, Ireland).

5.2.2 Calcium and contraction response to electrical pacing

Microtissues were loaded with 0.2 µmol/L Fura-2-acetoxymethyl ester (Invitrogen), a calcium-sensitive, ratiometric fluorescence dye, for 10 mins at RT and kept in the dark. An IonOptix system was used to conduct the experiments, including the Xenon arc lamp, hyperswitch and myopacer for myocyte stimulation and fluorescence excitation, myocam-S for the measurement of edge contraction, and a fluorescence system interface to integrate the different components (IonOptix Ltd). The Xenon arc lamp and fluorescence hyperswitch containing a galvonised mirror were used to alternate between wavelengths of 340 and 380 nM at a high frequency. Calcium fluorescence was recorded at 510 nm. Calcium traces represent the ratio of calcium bound: calcium free Fura-2- acetoxymethyl ester dye, and hence changes in free intracellular calcium. Simultaneous edge contraction

and calcium recordings for the microtissues were taken while perfusing with the microtissue media solution and field stimulating with suprathreshold voltage (7V) at various pacing frequencies (0.5, 1, 2 and 3Hz) with a bipolar pulse of 6 ms duration, using a pair of platinum wires placed on opposite sides of the microscope chamber connected to a MyoPacer EP stimulator (IonOptix™). Microtissues responded to an increase in electrical stimulation frequency by decreasing transient peak height and increasing contraction frequency (figure 5.2a (CMEF) & 5.2b (CM)). The alignment of the calcium-contraction transients shows that edge detection is a reliable measure of microtissue contraction in both CMEF (figure 5.2a) and CM (figure 5.2b) microtissues; peak bound calcium immediately precedes microtissue peak contraction.

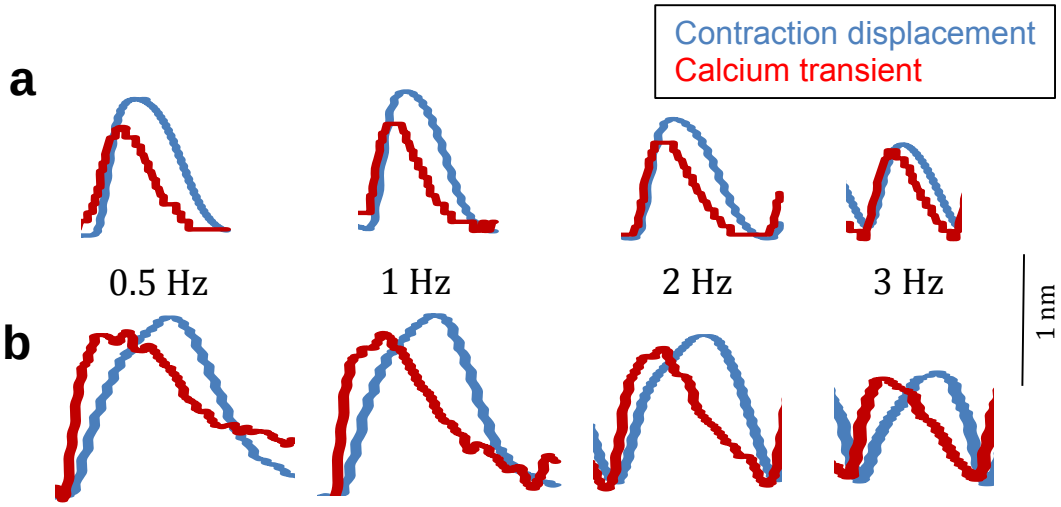

Figure 5.2 Representative edge contraction and calcium transients in (a) CMEF and (b) CM microtissues paced at 0.5Hz, 1Hz, 2Hz and 3Hz.

hESC-CMs were cultured either alone (CM microtissues) or with hCMECs and hCFs (CMEF microtissues) in 96 well round-bottomed ULA plates. After 2-3 days the cells have aggregated to form one tight microtissue in each well. After 2 weeks the microtissues spontaneously beat. Microtissues were transferred onto 0.1% (w/v) gelatin-coated coverslips for at least one hour before loading with 0.2 µmol/L Fura-2 for 30 mins and then mounted onto the IonOptix contractility system. Contractile properties and calcium fluorescence were assessed using the IonOptix system with field stimulation at 0.5, 1, 2, 3Hz with 7V for 6 ms.

Figure 5.3 shows quantification of the contraction (figure 5.3a) and calcium (figure 5.3b) transient peak heights from triplicate microtissues. The CM microtissues have a significantly higher peak amplitude at 1Hz than the CMEF microtissues ($p=0.0053$) but overall significantly lower maximum bound calcium (calcium peak height) ($p<0.001$), this already suggests a difference in calcium handling between the two microtissue types.

5.2.3 Validation of assay design and detection of negative inotropy in microtissues

The L-type calcium channel blocker verapamil was used as a typical 'negative' inotrope to test the capability of the Ionoptix in detecting changes in contraction displacement using video capture of the microtissue edge to measure changes in contraction displacement. Compound response was measured from one microtissue on triplicate occasions. After microtissues were added to the microscope stage, perfusion with microtissue media (with 0.1% (v/v) DMSO as the vehicle control) was started immediately. At this time field stimulation was also started (1Hz) and the microtissues allowed to acclimatise for at least 2 mins at 37^{o}C. A period of 30s of basal contractions were recorded for each microtissue before test compounds were applied in a cumulative manner with each concentration applied for 250 s or until steady-state was achieved. Figure 5.4 displays representative basal contraction transients of CMEF (figure 5.4a) and CM microtissues (figure 5.4b) followed by their contractility response to 1 μM verapamil. These 20s transient snapshots display a reduction in transient peak height in both microtissue types with 1 μM verapamil showing firstly the microtissues are capable of responding to a negative inotrope with a decrease in contraction displacement but also that this can be recorded using the IonOptix video-based edge detection.

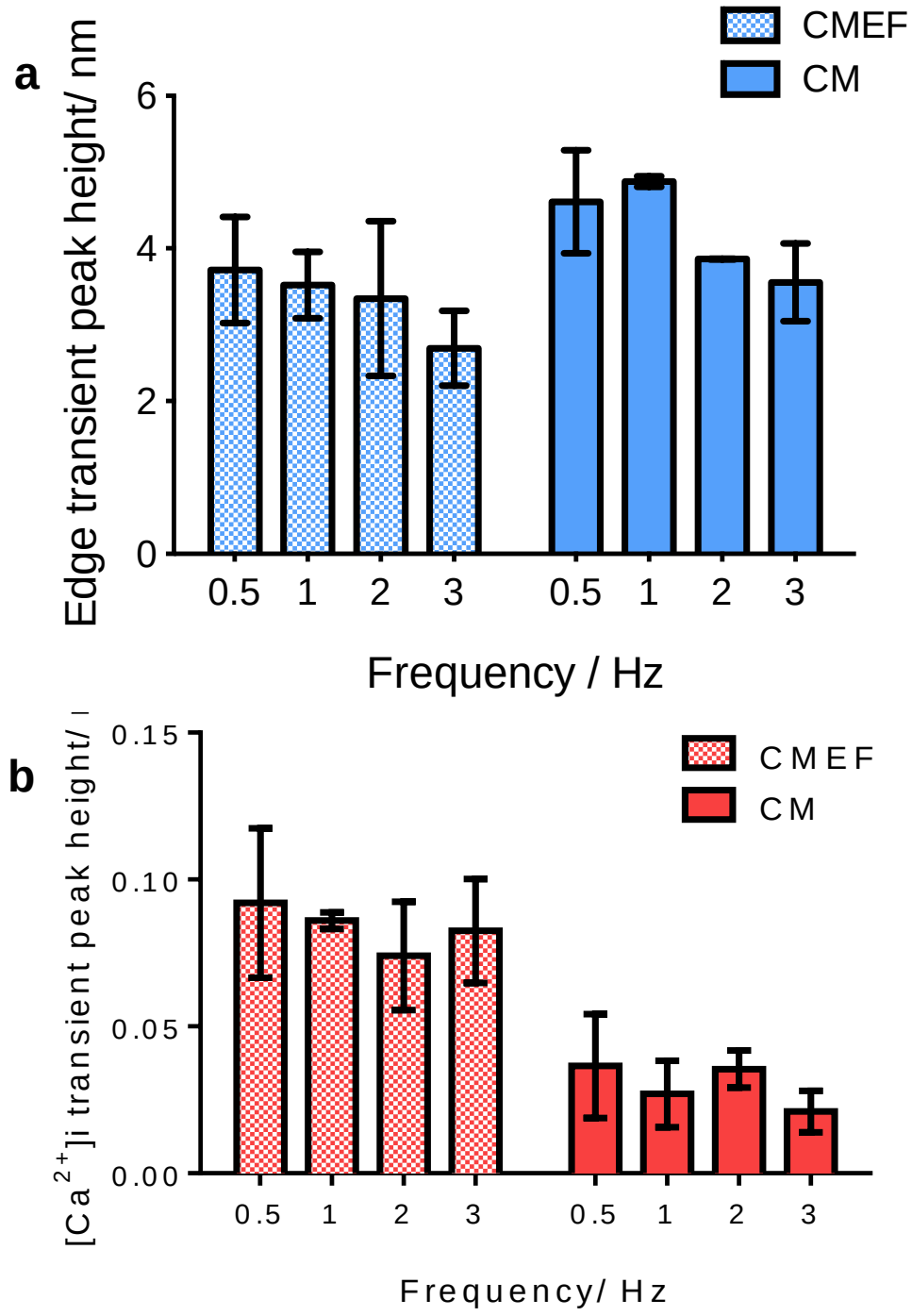

Figure 5.3 Quantification of (a) contraction and (b) calcium transient peak height at 0.5, 1, 2 and 3Hz.

hESC-CMs were cultured either alone (CM microtissues) or with hCMECs and hCFs (CMEF microtissues) in 96 well round-bottomed ULA plates. After 2-3 days the cells have aggregated to form one tight microtissue in each well. After 2 weeks the microtissues spontaneously beat. Microtissues were transferred onto 0.1% (w/v) gelatin-coated coverslips for at least one hour before loading with 0.2 µmol/L Fura-2 for 30 mins and then mounted onto the IonOptix contractility system. Contractile properties and calcium fluorescence were assessed using the IonOptix system with field stimulation at 0.5, 1, 2, 3Hz with 7V for 6 ms.

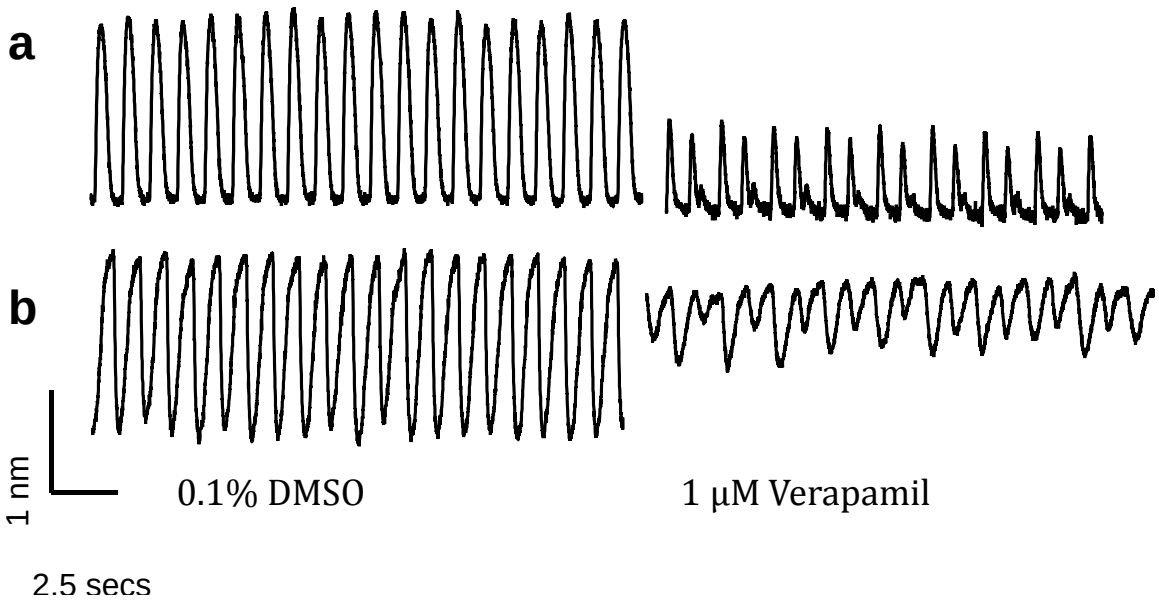

Figure 5.4 Contractility response of (a) CMEF and (b) CM microtissues to 1 µM verapamil.

hESC-CMs were cultured either alone (CM microtissues) or with hCMECs and hCFs (CMEF microtissues) in 96 well round-bottomed ULA plates. After 2 weeks the microtissues spontaneously beat. MT's were attached to gelatin-coated coverslips, mounted onto the IonOptix contractility system and field stimulated at 1.5Hz. The negative inotrope verapamil was applied in a cumulative manner with each concentration applied for 250s or until steady state. 20s of basal contraction transients (0.1% DMSO) (left side) and 20s of 1 µM verapamil contraction transients (right side) are shown.

Analysis was performed using the IonWizard™ software. For each test condition, data for 10 to 15 contractions were averaged to give a single representative monotonic contractility transient. From this analysis, 3 key parameters were used to quantify microtissue dynamics: 1) peak height, which indicates the percentage of peak contraction relative to the resting length. 2) Maximum contraction velocity, calculated as the maximum rate of change in peak height during the contraction phase. 3) Maximum relaxation velocity, calculated as the maximum rate of change in peak height during the relaxation phase. Figure 5.5 illustrates these parameters of a contraction transient.

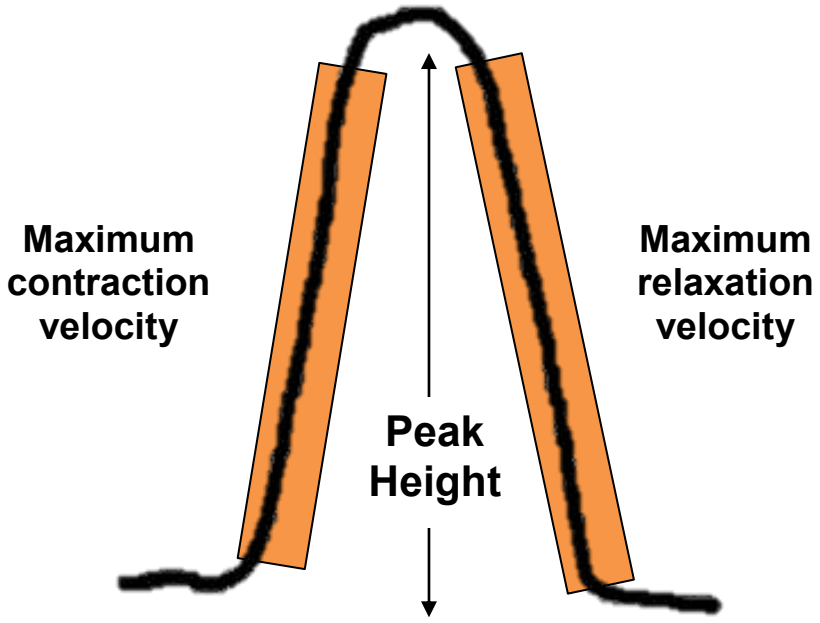

Figure 5.5 Illustration of contraction transient parameters.
Peak height, which indicates the percentage of peak contraction relative to the resting length. Maximum contraction velocity, calculated as the maximum rate of change in peak height during the contraction phase. Maximum relaxation velocity, calculated as the maximum rate of change in peak height during the relaxation phase.

The verapamil concentration-effect curves for each of these parameters in CMEF and CM microtissues relative to 0.1% (v/v) DMSO are displayed in figure 5.6a,b & c. Each parameter shows a dose-dependent decline with verapamil; peak height was selected as the most reproducible parameter. These responses are not significantly different ($p>0.1$).

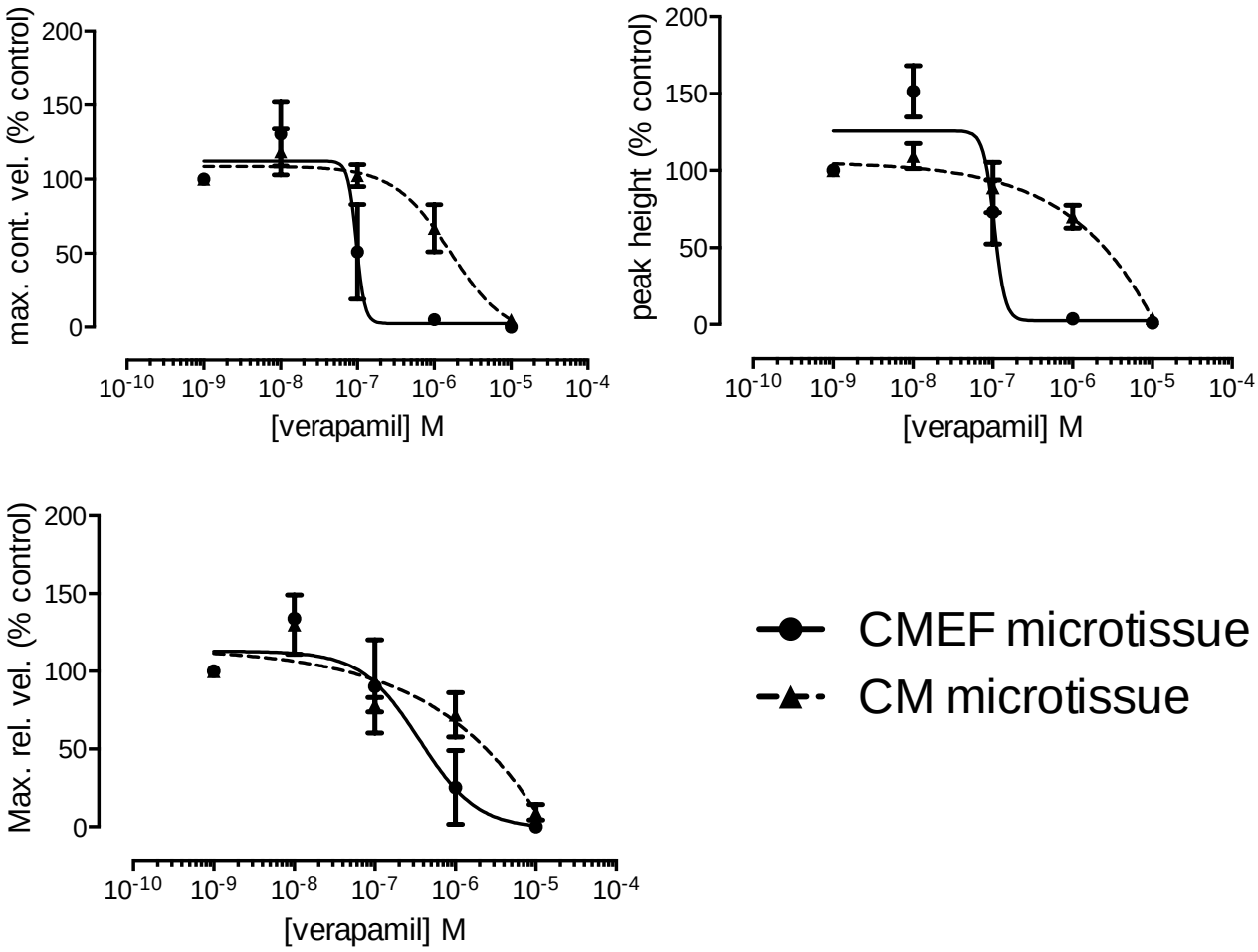

Figure 5.6 Verapamil concentration-effect curves for the 3 key transient parameters in CM and CMEF microtissues.

hESC-CMs were cultured either alone (CM microtissues) or with hCMECs and hCFs (CMEF microtissues) in 96 well round-bottomed ULA plates. After 2 weeks the microtissues spontaneously beat. Microtissues were attached to gelatin-coated coverslips, mounted onto the IonOptix contractility system and field stimulated at 1.5Hz. The negative inotrope verapamil was applied in a cumulative manner with each concentration applied for 250s or until steady state. 10-15 contraction transients were average for each test condition and the resulting monotonic contractility transient analysed to quantify maximum contraction velocity (max.cont.vel), peak height and maximum relaxation velocity (max.rel.vel), data is triplicate and relative to 0.1% (v/v) DMSO. *SD error bars.*

5.2.4 Detection of positive inotropy in microtissues

Having shown that both the single cell (CM) and multicell (CMEF) microtissues can respond to the negative inotrope verapamil, they were then assessed for their contractility response to a positive inotrope. A positive inotrope acts to increase contraction displacement; the beta-adrenergic receptor agonist dobutamine was selected as a test agent. As with the verapamil test in the previous section, the microtissues were applied to the IonOptix contractility system and field stimulated at 1.5Hz with flow of warm microtissue media. A period of 30s of basal contractions were recorded for each microtissue before dobutamine was applied in a cumulative manner with each concentration applied for 250 s or until steady-state was achieved. Figure 5.7 displays representative basal contraction transients of CMEF (figure 5.7a) and CM microtissues (figure 5.7b) followed by their contractility response to 10 μM dobutamine. These 20s transient snapshots display a increase in transient peak height in CMEF microtissues with the positive inotrope, interestingly the CM microtissues show no increase in peak height. From this we can see that, firstly, the video-based edge detection method is capable of recording an increase in microtissue contraction displacement as seen with CMEF, but the CM microtissues cannot respond with positive inotropy to dobutamine. A wider panel of inotropic agents with different mechanisms of action needs to be tested to determine the significance of this finding.

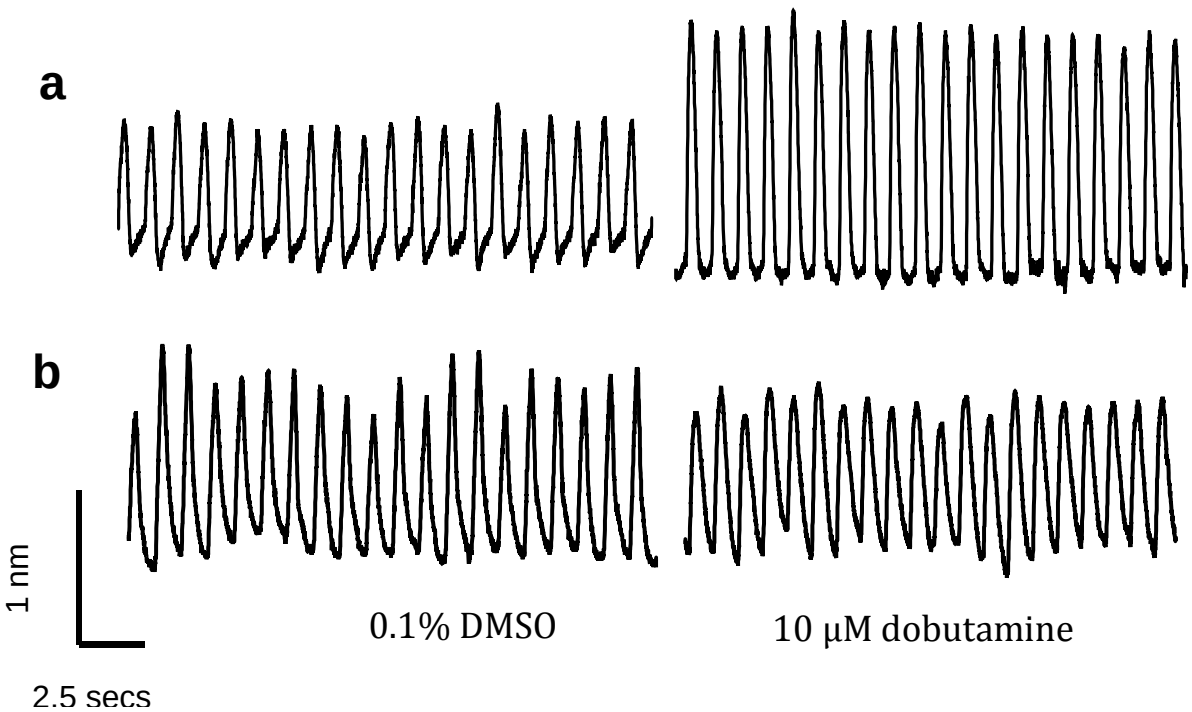

Figure 5.7 Contractility response of (a) CMEF and (b) CM microtissues to 10 µM dobutamine.

hESC-CMs were cultured either alone (CM microtissues) or with hCMECs and hCFs (CMEF microtissues) in 96 well round-bottomed ULA plates. After 2 weeks the microtissues spontaneously beat. Microtissues were attached to gelatin-coated coverslips, mounted onto the IonOptix contractility system and field stimulated at 1.5Hz. The positive inotrope dobutamine was applied in a cumulative manner with each concentration applied for 250s or until steady state. 20s of basal contraction transients (0.1% DMSO) (left side) and 20s of 10 µM dobutamine contraction transients (right side) are shown.

5.3 CMEF microtissues provide enhanced *in vitro* to *in vivo* correlation

5.3.1 Response of CMEF and CM microtissues to a panel of positive inotropic agents

CMEF and CM microtissues respond with decreased contraction displacement to the negative inotrope verapamil (figure 5.4a & b), however only CMEF respond with increased contraction displacement to the positive inotrope dobutamine (figure 5.7a). The contractile function of CM and CMEF microtissues were assessed against a panel of negative and positive inotropic agents. Positive inotropic agents with different mechanisms of action were selected. The microtissues were utilised between 2 and 4 weeks post seeding with verapamil response assessed throughout this time period to control for functional changes within the microtissues. As described in the previous *section 5.2.3*, the microtissues were attached to gelatin-coated coverslips, mounted on the IonOptix contractility system where they were field stimulated at 1-1.5Hz with microtissue media perfusion at 37^{o}C. A period of at least 30s of basal contractions were recorded for each microtissue before test compound was applied in a cumulative manner with each concentration applied for 250 s or until steady-state was achieved. Analysis was performed using the IonWizard™ software. For each test condition, data for 10 to 15 contractions were averaged to give a single representative monotonic contractility transient from which peak height was calculated using IonWizard™ software. Figure 5.8 shows CMEF and CM microtissue concentration-effect curves for isoproterenol, milrinone, epinephrine, glibenclamide and levosimenden. These curves show that all positive inotropy went undetected in CM microtissues. CMEF microtissues, however, responded to each positive inotrope with an increase in contraction displacement (peak height).

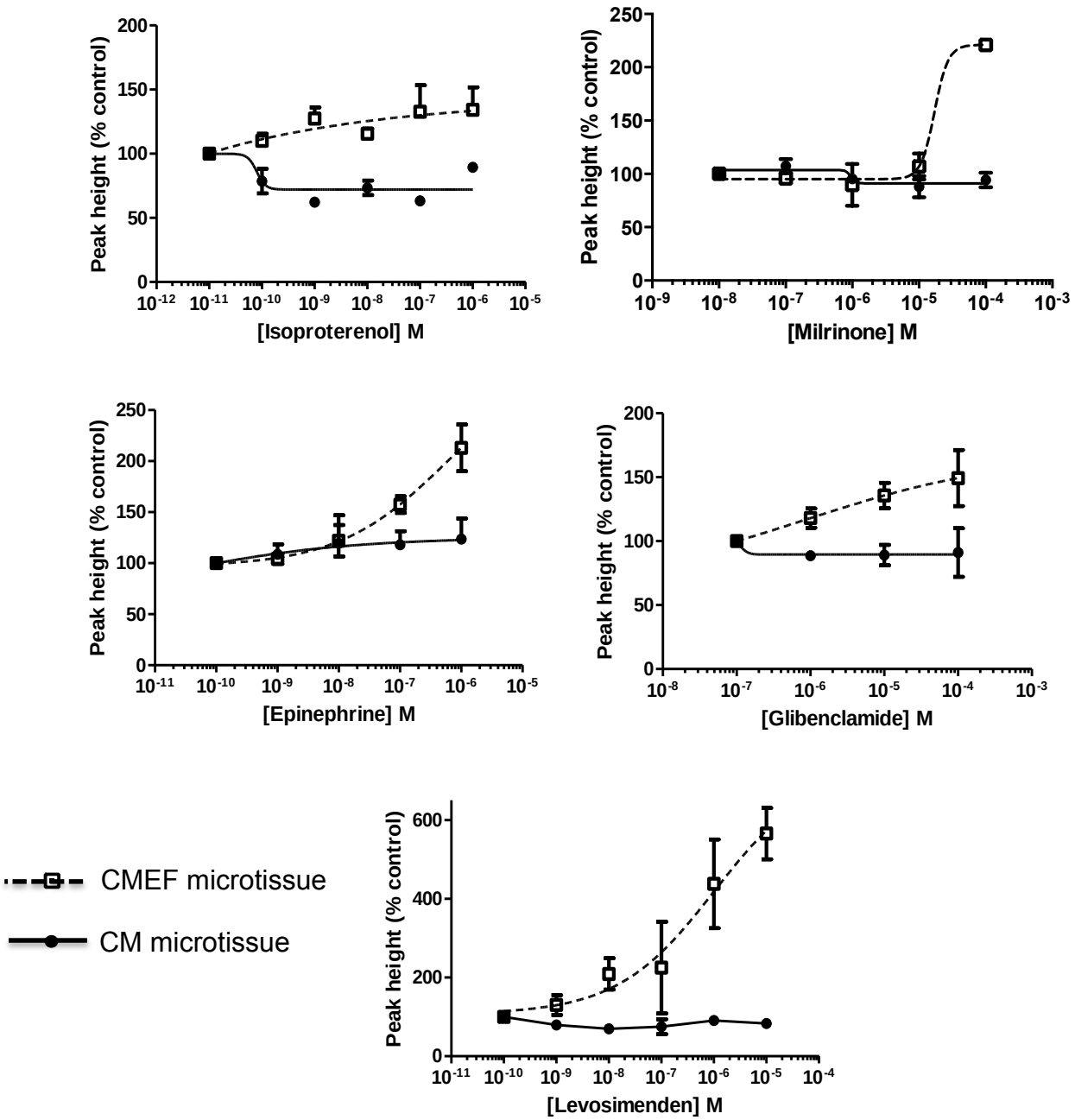

Figure 5.8 Concentration-effect curves of CMEF and CM microtissues in response to positive inotropes.

hESC-CMs were cultured either alone (CM microtissues) or with hCMECs and hCFs (CMEF microtissues) in 96 well ULA plates. After 2 weeks microtissues were attached to gelatin-coated coverslips, mounted onto the IonOptix contractility system and field stimulated at 1-1.5Hz, with a bipolar pulse of 6 ms duration and perfused at 37^{o}C. Test compounds were applied in a cumulative manner with each concentration applied for 250 s or until steady-state. For each test condition, data for 10 to 15 contractions were averaged to give a single representative monotonic contractility transient. Each plot shows the effect on peak height relative to 0.1% (v/v) DMSO (n=3*). SD error bars.*

5.3.2 The response of CMEF microtissues to a wider panel of inotropic agents

Since the CMEF microtissues can correctly predict the direction of inotropy, they were assessed against a wider panel of inotropic agents to gain better insight into their predictive strength. A total of 24 compounds were selected for testing based on their *in vivo* effect; 12 negative inotropes, 7 positive inotropes and 5 negative controls. Each of these compounds were tested in triplicate on separate CMEF microtissues. The aim was to determine whether this model could potentially offer a human relevant replacement for the current canine assay (Harmer *et al*, 2012). Data is summarised in table 5.1, for each compound the clinical target, top test concentration and IC_{50}/EC_{50} for peak height is shown. Representative concentration-effect curves for 12 of the 24 compounds are displayed in figure 5.9, peak height is relative to 0.1% (v/v) DMSO control. The CMEF microtissues correctly predicted negative inotropy for atenolol, doxorubicin and lapatinib; compounds which had no effect on canine cardiomyocyte contractility (Harmer *et al*, 2012). These compounds were subsequently tested in the CM microtissue model to assess whether the negative inotropy is a trait of the hESC-CMs or the tri-cultured microtissue. Table 5.1 shows the CM microtissues responded with negative inotropy to the anthracycline doxorubicin, but were unresponsive to atenolol and lapatinib. Despite responding to verapamil the CM microtissues did so with a 10-fold increased IC_{50} (1 μM), therefore diltiazem, also an L-type Ca^{2+} channel blocker, was tested in the CM microtissue model. Diltiazem behaved as a negative inotrope in CM microtissues but again with less potency (CM, 2.47 μM; CMEF, 0.38 μM). Paracetamol wrongly presented as a negative inotrope in the canine cardiomyocytes, had no inotropy effect in the CMEF microtissues (Table 5.1). Ivabradine and Phentolamine wrongly presented as negative inotropes in both assay models. Table 5.1 shows correctly predicted compounds in blue and incorrectly predicted compounds in pink, based on *in-vivo* effects. Comparison of the CMEF data (92% correctly predicted) with canine cardiomyocyte assay data from Harmer *et al* (75% correctly predicted), shows improved *in vitro* to *in vivo* correlation with the multicellular CMEF model.

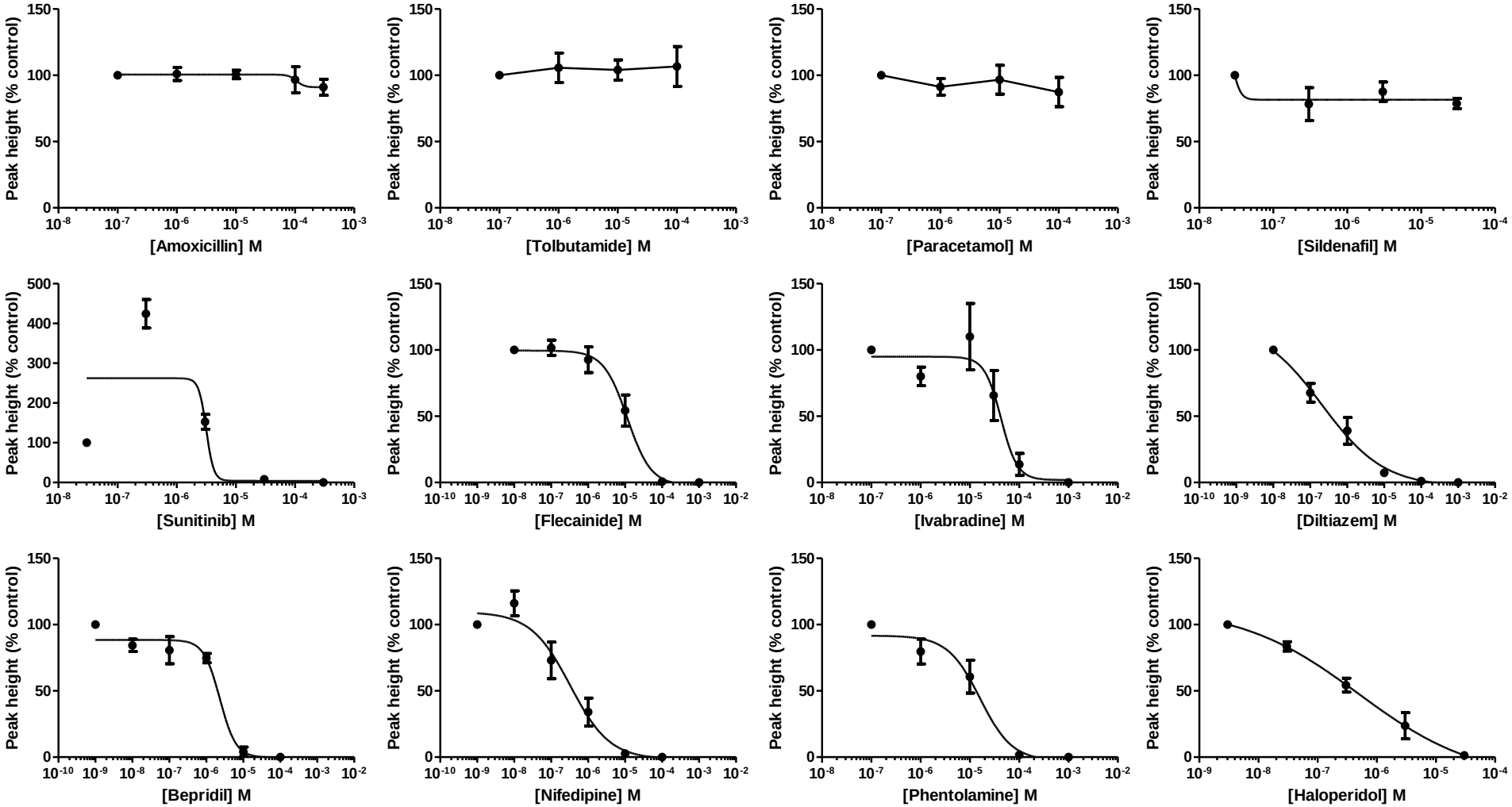

Figure 5.9 Representative concentration-effect curves of CMEF microtissues in response to inotropic and control agents. hESC-CMs were cultured with hCMECs and hCFs (CMEF microtissues) in 96 well ULA plates. After 2 weeks microtissues were mounted onto the IonOptix contractility system and field stimulated at 1-1.5Hz and perfused at 37ºC. Test compounds were applied in a cumulative manner with each concentration applied for 250 s or until steady-state. For each test condition, data for 10 to 15 contractions were averaged to give a single representative monotonic contractility transient. Each plot shows the effect on peak height relative to 0.1% (v/v) DMSO (n=3), *SD error bars*.

Table 5.1 Contraction peak height IC_{50}/ EC_{50}'s in CMEF microtissues, CM microtissues and canine cardiomyocytes.

Compound	Target	Top Test Conc.	EC_{50} / IC_{50} µM			Lowest IC_{50}/ EC_{50} CMEF Microtissue	Lowest IC_{50}/ EC_{50} Canine CM	Lowest IC_{50}/ EC_{50} CM Microtissue	*In vivo* effect
			Contraction Velocity (CV)	Peak Height (PH)	Relaxation Velocity (RV)				
No effect									
Amoxicillin	β-lactam antibiotic	100	NE	NE	NE	NE	NE	-	NE
Paracetamol	Cyclooxygenase inhibitor	100	NE	NE	NE	NE	44.98 ↓	-	NE
Sildenafil	PDE-5 inhibitor	30	NE	NE	NE	NE	NE	-	NE
Enalapril	Angiotensin-converting enzyme inhibitor	100	NE	NE	NE	NE	NE	-	NE
Tolbutamide	ATP-sensitive potassium channel inhibitor	100	NE	NE	NE	NE	NE	-	NE
-ve inotropy									
Atenolol	β1 receptor antagonist	100	NE	0.94	NE	0.94 ↓	NE	NE	-ve inotrope
Diltiazem	L-type Ca2+ channel blocker	100	0.42	0.38	7.78	0.38 ↓	7 ↓	2.47 ↓	-ve inotrope
Doxorubicin	Interacts with DNA	100	1.03	1.16	2.79	1.16 ↓	NE	1.16 ↓	-ve inotrope
Flecainide	Class Ic (Cardiac Na+ channel block)	100	7.05	11.14	10.46	11.14 ↓	7 ↓	-	-ve inotrope
Haloperidol	Dopamine D2-receptor antagonist	30	2.42	0.29	2.28	0.29 ↓	1 ↓	-	-ve inotrope
Lapatinib	EGFR and HER2/neu inhibitor	100	0.86	0.94	0.95	0.86 ↓	NE	NE	-ve inotrope
Nifedipine	L-type Ca2+ channel blocker	10	0.24	0.33	0.31	0.24 ↓	0.18 ↓		-ve inotrope
Sunitinib	Multi-targeted receptor tyrosine kinase inhibitor	30	18.33	18.82	20.12	18.33 ↓	5 ↓	-	-ve inotrope
Verapamil	L-type Ca2+ channel blocker	10	0.21	0.11	0.11	0.11 ↓	0.35 ↓	1 ↓	-ve inotrope
Bepridil	L-type Ca2+ channel blocker	10	2	2	0.3	0.3 ↓	1.4 ↓	-	-ve inotrope
Ivabradine	Inhibits the pacemaker	100	30.3	32.71	35.9	30.3 ↓	20 ↓	-	NE
Phentolamine	Non-selective alpha adrenergic receptor antagonist	100	20	20	20	20 ↓	15 ↓	-	NE
+ve inotropy									
Epinephrine	Non-selective adrenergic receptor agonist	1	NE	0.07	NE	0.07 ↑	0.1 ↑	0.0012 ↑	+ve inotrope
Glibenclamide	ATP-sensitive potassium channel inhibitor	100	0.8	0.96	24.01	0.8 ↑	1.58 ↑	NE	+ve inotrope
Levosimenden	calcium sensitiser (binds to cardiac troponin C)	10	0.13	0.15	0.14	0.13 ↑	0.09 ↑	NE	+ve inotrope
Digoxin	inhibits Na+ / K+ ATPase membrane pump	10	3.54	10.00	10	3.54 ↑	2.6 ↑	0.4	+ve inotrope
Dobutamine	β1-adrenergic agonist	10	8.38	0.29	0.83	0.29 ↑	1 ↑	0.03 ↓	+ve inotrope
Isoproterenol	betaadrenergic receptor agonist	0.1	0.0004	0.003	0.08	0.0004 ↑	0.002 ↑	0.00009 ↓	+ve inotrope
Milrinone	PDE-3 inhibitor	100	NE	83.68	NE	83.68 ↑	0.9 ↑	NE	+ve inotrope

Correlates with *in vivo* effect
No correlation with *in vivo* effect

↓ Decrease in CF
↑ Increase in CF

Compounds were subdivided into their *in vitro* effects; no effect, -ve inotrope, +ve inotrope. IC_{50}/ EC_{50}'s for CMEF, CM microtissues and canine CM are shown for contraction velocity, peak height and relaxation velocity for each compound tested. Data is the mean of triplicate experiments. The parameter with the lowest IC_{50}/ EC_{50} is used to compare the models. Top concentration tested is shown (Top Test Conc.). NE = no effect, - = not tested.

5.4 Contractile maturity is dependent upon the cardiac tri-culture system

To investigate the apparent contractile maturity of the CMEF microtissues; hESC-CMs were cultured in ULA plates with hCMECs (CME microtissues) or hCFs (CMF microtissues) and additionally in a tri-culture with human dermal microvascular endothelial cells (hDMECs) and human dermal fibroblasts (NhDFs) (DMEF microtissues). Once again, 200 μm spontaneously beating microtissues formed after two weeks and displayed uniform size, shape and even cell marker distribution (data shown in *chapter 3*). Their response to positive and negative inotropes was assessed using the IonOptix contractility assay. Only CMEF and CMF showed negative inotropy with atenolol (IC_{50}; 1 μM, $p<0.0009$) (figure 5.10a). Similarly, only CMEF and CME responded with negative inotropy to lapatinib (IC_{50}; 2 μM, $p=0.003$) (figure 5.10b). An increase in contraction magnitude in response to positive inotropic agents was not detected in CM, CMF, CME or DMEF (figure 5.11a & b). The mature contractile response to positive inotropy therefore remains a trait of the CMEF microtissues (Dobutamine IC_{50}; 0.3 μM, Digoxin IC_{50}; 2 μM).

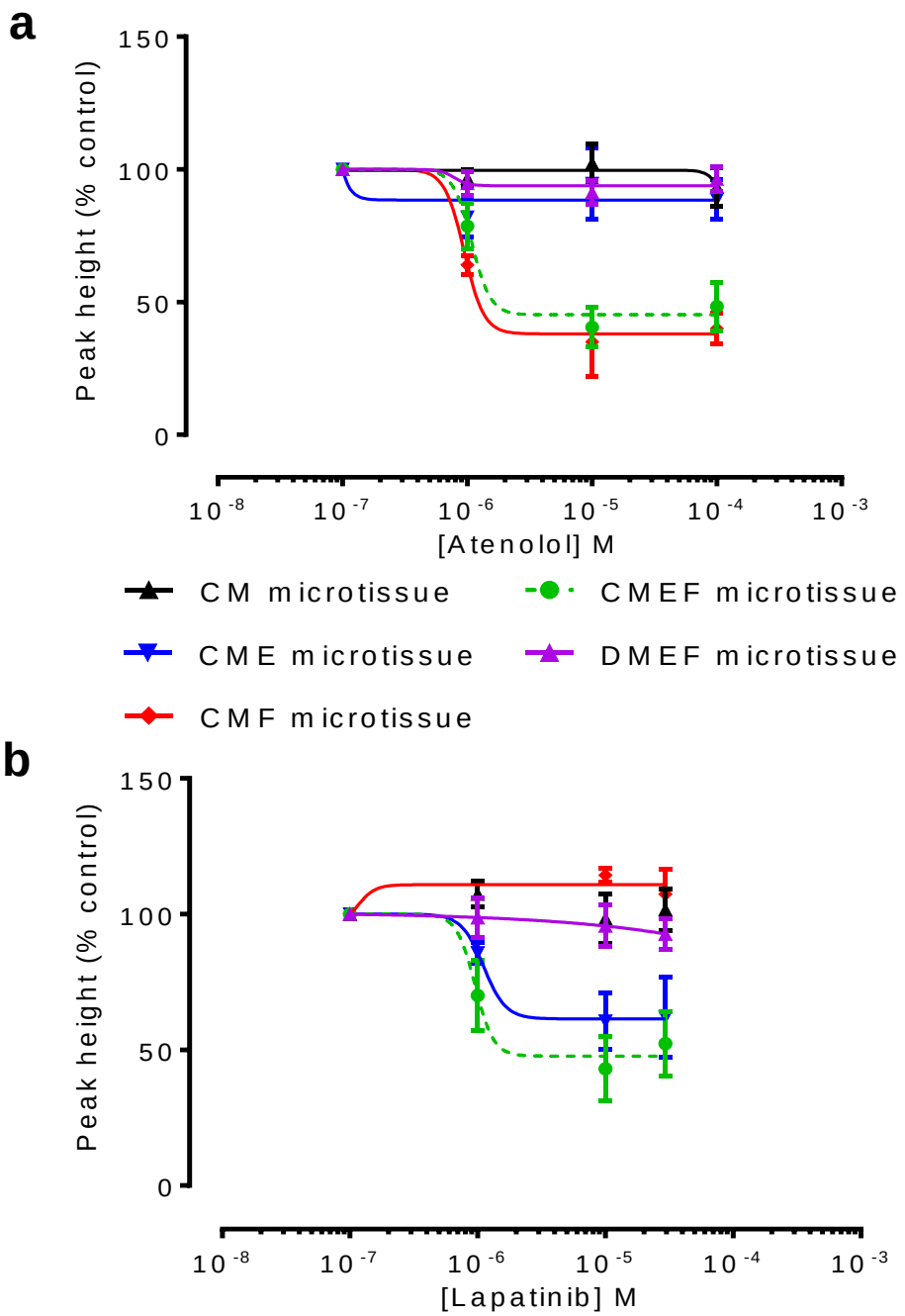

Figure 5.10 Response of CMEF, CM, DMEF, CME & CMF microtissues to negative inotropes atenolol and lapatinib. hESC-CMs were cultured either alone (CM microtissue), with hCMECs (CME microtissue) or hCFs (CMF microtissue) or both (CMEF microtissues) or hDMECs and NhDFs (DMEF microtissue) with in 96 well ULA plates. After 2 weeks microtissues were mounted onto the IonOptix contractility system and field stimulated at 1-1.5Hz. Test compounds were applied in a cumulative manner with each concentration applied for 250 s or until steady-state. For each test condition, data for 10 to 15 contractions were averaged to give a single representative monotonic contractility transient. Each plot shows the effect on peak height relative to 0.1% (v/v) DMSO (n=3), *SD error bars*.

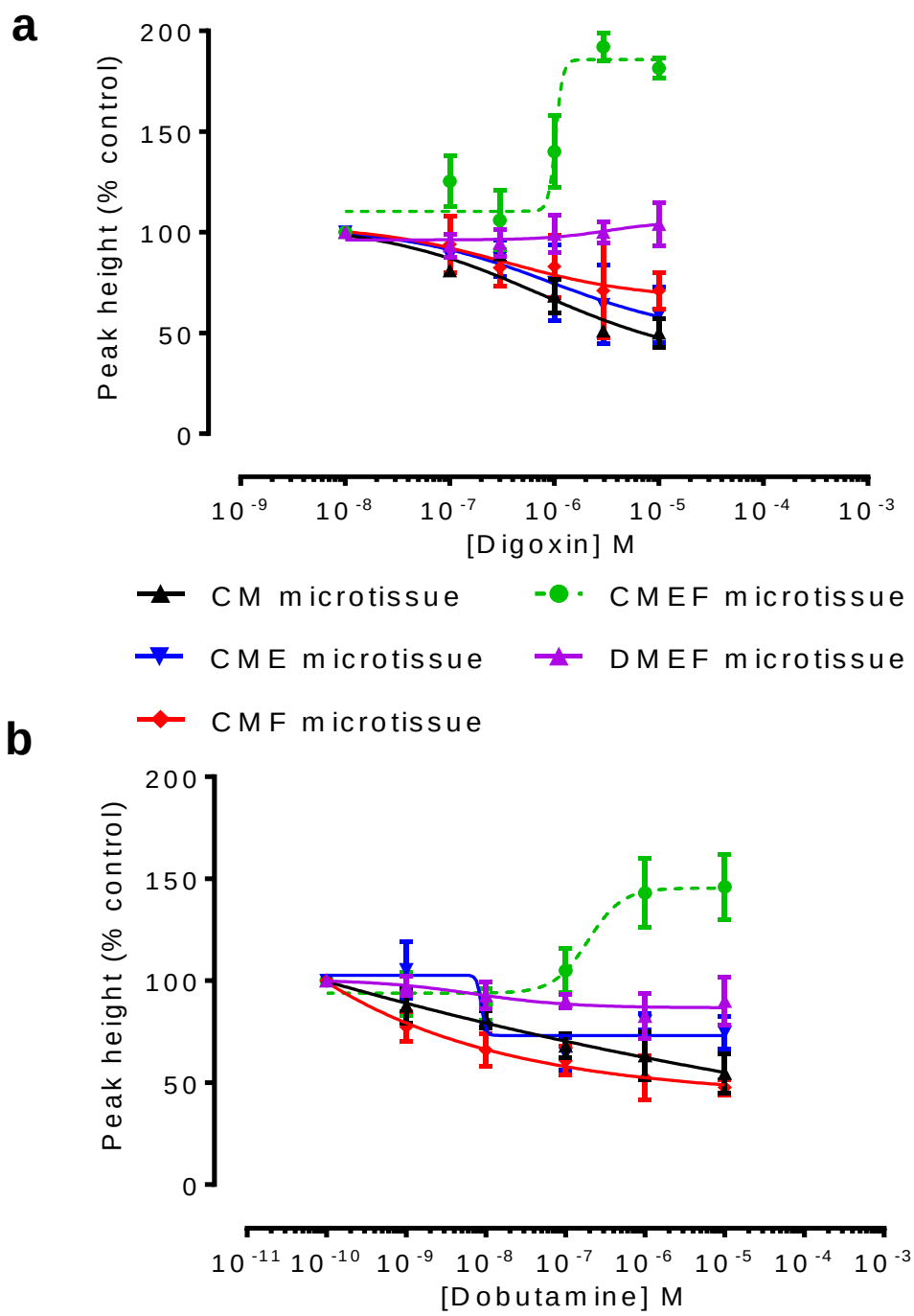

Figure 5.11 Response of CMEF, CM, DMEF, CME & CMF microtissues to positive inotropes digoxin and dobutamine. hESC-CMs were cultured either alone (CM microtissue), with hCMECs (CME microtissue) or hCFs (CMF microtissue) or both (CMEF microtissues) or hDMECs and NhDFs (DMEF microtissue) with in 96 well ULA plates. After 2 weeks microtissues were mounted onto the IonOptix contractility system and field stimulated at 1-1.5Hz. Test compounds were applied in a cumulative manner with each concentration applied for 250 s or until steady-state. For each test condition, data for 10 to 15 contractions were averaged to give a single representative monotonic contractility transient. Each plot shows the effect on peak height relative to 0.1% (v/v) DMSO (n=3), *SD error bars.*

5.5 Cardiac non-myocytes promote gene upregulation in CMEF microtissues

All microtissue models were subjected to gene expression analysis in order to determine whether the enhanced contractile performance of the CMEF microtissues correlates to an increase in gene maturity. A selection of structural and functional genes were selected based on maturation stages of cardiomyocytes (Robertson *et al.,* 2013) and in-house next generation sequencing (NGS) data generated for adult ventricle tissue, foetal heart tissue, hESC-CMs, hCMECs, hDMECs and hCFs, looking for genes specifically upregulated in adult ventricle and foetal heart. Microtissues were harvested for RNA extraction 2 weeks post seeding. Microtissues were pooled and washed in pre-warmed DPBS before lysis in buffer RLT containing 1% (v/v) 2-mercaptoethanol. Total RNA was extracted from cells using the RNeasy mini kit (Qiagen, Crawley, U.K.) and quantified using a NanoDrop spectrophotometer (NanoDrop Technologies). Total RNA was diluted to 20 ng and reverse transcribed using a SuperScript® III first-strand synthesis supermix kit (Life technologies) following manufacturers instructions. cDNA samples were preamplified using the TaqMan® PreAmp Master mix kit with TaqMan® Probes. QRT-PCR reactions were performed in a 7900 HT Fast Real-Time PCR System (Applied Biosystems, Foster City, CA, U.S.A.), 2.5 µl of preamplified cDNA was used with TaqMan® Gene Expression probes (Table 2.8) and master mix to monitor amplification under standard cycling conditions. Gene expression is expressed as fold change relative to GAPDH and adult ventricle using the ΔΔ*C*T method. Fold change relative to adult ventricle is plotted for adult, foetal, CMEF, DMEF, CM, CME, CMF and monolayer models (hESC-CMs, hCFs, hCMECs).

This investigation revealed two levels of mRNA upregulation: (i) an initial state of maturity which was promoted by a three dimensional (3D) culture environment, and (ii) an enhanced maturity state which was induced by culturing with both hCMECs and hCFs.

The gene expression pattern of MYH6 and MYH7 is traditionally used to monitor maturity in cardiomyocytes; during development there is a switch from high gene expression of MYH7 and low MYH6 to high MYH6 and low MYH7 in the fully matured cardiomyocyte. Figure 5.12 shows higher expression of MYH7 in foetal heart compared to adult ventricle and higher levels of MYH6 in adult ventricle than foetal heart, as would be expected. Both CM and CMEF show a downregulation of MYH7 and an upregulation of MYH6 when compared to hESC-CM monolayer expression. Cardiac troponin I (cTNI) and connexin43 (GJA1) mRNA levels were upregulated in both CM and CMEF microtissue models when compared to hESC-CM monolayer cells.

Table 5.2 Gene reference

Gene	Encodes
MYH6	Myosin heavy chain 6
MYH7	Myosin light chain 7
TNNI3	Cardiac troponin I
GJA1	Connexin43
ATP2A2	SERCA Ca^{2+} ATPase, slow twitch
ATP5B	Mitochondrial ATP synthase
KCNQ1	Potassium voltage gated channel
KCNJ2	Potassium inwardly rectifying channel
ADRB1	β-adrenergic receptor 1
S100A1	S100A1 calcium binding protein
TCAP	Titin-cap protein
NOS3	Endothelial nitric oxide synthase 3
PDE3A	Phosphodiesterase 3A

Reference table summarising the genes studied in this chapter with the corresponding protein complex encoded.

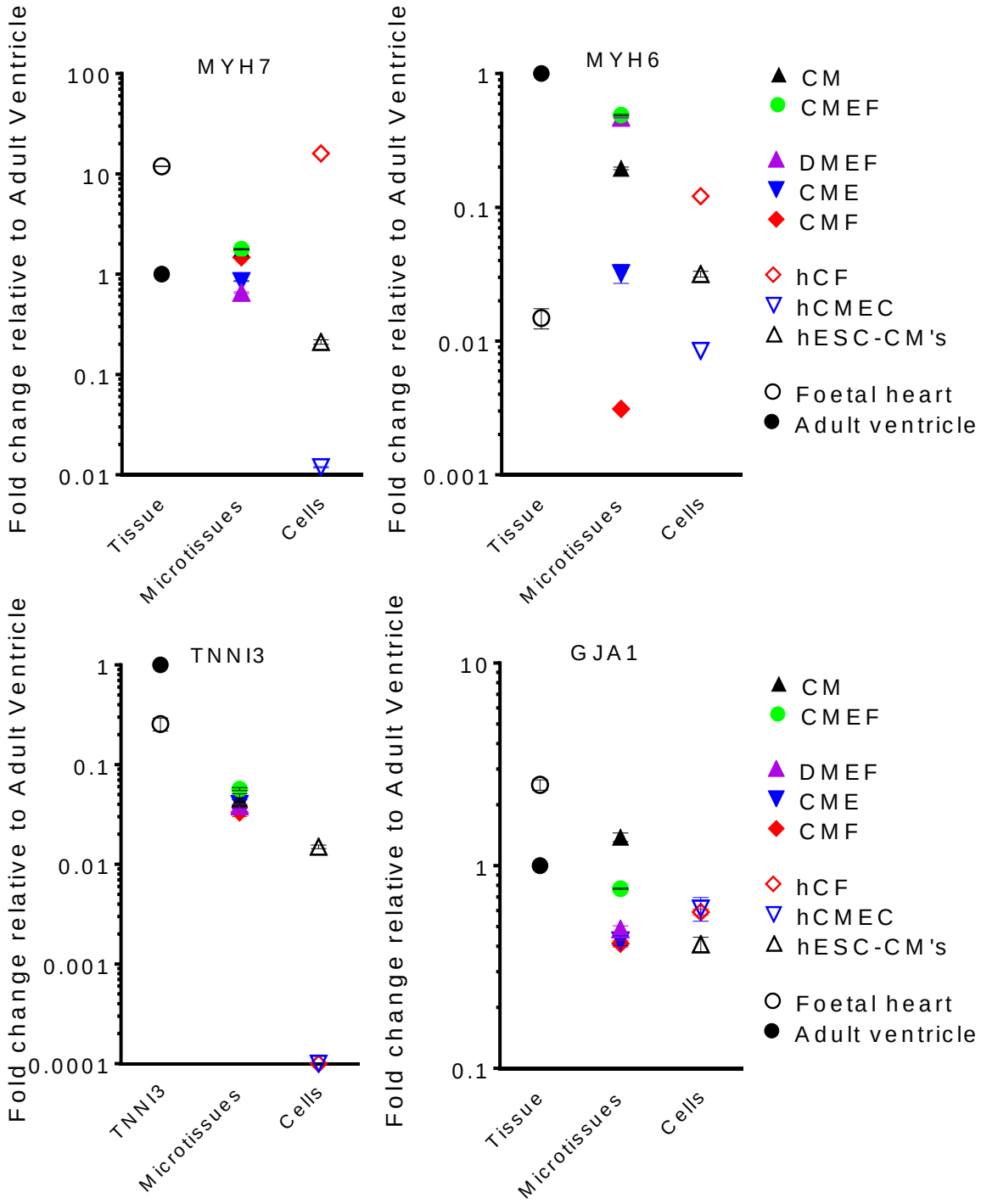

Figure 5.12 Expression of MYH7 and MYH6 in cardiac tissue, microtissues and monolayer cells.

Total RNA extracted using RNeasy mini kit (Qiagen, Crawley, U.K.). Total RNA was diluted to 20 ng and reverse transcribed using a SuperScript® III first-strand synthesis supermix kit (Life technologies). cDNA samples were preamplified using the TaqMan® PreAmp Master mix kit. QRT-PCR reactions were performed using TaqMan® Gene Expression probes and master mix to monitor amplification under standard cycling conditions. Gene expression is expressed as fold change relative to GAPDH and adult ventricle using the ΔΔ*C*T method. Fold change relative to adult ventricle is plotted for tissues, adult ventricle and foetal heart; microtissues, CMEF, DMEF, CM, CME and CMF; and cells, hESC-CMs, hCFs, hCMECs. *n=3, error bars represent SD.*

The SERCA Ca^{2+} ATPase (ATP2A2) and mitochondrial synthase (ATP5B) were upregulated at the gene level alongside adrenergic receptor β_1 (ADRB1). The levels of these genes were upregulated either towards adult ventricle or foetal heart dependent upon intial expression level. Similarly, various ion channels including K+ inwardly-rectifying channel (KCNJ2), K+ voltage-gated channel (KCNQ1) mRNA levels were found to be upregulated by 3D culturing.

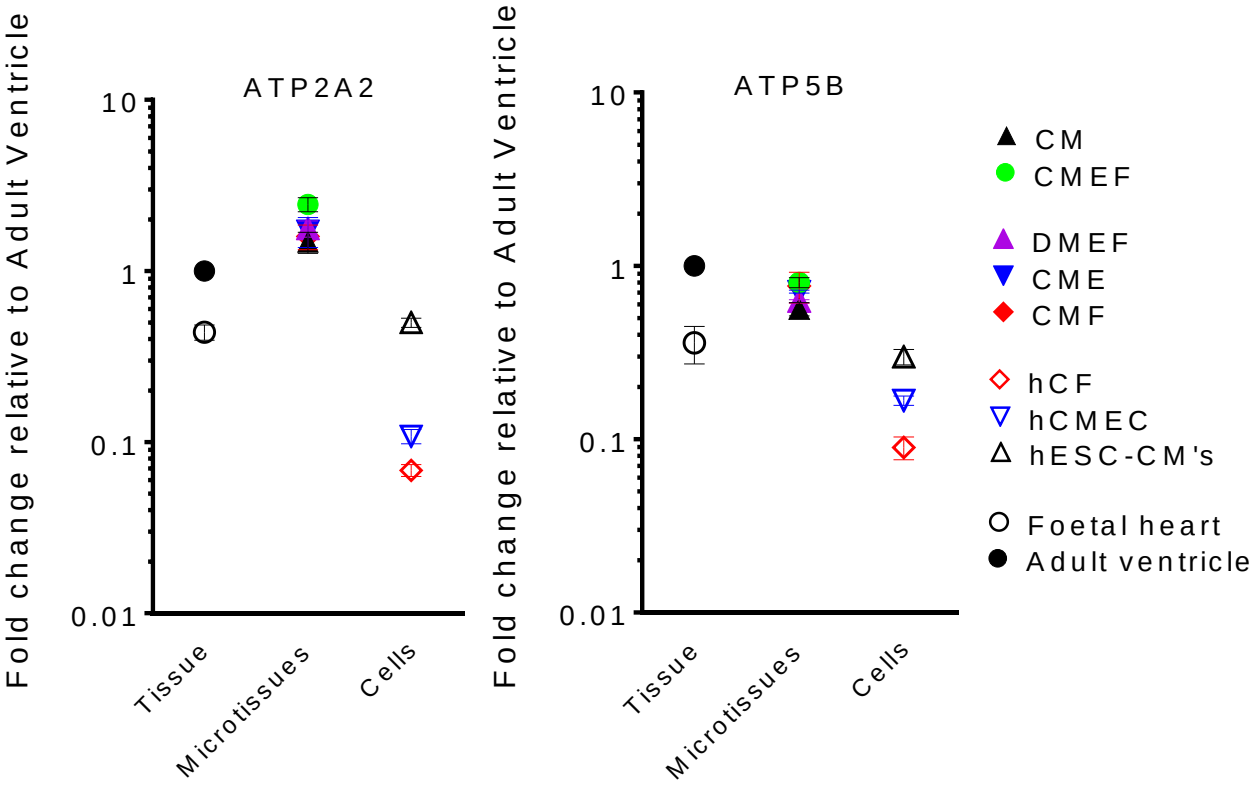

Figure 5.13 Expression of ATP2A2 and ATP5B in cardiac tissue, microtissues and monolayer cells.

Total RNA extracted using RNeasy mini kit (Qiagen, Crawley, U.K.). Total RNA was diluted to 20 ng and reverse transcribed using a SuperScript® III first-strand synthesis supermix kit (Life technologies). cDNA samples were preamplified using the TaqMan® PreAmp Master mix kit with TaqMan® Probes. QRT-PCR reactions were performed using TaqMan® Gene Expression probes and master mix to monitor amplification under standard cycling conditions. Gene expression is expressed as fold change relative to GAPDH and adult ventricle using the ΔΔCT method. Fold change relative to adult ventricle is plotted for tissues, adult ventricle and foetal heart; microtissues, CMEF, DMEF, CM, CME and CMF; and cells, hESC-CMs, hCFs, hCMECs. *n=3, error bars represent SD.*

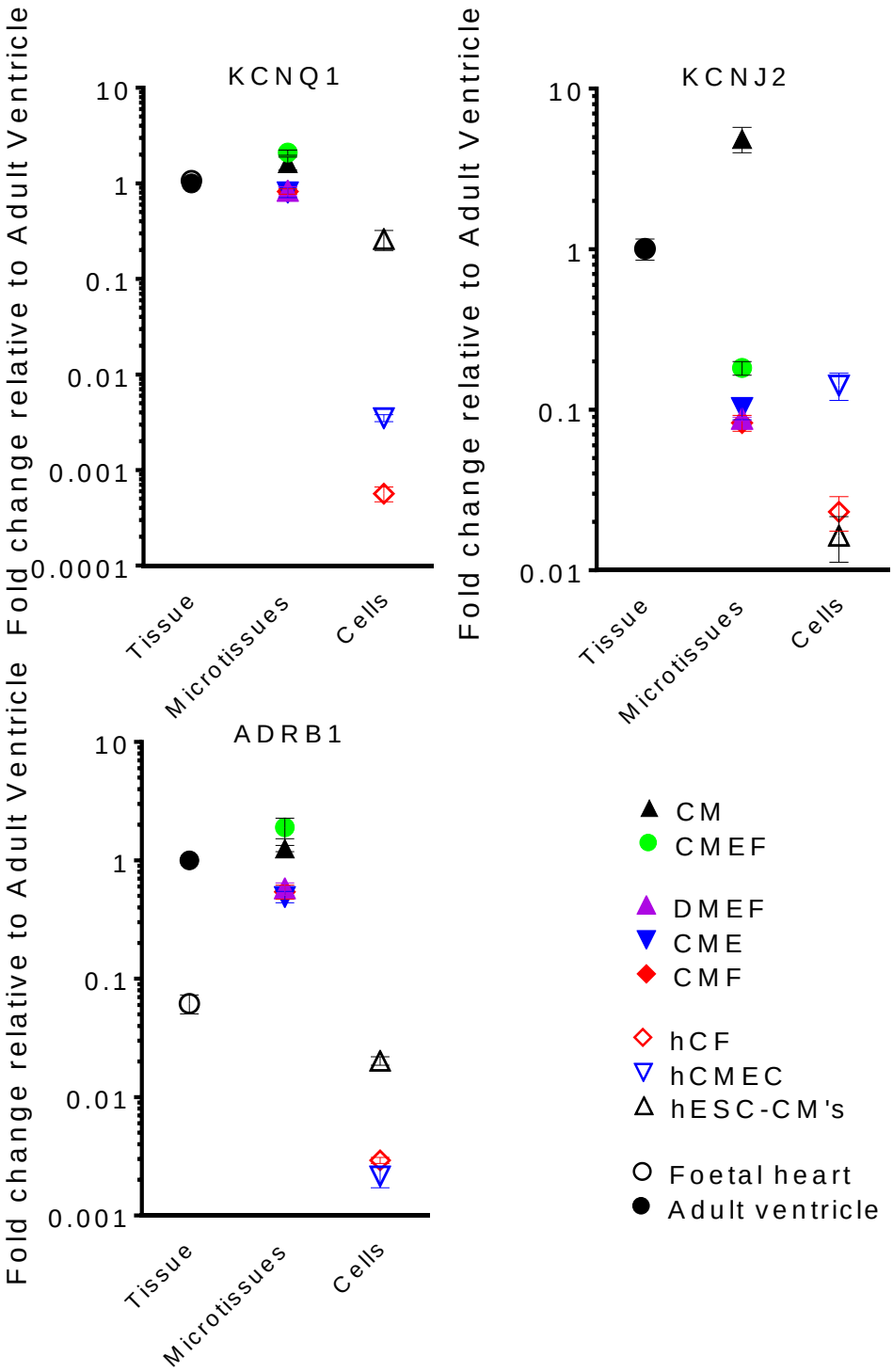

Figure 5.14 Expression of KCNQ1, KCNJ2 and ADRB1 in cardiac tissue, microtissues and monolayer cells.

Total RNA extracted using RNeasy mini kit (Qiagen, Crawley, U.K.). Total RNA was diluted to 20 ng and reverse transcribed using a SuperScript® III first-strand synthesis supermix kit (Life technologies). cDNA samples were preamplified using the TaqMan® PreAmp Master mix kit. QRT-PCR reactions were performed using TaqMan® Gene Expression probes and master mix to monitor amplification under standard cycling conditions. Gene expression is expressed as fold change relative to GAPDH and adult ventricle using the ΔΔCT method. Fold change relative to adult ventricle is plotted for tissues, adult ventricle and foetal heart; microtissues, CMEF, DMEF, CM, CME and CMF; and cells, hESC-CMs, hCFs, hCMECs. *n=3, error bars represent SD.*

A selection of genes showed enhanced upregulation specifically in the CMEF microtissues. An S100 Ca^{2+} binding protein (S100A1) and titin cap (TCAP) were found to have enhanced upregulation in the CMEF microtissues (figure 5.15); only the CMEF microtissues showed mRNA expression of S100A1 above that of the foetal heart, an increase of at least 10 fold relative to other microtissue types. Nitric oxide synthase 3 (NOS3), an endothelial derived form of NOS and phosphodiesterase 3 (PDE3A) were also found to have enhanced upregulation within the CMEF microtissues (figure 5.15).

5.6 S100A1 upregulation correlates with calcium handling maturity

Having studied the maturity of the microtissues at the gene expression level (*section 5.5*), this highlighted an upregulation of the S100A1 gene specifically in the CMEF microtissues. This was the only gene upregulated specifically in the CMEF's relative to the other microtissues at a level that was above foetal heart tissue, towards adult cardiomyocytes. S100A1 is suggested to modulate SR function in the mature cardiomyocyte. A high caffeine concentration of 10 mM was used to study SR function. Caffeine opens the RyRs and releases the SR ca^{2+} stores into the cytosolic domain. In the myocardium the strength of the contraction (inotropy) is dependent upon the magnitude of the Ca^{2+} released into the cytosol. In immature cardiomyocytes we see a lack of SR function therefore dysfunctional excitation contraction coupling upon caffeine-induced calcium release (caff-ICR).

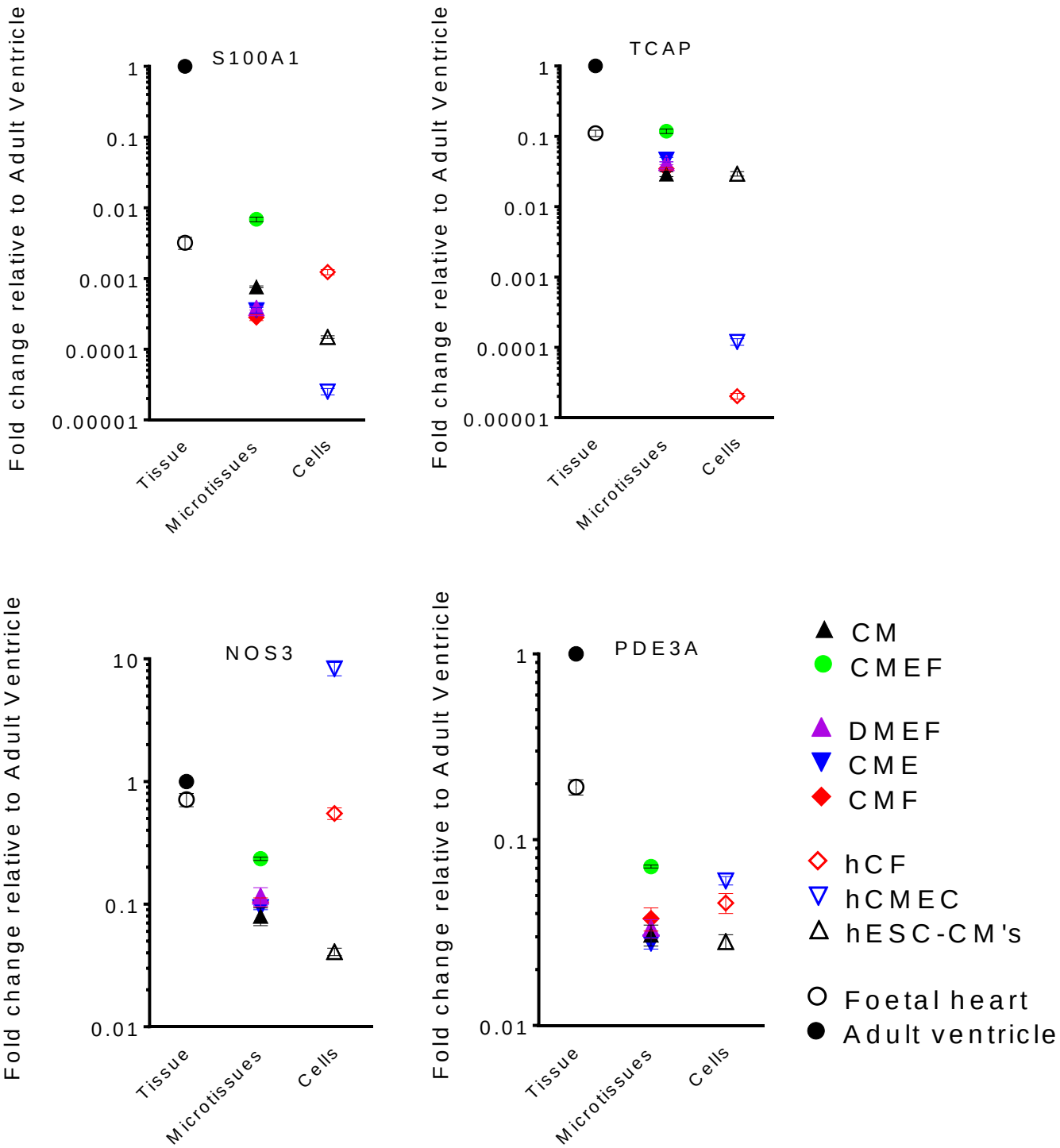

Figure 5.15 Expression of S100A1, TCAP, NOS3 and PDE3A in cardiac tissue, microtissues and monolayer cells.

Total RNA extracted using RNeasy mini kit (Qiagen, Crawley, U.K.). Total RNA was diluted to 20 ng and reverse transcribed using a SuperScript® III first-strand synthesis supermix kit (Life technologies). cDNA samples were preamplified using the TaqMan® PreAmp Master mix kit. QRT-PCR reactions were performed using TaqMan® Gene Expression probes and master mix to monitor amplification under standard cycling conditions. Gene expression is expressed as fold change relative to GAPDH and adult ventricle using the ΔΔCT method. Fold change relative to adult ventricle is plotted for tissues, adult ventricle and foetal heart; microtissues, CMEF, DMEF, CM, CME and CMF; and cells, hESC-CMs, hCFs, hCMECs. *n=3, error bars represent SD.*

CMEF, CM and DMEF microtissues were exposed to a high concentration of caffeine (10 mM) and contraction response recorded using the IonOptix cell geometry measurement system (figure 5.16). CMEF microtissues displayed a caffeine response reminiscent of the mature behavioral pattern expected; an acute increase in transient peak height (contraction displacement) as a result of caffeine-ICR followed by an abrupt halt in contractions once SR Ca^{2+} stores are depleted. CM and DMEF microtissue contractions were abruptly halted by caffeine, however, the acute increase in contraction displacement did not occur.

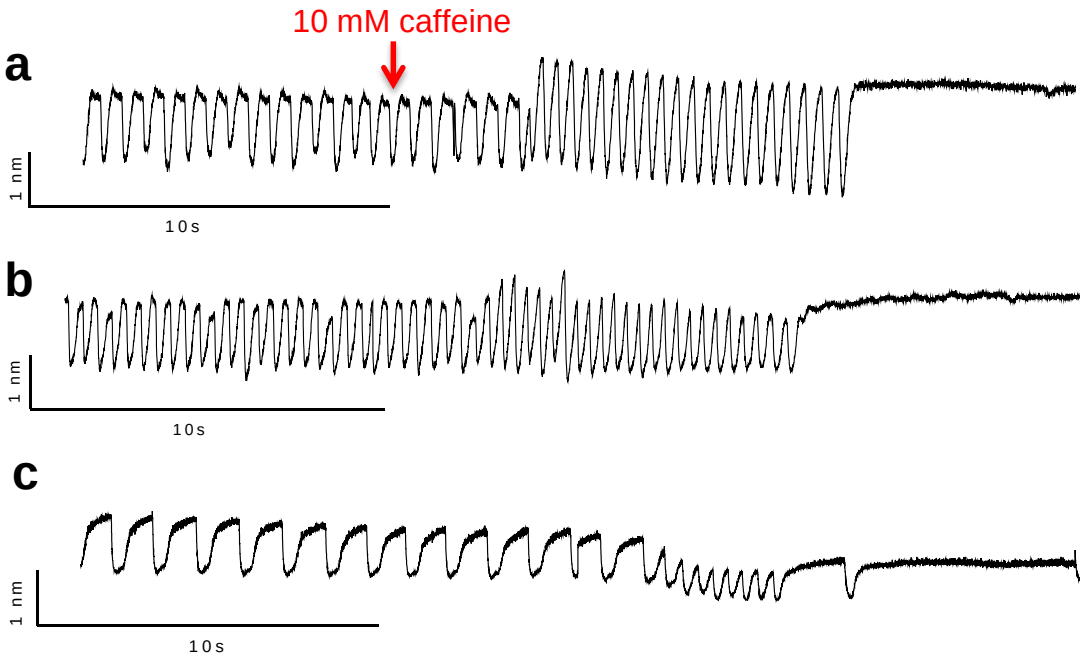

Figure 5.16 Contractile response of (a) CMEF, (b) DMEF and (c) CM microtissue models to 10 mM caffeine.

Microtissues were formed and incubated for 14 days prior to transfer and attachment to gelatin-coated coverslips for application to the IonOptix cell geometry system. 10 mM caffeine in 5050 microtissue media was applied and contractile response recorded until steady state.

To investigate the role of S100A1, a knockdown of S100A1 using siRNA was performed in CMEF microtissues and its effect on the mature CMEF caffeine response studied. A partial knockdown was desired to replicate loss of the upregulation but not any potential housekeeping roles of S100A1. Microtissues were formed and incubated for 14 days prior to use. Microtissues were transfected with 10 nM S100A1 siRNA or scrambled siRNA (negative control) using Lipofectamine™ RNAiMAX transfection reagent. Microtissues were incubated with the transfection solution at 37 °C, 5% CO_2 for 24 h prior to use. At this point microtissues were transferred and attached to gelatin-coated coverslips for application to the IonOptix cell geometry system. 10 mM caffeine in microtissue media was applied to the microtissues and contractile response recorded until steady state. Microtissues not used for contractile analysis were pooled and lysed for total RNA extraction. Following cDNA generation and amplification, qRT-PCR was performed to quantify the expression level of S100A1 in the CMEF microtissues transfected with 10 nM S100A1 siRNA, expression shown in figure 5.15 is fold change relative to the scrambled siRNA control CMEF's. S100A1 mRNA levels have been significantly downregulated by approximately 0.4 fold compared to the scrambled control ($p<0.0001$) (figure 5.17).

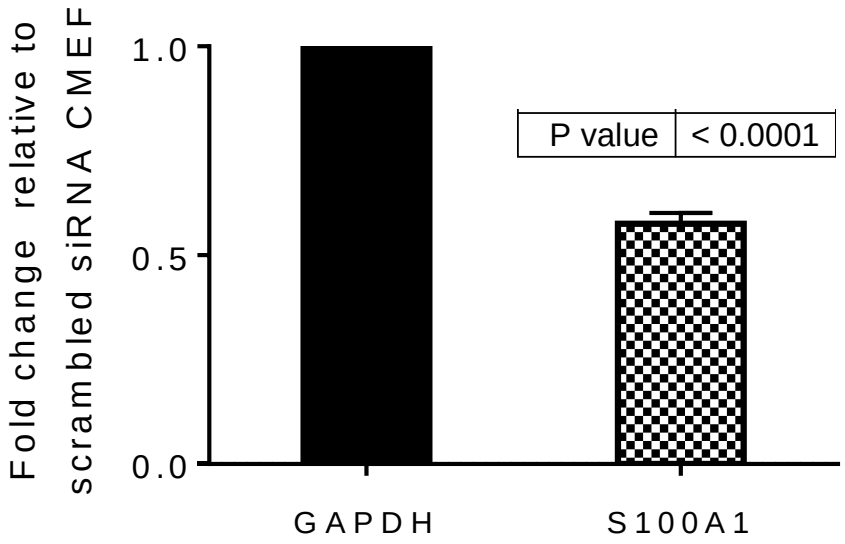

Figure 5.17 Expression of S100A1 in CMEF knockdown model.

Microtissues were formed and incubated for 14 days prior to transfection with 10 nM S100A1 siRNA or 10 nM scrambled siRNA (negative control) using Lipofectamine™ RNAiMAX transfection reagent. Microtissues were incubated with the transfection solution at 37 °C, 5% CO_2 for 24 h prior to use. Total RNA extracted using RNeasy mini kit (Qiagen, Crawley, U.K.). Total RNA was diluted to 20 ng and reverse transcribed using a SuperScript® III first-strand synthesis supermix kit (Life technologies). cDNA samples were preamplified using the TaqMan® PreAmp Master mix kit with TaqMan® Probes. QRT-PCR reactions were performed using TaqMan® Gene Expression probes and master mix to monitor amplification under standard cycling conditions. Data is expressed as fold change relative to GAPDH and CMEF scrambled siRNA control using the ΔΔ*C*T method from triplicate experiments, SD error bars shown.

Figure 5.18 displays representative contractility traces of the caffeine responses exerted by the control microtissues (figure 5.18a) and the S100A1KD CMEF's (figure 5.18b). These traces show that the control CMEF's are still able to respond to caffeine with an acute increase in contraction displacement, however the S100A1kd CMEF's show loss of this characteristic.

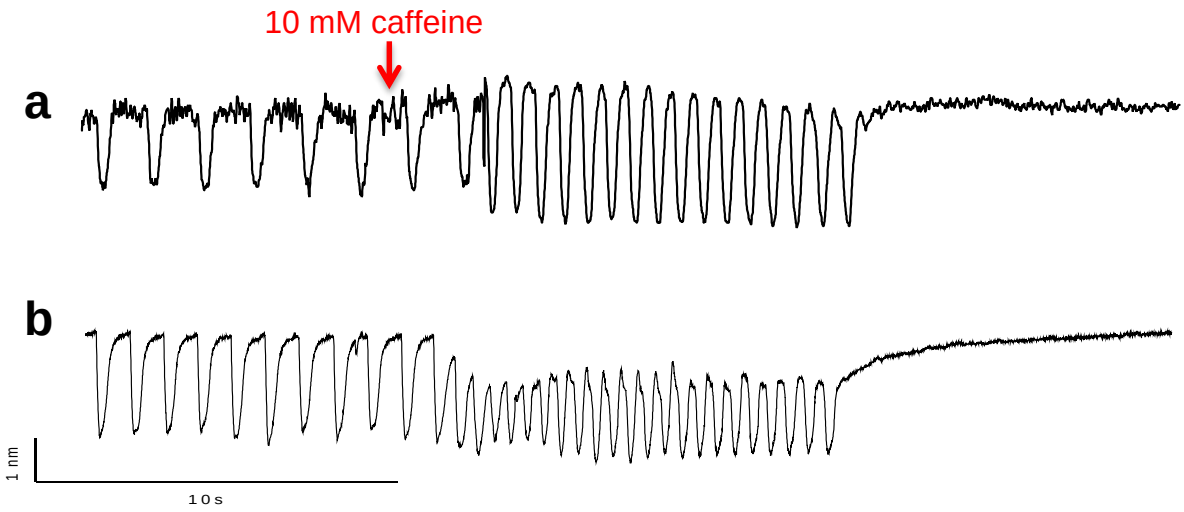

Figure 5.18 Response of CMEF S100A1 knockdown model to 10 mM caffeine.

Microtissues were formed and incubated for 14 days prior to transfection with 10 nM S100A1 siRNA or 10 nM scrambled siRNA (negative control) using Lipofectamine™ RNAiMAX transfection reagent. Microtissues were incubated with the transfection solution at 37 °C, 5% CO_2 for 24 h prior to use. Microtissues were transferred and attached to gelatin-coated coverslips for application to the IonOptix cell geometry system. 10 mM caffeine in 5050 microtissue media was applied and contractile response recorded until steady state. (a) scrambled siRNA control CMEF microtissue, (b) S100A1 CMEF knockdown microtissue model.

5.7 Discussion

The ultimate aim of this chapter was to assess the contractile maturity of the microtissues and establish their ability to predict drug-induced functional cardiotoxicity.

5.7.1 Detection of inotropy direction in CMEF microtissues

To assess the contractile maturity of the microtissues, firstly the basal spontaneous contractions were compared. Figure 5.1 showed clearly that the CMEF microtissues have a faster basal contraction rate than the CM microtissues. Literature suggests that an increase in the spontaneous contraction rate of hESC-CMs can occur with prolonged time in culture (Robertson *et al*., 2013). One hypothesis could be that prolonged culture is permitting further differentiation of the mixed population stem cell derived cardiomyocytes (ventricular and/or nodal cardiomyocytes) and hence the increased beat rate. Given the microtissues are cultured for equal periods it could be the adult cardiac non-myocytes are promoting this differentiation earlier in the CMEF microtissue model. Another interesting difference between the monoculture CM microtissue and the tri-cultured CMEF microtissue was their calcium transient amplitudes. CMEF microtissues display significantly higher Ca^{2+} transient amplitudes, this was the first indicator that the Ca^{2+} handling differs between the microtissue models and that calcium handling maturation may have ocurred. The next step in assessing the contractile maturity of the microtissues was their response to positive and negative inotropic agents. It has been suggested that immature cardiomyocytes such as hESC-CMs cannot increase their contraction displacement in response to positive inotropic agents (Robertson *et al*., 2013). The CMEF microtissues responded with increased contraction displacement to all positive inotropes whereas none of the other microtissue models could increase their displacement of contraction when positive inotropes were applied. These differences in their responses suggest maturation has been promoted in the CMEF microtissues.

Major morphological changes occur from embryonic cardiomyocytes through to adult. The sarcoplasmic reticulum (SR) are relatively sparse in the immature

myocyte with inositol 1,4,5-trisphosphate (IP3)-gated Ca^{2+} release channels (IP3Rs) playing significant roles in calcium mobilization from the SR (Robertson *et al*., 2013). This lack of SR function could be one mechanism limiting an immature cardiomyocytes response to positive inotropic agents. In normal excitation-contraction coupling a relatively small amount of extracellular Ca^{2+} enters the cardiomyocyte via L-type Ca^{2+} channels after depolarization and binds to the RyRs to release a much greater amount of Ca^{2+} from the intracellular calcium stores of the SR (Bers, 2002). This results in a fast synchronous rise in free cytosolic Ca^{2+}. The immature cardiomyocyte however relies on the diffusion of extracellular Ca^{2+} across the cell cytoplasm (Robertson *et al*., 2013), this lacks the fast synchronisity of the mature cardiomyocyte. This could be one reason why immature cardiomyocytes such as the hESC-CM cannot increase their contraction displacement in response to positive inotropic agents and suggests that maturation of SR function has been promoted within the CMEF microtissues.

Both CM and CMEF microtissue models responded to the negative inotrope verapamil. Interestingly, verapamil, which acts to block the L-type Ca^{2+} channels of the cell membrane thereby blocking Ca^{2+} entry into the cell, was more potent in the CMEF model. This was also seen further into the chapter when diltiazem, also an L-type Ca^{2+} channel blocker, was tested and the same pattern displayed. Immature CM's rely heavily on extracellular Ca^{2+} for excitation-contraction coupling, therefore it was surprising that the CMEF were more sensitive. However, this could support the idea of Ca^{2+} handling maturity in the CMEF model; more efficiency and reliance upon Ca^{2+} handling may result in more sensitivity to disruption.

Since the CMEF model displayed contractile maturity compared with the CM microtissues, it was selected for assessment with a wider panel of positive and negative inotropes. This model showed not only the correct detection of inotropy direction, but also predicted negative inotropy of compounds previously undetected in the "gold standard" canine cardiomyocyte assay. Therefore the CMEF model is a human relevant model with *in vivo* physiological relevance and *in vitro* contractile maturity that can be used to better predict cardiac toxicity.

5.7.2 Promotion of maturity in microtissues

The next step was to define how the contractile maturity of the CMEF model was promoted. The first question was whether both endothelial and fibroblasts are needed and whether they need to be from a cardiac origin. The two negative inotropes lapatinib and atenolol, previously undetected in CM microtissues and canine cardiomyocyte contractility assessment, were tested alongside the two positive inotropes digoxin and dobutamine. The CMEF microtissues were the only model to respond to the positive inotropes, therefore a tri-culture of cardiac originating cells is required to achieve contractile maturity. Neither DMEF nor CM microtissues responded to either of the negative inotropes while the CMEF again responded to both. Curiously, the di-culture microtissue, CME, responded to lapatinib while the di-culture microtissue, CMF, responded to atenolol. The first interesting aspect is that each of these negative inotropic responses must be cardiac specific since the dermal microtissue did not respond. However by utilising the di-culture models, we have highlighted a potential role for endothelial cells in lapatinib inotropy and fibroblasts in atenolol inotropy.

Gene expression analysis of all microtissues using adult ventricle (AV) and foetal heart as mature and relatively mature references, respectively, we were able to identify two promoters of maturity; three dimensional cell culture and co-culture with adult cardiac specific cells. Given the lack of response from the non-CMEF microtissues to positive inotropes it was perhaps surprising to see that at the gene level there is actually some degree of gene maturity towards AV and/ or foetal heart when compared to the monolayer hESC-CMs. In many ways this should not be surprising as it is widely accepted that 3D cell culturing can promote a more mature cell phenotype *in vitro*.

An interesting aspect of the gene expression study was the upregulation of S100A1 above foetal heart, towards AV, specifically in the CMEF microtissues. S100A1 is a Ca^{2+} binding protein of the EF-hand type and a member of the S100 protein family

with known roles in striated muscle sarcoplasmic reticulum (SR) Ca^{2+} handling. Given its preferential cardiac expression and localisation patterns close to the SR and contractile filaments of cardiomyocytes, S100A1 has become a target of interest with respect to cardiac contractility. S100A1 has been shown to regulate and improve the function of key proteins involved in the control of SR Ca^{2+} handling as well as myofilament and mitochondrial function, thereby enhancing the heart's inotropic and lusitropic state [reviewed in (Most *et al*, 2007; Ritterhoff & Most, 2012; Rohde *et al*, 2010)]. Additionally studies have highlighted a correlation between S100A1 protein expression and β-adrenergic inotropy response (Bennett, 2014). The upregulation of S100A1 in CMEF relative to other microtissue models and combined unique response to positive inotropes suggests a critical role for S100A1 during cardiomyocyte contraction. The role of S100A1 in CMEF contractile maturity was then assessed using gene knockdown.

5.7.3 Potential role of S100A1 in sarcoplasmic reticulum function

Caffeine is commonly used in electrophysiology to study sarcoplasmic reticulum (SR) function; it acts to increase the open probability of the SR ryanodine receptors thereby releasing calcium into the cytoplasm. In many ways caffeine-induced calcium release (caffeine-ICR) is a replication of calcium-induced calcium release (CICR). During excitation-contraction coupling a small amount of Ca^{2+} enters the cytoplasm, activates the ryanodine receptors and initiates a huge release of Ca^{2+} from the SR stores, this release is known as CICR. Only mature cardiomyocytes are thought to have this functional CICR pathway and reliance upon SR RyRs. As caffeine quickly releases Ca^{2+} from the functional SR you see a sharp increase in inotropy, until the stores are empty at which point contraction stops (during unpaced conditions; paced conditions would allow Ca^{2+} entry via the L-type Ca^{2+} channels). The CMEF microtissues displayed this behavioural pattern, whereas the CM and DMEF microtissues experienced a slow decrease in inotropy. These findings support the theory that the lack of positive inotropy displayed by the CM and DMEF models was due to immature Ca^{2+} handling and that cardiac non-myocytes have promoted SR function and therefore synchronisation of Ca^{2+} signalling to increase contraction displacement.

Caffeine-induced calcium release (caff-ICR) was then used to assess the role of the Ca^{2+} binding protein S100A1 and its potential role in SR function. A knockdown of the S100A1 gene was performed in the CMEF model; a knockdown rather than knockout was desired to study as closely as possible the upregulation of S100A1 rather than its general presence. A reduction in the expression of S100A1 resulted in a caff-ICR response phenotypically the same as the DMEF model, therefore loss of the contractile maturity. This suggests a critical role for S100A1 in SR function and hence contractile maturity of the CMEF model.

5.7.4 Conclusion

The ultimate conclusion from this chapter is adult cardiac non-myocyte cells can be used to promote contractile maturity of embryonic stem cell-derived cardiomyocytes *in vitro* when co-cultured as a three dimensional microtissue. The induction of maturity is very much multi-parameter dependent requiring a) both non-myocyte cell types, b) cells of cardiac origin and c) a 3D culture environment. However, it should be noted that despite achieving a functionally relevent degree of maturity, this *in vitro* myocardial model still lacks many of the characteristics of fully matured myocardial tissue.

Chapter Six

General Discussion

The aim of this thesis was to investigate the role of non-myocytes in drug-induced cardiovascular toxicity. Current methods of drug safety screening primarily focus on cardiomyocytes in isolation (Harmer *et al*., 2012; Pollard *et al*., 2010), ignoring other cellular components of the myocardium. Given the high level of drug attrition resulting from cardiotoxic events, the need for more physiologically relevant *in vitro* models has arisen. The first aim of this investigation was to determine whether non-myocyte cells (microvascular endothelial and fibroblasts) from the myocardium exhibit sensitivity to known structural cardiotoxins and whether this sensitivity is also displayed in dermal-derived and macrovascular-derived non-myocytes.

The second aim of this investigation was to incorporate these myocardial derived non-myocytes into a cell-based 3D *in vitro* model alongside cardiomyocytes for use in preclinical drug-induced cardiotoxicity screening. This model has been evaluated for its structural, gene expression and electrophysiological maturity.

6.1 The role of non-myocytes in drug-induced structural cardiovascular toxicity

The cardiomyocytes and non-myocytes studied in this thesis were evaluated for their individual sensitivities to known structural cardiotoxins utilizing high content biology in combination with a cytoxicity assay measuring ATP content. This combined approach increases the overall predictive strength of the toxicity screen (see chapter 3 and Pointon *et al*., 2013).

Despite studying both structural and cytotoxic endpoints, no cardiac microvascular specific endothelial toxicity was detected. These findings are not particurlaly surprising if we consider the limitations of this study. Endothelial cells are highly adaptive cells designed to rapidly respond to changes in their microenvironment in order to maintain the flow of oxygen and nutrients to their tissue (and removal of waste products) (Aird, 2007a; b; Aird, 2012). A major but unavoidable draw-back of this study is that the primary endothelial cells have been removed from their specific microenvironments *in vivo* and cultured alone *in vitro* under general endothelial cell culture conditions. The endothelial cell models were cultured in almost identical

conditions therefore it is not surprising that they should respond to compounds in an almost identical manner. Traditional *in vitro* cell culture involves cell attachment to plastic labware; this restricts the cell to an almost 2D morphology. A major *in vivo* characteristic of endothelial cells is their formation of vessel structures throughout their tissue. *In vitro* the endothelial cells lack this 3D morphology, blood flow through the vessels and intercellular communications; *in vitro* endothelial cells, therefore, could almost be considered immature compared with their *in vivo* counterparts. This highlights the need for more complex *in vitro* cell models when studying drug toxicity.

Interestingly, much more variation in structural cardiotoxin sensitivity was observed between the cardiac and dermal fibroblasts, this suggests that the fibroblasts perhaps are not as dependent upon their microenvironment for their phenotype as the endothelial cells. The cardiac fibroblasts displayed enhanced sensitivity to imatinib mesylate when compared to dermal fibroblasts. However, interestingly the dermal fibroblasts showed overall the most sensitivity to tyrosine kinase inhibitors suggesting they could be a target during incidences of skin toxicity reported by these compounds e.g. skin rashes following lapatinib dosage (Moy & Goss, 2007). However, keratinocytes are an alternative target since they are known to express epidermal growth factor receptors (EGFR) targeted by these compounds (Kolev *et al*, 2008). These findings suggest that *in vitro* preclinical safety assessments should utilise cells derived from the tissue of interest whenever possible otherwise important toxicities could be missed.

When the sensitivities of the cells from the myocardium (hCFs, hCMECs and hESC-CMs) were globally compared we see that the non-myocytes are sensitive to structural cardiotoxicity at the acute time point of 6 h, whereas the hESC-CMs display toxicity only after 72 h. *In vivo* the early compound toxicity of the non-myocytes could potentially translate into enhanced cardiomyocyte sensitivity. Fibroblasts are in close proximity to myocytes and their ability to manipulate the ECM provides them with the potential to influence cardiomyocyte phenotype (Souders *et al.*, 2009). Cardiomyocytes are highly energetic cells that require an abundance of oxygen and nutrients from the dense microvasculature. Loss or

damage to the microvasculature would ultimately affect cardiomyocyte health and mechanical output. On the other hand, in the *in vivo* environment the cardiomyocytes could potentially have a protective effect over the non-myocytes (Chen *et al.*, 2010) and therefore this early sensitivity is prevented. The exposure of co-cultured microtissue models to structural cardiotoxins in chapter four suggests that a protection mechanism exists between cardiomyocytes and non-myocytes since the tri-cultured microtissues displayed less sensitivity than di- or mono-cultured microtissues. Data from chapters three and five suggests the promotion of maturity in CMEF microtissue therefore it may be that mature cardiac tissue is better equipped to respond to stress conditions elicited by cardiotoxins.

Our current single cell type preclinical *in vitro* models lack the complexity required to establish whether these early events enhance or protect against cardiotoxicity. The microtissue models represent a human relevant *in vitro* model that better reconstitutes the *in vivo* cellular physiology. These models have improved *in vivo* relevance compared with the monolayer assays previously used, since they conform the cells into their natural 3D structure and allow multicellular interactions. However current assay endpoints available to study compound toxicities in microtissues are limited. Microtissues can be difficult to manipulate for image-based endpoints and chemical reaction-based assays often lack the sensitivity required to detect responses from the low cell numbers present within microtissues. An additional limitation of the microtissues was a lack of vessel formation by the endothelial cells. The mature myocardium has a dense vascular network formed by the endothelial cells. Without this arrangement the endothelial cells may lack the maturity and physiological relevance required for accurate toxicity prediction. One possible explanation for this poor vessel formation is the diameter of the microtissue. They were designed to have a diameter small enough to prevent a hypoxic core; literature suggests oxygen and nutrients can diffuse through a microtissue of up to 200 μm in diameter therefore evading the need for a vascular structure (Breslin & O'Driscoll, 2013). This lack of vascularisation therefore limits the use of these microtissues in structural cardiovascular toxicity screening. In hindsight larger microtissues may have induced a vascular network and overcome the sensitivity issues of chemical-based assays. Despite this electrophysiological assessment of the microtissues

suggests that the CMEF microtissues are functionally matured and therefore provide an improved *in vitro* model for functional cardiotoxicity screening.

6.2 Non-myocytes promote contractile maturity in cardiac microtissues

To assess the contractile maturity of the microtissues, firstly the basal spontaneous contractions were compared; CMEF microtissues have a faster basal contraction rate than the CM microtissues. Literature suggests that an increase in the spontaneous contraction rate of hESC-CMs is an indicator of maturity (Robertson *et al.*, 2013). Another interesting difference between the monoculture CM microtissue and the tri-cultured CMEF microtissue is their calcium transient amplitudes. CM microtissues display significantly lower Ca^{2+} transient amplitudes, suggesting immature calcium handling compared with the CMEF microtissues.

It has also been suggested that immature cardiomyocytes such as hESC-CMs cannot increase their contraction displacement in response to positive inotropic agents (Robertson *et al.*, 2013). Major morphological changes occur from embryonic cardiomyocytes through to adult. Sarcoplasmic reticulum (SR) are found to be relatively sparse in the immature myocyte with inositol 1,4,5-trisphosphate (IP3)-gated Ca^{2+} release channels (IP3Rs) playing significant roles in calcium mobilization from them. This lack of SR function has been suggested as one mechanism limiting an immature cardiomyocytes response to positive inotropic agents. In normal excitation-contraction coupling a relatively small amount of extracellular Ca^{2+} enters the cardiomyocyte via L-type Ca^{2+} channels after depolarization and binds to the RyRs to release a much greater amount of Ca^{2+} from the intracellular calcium stores of the SR. This results in a fast synchronous rise in free cytosolic Ca^{2+}. The immature cardiomyocyte however relies on the diffusion of extracellular Ca^{2+} across the cell cytoplasm, this lacks the fast synchronisty of the mature cardiomyocyte (Robertson *et al.*, 2013). This could be one reason why immature cardiomyocytes such as the hESC-CM cannot increase their contraction displacement in response to positive inotropic agents. The tri-cultured cardiac microtissue (CMEF) was the only model to respond to positive inotropes. This model (CMEF) showed, not only the correct detection of inotropy direction but also predicted negative inotropy of

compounds previously undetected in the gold standard canine cardiomyocyte assay. Therefore the CMEF model is a human relevant model with *in vivo* physiological relevance and *in vitro* contractile maturity that can be used to predict cardiac toxicity. This investigation highlights the need for cardiac originating non-myocytes to be incorporated into our pre-clinical cardiac safety screens.

Gene expression analysis of all microtissues using adult ventricle and foetal heart as mature and maturing references, respectively, we were able to identify two promoters of maturity. Given the lack of response from the non-CMEF microtissues to positive inotropes it was interesting to see that at the gene level there is actually some degree of gene maturity towards AV and/ or foetal when compared to the monolayer hESC-CMs. In many ways this should not be surprising as it is widely accepted that 3D cell culturing can promote a more mature cell phenotype *in vitro*.

The most intriguing aspect of the gene expression study in chapter five was perhaps the upregulation of S100A1 above foetal heart, towards AV, specifically in the CMEF microtissues. S100A1 is a Ca^{2+} binding protein of the EF-hand type and a member of the S100 protein family with known roles in striated muscle sarcoplasmic reticulum (SR) Ca^{2+} handling. Given its preferential cardiac expression and localisation patterns close to the SR and contractile filaments of cardiomyocytes, S100A1 has become a target of interest with respect to cardiac contractility. S100A1 has been shown to regulate and improve the function of key proteins involved in the control of SR Ca^{2+} handling as well as myofilament and mitochondrial function, thereby enhancing the heart's inotropic and lusitropic state [reviewed in (Most *et al*, 2007; Ritterhoff & Most, 2012; Rohde *et al*, 2010)]. Additionally studies have highlighted a correlation between S100A1 protein expression and β-adrenergic inotropy response (Bennett, 2014). Caffeine response with gene knockdown experience has suggested the gene upregulation of S100A1 plays a major role in the contractile maturity established within the CMEF microtissue.

6.3 Future work

In further work, it would be interesting to look at structural cardiotoxin sensitivities in non-myocytes at an earlier timepoint than six hours to allow improved mechanistic insight from the high content biology. This could help to highlight any common toxicity mechanism between non-myocytes and cardiomyocytes and ultimately provide knowledge for future drug development.

Despite displaying increased maturity, the CMEF microtissues are still an immature cardiac model. The size of the microtissues could be increased and additional cell types such as pericytes could be incorporated to help induce vasculaturisation. *In vivo* the myocardium is under constant electrical pacing conditions therefore the *in vitro* culture of microtissues under constant electrical pacing may be another step to help promote further model maturity. It may also be interesting to expose microtissues to structural cardiotoxins under electrical pacing conditions to see whether this affects the toxicity we see. Pointon *et al* (2013) showed a reduction in cardiomyocyte structural cardiotoxin sensitivity when co-administered with BTS, a negative inotrope. These findings suggest increased cardiomyocyte activity, for example electrical pacing, could enhance structural compound sensitivities.

6.4 Overall conclusions

This investigation has suggested a role for non-myocytes in early drug-induced structural and functional cardiotoxicity. Structural compound toxicity assessments were limited by current available models and assay endpoints for 3D models, however cell type specific toxicities were detected and utilization of microtissues suggests the role of non-myocytes in drug-induced structural cardiovascular toxicity could in fact be one of protection. Incorporation of non-myocytes into co-cultured microtissue models for the study of functional cardiotoxicity has highlighted the importance of utilizing firstly non-myocytes but also non-myocytes of cardiac origin in our *in vitro* cardiotoxicity screens. This investigation has successfully shown adult cardiac non-myocyte cells can be used to promote contractile maturity of embryonic stem cell-derived cardiomyocytes *in vitro* when co-cultured as a three dimensional microtissue and that the induction of cardiac maturity is very much multi-parameter

dependent. The incorporation of more complex cell models into *in vitro* cardiac safety screening is needed to improve drug attrition at the early stages of drug development.

Reference List

Aird, W. C. (2007a). Phenotypic heterogeneity of the endothelium I. Structure, function, and mechanisms. *Circulation Research*. **100**, 158-173.

Aird, W. C. (2007b). Phenotypic heterogeneity of the endothelium II. Representative vascular beds. *Circulation Research*. **100,** 174-190.

Aird, W. C. (2012). Endothelial cell heterogeneity. *Cold Spring Harbor Perspectives in Medicine.* **2**, (1).

Ajithkumar, G., Ramachandran, S., & Kartha, C. (2011). Drug induced endothelial dysfunction: functional role of oxidative stress. *The IIOAB Journal.* **2,** 62-70**.**

Bennett, M. K., Sweet, W. E., Baicker-McKee, S., Looney, E., Karohl, K., Mountis, M., Tang, W. H. W., Starling, R. C. & Moravec, C. S. (2014). S100A1 in human heart failure: lack of recovery following left ventricular assist device support. *Circulation. Heart Failure**.*** **7,** 612-618.

Bers, D. M. (2001). Excitation-contraction coupling and cardiac contractile force*. Developments in cardiovascular medicine.* **237,** 203-244.

Bers, D. M. (2002). Cardiac excitation-contraction coupling. *Nature*. **415,** 198-205.

Bocci, G., Danesi, R., Paolo, A., Innocenti, F., Allegrini, G., Falcone, A., Melosi, A., Battistoni, M., Barsanti, G., Franco Conte, P. and Del Tacca, M. (2000). Comparative Pharmacokinetic Analysis of 5-Fluorouracil and Its Major Metabolite 5-Fluoro-5,6-dihydrouracil after Conventional and Reduced Test Dose in Cancer Patients. *Clin Cancer Res.* **6,** 3032

Brana, I. & Tabernero, J. (2010). Cardiotoxicity. *Annals of Oncology.* **21,** 173-179.

Breslin, S. & O'Driscoll, L. (2013). Three-dimensional cell culture: The missing link in drug discovery. *Drug Discovery Today.* **18,** 240-249.

Brinks, H., Rohde, D., Voelkers, M., Qiu, G., Pleger, S. T., Herzog, N., Rabinowitz, J., Ruhparwar, A., Silvestry, S., Lerchenmüller, C., Mather, P. J., Eckhart, A. D., Katus, H. A., Carrel, T., Koch, W. J. & Most, P. (2011). S100A1 Genetically Targeted Therapy Reverses Dysfunction of Human Failing Cardiomyocytes. *Journal of the American College of Cardiology (JACC).* **58,** 966-973.

Brutsaert, D. L. (2003). Cardiac endothelial-myocardial signaling: Its role in cardiac growth, contractile performance, and rhythmicity. *Physiological Reviews* .**83,** 59-115.

Calderone, A., Thaik, C.M., Takahashi, N., Chang, D.L.F., & Colucci, W.S. (1998). Nitric oxide, atrial natriuretic peptide, and cyclic GMP inhibit the growth-promoting effects of norepinephrine in cardiac myocytes and fibroblasts. *Journal of Clinical Investigation.* **101,** 812-818.

Campbell, J.R. (2007). Arachidonic acid metabolites as endothelium-derived hyperpolarizing factors. *Hypertension.* **49,** 590-596.

Castro, L. R. V., Schittl, J., & Fischmeister, R. (2010). Feedback Control Through cGMP-Dependent Protein Kinase Contributes to Differential Regulation and Compartmentation of cGMP in Rat Cardiac Myocytes. *Circulation Research.* **107,** 1232-1240.

Chen, T. T., Zhou, G.Y., Zhu, Q.A., Liu, X.A., Ha, T.Z., Kelley, J.L., Kao, R.L., Williams, D.L., & Li, C.F. (2010). Overexpression of Vascular Endothelial Growth Factor 165 (VEGF(165)) Protects Cardiomyocytes Against Doxorubicin-Induced Apoptosis. *Journal of Chemotherapy.* **22,** 402-406.

Chintalgattu, V., Ai, D., Langley, R. R., Zhang, J., Bankson, J. A., Shih, T. L., Reddy, A. K., Coombes, K. R., Daher, I. N., Pati, S., Patel, S. S., Pocius, J. S., Taffet, G. E., Buja, L. M., Entman, M. L. & Khakoo, A. Y. (2010). Cardiomyocyte PDGFR-beta signaling is an essential component of the mouse cardiac response to load-induced stress. *Journal of Clinical Investigation.* **120,** 472-484.

Chintalgattu, V. & Khakoo, A. Y. (2010). Review: cardiovascular toxicities due to molecularly targeted cancer therapeutics. *Clinical advances in hematology & oncology : H&O.* **8,** 133-135.

Chintalgattu, V., Rees, M. L., Culver, J. C., Goel, A., Jiffar, T., Zhang, J., Dunner, K., Jr., Pati, S., Bankson, J. A., Pasqualini, R., Arap, W., Bryan, N. S., Taegtmeyer, H., Langley, R. R., Yao, H., Kupferman, M. E., Entman, M. L., Dickinson, M. E. & Khakoo, A. Y. (2013). Coronary Microvascular Pericytes Are the Cellular Target of Sunitinib Malate-Induced Cardiotoxicity. *Science Translational Medicine.* **5,** 187.

Chiusa, M., Hool, S.-L., Truetsch, P., Djafarzadeh, S., Jakob, S. M., Seifriz, F., Scherer, S. J., Suter, T. M., Zuppinger, C. & Zbinden, S. (2012). Cancer therapy modulates VEGF signaling and viability in adult rat cardiac microvascular endothelial cells and cardiomyocytes. *Journal of Molecular and Cellular Cardiology.* **52,** 1164-1175.

Cingolani, H. E., Villa-Abrille, M. C., Cornelli, M., Nolly, A., Ennis, I. L., Garciarena, C., Correa, M. V., Camilión De Hurtado, M. C., Aiello, E. A., Suburo, A. M. & Torbidoni, V. (2006). The positive inotropic effect of angiotensin II: Role of endothelin-1 and reactive oxygen species. *Hypertension.* **47,** 727-734.

Clauss, M. & Breier, G. (2005). Mechanisms of angiogenesis [electronic book] / edited by M. Clauss and G. Breier. Eds.), pp. Basel : Birkhäuser Verlag.

Díaz, M. E., Graham, H. K., O'Neill, S. C., Trafford, A. W. & Eisner, D. A. (2005). The control of sarcoplasmic reticulum Ca content in cardiac muscle. *Cell Calcium.* **38,** 391-396.

Duarte-Costa, S., Castro-Ferreira, R., Neves, J. S. & Leite-Moreira, A. F. (2014). S100A1: a major player in cardiovascular performance. Physiological Research / Academia Scientiarum Bohemoslovaca. Epub.

Edelberg, J. M., Aird, W.C., Wu, W., Rayburn, H., Mamuya, W.S., Mercola, M., & Rosenberg, R.D. . (1998). PDGF mediates cardiac microvascular communication. *Journal of Clinical Investigation.* **102,** 837-843.

Eisner, D., Bode, E., Venetucci, L. & Trafford, A. (2012). Calcium flux balance in the heart. *Journal of Molecular and Cellular Cardiology.* **58,** 110-7

Fabiato, A. & Fabiato, F. (1975). Contractions induced by a calcium triggered release of calcium from the sarcoplasmic reticulum of single skinned cardiac cells. *Journal of Physiology.* **249,** 469-495.

Fabiato, A. & Fabiato, F. (1977). Calcium release from the sarcoplasmic reticulum. *Circulation Research.* **40,** 119-129.

Fabiato, A. & Fabiato, F. (1979). Calcium and Cardiac Excitation-Contraction Coupling. *Annual Review of Physiology.* **41,** 473.

Flamme I, Frolich T, Risau W. (1997). Molecular mechanisms of vasculogenesis and embryonic angiogenesis. *J Cell Physiol.* **173,** 206–210.

Friedrich, J., Seidel, C., Kunz-Schughart, L. A. & Ebner, R. (2009). Spheroid-based drug screen: Considerations and practical approach. *Nature Protocols.* **4**, 309-324.

Garry, D. J. & Olson, E. N. (2006). A common progenitor at the heart of development. *Cell.* **127,** 1101-1104.

Gepstein, L. (2002). Derivation and potential applications of human embryonic stem cells. *Circulation Research*. **91,** 866-876.

Gianni, L., Herman, E.H., Lipshultz, S.E., Minotti, G., Sarvazyan, N., & Sawyer, D.B. (2008). Anthracycline cardiotoxicity: From bench to bedside. *Journal of Clinical Oncology.* **26,** 3777-3784.

Goldring, C. E. P., Duffy, P. A., Benvenisty, N., Andrews, P. W., Ben-David, U., Eakins, R., French, N., Hanley, N. A., Kelly, L., Kitteringham, N. R., Kurth, J., Ladenheim, D., Laverty, H., McBlane, J., Narayanan, G., Patel, S., Reinhardt, J., Rossi, A., Sharpe, M. & Park, B. K. (2011). Assessing the Safety of Stem Cell Therapeutics. *Cell Stem Cell.* **8,** 618-628.

Grocott-Mason, R., Anning, P., Evans, H., Lewis, M.J., & Shah, A.M. (1994). Modulation of left venticular relaxation in isolation ejecting heart by endogenous nitric oxide. *American Journal of Physiology.* **267,** 1804-1813.

Harding, P., Carretero, O.A., & Lapointe, M.C. (1995). Effects of Interleukin-1-Beta and Nitric-Oxide on Cardiac Myocytes. *Hypertension.* **25**, 421-430.

Harmer, A. R., Abi-Gerges, N., Easter, A., Woods, A., Lawrence, C. L., Small, B. G., Valentin, J. P. & Pollard, C. E. (2008). Optimisation and validation of a medium-throughput electrophysiology-based hNav1.5 assay using IonWorks™. *Journal of Pharmacological and Toxicological Methods.* **57**, 30-41.

Harmer, A. R., Abi-Gerges, N., Morton, M. J., Pullen, G. F., Valentin, J. P. & Pollard, C. E. (2012). Validation of an in vitro contractility assay using canine ventricular myocytes. *Toxicology and Applied Pharmacology.* **260**, 162-172.

Hasinoff, B. B., Patel, D. & Wu, X. (2013). The dual-targeted HER1/HER2 tyrosine kinase inhibitor lapatinib strongly potentiates the cardiac myocyte-damaging effects of doxorubicin. *Cardiovascular Toxicology.* **13**, 33-47.

Hayakawa, H. R., L. (1997). The link among nitric oxide synthase activity, endothelial function, and aortic and ventricular hypertrophy in hypertension. *Hypertension*. **29**, 235-241.

Hendrickx, J., Doggen, K., Weinberg, E. O., Van Tongelen, P., Fransen, P. & De Keulenaer, G. W. (2004). Molecular diversity of cardiac endothelial cells in vitro and in vivo. *Physiological Genomics.* **19**, 198-206.

Higashi, Y., Noma, K., Yoshizumi, M. & Kihara, Y. (2009). Endothelial Function and Oxidative Stress in Cardiovascular Diseases. *Circulation Journal.* **73**, 411-418.

Hirt, M. N., Hansen, A. & Eschenhagen, T. (2014). Cardiac Tissue Engineering State of the Art. *Circulation Research.* **114 (2),** 354-67.

Hsieh, P. C. H., Davis, M.E., Lisowski, L.K., & Lee, R.T. (2006). Endothelial-cardiomyocyte interactions in cardiac development and repair. *Annual Review Physiology.* **68**, 51-66.

Huang, X., Patel, S., Ahmed, N., Seiter, K. & Liu, D. (2008). Severe toxicity of skin rash, fever and diarrhea associated with imatinib: Case report and review of skin toxicities associated with tyrosine kinase inhibitors. *Drug Design, Development and Therapy.* **2,** 215-9.

Hussain, M. & Orchard, C. H. (1997). Sarcoplasmic reticulum Ca2+ content, L-type Ca2+ current and the Ca2+ transient in rat myocytes during beta-adrenergic stimulation. *The Journal of physiology.* **505,** 2.

Ichikawa, Y., Ghanefar, M., Bayeva, M., Wu, R., Khechaduri, A., Naga Prasad, S. V., Mutharasan, R. K., Naik, T. J. & Ardehali, H. (2014). Cardiotoxicity of doxorubicin is mediated through mitochondrial iron accumulation. *Journal of Clinical Investigation.* **124,** 617-630.

Ishii, Y., Langberg, J., Rosborough, K. & Mikawa, T. (2009). Endothelial cell lineages of the heart. *Cell and Tissue Research.* **335,** 67-73.

Iwanaga, Y., Kihara, Y., Hasegawa, K., Inagaki, K., Yoneda, T., Kaburagi, S., Araki, M., & Sasayama, S. (1998). Cardiac endothelin-1 plays a critical role in the functional deterioration of left ventricles during the transition from compensatory hypertrophy to congestive heart failure in salt-sensitive hypertensive rats. *Circulation.* **98,** 2065-2073.

Jiang, B., Hebert, V.Y., Li, Y., Mathis, J., Alexander, J., & Dugas, T.R. . (2007). HIV antiretroviral drug combination induces endothelial mitochondrial dysfunction and reactive oxygen species production, but not apoptosis. *Toxicology and Applied Pharmacology.* **224,** 60-71.

Kamkin, A., Kiseleva, I., Lozinsky, I. & Scholz, H. (2005). Electrical interaction of mechanosensitive fibroblasts and myocytes in the heart. *Basic Research in Cardiology.* **100**, 337-345.

Kao, J. P. Y., Harootunian, A. T. & Tsien, R. Y. (1989). Photochemically generated cytosolic calcium pulses and their detection by fluo-3. *Journal of Biological Chemistry.* **264,** 8179-8184.

Kattman, S. J., Huber, T. L. & Keller, Gordon M. (2006). Article: Multipotent Flk-1+ Cardiovascular Progenitor Cells Give Rise to the Cardiomyocyte, Endothelial, and Vascular Smooth Muscle Lineages. *Developmental Cell*. **11,** 723-732.

Katz, A. M. (2006). Physiology of the heart / Arnold M. Katz. Eds.), pp. Philadelphia ; Lippincott Williams & Wilkins. 4th ed.

Kehat, I., Gepstein, L., Coleman, R., Itskovitz-Eldor, J., Livne, E., Snir, M. & Gepstein, A. (2003). Assessment of the ultrastructural and proliferative properties of human embryonic stem cell-derived cardiomyocytes. *American Journal of Physiology - Heart and Circulatory Physiology.* **285,** H2355-H2363.

Kerkelä, R., Beahm, C., Shevtsov, S., Pesant, S., Force, T., Patten, R., Walters, B., Grazette, L., Rosenzweig, A., Yacobi, R., Van Etten, R. A., Iliescu, C., Durand, J. B., Clubb, F. J., Salomon, R. N. & Alroy, J. (2006). Cardiotoxicity of the cancer therapeutic agent imatinib mesylate. *Nature Medicine.* **12**, 908-916.

Kolev, V., Mandinova, A., Guinea- Viniegra, J., Hu, B., Lefort, K., Lambertini, C., Neel, V., Dummer, R., Wagner, E. F. and Dotto, P. (2008). EGFR signalling as a negative regulator of NOTCH1 gene transcription and function in proliferating keratinocytes and cancer. *Nature cell biology*. **10;** 902-911.

Kumar, D., Kamp, T. J. & LeWinter, M. M. (2005). Embryonic stem cells: differentiation into cardiomyocytes and potential for heart repair and regeneration. *Coron Artery Disruption.* **16**, 111-116.

Laflamme, M. A. & Murry, C. E. (2011). Heart regeneration. *Nature.* **473**, 326-335.

Laverty, A. A., Bottle, A., Majeed, A. & Millett, C. (2011). Blood pressure monitoring and control by cardiovascular disease status in UK primary care: 10 year retrospective cohort study 1998-2007. *Journal of Public Health.* **33**, 302-309.

Lieu, D. K., Siu, C. W., Abu-Khalil, A., Liu, J., Li, R. A., McNerney, G. P., Huser, T. & Tse, H. F. (2009). Absence of transverse tubules contributes to non-uniform Ca^{2+} wavefronts in mouse and human embryonic stem cell-derived cardiomyocytes. *Stem Cells and Development.* **18,** 1493-1500.

Liu, J., Ji, D. F., Chung, W. S. & Li, R. A. (2007). Functional sarcoplasmic reticulum for calcium handling of human embryonic stem cell-derived cardiomyocytes: Insights for driven maturation. *Stem Cells.* **25,** 3038-3044.

Loke, K. E., Messina, E.J., Shesely, E.G., Kaley, G., & Hintze, T.H. . (1999). ACE inhibitors induce the release of endogenous eNOS-derived nitric oxide to decrease myocardial oxygen consumption. *Circulation.* **100,** 1291-1297.

Maltman, D. J. & Przyborski, S. A. (2010). Developments in three-dimensional cell culture technology aimed at improving the accuracy of in vitro analyses. *Biochemical Society Transactions*. **38,** 1072-1075.

Maruyama, K., Mori, Y., Murasawa, S., Masaki, H., Takahashi, N., Tsutusmi, Y., Moriguchi, Y., Shibazaki, Y., Tanaka, Y., Shibuya, M., Inada, M., Matsubara, H., & Iwasaka, T. (1999). Interleukin-1 beta upregulates cardiac expression of vascular endothelial growth factor and its receptor KDR/flk-1 via activation of protein tyrosine kinases. *Journal of Molecular and Cellular Cardiology.* **31,** 607-617.

McNary, T. G., Spitzer, K. W., Holloway, H., Bridge, J. H. B., Kohl, P. & Sachse, F. B. (2012). Mechanical modulation of the transverse tubular system of ventricular cardiomyocytes. *Prog Biophys Mol Biol.* **110 (2-3),** 218-225.

Mellor, H. R., Bell, A.R., Valentin, J.P., & Roberts, R.R. (2011). Cardiotoxicity Associated with Targeting Kinase Pathways in Cancer. *Toxicological Sciences.* **120,** 14-32.

Mehta, G., Hsiao, A., Ingram, M., Luker, G. and Takayama, S. (2012). Opportunities and Challenges for use of Tumor Spheroids as Models to Test Drug Delivery and Efficacy. *J Control Release.* **164 (2),** 192-204.

Mikaelian, I., Buness, A., de Vera-Mudry, M.-C., Kanwal, C., Coluccio, D., Rasmussen, E., Char, H. W., Carvajal, V., Hilton, H., Funk, J., Hoflack, J.-C., Fielden, M., Herting, F., Dunn, M. & Suter-Dick, L. (2010). Primary Endothelial Damage Is the Mechanism of Cardiotoxicity of Tubulin-Binding Drugs. *Toxicological Sciences.* **117,** 144-151.

Minami, M., Matsumoto, S., & Horiuchi, H. (2010). Cardiovascular Side-Effects of Modern Cancer Therapy. *Circulation Journal.* **74,** 1779-1786.

Minamino, T. & Kitakaze, M. (2010). ER stress in cardiovascular disease. *Journal of Molecular & Cellular Cardiology.* **48,** 1105-1110.

Minta, A., Kao, J. P. Y. & Tsien, R. Y. (1988). Fluorescent indicators for cytosolic calcium based on rhodamine and fluorescein chromophores. *J Bio Chem.* **264 (14),** 8171- 8178.

Moretti, A., Caron, L., Nakano, A., Lam, J. T., Bernshausen, A., Chen, Y. H., Qyang, Y. B., Bu, L., Sasaki, M., Martin-Puig, S., Sun, Y. F., Evans, S. M., Laugwitz, K. L. & Chien, K. R. (2006). Multipotent embryonic Isl1(+) progenitor cells lead to cardiac, smooth muscle, and endothelial cell diversification. *Cell.* **127,** 1151-1165.

Most, P., Remppis, A., Pleger, S. T., Katus, H. A., Koch, W. J. (2007). S100A1: a novel inotropic regulator of cardiac performance. Transition from molecular physiology to pathophysiological relevance. *American Journal of Physiology - Regulatory, Integrative and Comparative Physiology*. **293 (2),** 568-577.

Murphy, J. F. F., D.J. (2001). Vascular endothelial cell growth factor (VEGF) induces cyclooxygenase (COX)-dependent proliferation of endothelial cells (EC) via the VEGF-2 receptor. *Faseb Journal.* **15,** 1667-1669.

Moy, B. & Goss, P. E. (2007). Lapatinib associated toxicity and practical management recommendations. *The oncologist*. **12 (7);** 756-765.

Nalbant, S., Akmaz, I., Kaplan, M., Avsar, K., Solmazgul, E., & Sahan, B. (2006). Does rofecoxib increase TNF-alpha levels? *Clinical and Experimental Rheumatology.* **24,** 361-365.

Nees, S., Weiss, D. R. & Juchem, G. (2013). Focus on cardiac pericytes. *Pflugers Archiv-European Journal of Physiology.* **465,** 779-787.

Nees, S., Weiss, D. R., Senftl, A., Knott, M., Foerch, S., Schnurr, M., Weyrich, P. & Juchem, G. (2012). Isolation, bulk cultivation, and characterization of coronary microvascular pericytes: the second most frequent myocardial cell type in vitro. *American Journal of Physiology-Heart and Circulatory Physiology.* **302,** H69-H84.

Ottaviano, F. G. & Yee, K. O. (2011). Communication Signals Between Cardiac Fibroblasts and Cardiac Myocytes. *Journal of Cardiovascular Pharmacology*. **57,** 513-521.

Oudit, G. Y. P., J.M. (2009). Cardiac regulation by phosphoinositide 3-kinases and PTEN. *Cardiovascular Research*. **82,** 250-260.

Palella, J.P. (2011). Cardiovascular disease in HIV infection. *Current Opinion in Hiv and Aids.* **6,** 266-271.

Paulus, W. J. (1999). NO and cardiac diastolic function. *Cardiovascular Research.* **43,** 595-606.

Pfaffl, M, W. & Hageleit, M. (2001). Validities of mRNA quantification using recombinant RNA and recombinant DNA external calibration curves in real-time RT-PCR. *Biotechnology Letters.* **23**, 275–282.

Pointon, A. V., Gerges, N. A. & Sidaway, J. E. (2013). In vitro detection of cardiotoxicity using human embryonic stem cell derived cardiomyocyte. *Journal of Pharmacological and Toxicological Methods.* **132 (2),** 317-326.

Pollard, C., Abi Gerges, N., Bridgland-Taylor, M. H., Easter, A., Hammond, T. G. and Valentin, J. P. (2010). An introduction to QT interval prolongation and non-clinical approaches to assessing and reducing risk. *British journal of pharmacology*. **159**; 12-21.

Ritchie, R. H., Marsh, J.D., Lancaster, W.D., Diglio, C.A., & Schiebinger, R.J. (1998a). Bradykinin blocks angiotensin II-induced hypertrophy in the presence of endothelial cells. *Hypertension.* **31,** 39-44.

Ritchie, R. H., Schiebinger, R.J., Lapointe, M.C., & Marsh, J.D. (1998b). Angiotensin II-induced hypertrophy of adult rat cardiomyocytes is blocked by nitric oxide. *American Journal of Physiology-Heart and Circulatory Physiology.* **275,** 1370-1374.

Ritterhoff, J. & Most, P. (2012). Targeting S100A1 in heart failure. *Gene Therapy*. **19 (6),** 613-621.

Robertson, C., George, S. C. & Tran, D. D. (2013). Concise review: Maturation phases of human pluripotent stem cell-derived cardiomyocytes. *Stem Cells.* **31,** 829-837.

Rohde, D., Schon, C., Boerries, M., Didrihsone, I., Ritterhoff, J., Kubatzky, K. F., Volkers, M., Herzog, N., Mahler, M., Tsoporis, J. N., Parker, T. G., Linke, B., Giannitsis, E., Gao, E. H., Peppel, K., Katus, H. A. & Most, P. (2014). S100A1 is released from ischemic cardiomyocytes and signals myocardial damage via Toll-like receptor. *EMBO Mol Med.* **15 (6),** 778-94.

Rossant, J. & Howard, L. (2002). Signalling pathways in vascular development. *Annual Review of Cell & Developmental Biology.* **18,** 541.

Rousseau, E. & Meissner, G. (1989). Single cardiac sarcoplasmic reticulum Ca2+-release channel: activation by caffeine. *American Journal of Physiology: Heart & Circulatory Physiology.* **25,** H328.

Seemann, I., te Poele, J. A. M., Song, J. Y., Hoving, S., Russell, N. S. & Stewart, F. A. (2014). Radiation- and anthracycline-induced cardiac toxicity and the influence of ErbB2 blocking agents. *Breast Cancer Research Treatment*. **141 (3),** 385–395.
Senkus, E. J. (2011). Cardiovascular effects of systemic cancer treatment. *Cancer Treatment Reviews.* **37,** 300-311.

Souders, C. A., Bowers, S. L. K. & Baudino, T. A. (2009). Cardiac Fibroblast The Renaissance Cell*. Circulation Research.* **105,** 1164-1176.

Srivastava, D. & Ivey, K. N. (2006). Potential of stem-cell-based therapies for heart disease. *Nature.* **444,** 512-512.

Suburo, A. M. & D'Amore, P. A. (2006). Development of the endothelium. *Handbook of experimental pharmacology.* **176,** 71-105.

Tan, Y., Dourdin, N., Wu, C., De Veyra, T., Elce, J. S., and Greer, P. A. (2006). Ubiquitous Calpains Promote Caspase-12 and JNK Activation during Endoplasmic Reticulum Stress-induced Apoptosis. *The Journal of Biological Chemistry.* **281,** 16016-16024.

Takeda, N. & Manabe, I. (2011). Cellular Interplay between Cardiomyocytes and Nonmyocytes in Cardiac Remodeling. *International Journal Of Inflammation.* **2011,** 535241-535241.

Tirziu, D., Giordano, F. J. & Simons, M. (2010). Cell Communications in the Heart. *Circulation.* **122**, 928-937.

Trafford, A. W., Diaz, M. E. & Eisner, D. A. (1998). Measurement of sarcoplasmic reticulum Ca content and sarcolemmal fluxes during the transient stimulation of the systolic Ca transient produced by caffeine. *Ann N Y Acad Sci.* **853,** 368-71.

Ueno, M., Kakinuma, Y., Yuhki, K., Murakoshi, N., Lemitsu, M., Miyauchi, T. & Yamaguchi, I. (2006). Doxorubicin induces apoptosis by activation of caspase-3 in cultured cardiomyocytes *in vitro* and rat cardiac ventricles *in vivo*. *J Pharm Sci.* **101 (2),** 151-158.

Völkers, M., Rohde, D., Goodman, C. & Most, P. (2010). S100A1: a regulator of striated muscle sarcoplasmic reticulum Ca2+ handling, sarcomeric, and mitochondrial function. *Journal Of Biomedicine & Biotechnology.* **2010,** 178614-178614.

Will, Y., Dykens, J. A., Hirakawa, B., Jamieson, J., Marroquin, L. D., Jessen, B. A., Nadanaciva, S., Hynes, J. & Patyna, S. (2008). Effect of the multitargeted tyrosine kinase inhibitors imatinib, dasatinib, sunitinib, and sorafenib on mitochondrial function in isolated rat heart mitochondria and H9c2 cells. *Toxicological Sciences.* **106,** 153-161.

Wolf, A., Couttet, P., Dong, M., Grenet, O., Heron, M., Junker, U., Laengle, U., Ledieu, D., Marrer, E., Nussher, A., Persohn, E., Pognan, F., Rivière, G.-J., Roth, D. R., Trendelenburg, C., Tsao, J. & Roman, D. (2010). Imatinib does not induce cardiotoxicity at clinically relevant concentrations in preclinical studies. *Leukemia Research.* **34,** 1180-1188.

Wu, S., Ko, Y. S., Teng, M. S., Ko, Y. L., Hsu, L. A., Hsueh, C., Chou, Y. Y., Liew, C. C. & Lee, Y. S. (2002). Adriamycin-induced cardiomyocyte and endothelial cell apoptosis: In vitro and in vivo studies. *J Mol Cell Cardiol*. **12**, 1595-607.

Wu, S. M., Fujiwara, Y., Cibulsky, S. M., Clapham, D. E., Lien, C. L., Schultheiss, T. M. & Orkin, S. H. (2006). Developmental origin of a bipotential myocardial and smooth muscle cell precursor in the mammalian heart. *Cell.* **127**, 1137-1150.

Xu, L. & Meissner, G. (1998). Regulation of cardiac muscle Ca2+ release channel by sarcoplasmic reticulum lumenal Ca2+. *Biophysical Journal*. **75**, 2302-2312.

Zhang, Q. H., Scholz, P.M., He, Y.Q., Tse, J., & Weiss, H.R. . (2005). Cyclic GMP signaling and regulation of SERCA activity during cardiac myocyte contraction. *Cell Calcium.* **37**, 259-266.

Zhang, S., Bawa-Khalfe, T., Yeh, E. T. H., Liu, X., Lu, L. S., Lyu, Y. L. & Liu, L. F. (2012). Identification of the molecular basis of doxorubicin-induced cardiotoxicity. *Nature Medicine*. **18**, 1639-1642.

Ziche, M., Morbidelli, L., Choudhuri, R., Zhang, H.T., Donnini, S., Granger, H.J., & Bicknell, R. (1997). Nitric oxide synthase lies downstream from vascular endothelial growth factor-induced but not basic fibroblast growth factor-induced angiogenesis. *Journal of Clinical Investigation.* **99 (11),** 2625-34.

Appendix

Table 1. Summary of structural cardiotoxin IC_{50}'s at 6 hrs

6 hr	Imatinib	Fluorouracil	Doxorubicin	Sorafenib	Lapatinib	Sunitinib	Dasatinib	Idarubicin
hCMEC''s								
MMP	16.59	1.95	28.35	9.23	11.36	2.42	8.26	13.35
ER	15.29	2.00	28.35	9.28	13.58	2.49	8.43	6.52
Ca^{2+}	15.48	2.11	28.35	9.18	13.92	2.40	9.05	31.68
ATP	198.52	1000.00	78.50	3.28	9.57	3.28	26.03	16.81
hDMECs								
MMP	10.15	3.26	14.81	7.11	10.67	1.63	8.50	1.62
ER	10.07	3.26	8.28	7.45	10.67	2.83	7.67	1.81
Ca^{2+}	10.03	3.26	9.57	7.58	10.67	1.63	8.50	4.00
ATP	77.31	66.67	69.32	2.79	8.28	36.29	40.17	20.52
hCAECs								
MMP	5.97	3.00	3.50	6.43	18.39	15.37	6.81	14.33
ER	5.96	3.00	3.49	6.49	5.57	15.38	6.81	14.33
Ca^{2+}	6.10	3.00	3.50	6.57	12.61	3.73	6.81	14.33
ATP	9.44	35.33	14.65	2.86	47.49	33.14	68.04	22.57
hCFs								
MMP	2.87	21.68	6.52	0.30	0.40	44.36	1109.18	179.04
ER	3.64	21.68	6.52	0.38	0.50	67.01	1121.74	23.31
Ca^{2+}	3.62	21.68	6.52	0.43	0.50	71.13	1150.95	37.91
ATP	3.05	21.68	6.52	3.59	0.31	40.30	2117.24	85.11
NhDFs								
MMP	28.24	21.68	6.52	6.04	0.18	1.20	13824.65	812.09
ER	28.24	21.68	6.52	6.04	0.18	191.26	13824.65	812.09
Ca^{2+}	28.24	21.68	6.52	6.04	1.50	163.57	13824.65	812.09
ATP	23.37	462.53	35.24	4.07	8.02	136.17	4887.47	115.67
hESC-CMs								
MMP	26.68	100	28.31	100	46.4	83.46	85.79	7.2
ER	100	100	100	100	100	100	100	90.68
Ca^{2+}	100	100	27.05	100	83.9	100	100	2.56
ATP	41.52	100	100	73.06	21.25	51.63	56.35	21.9

Table 2. Summary of structural cardiotoxin IC_{50}'s at 24 hrs

24 hr	Imatinib	Fluorouracil	Doxorubicin	Sorafenib	Lapatinib	Sunitinib	Dasatinib	Idarubicin
hCMEC''s								
MMP	23.78	6.67	0.73	1.76	16.50	6.52	13.56	24.00
ER	23.99	6.67	0.77	15.75	21.50	6.50	15.64	0.70
Ca^{2+}	23.99	6.67	0.62	10.98	21.50	7.24	16.79	0.69
ATP	88.47	165.27	15.60	4.76	17.54	31.42	28.66	3.23
hDMECs								
MMP	4.13	1.25	2.84	2.40	16.59	0.88	2.72	9.62
ER	4.13	1.22	2.78	2.32	1.09	0.89	4.17	1.36
Ca^{2+}	4.13	1.23	2.09	3.56	16.63	0.58	2.24	0.86
ATP	47.72	3171.73	12.13	2.19	18.08	7.59	66.00	3.44
hCAECs								
MMP	21.92	1.62	2.92	19.69	19.68	2.41	1.97	1.98
ER	21.92	1.62	2.92	34.02	16.17	2.33	16.30	2.33
Ca^{2+}	19.29	1.62	2.92	19.69	15.47	2.55	1.97	2.33
ATP	73.45	293.33	94.17	28.10	28.88	27.69	101.77	42.03
hCFs								
MMP	0.25	21.68	0.13	0.06	3.84	9.22	297.13	4.46
ER	0.25	21.68	0.03	0.06	3.06	9.43	167.35	4.36
Ca^{2+}	0.24	21.68	0.13	0.06	3.17	8.79	155.34	4.27
ATP	22.98	21.68	6.52	3.56	0.67	66.53	5242.30	481.61
NhDFs								
MMP	3.25	21.68	0.44	0.06	0.02	0.41	12.45	10.15
ER	3.24	21.68	0.36	0.07	0.02	0.08	12.51	3.35
Ca^{2+}	3.26	21.68	0.43	0.08	0.02	0.44	12.27	12.37
ATP	110.79	15921.42	6.48	2.66	12.56	207.59	8865.28	408.32
hESC-CMs								
MMP	94.28	100	3.47	100	54.64	86.9	0.5	4.6
ER	100	100	100	63.92	100	100	100	4.11
Ca^{2+}	100	100	6.2	100	100	94.57	76.89	8.62
ATP	32.33	100	29.18	48.33	10.1	35.53	35.02	8.4

Table 3. Summary of structural cardiotoxin IC_{50}'s at 72 hrs

72 hr	Imatinib	Fluorouracil	Doxorubicin	Sorafenib	Lapatinib	Sunitinib	Dasatinib	Idarubicin
hCMECs								
MMP	35.33	7.01	2.87	12.40	10.35	6.25	13.68	0.36
ER	35.33	7.01	2.85	12.50	8.38	5.84	14.17	0.37
Ca^{2+}	35.33	7.01	3.30	12.31	10.86	6.29	15.05	0.38
ATP	41.42	76.67	0.57	1.53	4.80	3.76	14.19	1.65
hDMECs								
MMP	9.79	13.45	13.41	3.09	5.33	4.54	10.47	0.63
ER	10.00	13.38	13.41	3.07	7.83	4.58	5.44	0.65
Ca^{2+}	10.00	13.45	13.42	4.26	9.99	4.63	8.84	0.73
ATP	20.50	3246.67	0.63	1.48	5.38	2.47	13.56	2.83
hCAECs								
MMP	36.67	16.40	2.79	7.41	13.34	8.73	3.28	1.14
ER	36.67	16.40	2.81	7.01	9.68	7.79	3.28	1.16
Ca^{2+}	36.67	16.40	3.80	7.20	9.68	8.83	3.28	1.18
ATP	43.15	908.23	3.13	1.35	6.15	5.04	15.02	3.74
hCFs								
MMP	0.00	21.68	0.01	0.12	1.15	35.34	2140.75	0.01
ER	0.00	21.68	0.02	0.16	2.40	33.86	2308.72	0.00
Ca^{2+}	0.00	21.68	0.02	0.17	1.27	37.65	6764.40	0.00
ATP	1.58	21.68	0.10	0.58	0.33	13.13	283.13	0.63
NhDFs								
MMP	28.24	21.68	0.08	0.00	0.00	47.01	13824.65	471.58
ER	28.24	21.68	0.02	0.00	0.05	65.65	8972.20	459.48
Ca^{2+}	28.24	21.68	0.32	0.00	0.05	56.46	10550.28	475.48
ATP	141.91	0.50	0.50	3.64	12.01	126.82	7812.77	77.63
hESC-CMs								
MMP	26.000	0.090	10.600	2.900	12.500	0.510	0.770	0.013
ER	52.0	0.06	>100	48.1	0.05	9.8	57.0	0.002
Ca^{2+}	20.4	0.03	40.8	7.8	*0.08*	0.001	18.3	0.013
ATP	16.4	48.3	0.53	19.7	12.5	19.4	62.0	9.4